INTERNATIONAL DOCTORAL
SCHOOL OF THE USC

Mireya
López Borrajo

PhD Thesis

Nanoengineered delivery of RNA: impact on brain diseases and COVID-19 vaccination

Santiago de Compostela, 2023

Doctoral Programme in Drug Research and Development

DOCTORAL THESIS

NANOENGINEERED DELIVERY OF RNA: IMPACT ON BRAIN DISEASES AND COVID-19 VACCINATION

Mireya López Borrajo

INTERNATIONAL PHD SCHOOL OF THE UNIVERSITY OF SANTIAGO DE COMPOSTELA

PHD PROGRAMME IN DRUG RESEARCH AND DEVELOPMENT

SANTIAGO DE COMPOSTELA

2023

Aos que viron o lóstrego,

e quedaron baixo a tormenta

Aos meus

«*Tunc ego, ut sum satis curiosa, requirere coepei*»

(Entón eu, sendo bastante curiosa, empecei a preguntar)

Exeria

«Non crer sen ver, dubidar, confiar só nos sentidos»

Sés

«Unha muller é unha muller (…)»

Laura Borrajo

ACKNOWLEDGEMENTS

Es probable que lo más importante de lo que he aprendido durante esta tesis no esté referenciado en las páginas que siguen. Pero se puede llegar a intuir las horas, la resiliencia, lo que se ha perdido y ha ganado en el camino. La persona que empezó esto y la que está escribiendo estas líneas. Y, sobre todo, las personas que me acompañaron durante estos años. Porque esta tesis no se hubiera empezado, continuado y terminado sin ellas.

Ante todo, agradecer la confianza depositada por mi directora de tesis, María José Alonso Fernández, y por todos estos años de enseñanzas. Gracias por darme una oportunidad y por hacerme salir de mi zona de confort tantas y tantas veces. Por guiarme y confiar en mis ideas. Por enseñarme lo que es tenacidad y perseverancia, de las cuales espero estarme llevando un poco conmigo.

Grazas á Universidade de Santiago de Compostela, ao CiMUS e ao IDIS, por poñer á miña disposición todos os medios necesarios para desenvolver á miña investigación. Gracias al Insituto de Salud Carlo III por la financiación de mi tesis a través de los Contratos i-PFIS. Y gracias a Orlando, del IDIS, por la paciencia mientras pedíamos becas y las denegaban. Hasta la última. Porque la calidad de una investigadora se mide más allá de sus calificaciones, y nos costó encontrar quien lo reconociese.

Special thanks to the B-SMART collaborators, especially Raymond Schiffelers, Ruth Schmid, and Roos Vandenbroucke. Also, thanks to the talented PhD students from the consortium, Hannah Walgrave and Nele Plehiers, who played a crucial role in this thesis. Gracias a nuestros colaboradores del proyecto COVARNA, en especial a Felipe García, Montse Plana, Mariano Esteban, Carmen Elena Gómez, Andreas Meyerhans, y Marta Sisteré-Oró, entre otros, por intentar lo imposible en mitad de una pandemia.

Gracias a Loli y al resto del personal del programa de doctorado en Investigación y Desarrollo de Medicamentos, por ser parte fundamental en esta tesis y la ayuda prestada para navegar la extensa burocracia del mundo académico y de la búsqueda de financiación.

Grazas a todos os compañeiros e compañeiras cos que tiven o pracer de compartir laboratorio durante estes anos. Grazas pola paciencia e o agarimo.

Gracias a Belén, por ser la directora de orquesta de este circo. Solo puedo esperar que el título de psicología llegue pronto, porque no sabría que hacer sin tus consejos, apoyo y rezos durante todos estos años. Por todo el cariño y el amor que me has dado. Gracias a Balby, por aguantarme y ayudarme sin importar en que página del Excel estuviéramos, y recibirme siempre con una sonrisa. Gracias a Puri, por siempre estar ahí cuando me asomaba en la puerta de tu despacho necesitando mil y una firmas. Grazas a Jose, por ser conselleiro de quen fixese falta no laboratorio. Gracias a Desi, por enseñarme a cómo hacer bien las cosas y estar siempre dispuesta a escuchar. Grazas ao resto de compañeiros do CiMUS, en especial a Marcos, Noemi, Sheila, Maruthi, Carla, Sandra e moitos otros. Grazas aos colaboradores deste centro, Mabel Loza, Jose Labandeira, Anxo Vidal, Rita Valenzuela, Aloia Quijano e David Moreira, pola axuda inestimable durante toda a tese.

Gracias a los que comenzaron este camino conmigo, y lo hicieron más fácil. No puedo imaginarme lo que el futuro nos depara, pero estoy convencida de que será bueno. Germán, por ser axuda e apoio en máis ámbitos dos que podo mencionar. Grazas por estar sempre para min cando máis o necesitei, e recibirme sempre cos brazos abertos. Gracias a Ana López, por ser ejemplo y marcar el ritmo a seguir durante todos estos años. ¡Quien nos ha visto en las escaleras hace cinco años y quien nos ve! Ahora, espero, viene algo mejor de lo que dejamos atrás.

Gracias a Carmen, por enseñarme lo que es ser realmente valiente. Obrigada a Catarina, por ser la alegría del laboratorio, y siempre tener una sonrisa y un mimo cuando hacía más falta. Thank you Shubaash, for being the unofficial co-director of this thesis. Thank you for your guidance, (huge) patience, motivation and for always finding time for me, regardless of what you were doing.

Gracias a los que ya estaban. Gracias a Adri, Irene, Belén, Andrea, Sofía, Cecília, Mati, Sergio, Vanessa, Fernando y Iago, por ayudarme a encontrar el norte, especialmente en los primeros meses, cuando no sabía ni por donde me daba el aire. Especial grazas a Tamara, por ser guía espiritual e científica dentro e fóra do laboratorio. Non sei nin como darche as grazas por todo o que fixeches por min, e o feliz que son de poder contar contigo. Grazas a Ana Olivera, por entenderme sempre e atopar tempo para falar e rir cando fixera falta.

Gracias a los que vinieron después. Gracias a Gustavo, por llegar en el momento adecuado y enseñarme a cómo hacer que me escuchen. Grazas a Laura Piñeiro, por afrontar todo o que che veu cun sorriso e estar sempre enterada de todo; creeme que xa pasou o peor da tese. Gracias a Alfonso, por las conversaciones en broma que terminen en serio, por preocuparte siempre de como estoy. Gracias por ser semejante apoyo desde que llegaste. Espero que Boston te guste casi tanto como Vermount, y estoy convencida de que te irá bien allá a donde vayas. Thanks, Philipp, for all the support and help in the past few years. It has been a pleasure working with you. I feel confident saying that you're more from here (Santiago, Galicia, or Spain) than myself. Thanks to Elena and Giorgio, who conquered the P5L2 and made it seem like we were in Italy more than in Compostela for a season. Thank you Jovanna, for the passion for our experiments, and the conversations inside and outside the lab. It was a pleasure to be part of your academic journey.

Gracias también a Federico, Lucía, Avinash, Dario, Sagi, Alberto, Eugenia, Eva, Alicia y Ana Otero. Gracias a Anna, por los consejos y siempre darme ánimos. Gracias a Marta, por la tranquilidad y tus historias contadas siempre con una sonrisa. Gracias a Patri, porque se puede ser parte de la farándula vistiendo totalmente de negro. Grazas a Cris, pola alegría coa que enches o laboratorio.

Gracias a los que están llegando. Supongo que estaréis cansados de oírmelo decir, pero vosotras vais primero y el resto después, y no hay nada más importante que esto para hacer una tesis (esto implica muchas cosas). Ánimo y suerte, Elena, Julia, Elisa, María y Jorge. Y en especial, gracias a Inés, por la paciencia y por recibirme con tanto cariño a mi vuelta. Te espera un futuro increíble (y también te vas a hacer mayor y llegará alguien que te diga que eres vieja).

A huge part of this thesis, and part of my PhD, is related to Eli Lilly in Cambridge, Massachusetts. Thanks to Sammy, for giving me the opportunity to be part of such an amazing team of scientists. Thanks for trusting and listening to me and my ideas. Thanks to Sean, for being the supervisor that anyone can wish for. Thank you for all the advice and always checking on me. Thanks to Eddie, for being such an inspiring, kind, and supportive colleague. Thanks to Michelle, for the opportunity and for making me feel supported. Thanks to all the amazing scientists that I had the opportunity to meet and work with for a year. Special thanks to Toby, who took me under his wing and helped me with everything. Thanks to Saeideh, for being the ultimate role model and making me feel less alone there. Thanks to Isom (Kelly The 3rd) for being the best buddy, for the laughs, and for always having my back. I don't like whiskey, but I guess the one from Tennessee is good. Thanks to Pintu, for all the bad jokes and sensing my mood perfectly every day. Thanks to Zhe, for getting excited with me every step of the way.

Thanks to every beautiful memory in 9 Granite St. Thanks to Fatema, for being such a kind, loving friend since my first morning there, for the talks on the countertop, and for being an example that effort can take you everywhere. Obrigada Gabi, for being such a force of nature and an inspiration in many, many ways. I miss having you on the other side of the door. Thanks to JB, for the love that you brought to the house every single day, and for making me feel at home. Thanks to Alex, for all the joy that you brought into the entire house as soon as you arrived. Honestly, could not imagine a better group of now friends to share my life with.

Y es imposible hablar de Boston sin mencionar a quienes me hicieron sentirme en casa. Gracias a Diana, Fabi, Vittoria, Gizem, Iratxe, Alicia, Adri, y Luis. Gràcies a David per entendre'm i pels audios llarguíssims que ens manteneten a prop. Gracias a Enya, por todas y cada una de las conversaciones medio escondidas a mitad de tarde, y por volver cuando más frío hacía. Gracias a Eric, por ser el unicornio que nadie esperaba, porque algún día todo nos irá mejor. Gracias a Marcos, por la sinceridad y por todo lo que evolucionaste delante de mis ojos. Eskerrik asko Pablo, oraindik zure barrea buruan grabatuta dudalako eta ezingo nukeelako mutil-lagun bat imajinatu. Gracias a Javi, por siempre tener una sonrisa, palabras bonitas y ganas de bailar. Eskerrik asko Ainhoa, ez baitakit nola biziko nintzateke ondoko kalean zeundela jakingo ez banu. Thanks to Sean for protect my drinks, my back, and to (try) explain me all the crazy sports. Eskerrik asko Viaña, handiago amets egin dezakedala erakusteagatik. Yo solo espero que después de todo este tiempo, os haya quedado por fin claro que todo depende de la persona y del contexto.

Grazas á xente que coñecín en Compostela e fixeron que todo isto fose moito máis sinxelo. Grazas a Natalia, por entenderme, apoiarme, rir e chorar comigo. Es a perfecta definición de persoa vitamina, e parte importantísima desta viaxe. Grazas a Alberto, polo agarimo durante todos estes anos. Grazas Ro, Ansur, Aldara, Tamara e Manu, por acollerme con tanto amor, por todos os adestramentos, partidos, ceas e o apoio. Non sodes conscientes de canto fixestes por min. Gracias a Laura Taina, por aparecer y poder ver la tesis desde fuera, estando todavía aquí. Gracias por el apoyo, las charlas entre cañas, y por siempre alegrarte por mí. Si hemos podido con esto, podemos con cualquier cosa.

Gracias a las que todavía sigo sin entender como siguen aquí. Gracias a Mónica, por estar cerquita mío al principio y al final de esta aventura, por no irte de mi lado desde que éramos peluqueras. No eres consciente de lo orgullosa que estoy de ti en todos los aspectos de la vida. Gracias a Tania, por ser a quien puedo recurrir pase lo que pase, alegrarme los días y hacerme ver las cosas desde una perspectiva mejor. Eres de las personas que solo pasan una vez en la vida. Gracias a Lara, por mantenerme al tanto e informada de la realidad, y por cuidarnos a todas tan bien. Por saber que necesito oír en cada momento.

Grazas a Noel e a Teresa, por seguir aí a pesar do tempo e a distancia, por continuar queréndome como o primeiro día. Grazas a Bichu, porque este Nadal serán o primeiro da tradición no que non teremos que falar da tese.

Grazas a Pancho e a Laura, que sen entender moi ben o que estaba a facer (non pasa nada, eu tampouco o teño moi claro algúns días), continúano tentando. Grazas a Chisco, por seguir levando a cordura á casa. Grazas a Perfecto e Celia, polo apoio e o mimo. E a Víctor e a Rocío, porque ao final si que escribín un libro.

I gràcies a Àlexandre, per continuar aprenent al meu costat, per haver aguantat l'inaguantable, per ensenyar-me el que és la paciència i tindre-la pels dos. Hui no seria ací si no fos per haver-me donat suport i estimar-me tots aquests anys.

TABLE OF CONTENTS

Table of contents

Abstract / resumen 17

Resumo *in extenso* 21

Introduction 39

Background, hypothesis, and objectives 71

CHAPTER 1. Ionizable nanoemulsions as nanocarriers for RNA delivery to the brain 79

CHAPTER 2. Nanoemulsions and polymeric nanocapsules for nose-to-brain and intracerebroventricular delivery of siRNA 111

CHAPTER 3. Nanoemulsions and polymeric nanocapsules as SARS-CoV-2 vaccines 165

Overall discussion 213

Conclusions 237

List of abbreviations 241

Ethical considerations 251

Publications derived from this thesis 277

ABSTRACT / RESUMEN

ABSTRACT

Gene therapies hold the promise of treating a wide range of diseases by modulating the expression of specific genes responsible for their development or progression. However, to fully harness this potential, effective delivery systems are required to reach and transfect specific tissues and cells. This becomes particularly crucial in the context of challenging diseases, such as central nervous system (CNS) conditions, or the development of vaccines against the severe acute respiratory syndrome coronavirus 2 (SARS-CoV-2).

The primary objective of this thesis has been to leverage nanotechnology for the delivery of different types of ribonucleic acids (RNA) intended to address the said diseases. For this, we chose delivery systems that have been well-established in our laboratory, namely nanoemulsions (NEs) and nanocapsules (NCs), and tailored them to encapsulate, protect, and deliver RNA. Namely, we designed and developed NEs and NCs endowed with a high capacity for diffusion and transfection of brain tissue. Some prototypes were also adapted for the nose-to-brain (N-to-B) and intracerebroventricular (ICV) delivery of small interfering siRNA (siRNA). In addition, a large library of NEs and NCs was investigated as delivery platforms for messenger RNA (mRNA) vaccines against SARS-CoV-2.

Chapter 1 describes the development of ionizable NE (iNEs), combining elements from classical lipid nanoparticles (LNPs) and oily cores from NEs. The results demonstrated a high diffusion across the brain and an excellent capacity to transfect neurons and microglia cells.

Chapter 2 is focused on the investigation of a library of NEs and NCs regarding their capacity to transport siRNA from the N-to-B route and their diffusivity following ICV administration. As a result, a powerful candidate was identified, exhibiting outstanding diffusivity upon ICV injection, accessing multiple brain regions (including the frontal cortex, striatum, hippocampus, brain stem, and dorsal root ganglion), and significantly reducing its targeted mRNA levels.

Chapter 3 discloses the encapsulation of several mRNA constructs derived from SARS-CoV-2 into NEs and NCs, as well as their *in vitro* and *in vivo* evaluation in terms of safety, transfection efficiency, and capacity to elicit immune responses. Notably, one candidate demonstrated the ability to induce specific cellular immune responses following intramuscular administration.

Overall, this work highlights the potential of NEs and polymeric NCs for the delivery of different kinds of RNA in two different contexts: treatment of brain diseases and vaccination. The results emphasize the importance of the nanocarrier composition and its physicochemical properties in the efficacy of RNA-based therapies and open new possibilities for enhancing the efficacy of genetic therapies for the treatment of challenging diseases.

RESUMEN

Las terapias genéticas tienen el potencial de tratar una amplia gama de enfermedades al modular la expresión de genes específicos responsables de su desarrollo o progresión. Sin embargo, para aprovechar completamente este potencial, se requieren sistemas de liberación capaces de alcanzar y transfectar tejidos y células específicos. Esta necesidad es particularmente crucial en el contexto de enfermedades desafiantes, como afecciones del sistema nervioso central (CNS), o el desarrollo de vacunas contra el síndrome respiratorio agudo severo del coronavirus 2 (SARS-CoV-2).

El objetivo de esta tesis se centra en el uso de la nanotecnología para desarrollar nanotransportadores de diferentes tipos de ácidos ribonucleicos (RNAs) con potencial en el tratamiento y prevención de enfermedades. Para ello, hemos seleccionado sistemas originalmente desarrollados en nuestro laboratorio, nanoemulsions (NEs) y nanocápsulas (NCs), y los hemos adaptado para encapsular, proteger y liberar RNA. En concreto, hemos diseñado y desarrollado NEs y NCs con una alta capacidad de difusión y transfección en el tejido cerebral. Algunos prototipos también se adaptaron para el transporte de la entrega de RNA pequeño de interferencia (siRNA) desde la nariz a cerebro (N-to-B) y también para su administración porvía intracerebroventricular (ICV). Además, desarrollamos una amplia biblioteca de NEs y NCs destinadas a transportar vacunas de RNA mensajero (mRNA) contra el SARS-CoV-2.

El Capítulo 1 describe el desarrollo de una NE ionizable (iNE), combinando elementos de las nanopartículas lípidicas (LNPs) y núcleos oleosos de las NEs. Dicha iNE mostró una alta difusión en el cerebro y una excelente capacidad para transfectar neuronas y microglía.

El Capítulo 2 se centra en la investigación de una biblioteca de NEs y NCs en cuanto a su capacidad para transportar siRNA a través de la ruta N-to-B y su difusión después de su administración por vía ICV. Como resultado, se identificó un candidato que exhibió una difusión sobresaliente tras su inyección ICV, accediendo a múltiples regiones cerebrales (incluyendo la corteza frontal, el estriado, el hipocampo, el tronco encefálico y el ganglio de la raíz dorsal) y reduciendo significativamente los niveles del mRNA objetivo.

El Capítulo 3 recoge la encapsulación de secuencias de mRNA derivadas del SARS-CoV-2 en NEs y NCs, y su evaluación *in vitro* e *in vivo* en términos de seguridad, eficiencia de transfección y capacidad para inducir respuestas inmunitarias. Notablemente, un candidato demostró la capacidad de inducir respuestas inmunitarias celulares específicas significativas después de su administración intramuscular.

En resumen, este trabajo destaca el potencial de las NEs y NCs poliméricas para la entrega de RNA en dos contextos diferentes: el tratamiento de enfermedades cerebrales y la vacunación. Los resultados enfatizan la importancia de la composición de los nanosistemas y sus propiedades fisicoquímicas en la eficacia de las terapias basadas en RNA, abriendo nuevas posibilidades para mejorar la eficiencia de las terapias genéticas para el tratamiento de enfermedades desafiantes.

RESUMO *IN EXTENSO*

1. INTRODUCIÓN

As terapias xenéticas consisten en tratar unha enfermidade transferindo material xenético ás células do paciente, inducindo, inhibido ou alterando a expresión do xene obxectivo. Isto permite ou modifica a expresión de proteínas específicas, corrixindo en última instancia o mecanismo subxacente responsable da enfermidade [1,2]. Estas terapias poden clasificarse en función de diversos factores, como a natureza da enfermidade a tratar, o tipo de método de entrega do xene, ou o tipo de administración [3,4]. Esta clasificación tamén pode facerse en función da tecnoloxía do ácido desoxirribonucleico (ADN) ou o ácido ribonucleico (ARN).

As terapias de ADN baséanse principalmente na transfección viral do ADN, onde unha copia funcional do xene defectuoso introdúcese nas células desexadas, utilizando virus adenoasociados [5,6]. Actualmente, 8 terapias xenéticas baseadas en ADN foron aprobadas pola Administración de Alimentos e Medicamentos (FDA) [7]. Con todo, o principal desafío sen resolver segue sendo a resposta inmunolóxica contra o vector, o que dificulta a posibilidade de administrar múltiples doses [6,8]. Coa intención de resolver este problema, e previr completamente a posible integración xenómica, as terapias xenéticas baseadas en ARN foron exploradas en décadas recentes como alternativas ás terapias baseadas en ADN [9,10].

1.1. ARN DE INTERFERENCIA

O ARN de interferencia (ARNi) baséase no uso de pequenos ácidos nucleicos exóxenos para interferir ou modular a expresión de xenes responsables de certas enfermidades [11]. Despois de múltiples décadas de investigación, involucrando o desenvolvemento de sistemas de liberación e modificacións químicas, a FDA aprobou a primeira terapia ARNi, Ompattro® (patisiran). Esta terapia consiste nun ARN interferente pequeno (ARNip) para o tratamento da amiloidosis hereditaria por transtiretina (hATTR), encapsulado nunha nanopartícula lipídica (LNP) [12,13]. Este logro abriu novas posibilidades para a terapia xenética no tratamento de diversas enfermidades.

Entre os diferentes tipos de oligonucleótidos deseñados para terapias de ARNi, os ARNip exóxenos e os mímicos do microARN (miARN) son os máis amplamente explorados.

1.1.1. ARN pequeno de interferencia (ARNip)

Os ARNip son moléculas curtas de ARN en dúplex (21-23 nucleótidos) deseñadas especificamente para dirixirse e inhibir a expresión de ARN mensaxeiro (ARNm) específicos. A especificidade de secuencia dos ARNip permite dirixirse selectivamente a un só ARNm, mellorando a precisión de efecto do ARNi [14,15]. Dada esta característica única, a selección de secuencias é unha parte clave no deseño racional dos ARNip, e esforzos substanciais realizáronse para optimizar a súa potencia terapéutica, con modificacións químicas incorporadas no esqueleto de fosfato, na ribosa ou nas bases de nucleótido dos ARNip [16–18].

1.1.2. Mímicos de microARN (miARN)

Os miARN son moléculas pequenas de ARN de cadea simple (19-25 nucleótidos). Prodúcense naturalmente e poden desempeñar un papel crítico na regulación de polo menos o 60% dos xenes humanos que codifican proteínas [19,20]. Un só miARN pode dirixirse a múltiples ARNm dentro do citosol, o que resulta na degradación do ARNm obxectivo ou a supresión do proceso de tradución, detendo así a produción de certas proteínas [20–23]. Para mellorar a súa estabilidade, protección contra nucleasas e potencia de ARNi, as moléculas de miARN poden ser quimicamente modificando, utilizando as estratexias similares ás usadas para os ARNip [24,25].

1.2. ARN MENSAXEIRO (ARNM)

O ARNm consiste nun ARN codifícante de cadea simple, cunha lonxitude media de aproximadamente 3 kbps [26]. Do mesmo xeito que as terapias xenéticas con ADN, o ARNm contén a información xenética necesaria para a tradución de proteínas. Con todo, o ARNm non necesita ser entregado dentro do núcleo para realizar a súa acción; no seu lugar, tradúcese na proteína obxectivo no citosol la célula diana [15,27]. Tanto as construcións de ARNm endóxenas como as sintéticas constan de cinco rexións distintas (de 5 'a 3 '): a carapucha 5', a rexión non traducida do 5 ' (UTR), o marco de lectura aberto (ORF), o UTR do 3 ' e unha cola final de poli-adenina ou poli(A) [28,29].

1.3. A NANOTECNOLOXÍA NA TERAPIA ARN

Ademais das vantaxes das modificacións químicas para mellorar a estabilidade e o rendemento dos ARN, os sistemas de entrega son unha compoñente clave nas estratexias da terapia de ARN [30,31]. No caso dos ARNm, debido ao seu tamaño e inestabilidade inherente, requiren do uso de vehículos de entrega para evitar a degradación, independentemente das modificacións químicas aplicadas [9]. No caso dos ARNip, máis curtos e estables que o ARNm, seguíronse diversas estratexias que levaron á aprobación de multiples fármacos por parte das axencias reguladoras, como o uso de LNPs ou a modificación do ARNip cun ligando que contén unha N-acetilgalactosamina (GalNAc) tricatenaria, capaz de recoñecer especificamente un receptor presente no fígado [12,32–36].

A pesar dos prometedores resultados, ambas estratexias permiten unicamente a liberación controlada de ARN no fígado. Por iso, nanotransportadores ou estratexias de liberación alternativas están a ser exploradas para mellorar o transporte e a aplicación das terapias xenéticas [30,37]. Isto é particularmente relevante no caso de enfermidades desafiantes, como condicións do sistema nervioso central (SNC) ou o desenvolvemento de vacinas contra o síndrome respiratorio agudo severo coronavirus 2 (SARS-CoV-2). Polo tanto, o obxectivo final desta tese foi o deseño e desenvolvemento de nanosistemas para terapias de ARN, co enfoque de abordar enfermidades desafiantes, como condicións do SNC e o seu uso como vacinas contra o SARS-CoV-2.

2. NANOEMULSIÓNS IONIZABLES PARA A ENTREGA DE ARN AO CEREBRO

Entre os numerosos desafíos asociados para a entrega de material xenético ao SNC, un obstáculo importante sen resolver é a limitada difusión dos nanosistemas. Por exemplo, o actual estándar para a entrega de ARN, as LNPs, só pode difundir aproximadamente 1-1,5 mm dende o sitio de administración no cerebro [38,39]. Esta mobilidade limitada débese ao denso núcleo interno das LNPs, que lles confire unha elevada rixidez [40].

Dado este contexto, a nosa hipótese baseouse na combinación do potencial das LNPs con núcleos máis fluídos, similares aos presentes nas nanoemulsións (NEs), para deseñar NEs ionizables (iNEs). As resultantes iNEs conteñen C12-200 como lípido ionizable, coñecido por mellorar o escape endosomal [41]. O núcleo contén un aceite (Vitamina E), có obxectivo de mellorar a súa flexibilidade. Para demostrar a versatilidade da iNE desenvolvida, utilizáronse varios tipos de oligonucleótidos para formular o nanosistema (Táboa 1). Non se atoparon diferencias significativas entre as formulacións, con tamaños ao redor de 70 nm e carga superficial neutra. Máis do 80% do ARN quedou completamente encapsulado nas iNE.

Táboa 1. Propiedades fisicoquímicas da iNE, en combinación con siGFP, mGFP, e miR-132

Tipo de ARN	Tamaño (nm)	PDI	Potencial ζ (mV)	Eficiencia de encapsulación (%)
siGFP	64 ± 7	0.23 ± 0.03	-2 ± 1	80-90
miR-132	60 ± 7	0.2 ± 0.05	-1 ± 1	80-90
mGFP	72 ± 9	0.17 ± 0.07	-4 ± 2	80-90

A eficiencia de encapsulación foi medida por xel de agarosa, e os valores foron corroborados polo ensaio de RiboGreen. **Abreviaturas:** GFP: proteína verde fluorescente. mGFP: ARNm codificante para GFP. miR-132: mímico de miARN-132. PDI: índice de polidispersión. siGFP: ARNip anti-GFP. Os valores representan a media ± desviación estándar (n ≥ 3).

O potencial de difusión das iNEs avaliouse nun modelo de rato da enfermidade de Alzheimer, utilizando miR-132, que está regulado á baixa na progresión desta enfermidade (Ilustración 2) [42]. Os nanosistemas foron administrados no xiro dentado (DG), unha rexión gravemente afectada pola enfermidade de Alzheimer, e determináronse os niveles de miR-132 tanto no DG como no Corno Ammonis (CA), unha rexión do hipocampo circundante [43,44]. A iNE mostrou unha acumulación significativa no DG, seguida dunha difusión cara ao CA de maneira dependente da dose, indicando unha modulación específica dos niveis de miR-132. Mesmo na concentración máis baixa (75 pmol), iNE-miR-132 induciu un aumento de aproximadamente 300 veces tanto no DG como no CA, superando o rendemento de LNP-miR-132, testado como control positivo a unha concentración máis alta (160 pmol). Estes resultados salientan a capacidade de difusión de iNE, en comparación coas LNPs clásicas, o que lles permite chegar eficientemente a diferentes rexións do cerebro.

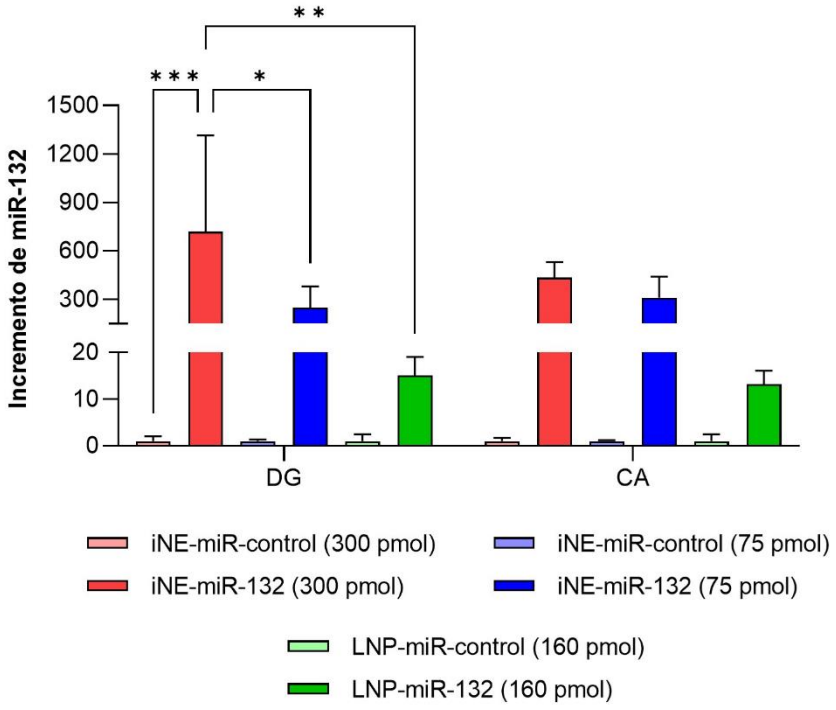

Ilustración 1. PCR semi-cuantitativa en tempo real dos niveis de miR-132 no DG e na rexión circundante CA, 48 horas despois da administración de iNE (a unha dose de 300 pmol en vermello, e 75 pmol en azul) e LNPs (verde), cargadas con miR-132 (cor brillante) ou miR-control (cor pálida)

Abreviacións: iNE: nanoemulsiones ionizables. LNP: nanopartículas lipidicas. miR-132: mímico de miARN-132. Análises de varianza (ANOVA) de 2 colas entre os grupos, seguido do método Tukey para comparacións múltiples. Valores $p < 0.05$ foron considerados estatisticamente significativos (*). Ademais, (**) se o valor $p < 0.01$, (***) se o valor $p < 0.001$. Os valores representan a media ± desviación estándar (n ≥ 3).

A capacidade de difusión das iNEs foi avaliado trala súa administración por vía intra-parenquimatosa, contendo ARNm que codifica para a proteína verde fluorescente (mGFP) (Ilustración 2). Os resultados demostraron unha difusión substancial das iNEs desde o sitio de administración, xunto cunha transfección celular prometedora, confirmando a eficiencia de difusión do nanosistema no hemisferio inxectado. Analizando os grupos celulares transfectados, observouse sinal GFP en neuronas e microglía, indicando a internalización e tradución da proteína fluorescente reporteira. Este comportamento foi menos prominente en astrocitos, suxerindo unha internalización específica por neuronas e microglía.

En resumo, este capítulo da tese describe o desenvolvemento de iNEs como novos nanotransportadores altamente difusores para a entrega de ARN ao cerebro. Aínda así, son necesarios máis estudos para validar a súa eficacia no tratamento de enfermidades do SNC, e explorar vías de administración menos invasivas.

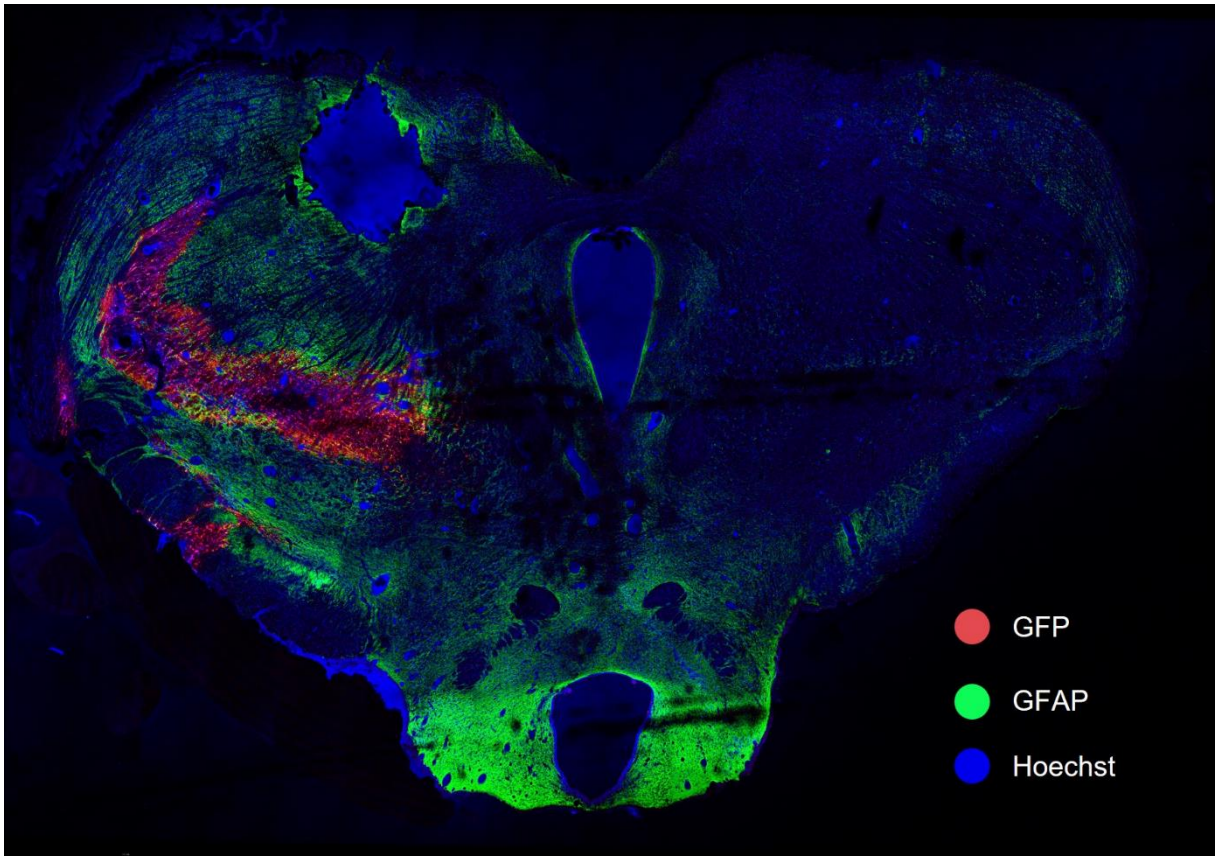

Ilustración 2. Dobre inmunomarcaxe no cerebro para GFP (vermello), e astrocitos (marcados con GFAP, verde), despois da administración intra-parenquimatosa de iNE-mGFP. Hoechst foi utilizado como marcador de núcleos (azul)

Abreviaturas: GFAP: proteína ácida fibrilar de glía. GFP: proteína de fluorescencia verde. iNE: nanoemulsión ionizable. mGFP: ARNm que codifica para GFP.

3. NANOEMULSIÓNS E NANOCÁPSULAS POLIMÉRICAS PARA A ENTREGA DE ARNIP DE POLAS VÍAS NARIZ A CEREBRO E INTRACEREBROVENTRICULAR

Un dos maiores desafíos na terapia de enfermidades do SNC é a presenza da barreira hematoencefálica (BBB). Esta barreira desempeña un papel fundamental na hemostase do SNC, e un mecanismo de defensa para a entrega de fármacos ao cerebro [45–48] Diferentes aproximacións tecnolóxicas para facilitar o transporte ao cerebro están sendo exploradas [49,50]. O uso de vías de administración alternativas en combinación con sistemas de libración controlada poden supoñer un avance no uso de terapias de ARN no contexto do SNC. Co obxectivo de entregar ARNip no SNC, desenvolvemos unha biblioteca de NEs e nanocápsulas (NCs) poliméricas con características específicas: un tamaño de partícula por baixo ou ao redor de 100 nm, produción reproducible e escalable, diversas cargas superficiais (incluíndo positivas, negativas e neutras), unha concentración final de ARNip de polo menos 0.25 mg/mL e estabilidade de polo menos un mes a 4°C. Estes nanosistemas están deseñados para

administrarse a través de vías de administración alternativas, incluíndo as administracións pola vía nariz a cerebro (N-to-B) e intracerebroventricular (ICV).

Cinco NEs diferentes cumpriron estes obxectivos en termos de tamaño de partícula (por baixo de 100 nm) e carga superficial (cargada positivamente), cunha eficiencia de encapsulación total próxima ao 100% (Táboa 2). Entre estes NEs, o NE-2 foi funcionalizado con éxito coa glicoproteína do virus da rabia (RVG), con capacidade de unirse ao receptor de acetilcolina nicotínica, presente no SNC [51].

Táboa 2. Propiedades fisicoquímicas das NE-1, NE-2, NE-3, NE-4 e NE-5 cargadas con ARNip

	NE-1	NE-2	NE-2-RVG	NE-3	NE-4	NE-5
Composición	DOTAP: Vit E: K-HS15®	DOTAP: Vit E: Tween 80	DOTAP: Vit E: Tween 80 + RVG	DOTAP: Lab™: Tween 80	DOTAP: Vit E: Labrasol®	DOTAP: Vit E: Inulin
Ratio molar (mol%)	16.9:65.8: 17.3	19.4:75.4: 5.2	19.4:75.4: 5.1:0.1	25:56.5: 18.5	19.4:75.4: 5.2	19.4:75.4: 5.2
Diámetro de partícula (nm)	90 ± 16	73 ± 10	84 ± 37	86 ± 10	100 ± 8	68 ± 5
PDI	0.20 ± 0.04	0.20 ± 0.04	0.25 ± 0.01	0.24 ± 0.03	0.18 ± 0.01	0.26 ± 0.03
Potencial ζ (mV)	+51 ± 3	+47 ± 4	+57 ± 6	+38 ± 6	+50 ± 3	+48 ± 2
Eficiencia de encapsulación (%)	100	100	100	100	100	100

A eficiencia de encapsulación foi medida por xel de agarosa, e os valores foron corroborados polo ensaio de RiboGreen e/ou análises por UPLC. **Abreviaturas:** DOTAP: 1,2-dioleoyl-3-trimethylammonium-propane chloride. K-HS15®: Kolliphor® HS15. Lab™: Labrafac™ Lipophile, WL 1349. NE: nanoemulsión. PDI: índice de polidispersión. RVG: glicoproteína do virus da rabia. Vit E: D, L-α-tocopherol. Os valores representan a media ± desviación estándar (n ≥ 3).

Debido ao seu pequeno tamaño de partícula, seleccionáronse NE-2 e NE-3 para recubrilos cunha cuberta polimérica, resultando na formación de NC cargadas con ARNip (Táboa 3). Os polímeros empregados foron o ácido poliglutámico conxugado a polietilenglicol (PEG-PGA), o ácido hialurónico (HA), o ácido polisialico (PSA) e o quitosano (CS). As NCs resultantes enxhibiron unha variedade de tamaños de partículas e cargas superficiais, dende altamente negativas (-48 mV, atribuída ao recubrimento de HA) ata altamente positivas (+49 mV, debido a dobre capa polimérica de HA e CS). Obtivéronse nanosistemas neutros, como NC-1, debido a cuberta de PEG-PGA.

Dada a capacidade destes nanosistemas, elixíronse diferentes candidatos específicos baseados nas súas propiedades fisicoquímicas para avalialos en modelos animais. Isto involucrou a exploración de vías de administración alternativas, como a N-to-B e a ICV.

Táboa 3. Propiedades fisicoquímicas das NC-1, NC-2, NC-3, NC-4, NC-5 e MNC-1 cargadas con ARNip

	NC-1	NC-2	NC-3	NC-4	NC-5	MNC-1
Nanosistema de base	NE-2	NE-2	NE-2	NE-3	NE-3	NC-2
Composición de base	DOTAP: Vit E: T80	DOTAP: Vit E: T80	DOTAP: Vit E: T80	DOTAP: Lab™: T80	DOTAP: Lab™: T80	DOTAP: Vit E: T80 + HA
Cuberta polimérica	PEG-PGA	HA	PSA	HA	PSA	CS
Ratio ARNip: polímero (mol/mol)	1:2	1:4	-	1:4	-	-
Ratio ARNip: polímero (w/w)	-	-	1:2	-	1:4	1:3.8
Diámetro de partícula (nm)	73 ± 5	87 ± 6	116 ± 3	70 ± 8	79 ± 11	100 ± 16
PDI	0.15 ± 0.03	0.15 ± 0.02	0.13 ± 0.03	0.24 ± 0.03	0.23 ± 0.02	0.18 ± 0.02
Potencial ζ (mV)	-1 ± 6	-28 ± 2	-48 ± 1	-23 ± 5	-44 ± 8	+49 ± 4
Eficiencia de encapsulación (%)	100	100	100	100	100	100

A eficiencia de encapsulación foi medida por xel de agarosa, e os valores foron corroborados polo ensaio de RiboGreen e/ou análises por UPLC. **Abreviaturas:** CS: quitosano. DOTAP: 1,2-dioleoyl-3-trimethylammonium-propane chloride. HA: ácido hialuronico (40 kDa). Lab™: Labrafac™ Lipophile, WL 1349. MNC: nanocápsula multi-capa. mol/mol: ratio mol/mol. NC: nanocápsula. NE: nanoemulsión. PEG-PGA: PEG (5 kDa)-b-PGA (10) (Na). PDI: índice de polidispersión. PSA: ácido polisiálico (30 kDa). T80: Tween 80. Vit E: D, L-α-tocopherol. w/w: ratio peso/peso. Os valores representan a media ± desviación estándar (n ≥ 3).

A administración N-to-B con diferentes candidatos (NE-2, NE-2-RVG, e NC-5) resultou nunha acumulación notable no epitelio nasal, o que podería facilitar o acceso aos nervios olfactivos e trixéminos [52,53]. Non obstante, unha modesta acumulación foi observada no bulbo olfactivo, no nervio trixémino e na cortiza frontal por parte de NE-2-RVG e NC-5, suxerindo un posible efecto do ligando ou da carga superficial. Estes resultados foron interpretados con precaución, debido á alta variabilidade experimental observada.

Finalmente, a formulación NC-1 foi elixida para avaliar a súa capacidade de difusión e rendemento de transfección tras a administración ICV. NC-1 resultou nunha redución dos niveis de ARNm obxectivo de máis do 50% en todas as áreas cerebrais analizadas (Ilustración 3). A observación adicional de ARNip confirmou o perfil de difusión e distribución en todo o cerebro (Ilustración 4). Curiosamente, a difusión observada supera á do estándar actual para a entrega de ARN, as LNPs, que só se difunden ata 4 mm desde o sitio de administración tras a inxección ICV [54]. Observouse unha difusión mellorada nas áreas próximas ao sitio de administración, como o estriado e a cortiza frontal, o que concorda cos resultados obtidos por análises de PCR.

En resumo, desenvolvemos unha biblioteca de múltiples NE e NC para a entrega de ARNip ao cerebro. De entre estes candidatos, NC-1 resultou ser un nanotransportador altamente prometedor para unha eficiente difusión e transfección de ARNip no cerebro. Dado o acceso preliminar ao bulbo olfactivo despois da administración de N-to-B de diferentes nanosistemas, as posibles aplicacións dos efectos de difusión e redución xénica de NC-1 poderían beneficiarse de vías menos invasivas, o que promete aínda máis o seu uso terapéutico. En conxunto, estes resultados teñen un gran potencial para o tratamento de enfermidades do SNC.

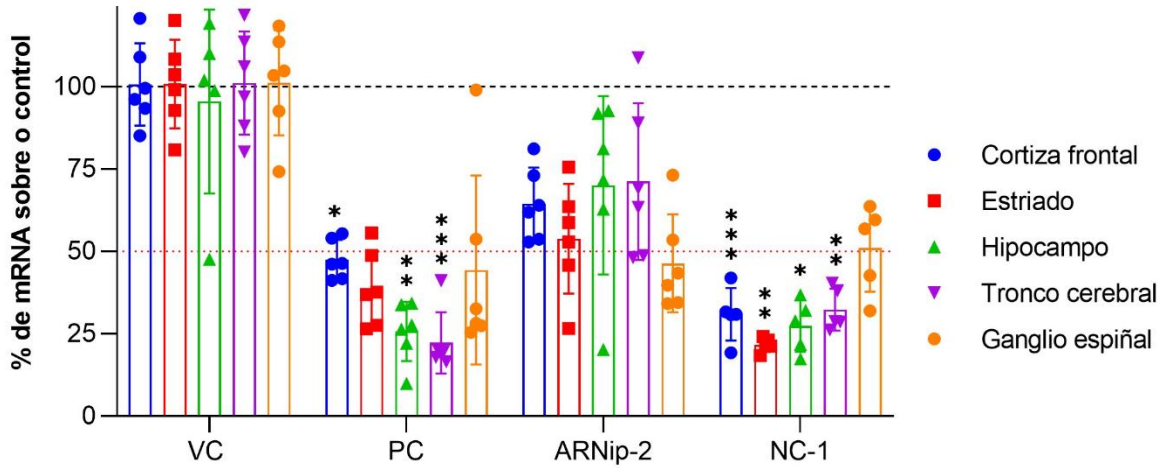

Ilustración 3. PRC cuantitativa dos niveis de ARNm obxectivo despois da administración ICV de NC-1 en diferentes áreas do cerebro, incluíndo a cortiza frontal, o estriado, o hipocampo, o tronco cerebral e o ganglio espiñal. Os resultados normalizáronse utilizando un xene de referencia

Abreviaturas: DRG: ganglio espiñal. NC: nanocápsula. PC: control positivo interno. VC: vehículo control (PBS). Análises de varianza (ANOVA) de 1 cola contra os grupos PC e NC-1 *vs* ARNip-2, seguido do método Tukey para comparacións múltiples. Valores $p < 0.05$ foron considerados estatisticamente significativos (*). Ademais, (**) se o valor $p < 0.01$, (***) se o valor $p < 0.001$. Os valores representan a media ± desviación estándar (n ≥ 3).

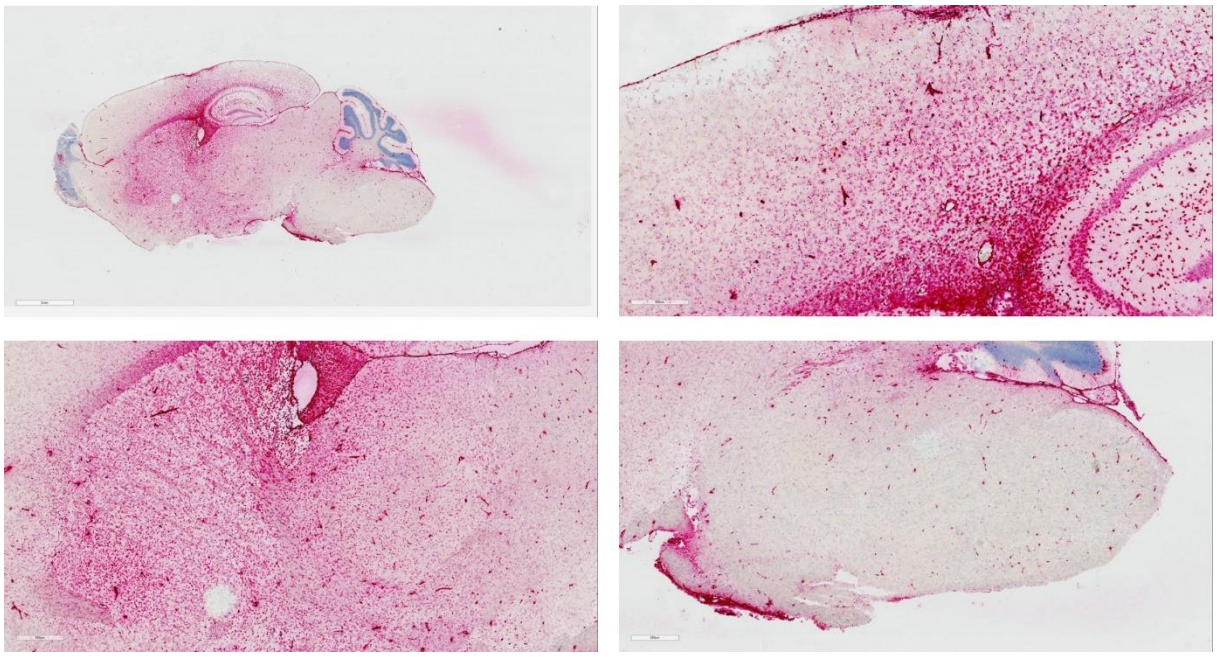

Ilustración 4. Detección de ARNip no cerebro despois da administración ICV de NC-1. Obtivéronse imaxes do cerebro completo (arriba, esquerda), e de preto da cortiza frontal (arriba, dereita), o hipocampo (abaixo, esquerda) e o tronco cerebral (abaixo, dereita)

3. NANOEMULSIÓNS E NANOCÁPSULAS POLIMÉRICAS COMO VACINAS CONTRA O SARS-COV-2

Durante a pandemia do coronavirus 2019 (COVID-19), investigadores de todo o mundo colaboraron para desenvolver vacinas contra o SARS-CoV-2, o virus responsable da enfermidade [55–58]. Este esforzo colectivo levou á aprobación de dúas vacinas de ARNm, Comirnaty® e Spikevax®, de BioNTech/Pfizer e Moderna, respectivamente. Ambas demostraron una eficacia superior ao 90% contra a infección sintomática por SARS-CoV-2 [59,60].

O noso laboratorio formou parte do consorcio COVARNA, co obxectivo de desenvolver unha vacina de ARNm contra o SARS-CoV-2. Diferentes ARNm foros sintetizados incluíndo un ARNm deseñado para estimular respostas de células T (ARNm de células T ou mT), un ARNm destinado a provocar unha resposta de células B (ARNm de células B ou mB), un ARNm que codifica para o dominio de unión ao receptor (RBD) da proteína espiga da superficie de SARS-CoV-2 (ARNm codificante para RBD ou mRBD), e un ARNm que codifica para un motivo altamente imunoxénico do dominio RBD (ARNm codificante para RBD_{epi} ou $mRBD_{epi}$). Desenvolvéronse aproximadamente 100 prototipos diferentes de NEs e NCs para a entrega de ARNm. Entre eles, seleccionáronse 15 en función da súa capacidade para cumprir cos criterios do perfil de produto obxectivo, que incluían un tamaño de partícula de menos de ou aproximadamente 200 nm, unha excelente monodispersidad de partículas, unha alta eficiencia de asociación de ARNm, estabilidade ou potencial de liofilización e cumprimento dos requisitos das axencias reguladoras.

Estes nanosistemas foron sometidos a varias avaliacións, incluíndo avaliacións *in vitro* utilizando múltiples liñas celulares (como células HeLa e células dendríticas humanas, usando mGFP) e administración intramuscular *in vivo* dun ARNm modelo (ARNm que codifica para luciferasa ou ovoalbumina). En xeral, NC-4-DX, que consiste nunha NE que contén DOTAP, DOPE e Tween 80 (denominada NE-4) e está recuberta por sulfato de dextrano (DX), mostrou un rendemento superior en comparación cos demais.

Táboa 4. Propiedades fisicoquímicas de NC-4-DX con diferentes tipos de ARNm contra SARS-CoV-2

Nanosistema	ARNm	Ratio w/w	Diámetro de partícula (nm)	PDI	Potencial ζ (mV)	EE (%)
NC-4-DX	mOVA	2: 1	132 ± 3	0.07 ± 0.03	-16 ± 2	100
NC-4-DX	mT	2: 1	111 ± 6	0.09 ± 0.02	-15 ± 5	100
NC-4-DX	mB	2: 1	114 ± 5	0.1 ± 0.02	-13 ± 5	100
NC-4-DX	mRBD	2: 1	109 ± 6	0.11 ± 0.01	-18 ± 2	90
NC-4-DX	$mRBD_{epi}$	2: 1	113 ± 6	0.09 ± 0.01	-19 ± 3	90
NC-4-DX	mT + mB	2: 1	113 ± 3	0.10 ± 0.02	-13 ± 4	100
NC-4-DX (n = 2)	mT + mRBD	2: 1	105 ± 1	0.09 ± 0.01	-19 ± 4	90
NC-4-DX (n = 2)	mT + $mRBD_{epi}$	2: 1	106 ± 1	0.10 ± 0.01	-17 ± 4	90

Abreviaturas: DX: sulfato de dextrano. EE: eficiencia de encapsulación. mB: ARNm de células B. mRBD: ARNm codificante RBD. $mRBD_{epi}$: ARNm codificante para RBD_{epi}. mT: ARNm de células T. NC: nanocápsula. PDI: índice de polidispersión. w/w: ratio peso/peso entre o polímero e o contido de ARNm. Os valores representan a media ± desviación estándar (n ≥ 3, a non ser indicado doutra forma).

Dado que NC-4-DX foi o noso candidato principal, realizouse a captura de diferentes ARNms para avaliar a súa versatilidade. Como se indica na Táboa 4, o tamaño de partícula de NC-4-DX variou de 105 a 130 nm, dependendo do tipo de ARNm utilizado, con índices de polidispersidad consistentemente baixos. Ademais, a carga superficial mantívose consistentemente negativa, oscilando entre -13 e -20 mV. En todos os casos, a eficiencia de encapsulación superou o 90%. Estes achados salientan o potencial de NC-4-DX como sistema de entrega para un candidato a vacina de ARNm. Isto é particularmente relevante no caso do SARS-CoV-2, xa que múltiples mutacións do virus requiriron axustes na carga de ARNm para manter unha eficacia protectora suficiente [61].

NC-4-DX avaliouse en termos da administración dun só ARNm contra o SARS-CoV-2 (utilizando mRBD e $mRBD_{epi}$, na Ilustración 5) ou a combinación de dous ARNms (un destinado a inducir respostas de células T, mT, en combinación con mB, mRBD ou $mRBD_{epi}$, na Ilustración 6).

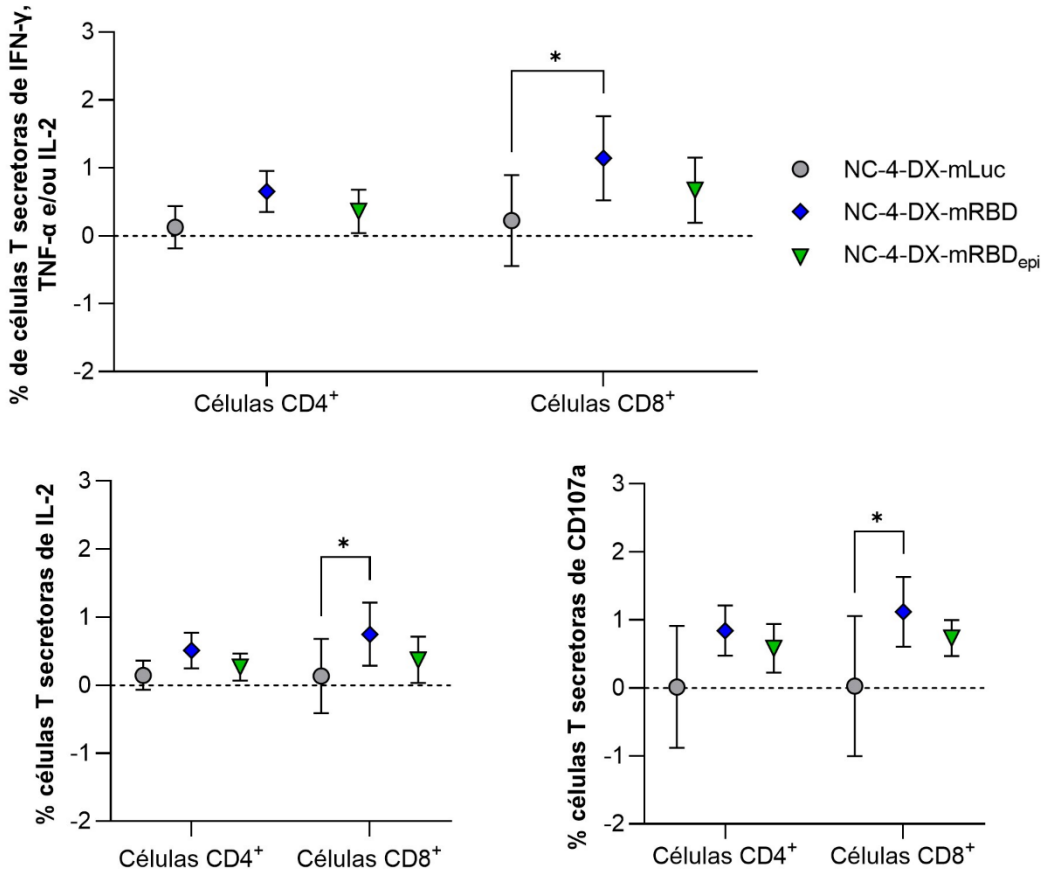

Ilustración 5. Respostas de células T $CD4^+$ e $CD8^+$ (arriba) considerando IFN-γ, TNF-α, e IL-2 (abaixo, esquerda). A secreción de CD107a por parte das células T foi tamén determinada (abaixo, dereita)

Abreviaturas: DX: sulfato de dextrano. IFN-γ: interferón gamma. IL-2: interleucina-2. mLuc: ARNm codificante para luciferasa. mRBD: ARNm codficante para RBD. $mRBD_{epi}$: ARNm codificante para RBD_{epi}. NC: nanocápsula. TNF-α: factor de necrose tumoral-alfa. Análises de varianza (ANOVA) de 1 cola, seguido do método Tukey para comparacións múltiples. Valores $p < 0.05$ foron considerados estatisticamente significativos (*). Os valores representan a media ± desviación estándar (n ≥ 3).

Coa intención de distinguir as diferenzas nas respostas inmunolóxicas de mRBD e $mRBD_{epi}$, ambos foron encapsulados en NC-4-DX e avaliáronse as súas respostas de células T $CD4^+$ e $CD8^+$ (Ilustración 5, parte superior). Esta avaliación revelou unha resposta inmunolóxica máis forte no caso das respostas de células T $CD8^+$, onde NC-4-DX-mRBD induciu respostas significativamente máis elevadas en termos de células T $CD8^+$ que segregan IL-2 e CD107a en comparación co grupo control. Estas dúas citoquinas desempeñan un papel crucial nas respostas inmunolóxicas medidas por células T [62,63]. Finalmente, avaliouse a combinación de NC-4-DX-mT con NC-DX-mB, -mRBD ou -$mRBD_{epi}$ (Ilustración 6). Atopáronse diferenzas significativas nas respostas de células T $CD8^+$ cando NC-4-DX-mT combinouse tanto con NC-4-DX-mRBD como con -RBDepi, en comparación co grupo de control (Figura 6, parte superior). A combinación de mT e mB aumentou significativamente os niveis de secreción de IFN-γ, en comparación cos outros grupos avaliados (Figura 6, parte inferior esquerda). Ademais, a combinación de mT e mRBD levou a niveis significativamente máis altos de IL-2 (Figura 6, parte inferior dereita).

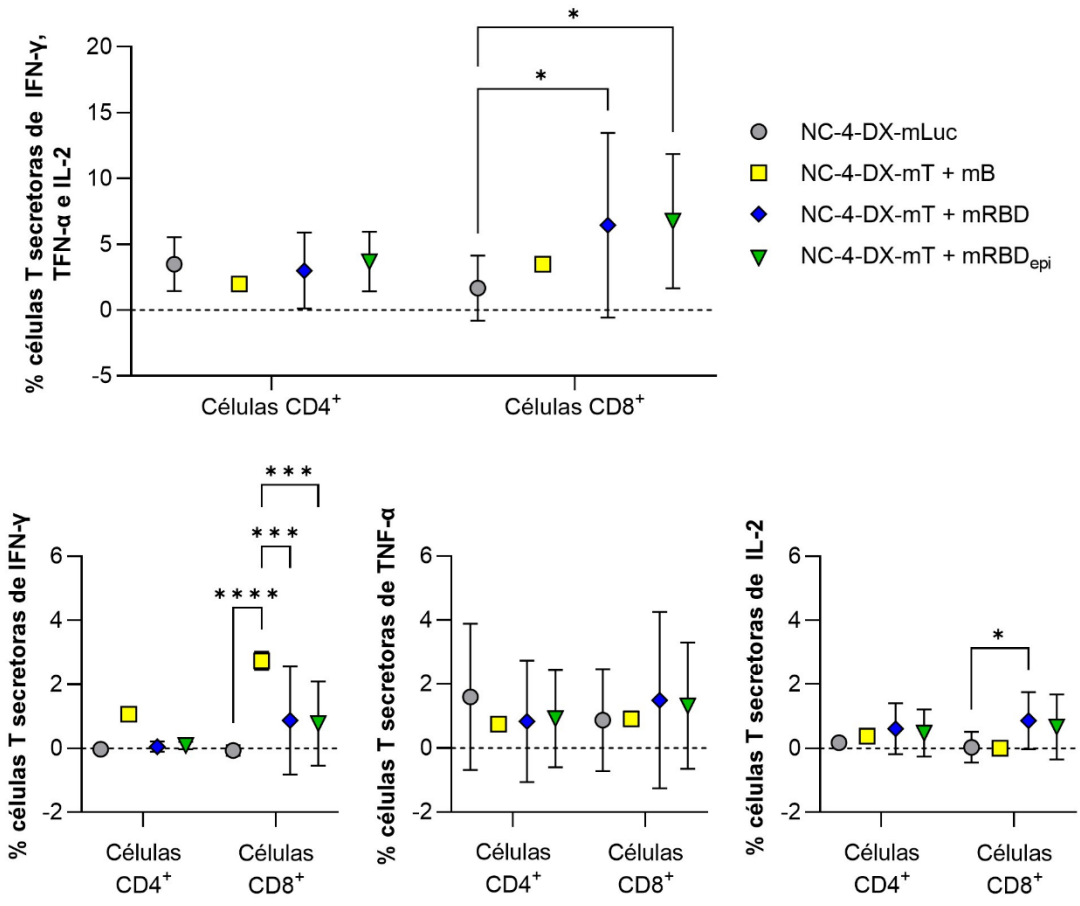

Ilustración 6. Resposta de células T $CD4^+$ e $CD8^+$ (arriba), considerando IFN-γ, TNF-α, e IL-2 (abaixo, esquerda, centro e dereita, respectivamente)

Abbreviations: DX: sulfato de dextrano. IFN-γ: interferón gamma. IL-2: interleucina-2. mB: ARNm de células B. mLuc: ARNm codificante para luciferasa. mRBD: ARNm codificante para RBD. $mRBD_{epi}$: ARNm codificante para RBD_{epi}. mT: ARNm de células T. NC: nanocápsula. TNF-α: factor de necrose tumoral-alfa. Análises de varianza (ANOVA) de 1 cola, seguido do método Tukey para comparacións múltiples. Valores $p < 0.05$ foron considerados estatisticamente significativos (*). Os valores representan a media ± desviación estándar (n ≥ 3).

En conclusión, nesta parte da tese deseñáronse e desenvolvéronse con éxito máis de 100 candidatos para unha vacina de ARNm e identificouse un posible candidato para unha vacina de ARNm contra o SARS-CoV-2, denominado NC-4-DX. Este nanosistema aumentou os niveis de respostas inmunolóxicas celulares específicas despois da administración intramuscular de ARNm derivados do SARS-CoV-2. Débense realizar estudos adicionais para optimizar a potencia de NC-4-DX ou as secuencias de ARNm para provocar respostas inmunolóxicas. En resumo, estes resultados salientan o potencial das NEs e NCs como portadores de entrega para vacinas de ARNm.

4. REFERENCIAS

[1] T. Wirth, N. Parker, S. Ylä-Herttuala, History of gene therapy, Gene. 525 (2013) 162–169. https://doi.org/10.1016/j.gene.2013.03.137.

[2] V. Sudhakar, R.M. Richardson, Gene Therapy for Neurodegenerative Diseases, Neurotherapeutics. 16 (2019) 166–175. https://doi.org/10.1007/s13311-018-00694-0.

[3] X.M. Anguela, K.A. High, Entering the modern era of gene therapy, Annu. Rev. Med. 70 (2019) 273–288. https://doi.org/10.1146/annurev-med-012017-043332.

[4] R. Tang, Z. Xu, Gene therapy: a double-edged sword with great powers, Mol. Cell. Biochem. 474 (2020) 73–81. https://doi.org/10.1007/s11010-020-03834-3.

[5] D. Wang, P.W.L. Tai, G. Gao, Adeno-associated virus vector as a platform for gene therapy delivery, Nat. Rev. Drug Discov. 18 (2019) 358–378. https://doi.org/10.1038/s41573-019-0012-9.

[6] J.T. Bulcha, Y. Wang, H. Ma, P.W.L. Tai, G. Gao, Viral vector platforms within the gene therapy landscape, Signal Transduct. Target. Ther. 6 (2021). https://doi.org/10.1038/s41392-021-00487-6.

[7] Food and Drug Administration, Approved Cellular and Gene Therapy Products, (2023). https://www.fda.gov/vaccines-blood-biologics/cellular-gene-therapy-products/approved-cellular-and-gene-therapy-products (accessed July 7, 2023).

[8] F. Mingozzi, K.A. High, Immune responses to AAV vectors: overcoming barriers to successful gene therapy, Blood. 122 (2013) 23–36. https://doi.org/10.1182/blood-2013-01-306647.

[9] T.R. Damase, R. Sukhovershin, C. Boada, F. Taraballi, R.I. Pettigrew, J.P. Cooke, The Limitless Future of RNA Therapeutics, Front. Bioeng. Biotechnol. 9 (2021) 1–24. https://doi.org/10.3389/fbioe.2021.628137.

[10] Y.-K. Kim, RNA therapy: rich history, various applications and unlimited future prospects, Exp. Mol. Med. 54 (2022) 455–465. https://doi.org/10.1038/s12276-022-00757-5.

[11] R.L. Setten, J.J. Rossi, S. ping Han, The current state and future directions of RNAi-based therapeutics, Nat. Rev. Drug Discov. 18 (2019) 421–446. https://doi.org/10.1038/s41573-019-0017-4.

[12] D. Adams, A. Gonzalez-Duarte, W.D. O'Riordan, C.-C. Yang, M. Ueda, A. V. Kristen, I. Tournev, H.H. Schmidt, T. Coelho, J.L. Berk, K.-P. Lin, G. Vita, S. Attarian, V. Planté-Bordeneuve, M.M. Mezei, J.M. Campistol, J. Buades, T.H. Brannagan, B.J. Kim, J. Oh, Y. Parman, Y. Sekijima, P.N. Hawkins, S.D. Solomon, M. Polydefkis, P.J. Dyck, P.J. Gandhi, S. Goyal, J. Chen, A.L. Strahs, S. V. Nochur, M.T. Sweetser, P.P. Garg, A.K. Vaishnaw, J.A.

Gollob, O.B. Suhr, Patisiran, an RNAi Therapeutic, for Hereditary Transthyretin Amyloidosis, N. Engl. J. Med. 379 (2018) 11–21. https://doi.org/10.1056/NEJMoa1716153.

[13] S.M. Hoy, Patisiran: First Global Approval, Drugs. 78 (2018) 1625–1631. https://doi.org/10.1007/s40265-018-0983-6.

[14] J.K.W. Lam, M.Y.T. Chow, Y. Zhang, S.W.S. Leung, siRNA Versus miRNA as Therapeutics for Gene Silencing, Mol. Ther. - Nucleic Acids. 4 (2015) e252. https://doi.org/10.1038/mtna.2015.23.

[15] M. Luo, L.K.C. Lee, B. Peng, C.H.J. Choi, W.Y. Tong, N.H. Voelcker, Delivering the Promise of Gene Therapy with Nanomedicines in Treating Central Nervous System Diseases, Adv. Sci. 9 (2022) 1–41. https://doi.org/10.1002/advs.202201740.

[16] B. Hu, Y. Weng, X. Xia, X. Liang, Y. Huang, Clinical advances of siRNA therapeutics, J. Gene Med. 21 (2019). https://doi.org/10.1002/jgm.3097.

[17] B. Hu, L. Zhong, Y. Weng, L. Peng, Y. Huang, Y. Zhao, X.J. Liang, Therapeutic siRNA: state of the art, Signal Transduct. Target. Ther. 5 (2020). https://doi.org/10.1038/s41392-020-0207-x.

[18] A. Khvorova, J.K. Watts, The chemical evolution of oligonucleotide therapies of clinical utility, Nat. Biotechnol. 35 (2017) 238–248. https://doi.org/10.1038/nbt.3765.

[19] R.C. Friedman, K.K.-H. Farh, C.B. Burge, D.P. Bartel, Most mammalian mRNAs are conserved targets of microRNAs, Genome Res. 19 (2009) 92–105. https://doi.org/10.1101/gr.082701.108.

[20] J. Godlewski, J. Lenart, E. Salinska, MicroRNA in Brain pathology: Neurodegeneration the Other Side of the Brain Cancer, Non-Coding RNA. 5 (2019) 20. https://doi.org/10.3390/ncrna5010020.

[21] M. Ghildiyal, P.D. Zamore, Small silencing RNAs: an expanding universe, Nat. Rev. Genet. 10 (2009) 94–108. https://doi.org/10.1038/nrg2504.Small.

[22] M. Guerau-de-Arellano, K.M. Smith, J. Godlewski, Y. Liu, R. Winger, S.E. Lawler, C.C. Whitacre, M.K. Racke, A.E. Lovett-Racke, Micro-RNA dysregulation in multiple sclerosis favours pro-inflammatory T-cell-mediated autoimmunity, Brain. 134 (2011) 3578–3589. https://doi.org/10.1093/brain/awr262.

[23] J. Peng, A. Omran, M.U. Ashhab, H. Kong, N. Gan, F. He, F. Yin, Expression Patterns of miR-124, miR-134, miR-132, and miR-21 in an Immature Rat Model and Children with Mesial Temporal Lobe Epilepsy, J. Mol. Neurosci. 50 (2013) 291–297. https://doi.org/10.1007/s12031-013-9953-3.

[24] R. Rupaimoole, F.J. Slack, MicroRNA therapeutics: Towards a new era for the management of cancer and other diseases, Nat. Rev. Drug Discov. 16 (2017) 203–221. https://doi.org/10.1038/nrd.2016.246.

[25] C. Diener, A. Keller, E. Meese, Emerging concepts of miRNA therapeutics: from cells to clinic, Trends Genet. 38 (2022) 613–626. https://doi.org/10.1016/j.tig.2022.02.006.

[26] X. Tang, S. Zhang, R. Fu, L. Zhang, K. Huang, H. Peng, L. Dai, Q. Chen, Therapeutic Prospects of mRNA-Based Gene Therapy for Glioblastoma, Front. Oncol. 9 (2019). https://doi.org/10.3389/fonc.2019.01208.

[27] J.A. Wolff, R.W. Malone, P. Williams, W. Chong, G. Acsadi, A. Jani, P.L. Felgner, Direct Gene Transfer into Mouse Muscle in Vivo, Science (80-.). 247 (1990) 1465–1468. https://doi.org/10.1126/science.1690918.

[28] N. Pardi, M.J. Hogan, F.W. Porter, D. Weissman, mRNA vaccines-a new era in vaccinology, Nat. Rev. Drug Discov. 17 (2018) 261–279. https://doi.org/10.1038/nrd.2017.243.

[29] N. Chaudhary, D. Weissman, K.A. Whitehead, mRNA vaccines for infectious diseases: principles, delivery and clinical translation, Nat. Rev. Drug Discov. 20 (2021) 817–838. https://doi.org/10.1038/s41573-021-00283-5.

[30] Y. Yan, X.-Y. Liu, A. Lu, X.-Y. Wang, L.-X. Jiang, J.-C. Wang, Non-viral vectors for RNA delivery, J. Control. Release. 342 (2022) 241–279. https://doi.org/10.1016/j.jconrel.2022.01.008.

[31] A. Cox, S.A. Lim, E.J. Chung, Strategies to deliver RNA by nanoparticles for therapeutic potential, Mol. Aspects Med. 83 (2022) 100991. https://doi.org/10.1016/j.mam.2021.100991.

[32] C.A. Sanhueza, M.M. Baksh, B. Thuma, M.D. Roy, S. Dutta, C. Préville, B.A. Chrunyk, K. Beaumont, R. Dullea, M. Ammirati, S. Liu, D. Gebhard, J.E. Finley, C.T. Salatto, A. King-Ahmad, I. Stock, K. Atkinson, B. Reidich, W. Lin, R. Kumar, M. Tu, E. Menhaji-Klotz, D.A. Price, S. Liras, M.G. Finn, V. Mascitti, Efficient Liver Targeting by Polyvalent Display of a Compact Ligand for the Asialoglycoprotein Receptor, J. Am. Chem. Soc. 139 (2017) 3528–3536. https://doi.org/10.1021/jacs.6b12964.

[33] A.D. Springer, S.F. Dowdy, GalNAc-siRNA Conjugates: Leading the Way for Delivery of RNAi Therapeutics, Nucleic Acid Ther. 28 (2018) 109–118. https://doi.org/10.1089/nat.2018.0736.

[34] A.A. D'Souza, P. V. Devarajan, Asialoglycoprotein receptor mediated hepatocyte targeting — Strategies and applications, J. Control. Release. 203 (2015) 126–139. https://doi.org/10.1016/j.jconrel.2015.02.022.

[35] M. Egli, M. Manoharan, Chemistry, structure and function of approved oligonucleotide therapeutics, Nucleic Acids Res. 51 (2023) 2529–2573. https://doi.org/10.1093/nar/gkad067.

[36] A. Akinc, M.A. Maier, M. Manoharan, K. Fitzgerald, M. Jayaraman, S. Barros, S. Ansell, X. Du, M.J. Hope, T.D. Madden, B.L. Mui, S.C. Semple, Y.K. Tam, M. Ciufolini, D. Witzigmann, J.A. Kulkarni, R. van der Meel, P.R. Cullis, The Onpattro story and the clinical translation of nanomedicines containing nucleic acid-based drugs, Nat. Nanotechnol. 14 (2019) 1084–1087. https://doi.org/10.1038/s41565-019-0591-y.

[37] H. Xu, Z. Li, J. Si, Nanocarriers in gene therapy: A review, J. Biomed. Nanotechnol. 10 (2014) 3483–3507. https://doi.org/10.1166/jbn.2014.2044.

[38] R.L. Rungta, H.B. Choi, P.J. Lin, R.W. Ko, D. Ashby, J. Nair, M. Manoharan, P.R. Cullis, B.A. MacVicar, Lipid Nanoparticle Delivery of siRNA to Silence Neuronal Gene Expression in the Brain, Mol. Ther. Acids. 2 (2013) e136. https://doi.org/10.1038/mtna.2013.65.

[39] L.E. Waggoner, K.F. Miyasaki, E.J. Kwon, Analysis of PEG-lipid anchor length on lipid nanoparticle pharmacokinetics and activity in a mouse model of traumatic brain injury, Biomater. Sci. (2023) 4238–4253. https://doi.org/10.1039/d2bm01846b.

[40] Y. Eygeris, S. Patel, A. Jozic, G. Sahay, Deconvoluting Lipid Nanoparticle Structure for Messenger RNA Delivery, Nano Lett. 20 (2020) 4543–4549. https://doi.org/10.1021/acs.nanolett.0c01386.

[41] X. Han, H. Zhang, K. Butowska, K.L. Swingle, M.G. Alameh, D. Weissman, M.J. Mitchell, An ionizable lipid toolbox for RNA delivery, Nat. Commun. 12 (2021) 8–13. https://doi.org/10.1038/s41467-021-27493-0.

[42] H. Walgrave, S. Balusu, S. Snoeck, E. Vanden Eynden, K. Craessaerts, N. Thrupp, L. Wolfs, K. Horré, Y. Fourne, A. Ronisz, E. Silajdžić, A. Penning, G. Tosoni, Z. Callaerts-Vegh, R. D'Hooge, D.R. Thal, H. Zetterberg, S. Thuret, M. Fiers, C.S. Frigerio, B. De Strooper, E. Salta,

Restoring miR-132 expression rescues adult hippocampal neurogenesis and memory deficits in Alzheimer's disease, Cell Stem Cell. 28 (2021) 1805-1821.e8. https://doi.org/10.1016/j.stem.2021.05.001.

[43] K. Richetin, P. Steullet, M. Pachoud, R. Perbet, E. Parietti, M. Maheswaran, S. Eddarkaoui, S. Bégard, C. Pythoud, M. Rey, R. Caillierez, K. Q Do, S. Halliez, P. Bezzi, L. Buée, G. Leuba, M. Colin, N. Toni, N. Déglon, Tau accumulation in astrocytes of the dentate gyrus induces neuronal dysfunction and memory deficits in Alzheimer's disease, Nat. Neurosci. 23 (2020) 1567–1579. https://doi.org/10.1038/s41593-020-00728-x.

[44] P. Chauhan, K. Jethwa, A. Rathawa, G. Chauhan, S. Mehra, The Anatomy of the Hippocampus, in: Cereb. Ischemia, Exon Publications, 2021: pp. 17–30. https://doi.org/10.36255/exonpublications.cerebralischemia.2021.hippocampus.

[45] D.J. Begley, Delivery of therapeutic agents to the central nervous system: The problems and the possibilities, Pharmacol. Ther. 104 (2004) 29–45. https://doi.org/10.1016/j.pharmthera.2004.08.001.

[46] B. Obermeier, R. Daneman, R.M. Ransohoff, Development, maintenance and disruption of blood-brain barrier, Nat. Med. 19 (2013) 1584–1596. https://doi.org/10.1038/nm.3407.Development.

[47] B. Engelhardt, L. Sorokin, The blood-brain and the blood-cerebrospinal fluid barriers: function and dysfunction, Semin. Immunopathol. 31 (2009) 497–511. https://doi.org/10.1007/s00281-009-0177-0.

[48] J.J. Lochhead, R.G. Thorne, Intranasal delivery of biologics to the central nervous system, Adv. Drug Deliv. Rev. 64 (2012) 614–628. https://doi.org/10.1016/j.addr.2011.11.002.

[49] D.S. Hersh, A.S. Wadajkar, N. Roberts, J.G. Perez, N.P. Connolly, V. Frenkel, J.A. Winkles, G.F. Woodworth, A.J. Kim, Evolving Drug Delivery Strategies to Overcome the Blood Brain Barrier., Curr. Pharm. Des. 22 (2016) 1177–1193.

[50] D. Furtado, M. Björnmalm, S. Ayton, A.I. Bush, K. Kempe, F. Caruso, Overcoming the Blood–Brain Barrier: The Role of Nanomaterials in Treating Neurological Diseases, Adv. Mater. 30 (2018). https://doi.org/10.1002/adma.201801362.

[51] R. Hao, B. Sun, L. Yang, C. Ma, S. Li, RVG29-modified microRNA-loaded nanoparticles improve ischemic brain injury by nasal delivery, Drug Deliv. 27 (2020) 772–781. https://doi.org/10.1080/10717544.2020.1760960.

[52] H. Wu, K. Hu, X. Jiang, From nose to brain: understanding transport capacity and transport rate of drugs, Expert Opin. Drug Deliv. 5 (2008) 1159–1168. https://doi.org/10.1517/17425247.5.10.1159.

[53] P.G. Djupesland, J.C. Messina, R.A. Mahmoud, The nasal approach to delivering treatment for brain diseases: An anatomic, physiologic, and delivery technology overview, Ther. Deliv. 5 (2014) 709–733. https://doi.org/10.4155/tde.14.41.

[54] R.L. Rungta, H.B. Choi, P.J.C. Lin, R.W.Y. Ko, D. Ashby, J. Nair, M. Manoharan, P.R. Cullis, B.A. MacVicar, Lipid nanoparticle delivery of sirna to silence neuronal gene expression in the brain, Mol. Ther. - Nucleic Acids. 2 (2013) 1–12. https://doi.org/10.1038/mtna.2013.65.

[55] D. Cucinotta, M. Vanelli, WHO declares COVID-19 a pandemic, Acta Biomed. 91 (2020) 157–160. https://doi.org/10.23750/abm.v91i1.9397.

[56] B. Hu, H. Guo, P. Zhou, Z.L. Shi, Characteristics of SARS-CoV-2 and COVID-19, Nat. Rev. Microbiol. 19 (2021) 141–154. https://doi.org/10.1038/s41579-020-00459-7.

[57] Y. Liu, J. Liu, K.S. Plante, J.A. Plante, X. Xie, X. Zhang, Z. Ku, Z. An, D. Scharton, C. Schindewolf, S.G. Widen, V.D. Menachery, P.Y. Shi, S.C. Weaver, The N501Y spike substitution enhances SARS-CoV-2 infection and transmission, Nature. 602 (2022) 294–299. https://doi.org/10.1038/s41586-021-04245-0.

[58] World Health Organization, WHO Coronavirus (COVID-19) Dashboard, (2023). https://covid19.who.int/ (accessed May 29, 2023).

[59] F.P. Polack, S.J. Thomas, N. Kitchin, J. Absalon, A. Gurtman, S. Lockhart, J.L. Perez, G. Pérez Marc, E.D. Moreira, C. Zerbini, R. Bailey, K.A. Swanson, S. Roychoudhury, K. Koury, P. Li, W. V. Kalina, D. Cooper, R.W. Frenck, L.L. Hammitt, Ö. Türeci, H. Nell, A. Schaefer, S. Ünal, D.B. Tresnan, S. Mather, P.R. Dormitzer, U. Şahin, K.U. Jansen, W.C. Gruber, Safety and Efficacy of the BNT162b2 mRNA Covid-19 Vaccine, N. Engl. J. Med. 383 (2020) 2603–2615. https://doi.org/10.1056/nejmoa2034577.

[60] L.R. Baden, H.M. El Sahly, B. Essink, K. Kotloff, S. Frey, R. Novak, D. Diemert, S.A. Spector, N. Rouphael, C.B. Creech, J. McGettigan, S. Khetan, N. Segall, J. Solis, A. Brosz, C. Fierro, H. Schwartz, K. Neuzil, L. Corey, P. Gilbert, H. Janes, D. Follmann, M. Marovich, J. Mascola, L. Polakowski, J. Ledgerwood, B.S. Graham, H. Bennett, R. Pajon, C. Knightly, B. Leav, W. Deng, H. Zhou, S. Han, M. Ivarsson, J. Miller, T. Zaks, Efficacy and Safety of the mRNA-1273 SARS-CoV-2 Vaccine, N. Engl. J. Med. 384 (2021) 403–416. https://doi.org/10.1056/nejmoa2035389.

[61] A.M. Carabelli, T.P. Peacock, L.G. Thorne, W.T. Harvey, J. Hughes, T.I. de Silva, S.J. Peacock, W.S. Barclay, T.I. de Silva, G.J. Towers, D.L. Robertson, SARS-CoV-2 variant biology: immune escape, transmission and fitness, Nat. Rev. Microbiol. (2023). https://doi.org/10.1038/s41579-022-00841-7.

[62] R.A. Seder, R. Ahmed, Similarities and differences in CD4+ and CD8+ effector and memory T cell generation, Nat. Immunol. 4 (2003) 835–842. https://doi.org/10.1038/ni969.

[63] G. Alter, J.M. Malenfant, M. Altfeld, CD107a as a functional marker for the identification of natural killer cell activity, J. Immunol. Methods. 294 (2004) 15–22. https://doi.org/10.1016/j.jim.2004.08.008.

INTRODUCTION

1. INTRODUCTION

1.1. THE RISING POTENTIAL OF GENE THERAPY

Decision on the approach for the treatment of a medical condition is always challenging. Ideally, addressing the direct cause of diseases would provide greater advantages than treating the symptoms. In many pathologies, the cause of the disease lies in the deregulation of genes encoding proteins, resulting in a malfunction that triggers the symptomology of the disease.

Gene therapies consist of treating a disease by transferring genetic material into the patient's cells, inducing, inhibiting, or altering the expression of the targeted gene. This enables or modifies the expression of specific proteins, ultimately correcting the underlying mechanism responsible for the disease [1,2]. These therapies can be classified based on various factors, such as the nature of the disease to be treated (genetic disorder or acquired disease), the type of gene delivery method (integrating or non-integrating), or the type of administration (directly into the patient, known as *in vivo*; or into cultured cells, followed by transplantation into the patient, referred to as *ex vivo*) [3,4]. Classification can also be based on the target type and modulation of the genetic expression depicted, as summarized in the following sections. In this introduction, therapeutics will be classified based on deoxyribonucleic acid (DNA) or ribonucleic acids (RNA) technology.

1.2. DNA THERAPIES

DNA therapeutics are mainly based on viral transfection of DNA, where a functional copy of the defective gene is delivered into the desired cells through local or systemic administration. Typically, this delivery is performed using adeno-associated viruses (AAVs), which are capable of delivering single-stranded DNA with a low rate of integration into the genome of the host cells. This reduces the risk of unintended mutagenesis but limits the long-term expression of the defective gene [5,6]. Several DNA therapies have already been approved by regulatory agencies. For example, the Food and Drug Administration (FDA) has approved 32 cellular and genetic therapies based on the delivery of the correct copy of the targeted gene [7]. Among them, 24 involve *ex vivo* genetic modification of the patient's cells; while *in vivo* gene therapies comprise 8 drugs, most of which received approval in the last two years (Table 1).

Nevertheless, the primary unmet challenge remains immunogenicity against the vector itself, which hinders the possibility of redosing [6,8]. In the recent decade, DNA therapeutics have gained significant attention due to advancements in cluster regularly interspaced short palindromic repeats (CRISPR) and CRISPR-associated protein 9 (Cas9), commonly known as CRISPR- Cas9 technology. This genome editing tool enables the addition, removal, promotion, or suppression of genetic material at specific genomic locations [9,10]. Currently, the first CRISPR-Cas9 therapy, intended to treat sickle cell disease and beta-thalassemia, is waiting for FDA approval [11].

Table 1. FDA-approved *in vivo* DNA therapeutics [7]

Drug name	FDA approval	Company	Delivery system	Indication
Imlygic®	2015	BioVex	HSV	Melanoma
Luxturna®	2017	Spark Therapeutics	AAV	Retinal dystrophy
Zolgensma®	2019	Novartis	AAV	Spinal muscular atrophy
Hemgenix®	2022	CSL Behring	AAV	Hemophilia B
Adstiladrin®	2022	Ferring Pharmaceuticals	AAV	High-risk non-muscle invasive bladder cancer
Vyjuvek™	2023	Krystal Biotech	HSV	Dystrophic epidermolysis bullosa
Elevidys	2023	Sarepta Therapeutics	AAV	Duchenne muscular dystrophy
Roctavian™	2023	BioMarin Pharmaceutical	AAV	Hemophilia A

Abbreviations: AAV: adeno-associated virus. HSV: herpes simplex virus.

1.3. RNA THERAPIES

In recent decades, gene therapies based on RNA have been successfully explored as an alternative to DNA therapies, aiming to completely prevent genome integration and reduce the immunogenicity associated with DNA-based therapeutics [12,13].

1.3.1. RNA interference

RNA interference (RNAi) relies on the use of small exogenous nucleic acids to interfere with or modulate the expression of genes responsible for certain diseases. The initial reports of this phenomenon date from 1998, when researchers discovered double-stranded RNAs (dsRNAs) capable of silencing genes in *Caenorhabditis elegans* [14]. Subsequent investigations identified smaller dsRNAs of 21-22 nucleotides, that depicted similar effects in mammalian cells [15,16].

Despite the initial excitement surrounding this technology, early clinical trials using unmodified small interfering RNAs (siRNA) concluded in disappointing results, with highly toxic immune responses and inconclusive silencing effects [17,18]. Incorporating these molecules into appropriate delivery systems, such as nanoparticles (NPs), provided initial evidence of RNAi efficacy upon systemic administration. However, challenges persisted, including toxicity and inadequate therapeutic effects, which prevented the further development of these technologies [19]. Undesired immunogenicity associated with both dsRNAs and delivery excipients was also observed [17,20]. Moreover, the accumulation of RNAi therapeutics in non-targeted tissues emerged as a significant source of toxicity [21].

All these discouraging findings, obtained in the 2000s and early 2010s, broke the bubble of enthusiasm about this class of therapies. Nevertheless, researchers and companies continued to refine RNAi technology, aiming to overcome these challenges. Substantial progress was made, primarily in terms of structural motifs, sequence selection, chemical modifications, formulation, and delivery mechanisms [22]. These major improvements culminated in the FDA approval of the first RNAi therapy, Ompattro® (patisiran). This therapy consists of a siRNA for the treatment of hereditary transthyretin amyloidosis (hATTR), encapsulated onto a lipid NP (LNP) [23,24]. This achievement opened new possibilities for genetic therapy in the treatment of various diseases.

Among the different types of oligonucleotides designed for RNAi therapies, exogenous siRNA and microRNA-mimics (miRNA) are the most extensively explored (Figure 1). In both cases, administered oligonucleotides are internalized into the cell, and processed by the RNA-induced silencing complex (RISC), which unwinds the RNA duplex and discards the sense or passenger strand [25,26]. The antisense strand, or guide strand, contains the sequence responsible for recognizing the targeted mRNA, resulting in different responses depending on the type of therapy used [27,28]. These distinct responses will be discussed in the next sections, and a summary of overall differences among these oligonucleotides can be found in Table 2.

Table 2. Comparison of the general properties between siRNA and miRNA as RNAi therapeutics [29]

General property	siRNA	miRNA
Structure	21-23 nucleotides	19-25 nucleotides
Complementary to target mRNA	Fully complementary	Partially complementary
mRNA targets	One	Multiple (could be over 100 targets)
Mechanism of RNAi	mRNA degradation	mRNA degradation
		Translational suppression

1.3.1.1. Small interfering RNA (siRNA)

siRNAs are short duplex RNA molecules (21-23 nucleotides) specifically designed to target and inhibit the expression of specific mRNAs. The sequence specificity of siRNA allows to selectively target a single mRNA, enhancing the precision of the RNAi effect [29,30]. Given this unique feature, sequence selection is a key part of the rational design of siRNAs, and substantial efforts have been made to optimize their therapeutic potency [31,32]. For instance, specificity can be improved when siRNA strands are asymmetrical (a 2 nucleotide 3' overhang on the end) [33,34]. Additionally, guanine (G) and cytosine (C) content significantly impact the performance of siRNA therapeutics and have been optimized within the range of approximately 30-64% [27,35,36]. Moreover, certain sequence motifs, such as those containing uracil (U) and G, have been found to stimulate immune toxicity, as in the case of *UGGC* [37]. Other motifs, like *UGU*, can enhance the interaction between siRNA and its target mRNA [38].

If siRNAs exceed 21 base pairs in length, the intervention of the cytosolic RNAi pathway enzyme Dicer is needed. This enzyme facilitates the cleavage of the siRNA before its interaction with the RISC complex and processing of the siRNA strands [28,39]. The requirement of this initial processing step can enhance RNAi activity, resulting in improved selection of the antisense strand within the RISC complex [28]. Conversely, avoiding the involvement of the Dicer machinery allows for greater chemical modification on the siRNA duplex, thereby increasing its stability and potency, while reducing side effects associated with these therapeutics [32,40]. Extensive research has been conducted on the modification of siRNAs to enhance their properties, with chemical modifications incorporated into the phosphate backbone, ribose moiety, or nucleotide bases of the siRNA therapeutic (Table 3) [32,41].

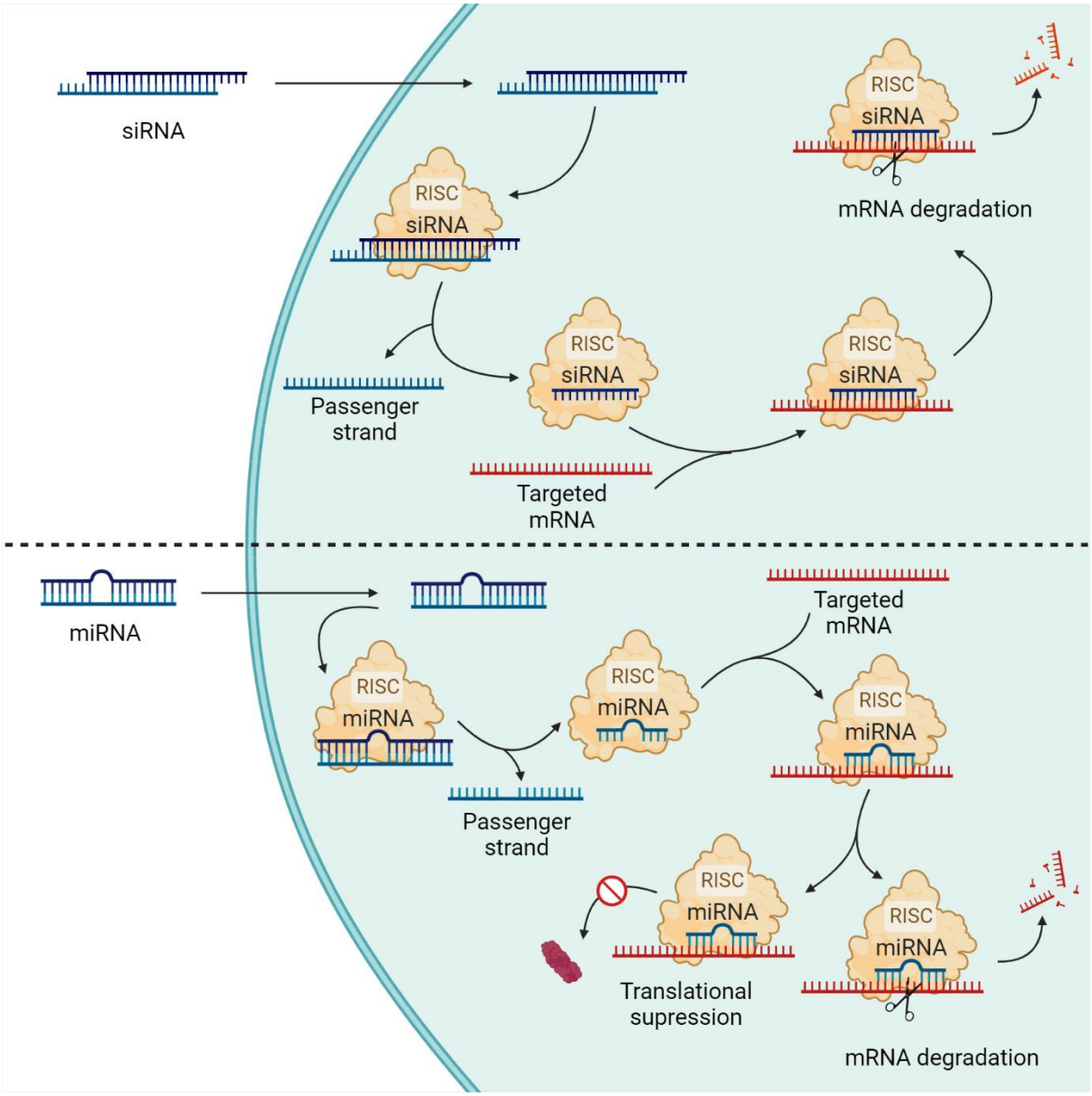

Figure 1. Schematic representation of RNA interference techniques, including siRNA (top) and miRNA (bottom)

The mechanism of action of both siRNA and miRNA in gene silencing within cells relies on the same cellular machinery, which involves the processing of these oligonucleotides by the RISC complex. This association facilitates the interaction with the targeted mRNA. In the case of siRNA, this interaction results in the complete degradation of the mRNA strand. However, due to the partial complimentary of miRNA with its target mRNAs, two distinct outcomes are possible: either degradation of the mRNA or suppression of the translation process. Created with https://biorender.com.

Table 3. Relevant chemical modifications applied to siRNA therapeutics

Modification family	Modification type	Effect on its performance as RNAi therapeutic
Phosphate modification	Phosphorothioate	Enhanced resistance to nucleases and longer circulation time [42,43].
	Phosphorodithioate	Increased affinity between RISC and siRNA [44]
	Methylphosphonate Methoxypropylphosphonate	Reduce hepatotoxicity [45]
	Phosphonate analogs	Increased stability and RISC loading [46–48]
	Peptide nucleic acid	Not as predominant, used to modify detection probes [49]
Sugar modification	2'-O-methyl	Enhanced stability and affinity for targeted mRNA [50,51]
	2'-O-methoxyethyl	Enhanced binding affinity and nuclease protection [41]
	2'-deoxy-2'-fluoro	Reduction immunotoxicity and enhanced binding affinity [41,52]
	2'-O-benzyl 2'-O-methyl-4-pyridine	Increased RNAi activity [53]
Base modification	Pseudouridine 2-thiouridine N-6-methyladenosine 5-methylcytidine *N*-ethylpiperidine 7-EAA triazole	Reduction of immunotoxicity and enhanced nuclease protection [54–56]
	6'-phenylpyrrolocytosine	Enhanced stability, RNAi activity, and fluorescence [57]
	5-nitroindole	Reduction of-targeted effects [58]
	5-fluoro-2'-deoxyuridine	Increased RNAi activity [59]

1.3.1.2. MicroRNA-mimics (miRNA)

miRNAs are small, single-stranded RNA molecules (19-25 nucleotides). They are naturally produced and can play a critical role in the regulation of at least 60% of human genes encoding for proteins, each containing various miRNA binding domains [60,61]. These oligonucleotides are critical in the development process, and their dysregulation has been associated with numerous human diseases [62,63]. A single miRNA can target multiple mRNAs within the cytosol, once loaded into the RISC complex, resulting in the degradation of the targeted mRNA or the suppression of the translation process, thereby stopping the production of certain proteins [25,61,64,65]. Different miRNA therapeutics can be classified into two different families: miRNA mimics and miRNA inhibitors. miRNA mimics consist of double-stranded RNA oligonucleotides, designed to mimick the naturally occurring miRNAs and their function; while miRNA inhibitors are single-stranded RNA molecules designed to interfere with miRNAs, inhibiting their function [12]. To enhance their stability, protection against nucleases, and RNAi potency, miRNA therapeutics can also be chemically modified, using the same strategies discussed for siRNA. Common chemical modifications include phosphorothioate, 2'-O-methyl, and locked nucleic acids (LNAs). [66,67].

1.3.2. Messenger RNA (mRNA)

Messenger RNA (mRNA) consists of a single-stranded coding RNA, with an average length of approximately 3 kbps [68]. Similar to plasmid DNA-gene therapies, mRNA contains the genetic information required for the translation of proteins. However, mRNA does not need to be delivered inside the nucleus to perform its action; instead, it is translated into the target protein in the cytosol of the targeted cell [30,69]. Both endogenous and synthetic mRNA constructs consist of five distinct regions (from 5' to 3'): 5' cap, 5' untranslated region (UTR), open reading frame (ORF), 3' UTR, and a final poly-adenine or poly(A) tail (Table 4) [70,71].

Table 4. Summary of the mRNA regions and their functions

mRNA regions	Function
5' cap	Reduction of immunotoxicity and endonuclease degradation. Involvement in the ORF translation [72,73].
5' UTR	Responsible for mRNA stability, cellular location, and protein translation regulation [74,75].
ORF	Sequence translated into protein [71].
3' UTR	Responsible for mRNA stability, cellular location, and protein translation regulation [74,75].
poly(A)	Responsible for mRNA stability [76].

Abbreviations: A: adenine. ORF: open read frame. UTR: untranslated region.

The 5' cap contains a 7-methylguanosine linked to the 5' end of the mRNA through a triphosphate bound. This structure reduces unwanted immune responses and enhances mRNA protection against degradation [72,73]. Additionally, in collaboration with the poly(A) section, it contributes to mRNA circularization and the recruiting of endosomes, optimizing protein translation [72,73,76]. The 5' and 3' UTR sections, located on either side of the ORF, are responsible for the oligonucleotide half-life, subcellular location, and the regulation of translation [72,74,75]. Typically, naturally occurring UTRs are optimized based on the cellular target and intended applications. These optimizations often involve the removal of miRNA-binding sites and AU-rich regions in the 3' UTR, to minimize unspecific mRNA degradation or the elimination of specific secondary and tertiary structures in the 5' UTR, which can prevent protein translation [77–79].

The ORF represents the most important portion of the mRNA construct, containing the sequence necessary for the translation of the target protein. Therefore, fewer modifications are typically made to this region compared to the rest of the oligonucleotide. The optimizations performed on the ORF can be summarized in improvements on the mRNA sequence or its production. [71]. Regarding modifications to the sequence, optimization can be used to reduce undesired immune responses. Since the immune system can recognize unmodified mRNA sequences, which are commonly found in viral mRNAs, mRNA constructs have been optimized with modified nucleosides, specially modified uridine, such us pseudo-uridine, and N1-methylpseudouridine. These modifications prevent the recognition of the mRNA sequence by pattern recognition receptors, such as toll-like receptors (TLR) [70,80,81]. Additionally, mRNA sequences can be optimized to improve translation efficiency without changing the final protein sequence. This can be achieved by modifying the sequence of frequently occurring codons. For

example, codons that rarely have specific nucleosides in a determined position can be replaced with other nucleosides, maintaining the resulting amino acid sequence [82].

Finally, the poly(A) tail is significantly important for mRNA translation and stability [76]. To ensure optimal tail length, the addition of poly(A) of an appropriate length can be achieved though direct modifications of the DNA template or by the use of a poly(A) polymerase [74]. Long poly(A) tails (greater than 100 bp) are known to significantly enhance the stability of therapeutic mRNAs; however, this length can destabilize DNA plasmids used to produce mRNA. Various modifications on the poly(A) tail, such as the incorporation of specific linkers, can enhance the stability of the DNA plasmid without compromising the therapeutic efficacy of the resulting mRNA [83,84].

1.3.3. Other relevant RNA therapy modalities

Gene therapy covers a wide range of technologies. In addition to siRNA, miRNA, and mRNA, RNA therapeutics also include other classes of oligonucleotides, such as antisense oligonucleotides (ASOs) or aptamers, some of which have been approved by regulatory agencies for the treatment of genetic diseases (Table 5) [85].

ASOs are synthetic, short, single-stranded oligonucleotides (12-22 nucleotides) capable of suppressing the expression of the targeted RNA, thereby modulating protein production [85,86]. This regulation can be performed by various mechanisms, including pre-mRNA processing and splicing, competitive inhibition, steric blockade, and degradation mediated by RNase H1 [87,88]. Over the past two decades, multiple ASOs have received approval, as summarized in Table 5. Vitravene® (fomivirsen) is the only first-generation ASO and antiviral oligonucleotide drug approved. It consists of a phosphorothioate-modified ASO, which enhances enzymatic resistance and circulation time while maintaining RNase H1 activity [89,90]. Second-generation ASOs incorporate ribose chemical modifications. For instance, Kynamro® (mipomersen), Tegsedi® (inotersen), and Waylivra® (volanesorsen) are approved drugs with RNAse H1 degradation therapeutic activity [91–93]. These ASOs have been chemically optimized to improve binding affinity to target RNA, overall stability, and nuclease protection, enabling the stability of these nucleic acids upon intravenous administration [94,95].

Further optimization has led to ASOs with the capacity to modulate alternative splicing by specifically binding to the target sequence and redirecting the spliceosome [96]. These features are used to either exclude or retain a specific exon of the targeted gene, a process known as exon skipping and exon inclusion, respectively [97]. The first approved drug in this modality was Spinraza® (nusinersen), which promotes exon inclusion by preventing the skipping of exon 7, leading to the production of the desired stable protein [98,99].

Additional modifications have resulted in the development of splice-switching ASOs, also known as phosphorodiamidate morpholino (PMO). These ASOs offer enhanced nuclease protection and facilitate exon skipping within the genome [100,101]. Exondys 51® (eteplirsen), Vyondys 53® (golodirsen), Viltepso® (vitolarsen), and Amondys 45® (casimersen) are clinically approved PMOs used to modify splicing in Duchenne muscular atrophy [102–105].

Table 5. ASO and aptamer therapeutics approved by FDA [85]

Drug name	Commercial name	FDA approval	Company	Type nucleic acid	Adm. route	Indication
Fomivirsen	Vitravene®	1998	Isis Pharmaceuticals	ASO	IVT	CMV retinitis
Pegaptanib	Macugen®	2004	Eyetech Pharmaceuticals	Aptamer	IVT	Neovascular AMD
Mipomersen	Kynamro®	2013	Genzyme Corporation	ASO	SC	HoFD
Eteplirsen	Exondys 51™	2016	Sarepta Therapeutics	ASO	IV	DMD
Nusinersen	Spinraza®	2016	Biogen	ASO	IT	SMA
Inotersen	Tegsedi®	2018	Ionis Pharmaceuticals	ASO	SC	hATTR
Golodirsen	Vyondys 53™	2019	Sarepta Therapeutics	ASO	IV	DMD
Volanesorsen	Waylivra®	2019	Akcea Therapeutics	ASO	SC	FCS
Vitolarsen	Viltepso®	2020	NS Pharma	ASO	IV	DMD
Casimersen	Amondys 45	2021	Sarepta Therapeutics	ASO	IV	DMD

Abbreviations: AMD: age-related macular degeneration. ASO: antisense oligonucleotide. CMV: cytomegalovirus. DMD: Duchenne muscular atrophy. FCS: familial chylomicronemia syndrome. hATTR: hereditary transthyretin amyloidosis. HoFD: homozygous familial hypercholesterolemia. IT: intrathecal. IV: intravenous. IVT: intravitreal. SC: subcutaneous.SMA: spinal muscular dystrophy.

Lastly, aptamers are short, single-stranded RNAs with the capacity to bind to a variety of targets, such as peptides and proteins, serving as agonists or antagonists of those biomolecules [12]. As an example, the only aptamer currently approved is Macugen® (pegaptanib), capable of targeting the vascular endothelial growth factor to treat macular degeneration [106].

1.4. NANOTECHNOLOGY AS AN ENABLING TECHNOLOGY IN RNA THERAPY

Besides the advantages that chemical modifications offer to enhance the stability and performance of oligonucleotides, delivery systems are a key component in RNA therapy strategies [107,108]. For example, due to its size and inherent instability, mRNA requires the use of delivery vehicles to prevent degradation, regardless of the chemical modifications applied [12].

In the case of siRNA, which is considerably shorter and more stable than mRNA, various strategies have been followed leading to approval by regulatory agencies (Table 6) [85]. The first approved siRNA drug, Onpattro® (patisiran) comprises a modified siRNA encapsulated within an LNP. Despite the chemical modifications applied to the siRNA sequence, Onpattro® still required the use of LNPs for the delivery of the siRNA to the liver [23,109]. LNPs are lipid-based nanosystems, typically composed of four distinct families of lipids: ionizable lipids, phospholipids, cholesterol, and polyethylene glycol (PEG)-lipids [110,111].

Table 6. siRNA therapeutics approved by FDA [85]

Drug name	Commercial name	FDA approval	Company	Delivery system	Indication
Patisiran	Onpattro®	2018	Alnylam	LNP	hATTR
Givosiran	Givlaari®	2019	Alnylam	GalNAc-siRNA	Acute hepatic porphyria
Lumasiran	Oxlumo®	2020	Alnylam	GalNAc-siRNA	PH1
Inclisiran	Leqvio®	2021	Novartis	GalNAc-siRNA	HeFH or ASCVD
Vutrisiran	Amvuttra®	2022	Alnylam	GalNAc-siRNA	hATTR

Abbreviations: ASCVD: clinical atherosclerotic cardiovascular disease. GalNAc: N-acetylgalactosamine. hATTR: hereditary transthyretin amyloidosis. HeFH: heterozygous familial hypercholesterolemia. LNP: lipid nanoparticle. PH1: primary hyperoxaluria type 1.

Ionizable lipids ensure high encapsulation of nucleic acids, maintaining a neutral surface charge at physiological pH, and facilitating the endosomal escape of the cargo upon cellular uptake. They have been extensively optimized to enhance their transfection efficiency while reducing toxicity and immune-related side effects [112]. Phospholipids, also known as helper lipids, contribute to the stability and endosomal scape properties of the LNPs due to their structural properties and the geometry of their saturated and unsaturated tails [80]. Cholesterol is fundamental for the overall stability and rigidity of the LNP [110]. PEGylated lipids play a significant role in the LNP stability and circulation time; however, inhibition of cellular uptake due to the PEGylated surface is known to reduce the transfection efficiency [113,114]. Consequently, various PEGylated lipids have been optimized, intended to balance the stability and transfection of the resulting LNPs [115].

The remaining approved siRNA therapeutics have been extensively modified, not only with chemical modifications to improve stability, nuclease protection, or therapeutic effect but also for targeted delivery to the liver. This modification entails the attachment of a ligand containing a triantennary N-acetylgalactosamine (GalNAc) [116,117]. GalNAc sugars can specifically recognize a receptor overexpressed on the hepatocyte surfaces, known as the asialoglycoprotein receptor carbohydrate recognition domine (ASGPR-CRD) [118]. Upon interaction with the receptor, GalNAc-siRNA conjugates enter the endosomal compartments, although some reports suggest that less than 0.1% of these conjugates successfully escape endosomes [117,119,120]. Furthermore, this delivery method achieves delivery solely to the liver due to the absence of ASGPR-CRD in other tissues and the specificity of GalNAc [118].

On the other hand, LNPs, and delivery nanosystems in general, can not only offer protection against degradation but can also lead to different biodistribution profiles, primarily determined by the nanocarrier composition. For example, the addition of different lipids (such as 1,2-dioleoyl-3-dimethylammonium propane or DODAP, or 1,2-dioleoyl-3-trimethyl-ammonium propane or DOTAP) into classical LNPs can alter their fate, redirecting them away from the liver to reach other organs, such as lung or spleen [121,122]. Furthermore, the ability to functionalize these nanocarriers with various targeting ligands provides the opportunity to reach different organs following intravenous administration [123]. Lastly, as mentioned earlier, different ionizable lipids have been optimized to enhance the endosomal escape of the RNA cargo, significantly improving the transfection performance of LNPs [111].

RNA delivery is not limited to LNPs or chemical modifications, as various other nanosystems are being explored for diverse purposes. In the following sections, different

promising nanocarriers designed for RNA delivery into the central nervous system (CNS) or as vaccines are going to be explored.

1.4.1. Gene therapy of central nervous system (CNS) diseases

Multiple types of nanocarriers have been developed for delivering oligonucleotides into the CNS to treat various disorders. In this section, we describe selected nanotechnological approaches involving RNA therapeutics that have been proven effective in treating CNS diseases in animal models (Table 7).

Numerous nanocarriers have been functionalized for the delivery of RNA into the brain upon intravenous administration. This route of administration poses several inherent challenges, including ensuring nanoparticle stability in the bloodstream, effectively delivering the cargo to the target tissue, and evading clearance mechanisms. Moreover, accessing the CNS from the bloodstream requires crossing the blood-brain barrier (BBB). This protective barrier surrounds cerebral blood vessels, maintaining CNS homeostasis and regulating the entry of potentially harmful substances. Unfortunately, it also hampers the transport of therapeutics and, consequently, delivery systems into the brain [124–126]. To overcome this challenge, nanocarriers intended to access the brain upon intravenous administration have been functionalized with various targeting ligands.

For this purpose, cell-penetrating peptides targeting specific receptors in the BBB have been widely used to functionalize nanocarriers, facilitating RNA delivery into the brain. Among them, Angiopep-2 has received significant attention, especially for transporting cargo of interest for the treatment of glioblastoma. This peptide specifically targets the low-density lipoprotein receptor-related protein-1 (LRP1), found in the BBB endothelial cells and human glioblastoma cells. These attributes confer Angiopep-2 the ability to enhance BBB penetration and target glioblastoma [127,128]. For example, liposomes functionalized with Angiopep-2 and loaded with siRNA targeting Golgi phosphoprotein 3 (GOLPH3) resulted in a modest increase in animal survival rates and a reduction in tumor volume in a glioblastoma mice model [129]. The same functionalization strategy was used in poly(lactic-co-glycolic acid) (PLGA)-NPs for co-delivery of siRNA GOLPH3 and the small molecule gefitinib, leading to successful accumulation in the brain and reduced levels of GOLPH3 in a glioblastoma model [130]. Notably, this study is one of the few that quantified the siRNA knockdown effect, providing valuable insights into RNAi therapy outcomes, whereas most investigations into glioblastoma focus primarily on tumor reduction and animal survival rates.

Polymeric nanosystems have also been functionalized with Angiopep-2 for the intravenous delivery of siRNA with the intention of crossing the BBB. For example, chitosan-PLGA NPs functionalized with Angiopep-2 and loaded with siRNA epidermal growth factor receptor (EGFR) and doxorubicin (DOX) resulted in significant tumor reduction [131]. Angiopep-2 was similarly used to functionalize guanidinium-PEG block-polymer NPs, for co-delivery of siRNA polo-like kinase 1 (PLK1) and vascular endothelial growth factor receptor 2 (VEGFR2) [132]; as well as miR-124 and anti-miR-21 [133]. Again, these positive results were mainly based on reduced tumor size and body weight loss, without a comprehensive assessment of the silencing effects on targeted mRNAs or protein production.

Another tumor-penetrating peptide, tLyp-1, was combined with Angiopep-2 for the functionalization of liposomes loaded with siRNA against vascular endothelial growth factor

(VEGF) and docetaxel (DTX). Again, the result was a decrease in the tumor size in a glioblastoma mice model [134]. A similar strategy was used in poly(amido amine) (PMAM) dendrimers, functionalized with both tLyp-1 and anti-NKG2A monoclonal antibody, to deliver siRNA targeting long stress-induced non-coding transcript 5 (LSINCT5), resulting in increased survival in a glioblastoma model [135].

Overall, despite the various approaches to treat glioblastoma through the use of nanocarriers functionalized with the said peptides, the reality is that the mechanistic details have not been well investigated and, therefore, the efficiency of the formulation approaches has not been well validated.

Table 7. Relevant examples of nanocarriers for the delivery of siRNA and miRNA into the CNS

Delivery system	Cargo	Disease	Size (nm)	Z-Pot (mV)	Targeting molecule	Administration route	Ref
Liposome	siRNA GOLPH3	Glioblastoma	88	+10	Angiopep-2	IV	[129]
PLGA-liposome	siRNA GOLPH3 and Ge	Glioblastoma	80	+20	Angiopep-2	IV	[130]
CS-PLGA NP	siRNA EGFR and DOX	Glioblastoma	190	+40	Angiopep-2	IV	[131]
Gu NP	siRNA PLK1 and VEGFR2	Glioblastoma	40	-	Angiopep-2	IV	[132]
Gu NP	miR-124 and anti-miR-21	Glioblastoma	30	-	Angiopep-2	IV	[133]
Liposome	siRNA VEGF and DTX	Glioblastoma	150	+25	tLyP-1 and Angiopep-2	IT and IV	[134]
PMAM dendrimer	siRNA LSINCT5	Glioblastoma	103	+7	tLyP-1 and anti-NKG2A Ab	IV	[135]
Liposome	siRNA mutant ataxin-3	SCA3	196	-	RVG	IV	[136]
Gu NP	siRNA BACE-1	AD	120	-	Galactose	IV	[137]
PEI NP	siRNA α-synucl	PD	90		-	ICV	[138,139]
LNP	siRNA PTEN	-	55	-	-	ICV	[140]

Abbreviations: AD: Alzheimer's disease. anti-NKG2A Ab: anti-NKG2A monoclonal antibody. BACE-1: β-secretase 1. CS: chitosan. DOX: doxorubicin. DTX: docetaxel. EGFR: epidermal growth factor receptor. Ge: gefitinib. GOLPH3: Golgi phosphoprotein 3. Gu: guanidinium. ICV: intracerebroventricular. IT: intratumoral. IV: intravenous. LNP: lipid nanoparticle. LSINCT5: long stress-induced non-coding transcript 5. miR: microRNA. NP: nanoparticle. PD: Parkinson's disease. PEI: poly(ethylenimine). PLGA: poly(lactic-co-glycolic acid). PLK1: polo-like kinase 1. PMAM: poly(amido amine). PTEN: phosphatase and tensin homolog 1. RNA: ribonucleic acid. RVG: rabies virus glycoprotein. SCA3: spinocerebellar ataxia 3. siRNA: small interfering RNA. tLyP-1: truncated form of LyP-1. VEGF: vascular endothelial growth factor. VEGFR2: vascular endothelial growth factor receptor 2.

Other diseases have been treated via intravenous administration, using various targeting ligands. For example, rabies virus glycoprotein (RVG) has been used to facilitate the transport of liposomes loaded with siRNA against mutant ataxin-3 into the brain in a spinocerebellar ataxia 3 (SCA3) model. This approach led to enhanced brain accumulation and reduced neuropathology by decreasing the levels of the mutant ataxin-3 [136]. On the other hand, guanidium NPs were functionalized with galactose, which binds to glucose transporter 1 (Glut1) receptors overexpressed in the BBB for the treatment of Alzheimer's disease. This targeting strategy enabled the delivery of siRNA β-secretase 1 (BACE-1), resulting in reduced BACE-1 mRNA and protein levels, as well as decreased amyloid-β levels in the hippocampus and the cortex areas [137].

In a different context, studies have attempted to understand the diffusivity and RNAi activity using different NPs upon intracerebroventricular (ICV) administration. For instance, poly(ethylenimine) (PEI) NPs were employed to deliver siRNA α-synuclein in a Parkinson's disease model. The results showed a reduction of α-synuclein levels in the striatum, this being attributed to an acceptable diffusion of the nanocomplexes in the brain [138,139]. However, this interpretation would require an adequate validation. In another example, LNPs loaded with siRNA against phosphatase and tensin homolog 1 (PTEN) were used to assess diffusivity after their ICV administration. The results showed a diffusion up to 4 mm from the injection site, accompanied by a 50% reduction in PTEN levels in the striatum and a 55% reduction in the hippocampus [140]. These comprehensive studies contribute to the understanding of NPs in the brain, as well as their ability to deliver RNAi therapeutics and to facilitate their function.

Table 7. Relevant examples of nanocarriers for the delivery of siRNA and miRNA into the CNS (continuation)

Delivery system	Cargo	Disease	Size (nm)	Z-Pot (mV)	Targeting molecule	Administration route	Ref
CS NP	siRNA Gal-1	Glioblastoma	141	+32	-	N-to-B	[146, 147]
PEG-PCL NP	siRNA Raf-1 and CPT	Glioblastoma	160	+9	Tat	N-to-B	[143]
PEG-PCL NP	siRNA TNF-α	Ischemia	62	+19	Tat	N-to-B	[144]
PEG-PLGA NPs	miR-124	Ischemia	204	-	RVG	N-to-B	[145]
PEG-PLA NPs	miR-132	AD/Ischemia	191	-25	WGA	N-to-B	[146]
PEG-PGA – r8-C12 NCX	miR-132	AD	96	+4	-	N-to-B	[147]

Abbreviations: AD: Alzheimer's disease. CPT: camptothecin. CS: chitosan. Gal-1: galectin-1. miR: microRNA. NCX: nanocomplex. NP: nanoparticle. N-to-B: nose-to-brain. PCL: poly(ε-caprolactone). PEG: polyethylene glycol. PGA: polyglutamic acid. PLA: poly(D,L-lactic acid). PLGA: poly(lactic-co-glycolic acid). r8-C12: octaarginine-lauric acid. Raf-1: serine-threonine kinase 1. RNA: ribonucleic acid. RVG: rabies virus glycoprotein. siRNA: small interfering RNA. Tat: trans-activator of transcription protein. TNF-α: tumor necrosis factor-α. WGA: wheat germ agglutinin.

Extensive research has also been done on less invasive administration routes, such as nose-to-brain (N-to-B), primarily using polymeric nanocarriers. In the case of glioblastoma, chitosan NPs administered through this route delivered siRNA targeting galectin-1 (Gal-1) to the brain, increasing animal survival rates. Furthermore, combining them with temozolomide or PD-1 blocking resulted in a synergetic effect, further increasing survival times [141,142]. Similarly, to treat glioblastoma, polyethylene glycol-poly(ε-caprolactone) (PEG-PCL) nanomicelles loaded with siRNA targeting serine-threonine kinase (Raf-1) and camptothecin (CPT), and functionalized with a truncated version of the trans-activator of transcription (Tat) protein of the human immunodeficiency virus (HIV), led to improved survival and tumor reduction [143]. This same nanosystem was used to deliver siRNA targeting tumor necrosis factor-α (TNF-α) in an ischemic stroke model, resulting in a significant reduction of the infracted area [144].

In addition, for ischemic stroke treatment, PEG-PLGA NPs functionalized with RVG were used to deliver miR-124, resulting in significant modulation of the targeted mRNAs and reduction in the infracted area [145]. A similar reduction of the infracted area was achieved with PEG-poly(D, L-lactic acid) (PEG-PLA) NPs loaded with miR-132 and chemically modified with wheat germ agglutinin (WGA). In the same study, the efficacy of this nanocarrier was evaluated in an Alzheimer's disease model, leading to significant behavioral improvements and decreased amyloid-β accumulation [146]. Additionally, our own group has developed an r8-C12 nanocomplex (NCX) coated with PEG-polyglutamic acid (PGA) for delivering miR-132, resulting in a significant modulation of mRNA targets in both the olfactory bulb and the hippocampus area [147].

In summary, most of the research focused on CNS delivery of RNAi therapeutics has been concentrated on glioblastoma treatment and the use of Angiopep-2 for CNS access. In cancer research, the primary focus appears to be assessing the anti-tumor effect of the therapeutics. While crucial for advancing these therapies, these findings alone do not provide sufficient insights into the fate of NPs in the brain or the silencing effects of RNAi therapeutics. Most research in this context is limited to *in vitro* studies, which may not always correlate with the *in vivo* outcomes.

Conversely, there is a growing trend in other CNS-related diseases, such as Alzheimer's disease, to assess targeted mRNA or protein levels. This may arise from the need for techniques to evaluate therapy results beyond behavioral improvements in animals. However, there remains a significant gap in understanding the processes NPs loaded with RNAi therapeutics undergo once they reach the CNS, including their diffusion, localization, and quantification of silencing effects. While reaching the CNS through targeting ligands or alternative administration routes is important, achieving the intended site of action within the brain and ensuring successful transfection is equally crucial, and at times, underestimated. Further research in this field would advance the development of genetic therapeutics for CNS diseases.

1.4.2. Vaccines

Different oligonucleotide vaccines have been approved in the past decade (Table 8). Only one DNA vaccine has been commercialized thus far. In 2017, the FDA approved Heplisav-B®, which consists of a phosphorothioate-modified DNA sequence capable of preventing hepatitis B liver infection, caused by the hepatitis B virus [148,149].

Table 8. Oligonucleotide vaccines approved by the FDA [85]

Drug name	Commercial name	FDA approval	Company	Type nucleic acid	Indication
Hepatitis B vaccine	Heplisav-B®	2017	Dynavax Technologies	DNA	Hepatitis B
Tozinameran	Comirnaty®	2021	BioNTech/Pfizer	mRNA	SARS-CoV-2
Elasomeeran	Spikevax®	2021	Moderna	mRNA	SARS-CoV-2

Abbreviations: DNA: deoxyribonucleic acid. mRNA: messenger RNA. RNA: ribonucleic acid. SARS-CoV-2: severe acute respiratory syndrome coronavirus 2.

Conversely, mRNA vaccines can be categorized into two different families: conventional non-replicating mRNA vaccines, which encode the protein of interest; and self-amplifying mRNA (SAM) vaccines, which additionally include the necessary machinery for RNA amplification within cells, thereby increasing antigen expression [70]. Currently, only two conventional mRNA vaccines have received regulatory authorization from the European Medicines Agency (EMA) and the FDA: Comirnaty® from BioNTech/Pfizer, and Spikevax® from Moderna. Both mRNA vaccines target the severe acute respiratory syndrome coronavirus 2 (SARS-CoV-2) and comprise a modified SARS-CoV-2 spike protein mRNA encapsulated onto LNPs [150]. These vaccines share certain similarities, such as the chemical modifications on the mRNA sequence and specific LNP characteristics (e.g., cholesterol content, use of the same helper lipid, and similar PEGylated components). Differences between Comirnaty® and Spikevax®, aside from the mRNA sequence, primarily involve the condensing lipid (ALC-0315 and SM-102, respectively) and the administered dose (30 µg and 100 µg, respectively) [110,151]. Both vaccines have reported efficacy rates of over 90% against SARS-CoV-2 infection, 100% efficacy against severe diseases, and favorable safety profiles [152,153].

Currently, more than 20 clinical trials are being conducted for mRNA vaccines encapsulated onto LNPs, intended for application in various diseases beyond SARS-CoV-2 [110,154]. For example, Moderna is developing an mRNA vaccine against influenza, named mRNA-1010, which encodes for the surface protein hemagglutinin of four influenza virus strains, encapsulated onto an LNP. In phases I and II (NCT04956575), this vaccine candidate elicited hemagglutination inhibition levels against all strains and exhibited a safety profile that supported its advancement to phase III (NCT05415462) [155]. Another promising clinical trial is being conducted for mRNA-1345, an adult respiratory syncytial virus (RSV) vaccine. This particular vaccine comprises an mRNA encoding for the prefusion F glycoprotein of the virus, encapsulated in the same LNP as Spikevax®. Phase I results demonstrated good tolerability across all tested doses in different age groups (NCT04528719), and phase II/III is currently assessing the efficacy of a single dose of the vaccine (NCT05127434) [156]. Clinical trials are also investigating the use of mRNA vaccines in cancer treatment, such as the personalized mRNA vaccine mRNA-4157 in combination with immune checkpoint inhibitors for melanoma

treatment. Phase I results highlighted the enhanced effect of the combination therapy compared to the anticancer drug alone, and phase II trials will commence soon (NCT03897881) [157,158].

In addition to LNPs, other types of nanocarriers have been extensively explored for the delivery of mRNA vaccines (Table 9). For instance, cationic nanoemulsions (NEs) containing DOTAP, squalene, Span 85, and Tween 80 have been used to deliver SAM vaccines for diseases like RSV, HIV, and human CMV (hCMV) in different animal models [159]. The RSV vaccine, consisting of a SAM encoding for the fusion glycoprotein (F), induced F-specific serum IgG in mice after two intramuscular administrations. The hCMV vaccine was tested in macaques, using a SAM encoding for both enveloped glycoprotein B (gB) and phosphoprotein 65-immediate early protein 1 (pp65-IE1), resulting in significant gB-specific IgG and neutralizing antibodies after a single intramuscular administration, with further amplification following a booster dose. Moreover, $CD4^+$ and $CD8^+$ T cells were detected in animals. Another relevant example is a SAM-based HIV vaccine, encoding for gp140 enveloped glycoprotein (gp140). Following intramuscular administration, this SAM vaccine formulated in a NE led to higher levels of gp140-specific serum IgG and neutralizing antibodies after two immunization sessions compared to the same free cargo and the SAM entrapped in a viral replicon particle. This same formulation was also used in macaques, resulting in a potent cellular immune response and neutralizing antibodies that exceeded those produced with the same mRNA cargo encapsulated in a viral replicon particle [160].

Table 9. Relevant examples of nanocarriers for the delivery of mRNA vaccines

Delivery system	Cargo	Disease	Size (nm)	Z-Pot (mV)	Administration route	Ref
NE	F SAM	RSV	130	+30	IM	[159]
NE	gB PP65-IE1 SAM	hCMV	130	+30	IM	[159]
NE	gp140 SAM	HIV	130	+30	IM	[159]
NE	gp140 SAM	HIV	~100	-	IM	[160]
PEI-SA NP	gag mRNA	HIV	120	-	SC	[161]
PEI-CD NP	gp120 mRNA	HIV	120	+26	IN	[162]
PGS NP	RBD mRNA	SARS-Cov-2	165	-4	IM	[163]
Dendrimer	HAp SAM	Influenza	~ 200	-	IM	[164]
Dendrimer	EBOV gp SAM	Ebola	~ 200	-	IM	[164]
Dendrimer	6-Ag SAM	*T. gondii*	~ 200	-	IM	[164]

Abbreviations: 6-Ag: six antigens onto same construct (GRA6, ROP2A, ROP18, SAG1, SAG2A, AMA1). AMA1: apical membrane antigen 1. EBOV gp: Ebola virus glycoprotein. F: fusion glycoprotein. gag: group-specific antigen. gB: envelope glyocoprotein B. gp120: enveloped glyocoprotein 120. gp140: envelope glycoprotein 140. GRA6: dense granule protein 6. HA: hemagglutinin protein. HIV: human immunodeficiency virus. IM: intramuscular. IN: intranasal. mRNA: messenger RNA. NE: nanoemulsion. NP: nanoparticle. PEI-CD: poly(ethylenimine)-cyclodextrin. PEI-SA: poly(ethylenimine)-stearic acid. PGS: polyglucan-spermidine. pp65-iE-1: phosphoprotein 65-immediate early protein 1. RBD: receptor binding domain. RNA: ribonucleic acid. ROP2A: rhoptry protein 2A. ROP18: rhoptry protein 18. RSV: respiratory syncytial virus. SAG1: surface antigen 1. SAG2A: surface antigen 2A. SAM: self-amplifying mRNA. SARS-CoV-2: severe acute respiratory syndrome coronavirus 2. SC: subcutaneous. *T. gondii*: *Toxoplasma gondii*.

Polymeric nanocarriers have also been extensively studied for their use as mRNA vaccines. For example, PEI modified with stearic acid nanoparticles (PEI-SA NP) have been used to deliver mRNA encoding the HIV group-specific antigen protein (gag). Subcutaneous administration in healthy mice led to greater antigen-specific immune responses compared to naked mRNA [161]. A similar nanocarrier, consisting of PEI-cyclodextrin NP loaded with mRNA encoding for HIV glycoprotein 120, was administered intranasally, resulting in an extended nasal residence time and HIV immune T cell response with increased cytokine production compared to unmodified PEI NP [162].

Polymers have also been used for the development of vaccines against SARS-CoV-2. For example, polyglucin-spermine complexed to mRNA encoding for the receptor binding domain (RBD) led to significant levels of specific neutralizing antibodies following intramuscular administration, surprising those produced by naked mRNA [163]. Dendrimers have been explored as delivery carriers for various SAM vaccines, including influenza virus, Ebola virus, and *Toxoplasma gondii* (*T. gondii*) [164]. A single dose of the dendrimer-encapsulated SAM encoding the hemagglutinin protein (HAp), a prime and boost administration of the SAM vaccine encoding the Ebola virus glycoprotein (EBOV gp), and a single administration of SAM vaccine for six antigens for *T gondii* protected the animals against a lethal dose of influenza virus, Ebola virus, and *T. gondii*, respectively.

Overall, despite the promising results achieved by several polymeric nanocarriers in preclinical animal studies, there are currently no polymeric nanocarriers in clinical trials for any mRNA vaccine candidates for any indication. We hypothesize that this could be due to multiple reasons. First, LNPs have demonstrated at the clinical level superior transfection efficiency in terms of mRNA delivery compared to any other nanocarrier. Secondly, there are some toxicity concerns related to the components of nanocarriers, such as DOTAP or PEI, for example. Lastly, previous failure of nanocarriers other than LNPs in advanced stages of clinical trials as protein vaccines has set a negative precedent. For example, ResVax^{TM}, developed by Novovax, was an RSV vaccine encapsulated onto a polysorbate 80 polymer in combination with an aluminum phosphate adjuvant. Initial clinical trials demonstrated overall safety and ability to induce strong RSV-neutralizing antibodies [165–167]. However, it failed in Phase III trials (NCT02608502), proving ineffective in preventing RSV disease. Examples like this could explain why the field is easily moving towards LNP vaccines, which already hold regulatory approval.

Significant efforts are underway to develop safer and more biodegradable polymers and lipids, and advances are being made to improve the transfection potency of mRNA using nanosystems, other than LNPs. These combined efforts may help address the various unmet challenges, allowing new nanotechnological approaches to emerge for their use as mRNA vaccines.

2. REFERENCES

[1] T. Wirth, N. Parker, S. Ylä-Herttuala, History of gene therapy, Gene. 525 (2013) 162–169. https://doi.org/10.1016/j.gene.2013.03.137.

[2] V. Sudhakar, R.M. Richardson, Gene Therapy for Neurodegenerative Diseases, Neurotherapeutics. 16 (2019) 166–175. https://doi.org/10.1007/s13311-018-00694-0.

[3] X.M. Anguela, K.A. High, Entering the modern era of gene therapy, Annu. Rev. Med. 70 (2019) 273–288. https://doi.org/10.1146/annurev-med-012017-043332.

[4] R. Tang, Z. Xu, Gene therapy: a double-edged sword with great powers, Mol. Cell. Biochem. 474 (2020) 73–81. https://doi.org/10.1007/s11010-020-03834-3.

[5] D. Wang, P.W.L. Tai, G. Gao, Adeno-associated virus vector as a platform for gene therapy delivery, Nat. Rev. Drug Discov. 18 (2019) 358–378. https://doi.org/10.1038/s41573-019-0012-9.

[6] J.T. Bulcha, Y. Wang, H. Ma, P.W.L. Tai, G. Gao, Viral vector platforms within the gene therapy landscape, Signal Transduct. Target. Ther. 6 (2021). https://doi.org/10.1038/s41392-021-00487-6.

[7] Food and Drug Administration, Approved Cellular and Gene Therapy Products, (2023). https://www.fda.gov/vaccines-blood-biologics/cellular-gene-therapy-products/approved-cellular-and-gene-therapy-products (accessed July 7, 2023).

[8] F. Mingozzi, K.A. High, Immune responses to AAV vectors: overcoming barriers to successful gene therapy, Blood. 122 (2013) 23–36. https://doi.org/10.1182/blood-2013-01-306647.

[9] F. Jiang, J.A. Doudna, CRISPR–Cas9 Structures and Mechanisms, Annu. Rev. Biophys. 46 (2017) 505–529. https://doi.org/10.1146/annurev-biophys-062215-010822.

[10] K.S. Makarova, Y.I. Wolf, J. Iranzo, S.A. Shmakov, O.S. Alkhnbashi, S.J.J. Brouns, E. Charpentier, D. Cheng, D.H. Haft, P. Horvath, S. Moineau, F.J.M. Mojica, D. Scott, S.A. Shah, V. Siksnys, M.P. Terns, Č. Venclovas, M.F. White, A.F. Yakunin, W. Yan, F. Zhang, R.A. Garrett, R. Backofen, J. van der Oost, R. Barrangou, E. V. Koonin, Evolutionary classification of CRISPR–Cas systems: a burst of class 2 and derived variants, Nat. Rev. Microbiol. 18 (2020) 67–83. https://doi.org/10.1038/s41579-019-0299-x.

[11] K. Kingwell, First CRISPR therapy seeks landmark approval, Nat. Rev. Drug Discov. 22 (2023) 339–341. https://doi.org/10.1038/d41573-023-00050-8.

[12] T.R. Damase, R. Sukhovershin, C. Boada, F. Taraballi, R.I. Pettigrew, J.P. Cooke, The Limitless Future of RNA Therapeutics, Front. Bioeng. Biotechnol. 9 (2021) 1–24. https://doi.org/10.3389/fbioe.2021.628137.

[13] Y.-K. Kim, RNA therapy: rich history, various applications and unlimited future prospects, Exp. Mol. Med. 54 (2022) 455–465. https://doi.org/10.1038/s12276-022-00757-5.

[14] A. Fire, S. Xu, M.K. Montgomery, S.A. Kostas, S.E. Driver, C.C. Mello, Potent and specific genetic interference by double-stranded RNA in Caenorhabditis elegans, Nature. 391 (1998) 806–811. https://doi.org/10.1038/35888.

[15] S.M. Elbashir, J. Harborth, W. Lendeckel, A. Yalcin, K. Weber, T. Tuschl, Duplexes of 21-nucleotide RNAs mediate RNA interference in cultured mammalian cells, Nature. 411 (2001) 494–498. https://doi.org/10.1038/35078107.

[16] N.J. Caplen, S. Parrish, F. Imani, A. Fire, R.A. Morgan, Specific inhibition of gene expression by small double-stranded RNAs in invertebrate and vertebrate systems, Proc. Natl. Acad. Sci. 98 (2001) 9742–9747. https://doi.org/10.1073/pnas.171251798.

[17] M.E. Kleinman, K. Yamada, A. Takeda, V. Chandrasekaran, M. Nozaki, J.Z. Baffi, R.J.C. Albuquerque, S. Yamasaki, M. Itaya, Y. Pan, B. Appukuttan, D. Gibbs, Z. Yang, K. Karikó, B.K. Ambati, T.A. Wilgus, L.A. DiPietro, E. Sakurai, K. Zhang, J.R. Smith, E.W. Taylor, J. Ambati, Sequence- and target-independent angiogenesis suppression by siRNA via TLR3, Nature. 452 (2008) 591–597. https://doi.org/10.1038/nature06765.

[18] J. DeVincenzo, R. Lambkin-Williams, T. Wilkinson, J. Cehelsky, S. Nochur, E. Walsh, R. Meyers, J. Gollob, A. Vaishnaw, A randomized, double-blind, placebo-controlled study of an RNAi-based therapy directed against respiratory syncytial virus, Proc. Natl. Acad. Sci. 107 (2010) 8800–8805. https://doi.org/10.1073/pnas.0912186107.

[19] M.E. Davis, J.E. Zuckerman, C.H.J. Choi, D. Seligson, A. Tolcher, C.A. Alabi, Y. Yen, J.D. Heidel, A. Ribas, Evidence of RNAi in humans from systemically administered siRNA via targeted nanoparticles, Nature. 464 (2010) 1067–1070. https://doi.org/10.1038/nature08956.

[20] J.E. Zuckerman, M.E. Davis, Clinical experiences with systemically administered siRNA-based therapeutics in cancer, Nat. Rev. Drug Discov. 14 (2015) 843–856. https://doi.org/10.1038/nrd4685.

[21] Y. Huang, Q. Cheng, J.-L. Ji, S. Zheng, L. Du, L. Meng, Y. Wu, D. Zhao, X. Wang, L. Lai, H. Cao, K. Xiao, S. Gao, Z. Liang, Pharmacokinetic Behaviors of Intravenously Administered siRNA in Glandular Tissues, Theranostics. 6 (2016) 1528–1541. https://doi.org/10.7150/thno.15246.

[22] R.L. Setten, J.J. Rossi, S. ping Han, The current state and future directions of RNAi-based therapeutics, Nat. Rev. Drug Discov. 18 (2019) 421–446. https://doi.org/10.1038/s41573-019-0017-4.

[23] D. Adams, A. Gonzalez-Duarte, W.D. O'Riordan, C.-C. Yang, M. Ueda, A. V. Kristen, I. Tournev, H.H. Schmidt, T. Coelho, J.L. Berk, K.-P. Lin, G. Vita, S. Attarian, V. Planté-Bordeneuve, M.M. Mezei, J.M. Campistol, J. Buades, T.H. Brannagan, B.J. Kim, J. Oh, Y. Parman, Y. Sekijima, P.N. Hawkins, S.D. Solomon, M. Polydefkis, P.J. Dyck, P.J. Gandhi, S. Goyal, J. Chen, A.L. Strahs, S. V. Nochur, M.T. Sweetser, P.P. Garg, A.K. Vaishnaw, J.A. Gollob, O.B. Suhr, Patisiran, an RNAi Therapeutic, for Hereditary Transthyretin Amyloidosis, N. Engl. J. Med. 379 (2018) 11–21. https://doi.org/10.1056/NEJMoa1716153.

[24] S.M. Hoy, Patisiran: First Global Approval, Drugs. 78 (2018) 1625–1631. https://doi.org/10.1007/s40265-018-0983-6.

[25] M. Ghildiyal, P.D. Zamore, Small silencing RNAs: an expanding universe, Nat. Rev. Genet. 10 (2009) 94–108. https://doi.org/10.1038/nrg2504.Small.

[26] J.M. Claycomb, Ancient Endo-siRNA Pathways Reveal New Tricks, Curr. Biol. 24 (2014) R703–R715. https://doi.org/10.1016/j.cub.2014.06.009.

[27] A. Reynolds, D. Leake, Q. Boese, S. Scaringe, W.S. Marshall, A. Khvorova, Rational siRNA design for RNA interference, Nat. Biotechnol. 22 (2004) 326–330. https://doi.org/10.1038/nbt936.

[28] N.M. Snead, X. Wu, A. Li, Q. Cui, K. Sakurai, J.C. Burnett, J.J. Rossi, Molecular basis for improved gene silencing by Dicer substrate interfering RNA compared with other siRNA variants, Nucleic Acids Res. 41 (2013) 6209–6221. https://doi.org/10.1093/nar/gkt200.

[29] J.K.W. Lam, M.Y.T. Chow, Y. Zhang, S.W.S. Leung, siRNA Versus miRNA as Therapeutics for Gene Silencing, Mol. Ther. - Nucleic Acids. 4 (2015) e252. https://doi.org/10.1038/mtna.2015.23.

[30] M. Luo, L.K.C. Lee, B. Peng, C.H.J. Choi, W.Y. Tong, N.H. Voelcker, Delivering the Promise of Gene Therapy with Nanomedicines in Treating Central Nervous System Diseases, Adv. Sci. 9 (2022) 1–41. https://doi.org/10.1002/advs.202201740.

[31] B. Hu, Y. Weng, X. Xia, X. Liang, Y. Huang, Clinical advances of siRNA therapeutics, J. Gene Med. 21 (2019). https://doi.org/10.1002/jgm.3097.

[32] B. Hu, L. Zhong, Y. Weng, L. Peng, Y. Huang, Y. Zhao, X.J. Liang, Therapeutic siRNA: state of the art, Signal Transduct. Target. Ther. 5 (2020). https://doi.org/10.1038/s41392-020-0207-x.

[33] M. Sano, M. Sierant, M. Miyagishi, M. Nakanishi, Y. Takagi, S. Sutou, Effect of asymmetric terminal structures of short RNA duplexes on the RNA interference activity and strand selection, Nucleic Acids Res. 36 (2008) 5812–5821. https://doi.org/10.1093/nar/gkn584.

[34] Z. Yuan, X. Wu, C. Liu, G. Xu, Z. Wu, Asymmetric siRNA: New Strategy to Improve Specificity and Reduce Off-Target Gene Expression, Hum. Gene Ther. 23 (2012) 521–532. https://doi.org/10.1089/hum.2011.145.

[35] A. Birmingham, E. Anderson, K. Sullivan, A. Reynolds, Q. Boese, D. Leake, J. Karpilow, A. Khvorova, A protocol for designing siRNAs with high functionality and specificity, Nat. Protoc. 2 (2007) 2068–2078. https://doi.org/10.1038/nprot.2007.278.

[36] H. Tafer, S.L. Ameres, G. Obernosterer, C.A. Gebeshuber, R. Schroeder, J. Martinez, I.L. Hofacker, The impact of target site accessibility on the design of effective siRNAs, Nat. Biotechnol. 26 (2008) 578–583. https://doi.org/10.1038/nbt1404.

[37] Y. Fedorov, E.M. Anderson, A. Birmingham, A. Reynolds, J. Karpilow, K. Robinson, D. Leake, W.S. Marshall, A. Khvorova, Off-target effects by siRNA can induce toxic phenotype, RNA. 12 (2006) 1188–1196. https://doi.org/10.1261/rna.28106.

[38] A.D. Judge, V. Sood, J.R. Shaw, D. Fang, K. McClintock, I. MacLachlan, Sequence-dependent stimulation of the mammalian innate immune response by synthetic siRNA, Nat. Biotechnol. 23 (2005) 457–462. https://doi.org/10.1038/nbt1081.

[39] H.Y. Lee, K. Zhou, A.M. Smith, C.L. Noland, J.A. Doudna, Differential roles of human Dicer-binding proteins TRBP and PACT in small RNA processing, Nucleic Acids Res. 41 (2013) 6568–6576. https://doi.org/10.1093/nar/gkt361.

[40] C.R. Allerson, N. Sioufi, R. Jarres, T.P. Prakash, N. Naik, A. Berdeja, L. Wanders, R.H. Griffey, E.E. Swayze, B. Bhat, Fully 2'-Modified Oligonucleotide Duplexes with Improved in Vitro Potency and Stability Compared to Unmodified Small Interfering RNA, J. Med. Chem. 48 (2005)

901–904. https://doi.org/10.1021/jm049167j.

[41] A. Khvorova, J.K. Watts, The chemical evolution of oligonucleotide therapies of clinical utility, Nat. Biotechnol. 35 (2017) 238–248. https://doi.org/10.1038/nbt.3765.

[42] C.F. Bennett, Therapeutic Antisense Oligonucleotides Are Coming of Age, Annu. Rev. Med. 70 (2019) 307–321. https://doi.org/10.1146/annurev-med-041217-010829.

[43] R.Z. Yu, T.-W. Kim, A. Hong, T.A. Watanabe, H.J. Gaus, R.S. Geary, Cross-Species Pharmacokinetic Comparison from Mouse to Man of a Second-Generation Antisense Oligonucleotide, ISIS 301012, Targeting Human Apolipoprotein B-100, Drug Metab. Dispos. 35 (2007) 460–468. https://doi.org/10.1124/dmd.106.012401.

[44] W. Marshall, M. Caruthers, Phosphorodithioate DNA as a potential therapeutic drug, Science (80-.). 259 (1993) 1564–1570. https://doi.org/10.1126/science.7681216.

[45] M.T. Migawa, W. Shen, W.B. Wan, G. Vasquez, M.E. Oestergaard, A. Low, C.L. De Hoyos, R. Gupta, S. Murray, M. Tanowitz, M. Bell, J.G. Nichols, H. Gaus, X. Liang, E.E. Swayze, S.T. Crooke, P.P. Seth, Site-specific replacement of phosphorothioate with alkyl phosphonate linkages enhances the therapeutic profile of gapmer ASOs by modulating interactions with cellular proteins, Nucleic Acids Res. 47 (2019) 5465–5479. https://doi.org/10.1093/nar/gkz247.

[46] R. Parmar, J.L.S. Willoughby, J. Liu, D.J. Foster, B. Brigham, C.S. Theile, K. Charisse, A. Akinc, E. Guidry, Y. Pei, W. Strapps, M. Cancilla, M.G. Stanton, K.G. Rajeev, L. Sepp-Lorenzino, M. Manoharan, R. Meyers, M.A. Maier, V. Jadhav, 5′-(E)-Vinylphosphonate: A Stable Phosphate Mimic Can Improve the RNAi Activity of siRNA-GalNAc Conjugates, ChemBioChem. 17 (2016) 985–989. https://doi.org/10.1002/cbic.201600130.

[47] E. Elkayam, R. Parmar, C.R. Brown, J.L. Willoughby, C.S. Theile, M. Manoharan, L. Joshua-Tor, siRNA carrying an (E)-vinylphosphonate moiety at the 5' end of the guide strand augments gene silencing by enhanced binding to human Argonaute-2, Nucleic Acids Res. 45 (2017) 3528–3536. https://doi.org/10.1093/nar/gkw1171.

[48] R.A. Haraszti, L. Roux, A.H. Coles, A.A. Turanov, J.F. Alterman, D. Echeverria, B.M.D.C. Godinho, N. Aronin, A. Khvorova, 5′-Vinylphosphonate improves tissue accumulation and efficacy of conjugated siRNAs in vivo, Nucleic Acids Res. 45 (2017) 7581–7592. https://doi.org/10.1093/nar/gkx507.

[49] B. Ndeboko, N. Ramamurthy, G.J. Lemamy, C. Jamard, P.E. Nielsen, L. Cova, Role of Cell-Penetrating Peptides in Intracellular Delivery of Peptide Nucleic Acids Targeting Hepadnaviral Replication, Mol. Ther. - Nucleic Acids. 9 (2017) 162–169. https://doi.org/10.1016/j.omtn.2017.09.003.

[50] H. Inoue, Y. Hayase, A. Imura, S. Iwai, K. Miura, E. Ohtsuka, Synthesis and hybridization studies on two complementary nona(2'-O-methyl)ribonucleotides, Nucleic Acids Res. 15 (1987) 6131–6148. https://doi.org/10.1093/nar/15.15.6131.

[51] B.P. Monia, E.A. Lesnik, C. Gonzalez, W.F. Lima, D. McGee, C.J. Guinosso, A.M. Kawasaki, P.D. Cook, S.M. Freier, Evaluation of 2'-modified oligonucleotides containing 2'-deoxy gaps as antisense inhibitors of gene expression, J. Biol. Chem. 268 (1993) 14514–14522. https://doi.org/10.1016/S0021-9258(19)85268-7.

[52] R. V. Fucini, H.J. Haringsma, P. Deng, W.M. Flanagan, A.T. Willingham, Adenosine

Modification May Be Preferred for Reducing siRNA Immune Stimulation, Nucleic Acid Ther. 22 (2012) 205–210. https://doi.org/10.1089/nat.2011.0334.

[53] D.M. Kenski, G. Butora, A.T. Willingham, A.J. Cooper, W. Fu, N. Qi, F. Soriano, I.W. Davies, W.M. Flanagan, siRNA-optimized Modifications for Enhanced In Vivo Activity, Mol. Ther. - Nucleic Acids. 1 (2012) e5. https://doi.org/10.1038/mtna.2011.4.

[54] K. Karikó, H. Muramatsu, F.A. Welsh, J. Ludwig, H. Kato, S. Akira, D. Weissman, Incorporation of Pseudouridine Into mRNA Yields Superior Nonimmunogenic Vector With Increased Translational Capacity and Biological Stability, Mol. Ther. 16 (2008) 1833–1840. https://doi.org/10.1038/mt.2008.200.

[55] B.R. Anderson, H. Muramatsu, B.K. Jha, R.H. Silverman, D. Weissman, K. Kariko, Nucleoside modifications in RNA limit activation of 2'-5'-oligoadenylate synthetase and increase resistance to cleavage by RNase L, Nucleic Acids Res. 39 (2011) 9329–9338. https://doi.org/10.1093/nar/gkr586.

[56] K.J. Phelps, J.M. Ibarra-Soza, K. Tran, A.J. Fisher, P.A. Beal, Click Modification of RNA at Adenosine: Structure and Reactivity of 7-Ethynyl- and 7-Triazolyl-8-aza-7-deazaadenosine in RNA, ACS Chem. Biol. 9 (2014) 1780–1787. https://doi.org/10.1021/cb500270x.

[57] A.S. Wahba, F. Azizi, G.F. Deleavey, C. Brown, F. Robert, M. Carrier, A. Kalota, A.M. Gewirtz, J. Pelletier, R.H.E. Hudson, M.J. Damha, Phenylpyrrolocytosine as an Unobtrusive Base Modification for Monitoring Activity and Cellular Trafficking of siRNA, ACS Chem. Biol. 6 (2011) 912–919. https://doi.org/10.1021/cb200070k.

[58] J. Zhang, J. Zheng, C. Lu, Q. Du, Z. Liang, Z. Xi, Modification of the siRNA Passenger Strand by 5-Nitroindole Dramatically Reduces its Off-Target Effects, ChemBioChem. 13 (2012) 1940–1945. https://doi.org/10.1002/cbic.201200349.

[59] S. -y. Wu, T. -m. Chen, W.H. Gmeiner, E. Chu, J.C. Schmitz, Development of modified siRNA molecules incorporating 5-fluoro-2'-deoxyuridine residues to enhance cytotoxicity, Nucleic Acids Res. 41 (2013) 4650–4659. https://doi.org/10.1093/nar/gkt120.

[60] R.C. Friedman, K.K.-H. Farh, C.B. Burge, D.P. Bartel, Most mammalian mRNAs are conserved targets of microRNAs, Genome Res. 19 (2009) 92–105. https://doi.org/10.1101/gr.082701.108.

[61] J. Godlewski, J. Lenart, E. Salinska, MicroRNA in Brain pathology: Neurodegeneration the Other Side of the Brain Cancer, Non-Coding RNA. 5 (2019) 20. https://doi.org/10.3390/ncrna5010020.

[62] Y.K. Adlakha, N. Saini, Brain microRNAs and insights into biological functions and therapeutic potential of brain enriched miRNA-128, Mol. Cancer. 13 (2014) 33. https://doi.org/10.1186/1476-4598-13-33.

[63] J. Wang, J. Chen, S. Sen, MicroRNA as Biomarkers and Diagnostics, J. Cell. Physiol. 231 (2016) 25–30. https://doi.org/10.1002/jcp.25056.

[64] M. Guerau-de-Arellano, K.M. Smith, J. Godlewski, Y. Liu, R. Winger, S.E. Lawler, C.C. Whitacre, M.K. Racke, A.E. Lovett-Racke, Micro-RNA dysregulation in multiple sclerosis favours pro-inflammatory T-cell-mediated autoimmunity, Brain. 134 (2011) 3578–3589. https://doi.org/10.1093/brain/awr262.

[65] J. Peng, A. Omran, M.U. Ashhab, H. Kong, N. Gan, F. He, F. Yin, Expression Patterns of miR-124, miR-134, miR-132, and miR-21 in an Immature Rat Model and Children with Mesial Temporal Lobe Epilepsy, J. Mol. Neurosci. 50 (2013) 291–297. https://doi.org/10.1007/s12031-013-9953-3.

[66] R. Rupaimoole, F.J. Slack, MicroRNA therapeutics: Towards a new era for the management of cancer and other diseases, Nat. Rev. Drug Discov. 16 (2017) 203–221. https://doi.org/10.1038/nrd.2016.246.

[67] C. Diener, A. Keller, E. Meese, Emerging concepts of miRNA therapeutics: from cells to clinic, Trends Genet. 38 (2022) 613–626. https://doi.org/10.1016/j.tig.2022.02.006.

[68] X. Tang, S. Zhang, R. Fu, L. Zhang, K. Huang, H. Peng, L. Dai, Q. Chen, Therapeutic Prospects of mRNA-Based Gene Therapy for Glioblastoma, Front. Oncol. 9 (2019). https://doi.org/10.3389/fonc.2019.01208.

[69] J.A. Wolff, R.W. Malone, P. Williams, W. Chong, G. Acsadi, A. Jani, P.L. Felgner, Direct Gene Transfer into Mouse Muscle in Vivo, Science (80-.). 247 (1990) 1465–1468. https://doi.org/10.1126/science.1690918.

[70] N. Pardi, M.J. Hogan, F.W. Porter, D. Weissman, mRNA vaccines-a new era in vaccinology, Nat. Rev. Drug Discov. 17 (2018) 261–279. https://doi.org/10.1038/nrd.2017.243.

[71] N. Chaudhary, D. Weissman, K.A. Whitehead, mRNA vaccines for infectious diseases: principles, delivery and clinical translation, Nat. Rev. Drug Discov. 20 (2021) 817–838. https://doi.org/10.1038/s41573-021-00283-5.

[72] A. Wadhwa, A. Aljabbari, A. Lokras, C. Foged, A. Thakur, Opportunities and Challenges in the Delivery of mRNA-Based Vaccines, Pharmaceutics. 12 (2020) 102. https://doi.org/10.3390/pharmaceutics12020102.

[73] S. Linares-Fernández, C. Lacroix, J.-Y. Exposito, B. Verrier, Tailoring mRNA Vaccine to Balance Innate/Adaptive Immune Response, Trends Mol. Med. 26 (2020) 311–323. https://doi.org/10.1016/j.molmed.2019.10.002.

[74] S. Holtkamp, S. Kreiter, A. Selmi, P. Simon, M. Koslowski, C. Huber, O. Türeci, U. Sahin, Modification of antigen-encoding RNA increases stability, translational efficacy, and T-cell stimulatory capacity of dendritic cells, Blood. 108 (2006) 4009–4017. https://doi.org/10.1182/blood-2006-04-015024.

[75] B.D. Berkovits, C. Mayr, Alternative 3′ UTRs act as scaffolds to regulate membrane protein localization, Nature. 522 (2015) 363–367. https://doi.org/10.1038/nature14321.

[76] D.R. Gallie, The cap and poly(A) tail function synergistically to regulate mRNA translational efficiency., Genes Dev. 5 (1991) 2108–2116. https://doi.org/10.1101/gad.5.11.2108.

[77] P.J. Sample, B. Wang, D.W. Reid, V. Presnyak, I.J. McFadyen, D.R. Morris, G. Seelig, Human 5′ UTR design and variant effect prediction from a massively parallel translation assay, Nat. Biotechnol. 37 (2019) 803–809. https://doi.org/10.1038/s41587-019-0164-5.

[78] C.-Y.A. Chen, A.-B. Shyu, AU-rich elements: characterization and importance in mRNA degradation, Trends Biochem. Sci. 20 (1995) 465–470. https://doi.org/10.1016/S0968-0004(00)89102-1.

[79] K. Leppek, R. Das, M. Barna, Functional 5′ UTR mRNA structures in eukaryotic translation regulation and how to find them, Nat. Rev. Mol. Cell Biol. 19 (2018) 158–174. https://doi.org/10.1038/nrm.2017.103.

[80] K.A. Hajj, K.A. Whitehead, Tools for translation: non-viral materials for therapeutic mRNA delivery, Nat. Rev. Mater. 2 (2017) 17056. https://doi.org/10.1038/natrevmats.2017.56.

[81] S. Vaidyanathan, K.T. Azizian, A.K.M.A. Haque, J.M. Henderson, A. Hendel, S. Shore, J.S. Antony, R.I. Hogrefe, M.S.D. Kormann, M.H. Porteus, A.P. McCaffrey, Uridine Depletion and Chemical Modification Increase Cas9 mRNA Activity and Reduce Immunogenicity without HPLC Purification, Mol. Ther. - Nucleic Acids. 12 (2018) 530–542. https://doi.org/10.1016/j.omtn.2018.06.010.

[82] P.S. Spencer, E. Siller, J.F. Anderson, J.M. Barral, Silent Substitutions Predictably Alter Translation Elongation Rates and Protein Folding Efficiencies, J. Mol. Biol. 422 (2012) 328–335. https://doi.org/10.1016/j.jmb.2012.06.010.

[83] G. Kudla, L. Lipinski, F. Caffin, A. Helwak, M. Zylicz, High Guanine and Cytosine Content Increases mRNA Levels in Mammalian Cells, PLoS Biol. 4 (2006) e180. https://doi.org/10.1371/journal.pbio.0040180.

[84] A. Thess, S. Grund, B.L. Mui, M.J. Hope, P. Baumhof, M. Fotin-Mleczek, T. Schlake, Sequence-engineered mRNA Without Chemical Nucleoside Modifications Enables an Effective Protein Therapy in Large Animals, Mol. Ther. 23 (2015) 1456–1464. https://doi.org/10.1038/mt.2015.103.

[85] M. Egli, M. Manoharan, Chemistry, structure and function of approved oligonucleotide therapeutics, Nucleic Acids Res. 51 (2023) 2529–2573. https://doi.org/10.1093/nar/gkad067.

[86] T.C. Roberts, R. Langer, M.J.A. Wood, Advances in oligonucleotide drug delivery, Nat. Rev. Drug Discov. 19 (2020) 673–694. https://doi.org/10.1038/s41573-020-0075-7.

[87] S.M. Hammond, E. Bernstein, D. Beach, G.J. Hannon, An RNA-directed nuclease mediates post-transcriptional gene silencing in Drosophila cells, Nature. 404 (2000) 293–296. https://doi.org/10.1038/35005107.

[88] J.A. Kulkarni, D. Witzigmann, S.B. Thomson, S. Chen, B.R. Leavitt, P.R. Cullis, R. van der Meel, The current landscape of nucleic acid therapeutics, Nat. Nanotechnol. 16 (2021) 630–643. https://doi.org/10.1038/s41565-021-00898-0.

[89] M.D. de Smet, C. Meenken, G.J. van den Horn, Fomivirsen – a phosphorothioate oligonucleotide for the treatment of CMV retinitis, Ocul. Immunol. Inflamm. 7 (1999) 189–198. https://doi.org/10.1076/ocii.7.3.189.4007.

[90] R.S. Geary, S.P. Henry, L.R. Grillone, Fomivirsen, Clin. Pharmacokinet. 41 (2002) 255–260. https://doi.org/10.2165/00003088-200241040-00002.

[91] E. Merki, M.J. Graham, A.E. Mullick, E.R. Miller, R.M. Crooke, R.E. Pitas, J.L. Witztum, S. Tsimikas, Antisense Oligonucleotide Directed to Human Apolipoprotein B-100 Reduces Lipoprotein(a) Levels and Oxidized Phospholipids on Human Apolipoprotein B-100 Particles in Lipoprotein(a) Transgenic Mice, Circulation. 118 (2008) 743–753. https://doi.org/10.1161/CIRCULATIONAHA.108.786822.

[92] L. Gales, Tegsedi (Inotersen): An Antisense Oligonucleotide Approved for the Treatment of Adult Patients with Hereditary Transthyretin Amyloidosis, Pharmaceuticals. 12 (2019) 78. https://doi.org/10.3390/ph12020078.

[93] J. Paik, S. Duggan, Volanesorsen: First Global Approval, Drugs. 79 (2019) 1349–1354. https://doi.org/10.1007/s40265-019-01168-z.

[94] K.-H. Altmann, D. Fabbro, N.M. Dean, T. Geiger, B.P. Monia, M. Müllert, P. Nicklin, Second-generation antisense oligonucleotides: structure—activity relationships and the design of improved signal-transduction inhibitors, Biochem. Soc. Trans. 24 (1996) 630–637. https://doi.org/10.1042/bst0240630.

[95] M. Manoharan, 2′-Carbohydrate modifications in antisense oligonucleotide therapy: importance of conformation, configuration and conjugation, Biochim. Biophys. Acta - Gene Struct. Expr. 1489 (1999) 117–130. https://doi.org/10.1016/S0167-4781(99)00138-4.

[96] J. Bauman, N. Jearawiriyapaisarn, R. Kole, Therapeutic Potential of Splice-Switching Oligonucleotides, Oligonucleotides. 19 (2009) 1–13. https://doi.org/10.1089/oli.2008.0161.

[97] R.N. Singh, N.N. Singh, Mechanism of Splicing Regulation of Spinal Muscular Atrophy Genes, in: 2018: pp. 31–61. https://doi.org/10.1007/978-3-319-89689-2_2.

[98] R.S. Finkel, E. Mercuri, B.T. Darras, A.M. Connolly, N.L. Kuntz, J. Kirschner, C.A. Chiriboga, K. Saito, L. Servais, E. Tizzano, H. Topaloglu, M. Tulinius, J. Montes, A.M. Glanzman, K. Bishop, Z.J. Zhong, S. Gheuens, C.F. Bennett, E. Schneider, W. Farwell, D.C. De Vivo, Nusinersen versus Sham Control in Infantile-Onset Spinal Muscular Atrophy, N. Engl. J. Med. 377 (2017) 1723–1732. https://doi.org/10.1056/NEJMoa1702752.

[99] C.A. Chiriboga, Nusinersen for the treatment of spinal muscular atrophy, Expert Rev. Neurother. 17 (2017) 955–962. https://doi.org/10.1080/14737175.2017.1364159.

[100] J. Summerton, D. Weller, Morpholino Antisense Oligomers: Design, Preparation, and Properties, Antisense Nucleic Acid Drug Dev. 7 (1997) 187–195. https://doi.org/10.1089/oli.1.1997.7.187.

[101] Y. Nan, Y.-J. Zhang, Antisense Phosphorodiamidate Morpholino Oligomers as Novel Antiviral Compounds, Front. Microbiol. 9 (2018). https://doi.org/10.3389/fmicb.2018.00750.

[102] K.R. Lim, R. Maruyama, T. Yokota, Eteplirsen in the treatment of Duchenne muscular dystrophy, Drug Des. Devel. Ther. Volume11 (2017) 533–545. https://doi.org/10.2147/DDDT.S97635.

[103] Y.-A. Heo, Golodirsen: First Approval, Drugs. 80 (2020) 329–333. https://doi.org/10.1007/s40265-020-01267-2.

[104] S. Dhillon, Viltolarsen: First Approval, Drugs. 80 (2020) 1027–1031. https://doi.org/10.1007/s40265-020-01339-3.

[105] M. Shirley, Casimersen: First Approval, Drugs. 81 (2021) 875–879. https://doi.org/10.1007/s40265-021-01512-2.

[106] E.W.M. Ng, D.T. Shima, P. Calias, E.T. Cunningham, D.R. Guyer, A.P. Adamis, Pegaptanib, a targeted anti-VEGF aptamer for ocular vascular disease, Nat. Rev. Drug Discov. 5 (2006) 123–132. https://doi.org/10.1038/nrd1955.

[107] Y. Yan, X.-Y. Liu, A. Lu, X.-Y. Wang, L.-X. Jiang, J.-C. Wang, Non-viral vectors for RNA delivery, J. Control. Release. 342 (2022) 241–279. https://doi.org/10.1016/j.jconrel.2022.01.008.

[108] A. Cox, S.A. Lim, E.J. Chung, Strategies to deliver RNA by nanoparticles for therapeutic potential, Mol. Aspects Med. 83 (2022) 100991. https://doi.org/10.1016/j.mam.2021.100991.

[109] A. Akinc, M.A. Maier, M. Manoharan, K. Fitzgerald, M. Jayaraman, S. Barros, S. Ansell, X. Du, M.J. Hope, T.D. Madden, B.L. Mui, S.C. Semple, Y.K. Tam, M. Ciufolini, D. Witzigmann, J.A. Kulkarni, R. van der Meel, P.R. Cullis, The Onpattro story and the clinical translation of nanomedicines containing nucleic acid-based drugs, Nat. Nanotechnol. 14 (2019) 1084–1087. https://doi.org/10.1038/s41565-019-0591-y.

[110] X. Hou, T. Zaks, R. Langer, Y. Dong, Lipid nanoparticles for mRNA delivery, Nat. Rev. Mater. 6 (2021) 1078–1094. https://doi.org/10.1038/s41578-021-00358-0.

[111] C. Hald Albertsen, J.A. Kulkarni, D. Witzigmann, M. Lind, K. Petersson, J.B. Simonsen, The role of lipid components in lipid nanoparticles for vaccines and gene therapy, Adv. Drug Deliv. Rev. 188 (2022) 114416. https://doi.org/10.1016/j.addr.2022.114416.

[112] X. Han, H. Zhang, K. Butowska, K.L. Swingle, M.G. Alameh, D. Weissman, M.J. Mitchell, An ionizable lipid toolbox for RNA delivery, Nat. Commun. 12 (2021) 8–13. https://doi.org/10.1038/s41467-021-27493-0.

[113] P. Harvie, F.M.P. Wong, M.B. Bally, Use of Poly(ethylene glycol)–Lipid Conjugates to Regulate the Surface Attributes and Transfection Activity of Lipid–DNA Particles, J. Pharm. Sci. 89 (2000) 652–663. https://doi.org/10.1002/(SICI)1520-6017(200005)89:5<652::AID-JPS11>3.0.CO;2-H.

[114] J.A. Kulkarni, D. Witzigmann, J. Leung, R. van der Meel, J. Zaifman, M.M. Darjuan, H.M. Grisch-Chan, B. Thöny, Y.Y.C. Tam, P.R. Cullis, Fusion-dependent formation of lipid nanoparticles containing macromolecular payloads, Nanoscale. 11 (2019) 9023–9031. https://doi.org/10.1039/C9NR02004G.

[115] B.L. Mui, Y.K. Tam, M. Jayaraman, S.M. Ansell, X. Du, Y.Y.C. Tam, P.J. Lin, S. Chen, J.K. Narayanannair, K.G. Rajeev, M. Manoharan, A. Akinc, M.A. Maier, P. Cullis, T.D. Madden, M.J. Hope, Influence of Polyethylene Glycol Lipid Desorption Rates on Pharmacokinetics and Pharmacodynamics of siRNA Lipid Nanoparticles, Mol. Ther. - Nucleic Acids. 2 (2013) e139. https://doi.org/10.1038/mtna.2013.66.

[116] C.A. Sanhueza, M.M. Baksh, B. Thuma, M.D. Roy, S. Dutta, C. Préville, B.A. Chrunyk, K. Beaumont, R. Dullea, M. Ammirati, S. Liu, D. Gebhard, J.E. Finley, C.T. Salatto, A. King-Ahmad, I. Stock, K. Atkinson, B. Reidich, W. Lin, R. Kumar, M. Tu, E. Menhaji-Klotz, D.A. Price, S. Liras, M.G. Finn, V. Mascitti, Efficient Liver Targeting by Polyvalent Display of a Compact Ligand for the Asialoglycoprotein Receptor, J. Am. Chem. Soc. 139 (2017) 3528–3536. https://doi.org/10.1021/jacs.6b12964.

[117] A.D. Springer, S.F. Dowdy, GalNAc-siRNA Conjugates: Leading the Way for Delivery of RNAi Therapeutics, Nucleic Acid Ther. 28 (2018) 109–118. https://doi.org/10.1089/nat.2018.0736.

[118] A.A. D'Souza, P. V. Devarajan, Asialoglycoprotein receptor mediated hepatocyte targeting — Strategies and applications, J. Control. Release. 203 (2015) 126–139. https://doi.org/10.1016/j.jconrel.2015.02.022.

[119] A. Wittrup, A. Ai, X. Liu, P. Hamar, R. Trifonova, K. Charisse, M. Manoharan, T. Kirchhausen, J. Lieberman, Visualizing lipid-formulated siRNA release from endosomes and target gene knockdown, Nat. Biotechnol. 33 (2015) 870–876. https://doi.org/10.1038/nbt.3298.

[120] S.F. Dowdy, Overcoming cellular barriers for RNA therapeutics, Nat. Biotechnol. 35 (2017) 222–229. https://doi.org/10.1038/nbt.3802.

[121] Q. Cheng, T. Wei, L. Farbiak, L.T. Johnson, S.A. Dilliard, D.J. Siegwart, Selective organ targeting (SORT) nanoparticles for tissue-specific mRNA delivery and CRISPR–Cas gene editing, Nat. Nanotechnol. 15 (2020) 313–320. https://doi.org/10.1038/s41565-020-0669-6.

[122] X. Wang, S. Liu, Y. Sun, X. Yu, S.M. Lee, Q. Cheng, T. Wei, J. Gong, J. Robinson, D. Zhang, X. Lian, P. Basak, D.J. Siegwart, Preparation of selective organ-targeting (SORT) lipid nanoparticles (LNPs) using multiple technical methods for tissue-specific mRNA delivery, Nat. Protoc. 18 (2023) 265–291. https://doi.org/10.1038/s41596-022-00755-x.

[123] R. Thiruppathi, S. Mishra, M. Ganapathy, P. Padmanabhan, Nanoparticle Functionalization and Its Potentials for Molecular Imaging, Adv. Sicence. 4 (2017). https://doi.org/10.1002/advs.201600279.

[124] D.J. Begley, Delivery of therapeutic agents to the central nervous system: The problems and the possibilities, Pharmacol. Ther. 104 (2004) 29–45. https://doi.org/10.1016/j.pharmthera.2004.08.001.

[125] B. Obermeier, R. Daneman, R.M. Ransohoff, Development, maintenance and disruption of blood-brain barrier, Nat. Med. 19 (2013) 1584–1596. https://doi.org/10.1038/nm.3407.Development.

[126] B. Engelhardt, L. Sorokin, The blood-brain and the blood-cerebrospinal fluid barriers: function and dysfunction, Semin. Immunopathol. 31 (2009) 497–511. https://doi.org/10.1007/s00281-009-0177-0.

[127] S.E. Storck, M. Kurtyka, C.U. Pietrzik, Brain endothelial LRP1 maintains blood–brain barrier integrity, Fluids Barriers CNS. 18 (2021) 27. https://doi.org/10.1186/s12987-021-00260-5.

[128] L. Maletínská, E.A. Blakely, K.A. Bjornstad, D.F. Deen, L.J. Knoff, T.M. Forte, Human glioblastoma cell lines: levels of low-density lipoprotein receptor and low-density lipoprotein receptor-related protein., Cancer Res. 60 (2000) 2300–3. http://www.ncbi.nlm.nih.gov/pubmed/10786698.

[129] Z. Yuan, L. Zhao, Y. Zhang, S. Li, B. Pan, L. Hua, Z. Wang, C. Ye, J. Lu, R. Yu, H. Liu, Inhibition of glioma growth by a GOLPH3 siRNA-loaded cationic liposomes, J. Neurooncol. 140 (2018) 249–260. https://doi.org/10.1007/s11060-018-2966-6.

[130] C. Ye, B. Pan, H. Xu, Z. Zhao, J. Shen, J. Lu, R. Yu, H. Liu, Co-delivery of GOLPH3 siRNA and gefitinib by cationic lipid-PLGA nanoparticles improves EGFR-targeted therapy for glioma, J. Mol. Med. 97 (2019) 1575–1588. https://doi.org/10.1007/s00109-019-01843-4.

[131] L. Wang, Y. Hao, H. Li, Y. Zhao, D. Meng, D. Li, J. Shi, H. Zhang, Z. Zhang, Y. Zhang, Co-delivery of doxorubicin and siRNA for glioma therapy by a brain targeting system: Angiopep-2-modified poly(lactic-co-glycolic acid) nanoparticles, J. Drug Target. 23 (2015) 832–846. https://doi.org/10.3109/1061186X.2015.1025077.

[132] M. Zheng, Y. Liu, Y. Wang, D. Zhang, Y. Zou, W. Ruan, J. Yin, W. Tao, J.B. Park, B. Shi, ROS-Responsive Polymeric siRNA Nanomedicine Stabilized by Triple Interactions for the Robust Glioblastoma Combinational RNAi Therapy, Adv. Mater. 31 (2019) 1903277. https://doi.org/10.1002/adma.201903277.

[133] Y. Liu, M. Zheng, M. Jiao, C. Yan, S. Xu, Q. Du, M. Morsch, J. Yin, B. Shi, Polymeric nanoparticle mediated inhibition of miR-21 with enhanced miR-124 expression for combinatorial glioblastoma therapy, Biomaterials. 276 (2021) 121036. https://doi.org/10.1016/j.biomaterials.2021.121036.

[134] Z.-Z. Yang, J.-Q. Li, Z.-Z. Wang, D.-W. Dong, X.-R. Qi, Tumor-targeting dual peptides-modified cationic liposomes for delivery of siRNA and docetaxel to gliomas, Biomaterials. 35 (2014) 5226–5239. https://doi.org/10.1016/j.biomaterials.2014.03.017.

[135] Z. Jin, L. Piao, G. Sun, C. Lv, Y. Jing, R. Jin, Dual functional nanoparticles efficiently across the blood–brain barrier to combat glioblastoma via simultaneously inhibit the PI3K pathway and NKG2A axis, J. Drug Target. 29 (2021) 323–335. https://doi.org/10.1080/1061186X.2020.1841214.

[136] M. Conceição, L. Mendonça, C. Nóbrega, C. Gomes, P. Costa, H. Hirai, J.N. Moreira, M.C. Lima, N. Manjunath, L. Pereira de Almeida, Intravenous administration of brain-targeted stable nucleic acid lipid particles alleviates Machado-Joseph disease neurological phenotype, Biomaterials. 82 (2016) 124–137. https://doi.org/10.1016/j.biomaterials.2015.12.021.

[137] Y. Zhou, F. Zhu, Y. Liu, M. Zheng, Y. Wang, D. Zhang, Y. Anraku, Y. Zou, J. Li, H. Wu, X. Pang, W. Tao, O. Shimoni, A.I. Bush, X. Xue, B. Shi, Blood-brain barrier–penetrating siRNA nanomedicine for Alzheimer's disease therapy, Sci. Adv. 6 (2020). https://doi.org/10.1126/sciadv.abc7031.

[138] S. Werth, B. Urban-Klein, L. Dai, S. Höbel, M. Grzelinski, U. Bakowsky, F. Czubayko, A. Aigner, A low molecular weight fraction of polyethylenimine (PEI) displays increased transfection efficiency of DNA and siRNA in fresh or lyophilized complexes, J. Control. Release. 112 (2006) 257–270. https://doi.org/10.1016/j.jconrel.2006.02.009.

[139] C. Helmschrodt, S. Höbel, S. Schöniger, A. Bauer, J. Bonicelli, M. Gringmuth, S.A. Fietz, A. Aigner, A. Richter, F. Richter, Polyethylenimine Nanoparticle-Mediated siRNA Delivery to Reduce α-Synuclein Expression in a Model of Parkinson's Disease, Mol. Ther. - Nucleic Acids. 9 (2017) 57–68. https://doi.org/10.1016/j.omtn.2017.08.013.

[140] R.L. Rungta, H.B. Choi, P.J. Lin, R.W. Ko, D. Ashby, J. Nair, M. Manoharan, P.R. Cullis, B.A. MacVicar, Lipid Nanoparticle Delivery of siRNA to Silence Neuronal Gene Expression in the Brain, Mol. Ther. Acids. 2 (2013) e136. https://doi.org/10.1038/mtna.2013.65.

[141] M. Van Woensel, T. Mathivet, N. Wauthoz, R. Rosière, A.D. Garg, P. Agostinis, V. Mathieu, R. Kiss, F. Lefranc, L. Boon, J. Belmans, S.W. Van Gool, H. Gerhardt, K. Amighi, S. De Vleeschouwer, Sensitization of glioblastoma tumor micro-environment to chemo- and immunotherapy by Galectin-1 intranasal knock-down strategy, Sci. Rep. 7 (2017) 1217. https://doi.org/10.1038/s41598-017-01279-1.

[142] M. Van Woensel, N. Wauthoz, R. Rosière, V. Mathieu, R. Kiss, F. Lefranc, B. Steelant, E. Dilissen, S.W. Van Gool, T. Mathivet, H. Gerhardt, K. Amighi, S. De Vleeschouwer, Development of siRNA-loaded chitosan nanoparticles targeting Galectin-1 for the treatment of glioblastoma multiforme via intranasal administration, J. Control. Release. 227 (2016) 71–81.

https://doi.org/10.1016/j.jconrel.2016.02.032.

[143] T. Kanazawa, K. Morisaki, S. Suzuki, Y. Takashima, Prolongation of life in rats with malignant glioma by intranasal siRNA/drug codelivery to the brain with cell-penetrating peptide-modified micelles, Mol. Pharm. 11 (2014) 1471–1478. https://doi.org/10.1021/mp400644e.

[144] T. Kanazawa, T. Kurano, H. Ibaraki, Y. Takashima, T. Suzuki, Y. Seta, Therapeutic effects in a transient middle cerebral artery occlusion rat model by nose-to-brain delivery of anti-tnf-alpha sirna with cell-penetrating peptide-modified polymer micelles. (pharmaceutics, (2019), 11(9), 478, 10.3390/pharmaceutics11090478), Pharmaceutics. 11 (2019) 478. https://doi.org/10.3390/pharmaceutics11120689.

[145] R. Hao, B. Sun, L. Yang, C. Ma, S. Li, RVG29-modified microRNA-loaded nanoparticles improve ischemic brain injury by nasal delivery, Drug Deliv. 27 (2020) 772–781. https://doi.org/10.1080/10717544.2020.1760960.

[146] Y. Su, B. Sun, X. Gao, X. Dong, L. Fu, Y. Zhang, Z. Li, Y. Wang, H. Jiang, B. Han, Intranasal Delivery of Targeted Nanoparticles Loaded With miR-132 to Brain for the Treatment of Neurodegenerative Diseases, Front. Pharmacol. 11 (2020). https://doi.org/10.3389/fphar.2020.01165.

[147] E. Samaridou, H. Walgrave, E. Salta, D.M. Álvarez, V. Castro-López, M. Loza, M.J. Alonso, Nose-to-brain delivery of enveloped RNA - cell permeating peptide nanocomplexes for the treatment of neurodegenerative diseases, Biomaterials. 230 (2020) 119657. https://doi.org/10.1016/j.biomaterials.2019.119657.

[148] N.F. Eng, N. Bhardwaj, R. Mulligan, F. Diaz-Mitoma, The potential of 1018 ISS adjuvant in hepatitis B vaccines, Hum. Vaccin. Immunother. 9 (2013) 1661–1672. https://doi.org/10.4161/hv.24715.

[149] J.D. Campbell, Development of the CpG Adjuvant 1018: A Case Study, Methods Mol. Biol. 1494 (2017) 15–27. https://doi.org/10.1007/978-1-4939-6445-1_2.

[150] M. Li, H. Wang, L. Tian, Z. Pang, Q. Yang, T. Huang, J. Fan, L. Song, Y. Tong, H. Fan, COVID-19 vaccine development: milestones, lessons and prospects, Signal Transduct. Target. Ther. 7 (2022) 146. https://doi.org/10.1038/s41392-022-00996-y.

[151] L. Schoenmaker, D. Witzigmann, J.A. Kulkarni, R. Verbeke, G. Kersten, W. Jiskoot, D.J.A. Crommelin, mRNA-lipid nanoparticle COVID-19 vaccines: Structure and stability, Int. J. Pharm. 601 (2021) 120586. https://doi.org/10.1016/j.ijpharm.2021.120586.

[152] F.P. Polack, S.J. Thomas, N. Kitchin, J. Absalon, A. Gurtman, S. Lockhart, J.L. Perez, G. Pérez Marc, E.D. Moreira, C. Zerbini, R. Bailey, K.A. Swanson, S. Roychoudhury, K. Koury, P. Li, W. V. Kalina, D. Cooper, R.W. Frenck, L.L. Hammitt, Ö. Türeci, H. Nell, A. Schaefer, S. Ünal, D.B. Tresnan, S. Mather, P.R. Dormitzer, U. Şahin, K.U. Jansen, W.C. Gruber, Safety and Efficacy of the BNT162b2 mRNA Covid-19 Vaccine, N. Engl. J. Med. 383 (2020) 2603–2615. https://doi.org/10.1056/nejmoa2034577.

[153] L.R. Baden, H.M. El Sahly, B. Essink, K. Kotloff, S. Frey, R. Novak, D. Diemert, S.A. Spector, N. Rouphael, C.B. Creech, J. McGettigan, S. Khetan, N. Segall, J. Solis, A. Brosz, C. Fierro, H. Schwartz, K. Neuzil, L. Corey, P. Gilbert, H. Janes, D. Follmann, M. Marovich, J. Mascola, L. Polakowski, J. Ledgerwood, B.S. Graham, H. Bennett, R. Pajon, C. Knightly, B. Leav, W. Deng, H. Zhou, S. Han, M. Ivarsson, J. Miller, T. Zaks, Efficacy and Safety of the mRNA-1273 SARS-

CoV-2 Vaccine, N. Engl. J. Med. 384 (2021) 403–416. https://doi.org/10.1056/nejmoa2035389.

[154] A.J. Barbier, A.Y. Jiang, P. Zhang, R. Wooster, D.G. Anderson, The clinical progress of mRNA vaccines and immunotherapies, Nat. Biotechnol. 40 (2022) 840–854. https://doi.org/10.1038/s41587-022-01294-2.

[155] I.T. Lee, R. Nachbagauer, D. Ensz, H. Schwartz, L. Carmona, K. Schaefers, A. Avanesov, D. Stadlbauer, C. Henry, R. Chen, W. Huang, D.R. Schrempp, J. Ananworanich, R. Paris, Safety and immunogenicity of a phase 1/2 randomized clinical trial of a quadrivalent, mRNA-based seasonal influenza vaccine (mRNA-1010) in healthy adults: interim analysis, Nat. Commun. 14 (2023) 3631. https://doi.org/10.1038/s41467-023-39376-7.

[156] X. Qiu, S. Xu, Y. Lu, Z. Luo, Y. Yan, C. Wang, J. Ji, Development of mRNA vaccines against respiratory syncytial virus (RSV), Cytokine Growth Factor Rev. 68 (2022) 37–53. https://doi.org/10.1016/j.cytogfr.2022.10.001.

[157] H.A. Burris, M.R. Patel, D.C. Cho, J.M. Clarke, M. Gutierrez, T.Z. Zaks, J. Frederick, K. Hopson, K. Mody, A. Binanti-Berube, C. Robert-Tissot, B. Goldstein, B. Breton, J. Sun, S. Zhong, S.K. Pruitt, K. Keating, R.S. Meehan, J.F. Gainor, A phase I multicenter study to assess the safety, tolerability, and immunogenicity of mRNA-4157 alone in patients with resected solid tumors and in combination with pembrolizumab in patients with unresectable solid tumors., J. Clin. Oncol. 37 (2019) 2523–2523. https://doi.org/10.1200/JCO.2019.37.15_suppl.2523.

[158] J. Bauman, H. Burris, J. Clarke, M. Patel, D. Cho, M. Gutierrez, R. Julian, A. Scott, P. Cohen, J. Frederick, C. Robert-Tissot, H. Zhou, K. Mody, K. Keating, R. Meehan, J. Gainor, 798 Safety, tolerability, and immunogenicity of mRNA-4157 in combination with pembrolizumab in subjects with unresectable solid tumors (KEYNOTE-603): an update, in: Late-Breaking Abstr., BMJ Publishing Group Ltd, 2020: p. A477.1-A477. https://doi.org/10.1136/jitc-2020-SITC2020.0798.

[159] L.A. Brito, M. Chan, C.A. Shaw, A. Hekele, T. Carsillo, M. Schaefer, J. Archer, A. Seubert, G.R. Otten, C.W. Beard, A.K. Dey, A. Lilja, N.M. Valiante, P.W. Mason, C.W. Mandl, S.W. Barnett, P.R. Dormitzer, J.B. Ulmer, M. Singh, D.T. O'Hagan, A.J. Geall, A Cationic Nanoemulsion for the Delivery of Next-generation RNA Vaccines, Mol. Ther. 22 (2014) 2118–2129. https://doi.org/10.1038/mt.2014.133.

[160] W.M. Bogers, H. Oostermeijer, P. Mooij, G. Koopman, E.J. Verschoor, D. Davis, J.B. Ulmer, L.A. Brito, Y. Cu, K. Banerjee, G.R. Otten, B. Burke, A. Dey, J.L. Heeney, X. Shen, G.D. Tomaras, C. Labranche, D.C. Montefiori, H.-X. Liao, B. Haynes, A.J. Geall, S.W. Barnett, Potent Immune Responses in Rhesus Macaques Induced by Nonviral Delivery of a Self-amplifying RNA Vaccine Expressing HIV Type 1 Envelope With a Cationic Nanoemulsion, J. Infect. Dis. 211 (2015) 947–955. https://doi.org/10.1093/infdis/jiu522.

[161] M. Zhao, M. Li, Z. Zhang, T. Gong, X. Sun, Induction of HIV-1 gag specific immune responses by cationic micelles mediated delivery of gag mRNA, Drug Deliv. 23 (2016) 2596–2607. https://doi.org/10.3109/10717544.2015.1038856.

[162] M. Li, M. Zhao, Y. Fu, Y. Li, T. Gong, Z. Zhang, X. Sun, Enhanced intranasal delivery of mRNA vaccine by overcoming the nasal epithelial barrier via intra- and paracellular pathways, J. Control. Release. 228 (2016) 9–19. https://doi.org/10.1016/j.jconrel.2016.02.043.

[163] L.I. Karpenko, A.P. Rudometov, S. V. Sharabrin, D.N. Shcherbakov, M.B. Borgoyakova, S.I. Bazhan, E.A. Volosnikova, N.B. Rudometova, L.A. Orlova, I.A. Pyshnaya, B.N. Zaitsev, N. V.

Volkova, M.S. Azaev, A. V. Zaykovskaya, O. V. Pyankov, A.A. Ilyichev, Delivery of mRNA Vaccine against SARS-CoV-2 Using a Polyglucin:Spermidine Conjugate, Vaccines. 9 (2021) 76. https://doi.org/10.3390/vaccines9020076.

[164] J.S. Chahal, O.F. Khan, C.L. Cooper, J.S. McPartlan, J.K. Tsosie, L.D. Tilley, S.M. Sidik, S. Lourido, R. Langer, S. Bavari, H.L. Ploegh, D.G. Anderson, Dendrimer-RNA nanoparticles generate protective immunity against lethal Ebola, H1N1 influenza, and Toxoplasma gondii challenges with a single dose, Proc. Natl. Acad. Sci. 113 (2016). https://doi.org/10.1073/pnas.1600299113.

[165] G. Smith, R. Raghunandan, Y. Wu, Y. Liu, M. Massare, M. Nathan, B. Zhou, H. Lu, S. Boddapati, J. Li, D. Flyer, G. Glenn, Respiratory Syncytial Virus Fusion Glycoprotein Expressed in Insect Cells Form Protein Nanoparticles That Induce Protective Immunity in Cotton Rats, PLoS One. 7 (2012) e50852. https://doi.org/10.1371/journal.pone.0050852.

[166] R. Raghunandan, H. Lu, B. Zhou, M.G. Xabier, M.J. Massare, D.C. Flyer, L.F. Fries, G.E. Smith, G.M. Glenn, An insect cell derived respiratory syncytial virus (RSV) F nanoparticle vaccine induces antigenic site II antibodies and protects against RSV challenge in cotton rats by active and passive immunization, Vaccine. 32 (2014) 6485–6492. https://doi.org/10.1016/j.vaccine.2014.09.030.

[167] L. Fries, V. Shinde, J.J. Stoddard, D.N. Thomas, E. Kpamegan, H. Lu, G. Smith, S.P. Hickman, P. Piedra, G.M. Glenn, Immunogenicity and safety of a respiratory syncytial virus fusion protein (RSV F) nanoparticle vaccine in older adults, Immun. Ageing. 14 (2017) 8. https://doi.org/10.1186/s12979-017-0090-7.

BACKGROUND, HYPOTHESIS, AND OBJECTIVES

1. BACKGROUND

Genetic therapies hold promise for treating a wide range of diseases by successfully regulating the expression of effective genes responsible for the development and progression of various conditions. To harness this potential, the design of specific nanocarriers for delivering genetic material, such as ribonucleic acids (RNA), to their target site, is fundamental [1,2]. Lipid nanoparticles (LNPs) are currently recognized as the standard nanosystems for RNA delivery, being the only nanosystems currently approved for the transport of this type of cargo [3,4]. Nevertheless, despite their favorable regulatory status, several challenges are still unmet. These challenges include their predominant accumulation in the liver following intravenous administration and their limited access and diffusion across the targeted site. These limitations constrain their applications for the treatment of diseases in challenging tissues, such as the central nervous system (CNS) [5–8].

Over recent decades, CNS-related diseases have become the second leading cause of mortality worldwide [9]. These conditions remain inadequately treated due to the limited effectiveness of conventional therapies. Hence, these diseases could potentially benefit from therapies intended to deal with the cause of the disease rather than with the symptoms [10–12]. However, the multiple protective barriers surrounding the CNS impede the delivery of therapeutic agents, notably those with high hydrophilicity. Moreover, in the case of genetic therapies, the polynucleotides have to be transported not only to the tissue but also to the inner of the targeted cells. In such situation, the use of adequate delivery carriers becomes critically important [13,14]. Ideally, an effective delivery carrier should possess the capacity to diffuse across the CNS, enabling the distribution of the genetic cargo to cells located in multiple regions of the brain [15]. The exploration of non-invasive modalities of administration has also become important for enhancing patient compliance [16,17].

Another RNA-based application that has gained significant attention in recent years is messenger RNA (mRNA) vaccines [18,19]. This is largely due to their role during the coronavirus disease 2019 (COVID-19) pandemic and the development of two mRNA vaccines, both using LNPs as delivery systems [20,21]. Substantial efforts have been dedicated to developing nanocarriers for mRNA vaccines, with the objectives of protecting the cargo and eliciting immune responses capable of mitigating the effects of multiple infectious diseases, including the severe acute respiratory syndrome coronavirus 2 (SARS-CoV-2) [22].

2. HYPOTHESIS

1. The formulation of lipids typically used on LNPs in the form of nanoemulsions (NEs), may lead to novel RNA-loaded ionizable NEs (iNEs) with improved diffusivity within the brain while ensuring an efficient transfection.

2. Following a rational design, NEs, and polymer NCs can be engineered to efficiently encapsulate small interfering RNA (siRNA) and have access and diffuse across the CNS through nose-to-brain (N-to-B) and intracerebroventricular (ICV) administration.

3. NEs and polymeric NCs can be formulated as potential delivery systems for mRNA vaccines. The specific compositions of these nanocarriers may determine their safety profiles and the immune responses elicited against SARS-CoV-2.

3. OBJECTIVES

Based on the background information, the final goal of this thesis was to design and develop delivery systems for RNA therapeutics, with a focus on addressing challenging diseases, such as CNS conditions and SARS-CoV-2. This main goal involves two primary experimental directions:

- To design and develop versatile, diverse NEs and polymeric NCs for brain delivery of RNA, allowing the diffusion from the administration point to multiple brain regions and achieving the modulation of the target expression. Different administration routes and oligonucleotides cargos were explored.
- To engineer NEs and polymeric NCs as delivery carriers for mRNA vaccines, ensuring cargo protection and capacity to elicit immune responses against SARS-CoV-2.

More precisely, to achieve these objectives, the following experimental activities were undertaken:

1. Design and development of an iNE for RNA delivery in the CNS, capable of diffusing within the brain and efficiently transferring the genetic cargo into brain cells. This activity has involved:
    a. The formulation and characterization of an iNE loaded with different RNA cargos, including siRNA, miRNA, and mRNA.
    b. The assessment of the transfection capacity in brain cell models.
    c. The evaluation of the diffusion and transfection capacity *in vivo*.

    The results corresponding to this objective are presented in Chapter 1: “Ionizable nanoemulsions for RNA delivery in the brain”.

2. Design and development of NEs and polymeric NCs loaded with siRNA, and their evaluation following different alternative routes to access the brain. This activity has involved:
    a. The design, development, and characterization of a library of NEs and polymeric NCs loaded with siRNA.
    b. The functionalization of a promising candidate with a targeting ligand.
    c. The evaluation of the *in vitro* cytotoxicity and transfection profiles.

d. The assessment of brain distribution and knockdown effect through N-to-B and ICV administration.

The results corresponding to this objective are presented in Chapter 2: "Nanoemulsions and polymeric nanocapsules for nose-to-brain and intracerebroventricular delivery of siRNA".

3. Design and development of NEs and polymeric NCs as an mRNA vaccine candidate against SARS-CoV-2. This activity has involved:

   a. The design, development, and characterization of a library of NEs and polymeric NCs loaded with mRNA.

   b. The evaluation of the *in vitro* cytotoxicity and transfection profile in relevant cellular lines.

   c. The evaluation of the *in vivo* transfection efficiency and capacity to elicit immune response using model mRNAs.

   d. The assessment of the immune responses *in vivo* using SARS-CoV-2 derived mRNA.

   The results corresponding to this objective are presented in Chapter 3: "Nanoemulsions and polymeric nanocapsules as SARS-CoV-2 vaccines".

4. REFERENCES

[1] T. Wirth, N. Parker, S. Ylä-Herttuala, History of gene therapy, Gene. 525 (2013) 162–169. https://doi.org/10.1016/j.gene.2013.03.137.

[2] V. Sudhakar, R.M. Richardson, Gene Therapy for Neurodegenerative Diseases, Neurotherapeutics. 16 (2019) 166–175. https://doi.org/10.1007/s13311-018-00694-0.

[3] X. Hou, T. Zaks, R. Langer, Y. Dong, Lipid nanoparticles for mRNA delivery, Nat. Rev. Mater. 6 (2021) 1078–1094. https://doi.org/10.1038/s41578-021-00358-0.

[4] C. Hald Albertsen, J.A. Kulkarni, D. Witzigmann, M. Lind, K. Petersson, J.B. Simonsen, The role of lipid components in lipid nanoparticles for vaccines and gene therapy, Adv. Drug Deliv. Rev. 188 (2022) 114416. https://doi.org/10.1016/j.addr.2022.114416.

[5] Y. Yan, X.-Y. Liu, A. Lu, X.-Y. Wang, L.-X. Jiang, J.-C. Wang, Non-viral vectors for RNA delivery, J. Control. Release. 342 (2022) 241–279. https://doi.org/10.1016/j.jconrel.2022.01.008.

[6] R.L. Rungta, H.B. Choi, P.J. Lin, R.W. Ko, D. Ashby, J. Nair, M. Manoharan, P.R. Cullis, B.A. MacVicar, Lipid Nanoparticle Delivery of siRNA to Silence Neuronal Gene Expression in the Brain, Mol. Ther. Acids. 2 (2013) e136. https://doi.org/10.1038/mtna.2013.65.

[7] L.E. Waggoner, K.F. Miyasaki, E.J. Kwon, Analysis of PEG-lipid anchor length on lipid

nanoparticle pharmacokinetics and activity in a mouse model of traumatic brain injury, Biomater. Sci. (2023) 4238–4253. https://doi.org/10.1039/d2bm01846b.

[8] H. Xu, Z. Li, J. Si, Nanocarriers in gene therapy: A review, J. Biomed. Nanotechnol. 10 (2014) 3483–3507. https://doi.org/10.1166/jbn.2014.2044.

[9] V.L. Feigin, A.A. Abajobir, K.H. Abate, F. Abd-Allah, A.M. Abdulle, S.F. Abera, G.Y. Abyu, M.B. Ahmed, A.N. Aichour, I. Aichour, M.T.E. Aichour, R.O. Akinyemi, S. Alabed, R. Al-Raddadi, N. Alvis-Guzman, J.R. Zunt, C.J.L. Murray, T. Vos, Global, regional, and national burden of neurological disorders during 1990–2015: a systematic analysis for the Global Burden of Disease Study 2015, Lancet Neurol. 16 (2017) 877–897. https://doi.org/10.1016/S1474-4422(17)30299-5.

[10] R.L. Setten, J.J. Rossi, S. ping Han, The current state and future directions of RNAi-based therapeutics, Nat. Rev. Drug Discov. 18 (2019) 421–446. https://doi.org/10.1038/s41573-019-0017-4.

[11] J. Sun, S. Roy, Gene-based therapies for neurodegenerative diseases, Nat. Neurosci. 24 (2021) 297–311. https://doi.org/10.1038/s41593-020-00778-1.

[12] M. Luo, L.K.C. Lee, B. Peng, C.H.J. Choi, W.Y. Tong, N.H. Voelcker, Delivering the Promise of Gene Therapy with Nanomedicines in Treating Central Nervous System Diseases, Adv. Sci. 9 (2022) 1–41. https://doi.org/10.1002/advs.202201740.

[13] D.J. Begley, Delivery of therapeutic agents to the central nervous system: The problems and the possibilities, Pharmacol. Ther. 104 (2004) 29–45. https://doi.org/10.1016/j.pharmthera.2004.08.001.

[14] B. Engelhardt, L. Sorokin, The blood-brain and the blood-cerebrospinal fluid barriers: function and dysfunction, Semin. Immunopathol. 31 (2009) 497–511. https://doi.org/10.1007/s00281-009-0177-0.

[15] D.J. Wolak, R.G. Thorne, Diffusion of Macromolecules in the Brain: Implications for Drug Delivery, Mol. Pharm. 10 (2013) 1492–1504. https://doi.org/10.1021/mp300495e.

[16] M.L. Borrajo, M.J. Alonso, Using nanotechnology to deliver biomolecules from nose to brain — peptides, proteins, monoclonal antibodies and RNA, Drug Deliv. Transl. Res. 12 (2022) 862–880. https://doi.org/10.1007/s13346-021-01086-2.

[17] C.M. Gorick, V.R. Breza, K.M. Nowak, V.W.T. Cheng, D.G. Fisher, A.C. Debski, M.R. Hoch, Z.E.F. Demir, N.M. Tran, M.R. Schwartz, N.D. Sheybani, R.J. Price, Applications of focused ultrasound-mediated blood-brain barrier opening, Adv. Drug Deliv. Rev. 191 (2022) 114583. https://doi.org/10.1016/j.addr.2022.114583.

[18] K.S. Corbett, D.K. Edwards, S.R. Leist, O.M. Abiona, S. Boyoglu-Barnum, R.A. Gillespie, S. Himansu, A. Schäfer, C.T. Ziwawo, A.T. DiPiazza, K.H. Dinnon, S.M. Elbashir, C.A. Shaw, A. Woods, E.J. Fritch, D.R. Martinez, K.W. Bock, M. Minai, B.M. Nagata, G.B. Hutchinson, K. Wu, C. Henry, K. Bahl, D. Garcia-Dominguez, L.Z. Ma, I. Renzi, W.P. Kong, S.D. Schmidt, L. Wang, Y. Zhang, E. Phung, L.A. Chang, R.J. Loomis, N.E. Altaras, E. Narayanan, M. Metkar, V. Presnyak, C. Liu, M.K. Louder, W. Shi, K. Leung, E.S. Yang, A. West, K.L. Gully, L.J. Stevens, N. Wang, D. Wrapp, N.A. Doria-Rose, G. Stewart-Jones, H. Bennett, G.S. Alvarado, M.C. Nason, T.J. Ruckwardt, J.S. McLellan, M.R. Denison, J.D. Chappell, I.N. Moore, K.M. Morabito, J.R. Mascola, R.S. Baric, A. Carfi, B.S. Graham, SARS-CoV-2 mRNA vaccine design

enabled by prototype pathogen preparedness, Nature. 586 (2020) 567–571. https://doi.org/10.1038/s41586-020-2622-0.

[19] G.T. Szabó, A.J. Mahiny, I. Vlatkovic, COVID-19 mRNA vaccines: Platforms and current developments, Mol. Ther. 30 (2022) 1850–1868. https://doi.org/10.1016/j.ymthe.2022.02.016.

[20] F.P. Polack, S.J. Thomas, N. Kitchin, J. Absalon, A. Gurtman, S. Lockhart, J.L. Perez, G. Pérez Marc, E.D. Moreira, C. Zerbini, R. Bailey, K.A. Swanson, S. Roychoudhury, K. Koury, P. Li, W. V. Kalina, D. Cooper, R.W. Frenck, L.L. Hammitt, Ö. Türeci, H. Nell, A. Schaefer, S. Ünal, D.B. Tresnan, S. Mather, P.R. Dormitzer, U. Şahin, K.U. Jansen, W.C. Gruber, Safety and Efficacy of the BNT162b2 mRNA Covid-19 Vaccine, N. Engl. J. Med. 383 (2020) 2603–2615. https://doi.org/10.1056/nejmoa2034577.

[21] L.R. Baden, H.M. El Sahly, B. Essink, K. Kotloff, S. Frey, R. Novak, D. Diemert, S.A. Spector, N. Rouphael, C.B. Creech, J. McGettigan, S. Khetan, N. Segall, J. Solis, A. Brosz, C. Fierro, H. Schwartz, K. Neuzil, L. Corey, P. Gilbert, H. Janes, D. Follmann, M. Marovich, J. Mascola, L. Polakowski, J. Ledgerwood, B.S. Graham, H. Bennett, R. Pajon, C. Knightly, B. Leav, W. Deng, H. Zhou, S. Han, M. Ivarsson, J. Miller, T. Zaks, Efficacy and Safety of the mRNA-1273 SARS-CoV-2 Vaccine, N. Engl. J. Med. 384 (2021) 403–416. https://doi.org/10.1056/nejmoa2035389.

[22] V. Gote, P.K. Bolla, N. Kommineni, A. Butreddy, P.K. Nukala, S.S. Palakurthi, W. Khan, A Comprehensive Review of mRNA Vaccines, Int. J. Mol. Sci. 24 (2023) 2700. https://doi.org/10.3390/ijms24032700.

CHAPTER 1

Ionizable nanoemulsions as nanocarriers for RNA delivery to the brain

Chapter 1: Ionizable nanoemulsions as nanocarriers for RNA delivery to the brain

This work has been done in collaboration with the BioFarma Research Group and the Cell and Molecular Neurobiology of Parkinson's disease Group, Center for Research in Molecular Medicine and Chronic Diseases (CiMUS), University of Santiago de Compostela (Santiago de Compostela, Spain), the Vlaams Instituut voor Biotechnologie (VIB) Center for Brain and Disease, VIB-Leuven, Center for Human Genetics, Universitaire Zeikenhuizen and Leuven Research Institute for Neuroscience and Diseases, KU-Leuven (Leuven, Belgium).

ABSTRACT

Currently, lipid nanoparticles (LNPs) are considered the gold standard for RNA delivery. However, this delivery platform lacks the necessary diffusivity to enable the dissemination of RNA payload in the targeted tissue, making it challenging to deliver the cargo to specific cells. This limitation is particularly relevant for tissues with difficult access, such as the central nervous system (CNS), to maximize the effectiveness of genetic therapy after overcoming the multiple challenging protective barriers.

The objective of this work was the development of a new generation of nanocarriers, named ionizable nanoemulsions (iNE), capable of efficiently delivering RNA and diffusing within the targeted tissue. The developed iNE exhibited a size smaller than 100 nm, a neutral surface charge, high RNA loading capacity, and stability in relevant simulated media. Furthermore, *in vitro* studies conducted in numerous cellular models (including neuron, astrocyte, and microglia models) resulted in a high viability profile as well as a remarkable transfection efficiency. Subsequently, intra-dentate administration was performed in an Alzheimer's disease animal model, and the results showed that iNEs containing miR-132 could diffuse from the site of injection to surrounding areas. The same formulation was finally tested for its ability to transfect brain tissue using mRNA GFP as a model, confirming the extraordinary diffusivity profile of these nanocarriers and their selective transfection of neurons and microglia *in vivo*.

GRAPHICAL ABSTRACT

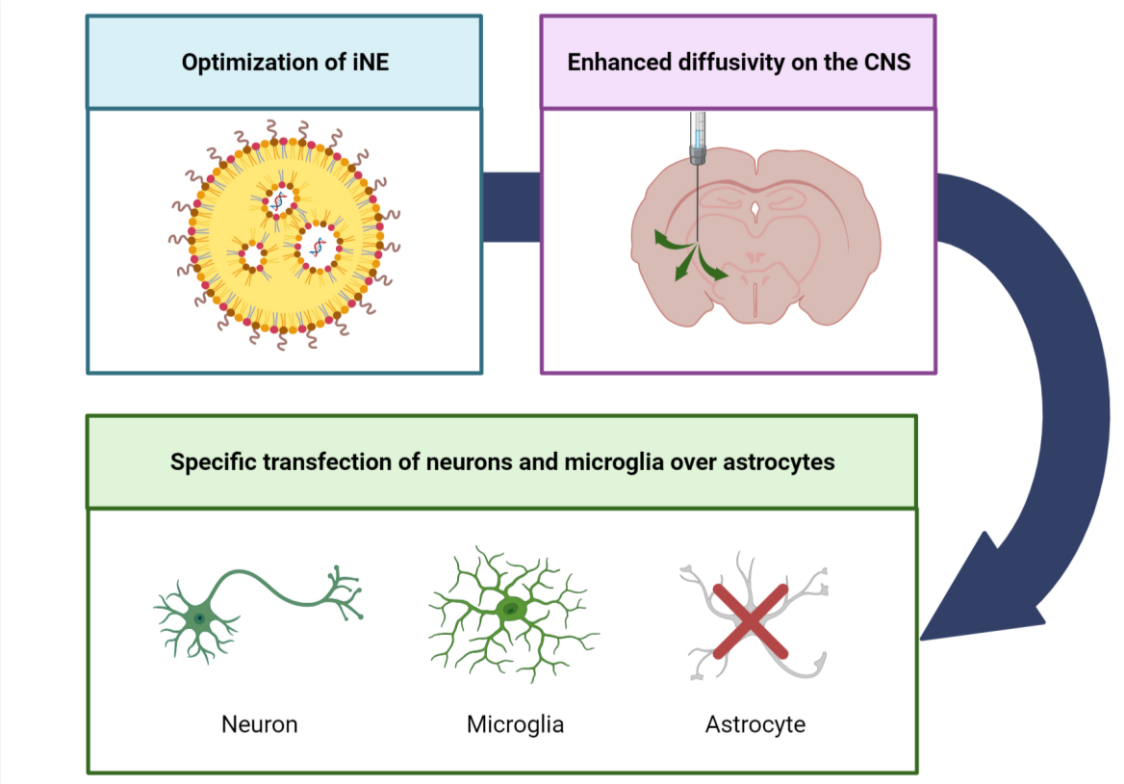

Created with https://biorender.com.

1. INTRODUCTION

Currently, the potential of RNA therapeutics for the treatment of multiple medical conditions relies heavily on the use of nanotechnology. Among the different nanocarriers developed, lipid nanoparticles (LNPs) are the only ones commercialized for the delivery of messenger RNA (mRNA) and small interfering RNA (siRNA) [1]. The first LNP-based genetic medicine approved was Onpattro® (Alnylam) in 2018, which consisted of a siRNA-based technology for treating hereditary transthyretin-mediated amyloidosis [2]. In late 2020, mRNA vaccines Comirnaty® (BioNTech/Pfizer) and Spikevax® (Moderna) were approved against the severe acute respiratory syndrome coronavirus 2 (SARS-CoV-2), the cause of the coronavirus disease 2019 (COVID-19) [3].

In these formulations mRNA molecules were encapsulated into LNPs, containing a cationic or ionizable lipid, cholesterol, a helper lipid, and a PEGylated lipid [4] (Figure 1). Ionizable lipids are responsible for the complexation of RNA. They are neutral at physiological pH and become positively charged at the acidic pH of the endosomal compartment. This property facilitates their fusion with the endosomal membrane, ultimately leading to the release of the cargo in the cytoplasm of the targeted cell [5–7]. In the case of Onpattro®, the unsaturated ionizable lipid DLin-MC3-DMA was used. [8,9]. Further optimization of these unsaturated ionizable lipids has resulted in the synthesis of multi-tail ionizable lipids, such as C12-200, with a cone-shaped structure, which enhances their ability to disrupt the endosome [10]. However, a limitation of this type of ionizable lipids is their low degradability, mainly due to their stable backbones [11].

Although ionizable lipids are critical for the effective entrapment of oligonucleotides, the rest of the components of the LNPs are equally fundamental for the proper delivery of the cargo. Cholesterol promotes the stability of the resulting nanosystems and assists in the fusion of the LNPs with the endosomal membrane [12]. Helper lipids are involved in the nanocarrier fluidity and facilitate the lipid phase transition, which is necessary for the fusion of the endosomal membrane [13]. Finally, PEGylated lipids play a significant role in the LNP stability and circulation time [14,15].

However, when designing a nanocarrier successful in vivo transfection is not the only requirement. Following in vivo administration, the nanocarrier must reach the desired tissue; once there, the nanocarrier must diffuse across the tissue and effectively reach the targeted cell. Different studies have evaluated the diffusion of LNPs upon direct administration in the brain. Administration of LNPs carrying PTEN (phosphatase and tensin homolog 1)-siRNA showed lowered levels of PTEN in neurons less than 1 mm [16]. This result was corroborated after the administration of Cy5-labeled mRNA LNPs into the striatum, as the signal was detected 1-1.5 mm away from the injection site [17]. However, other studies performed to determine the delivery of oligonucleotides on the brain are based on total brain quantification, which only provides information about the overall effect, not where this is being depicted [18,19]. This lack of mobility could be explained due to the dense inner core and relative rigidity of LNPs [20]. Interestingly, similar results have been obtained with inorganic nanoparticles [21,22]. In other contexts, diffusivity studies in mucus and brain demonstrated that PEGylation of nanoparticles could enhance their diffusivity profile in a size-dependent manner [23,24]. These results suggest

that both particle size and the internal composition of the nanoparticles play a crucial role in diffusion within the brain.

Considering that the results reported so far refer to relatively dense, rigid inner cores, our hypothesis relied on the use of softer, fluid, and more deformable cores, as those present in nanoemulsions (NEs), illustrated in Figure 1. NEs consist of an oil-in-water suspension containing oils and surfactants, with a typical droplet size in the nanometric range [25,26]. Unfortunately, these nanocarriers have been mainly used for the controlled delivery of different lipophilic moieties, which can be dissolved within the hydrophobic core of the NE [27]. Therefore, a specific formulation strategy had to be adopted to accommodate the RNA molecules with these nanostructures. Recently, the incorporation of cationic lipids and surfactants into NE compositions has allowed the entrapment of RNA molecules, particularly in the context of vaccination [28–30]. In other cases, cationic NEs have been used for brain delivery. For example, flaxseed oil NEs containing 1,2-dioleoyl-3-trimethylammonium propane (DOTAP) for the entrapment of siRNA anti-tumor necrosis factor-α (TNF-α) were found to effectively work following intranasal administration [31]. Similarly, a NE containing DOTAP was used for the intranasal delivery of siRNA CD73 for glioblastoma treatment, leading to a significant reduction of tumor growth in an animal model [32].

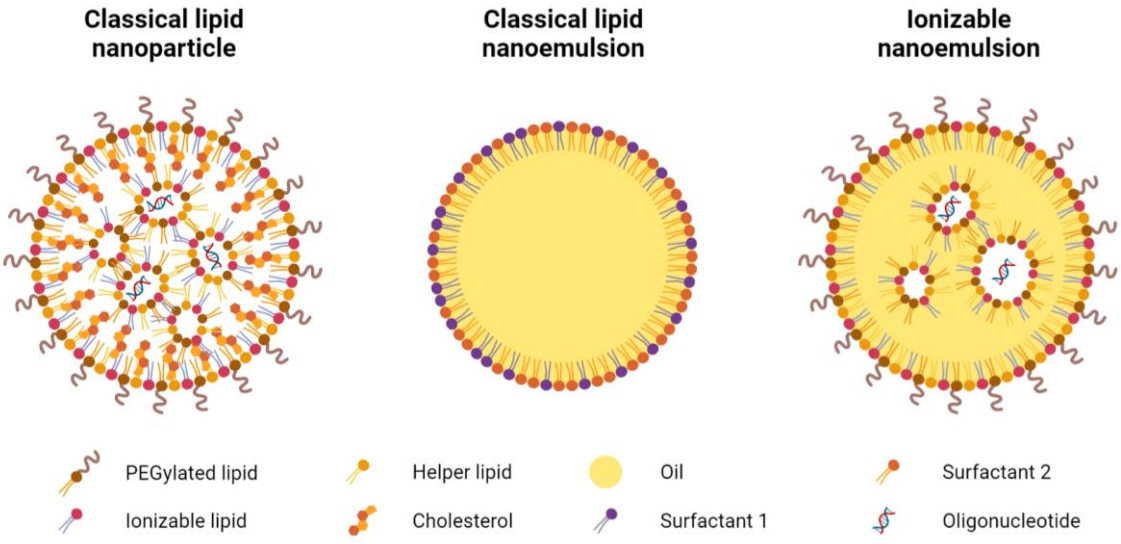

Figure 1. Hypothetical schematic representation of LNPs (left), NEs (middle), and iNE (right)

Abbreviations: iNE: ionizable nanoemulsion. NE: nanoemulsion. LNP: lipid nanoparticle. Created with https://biorender.com.

Here, we leverage the knowledge of NEs to develop the next-generation ionizable NEs (iNE), combining the versatility of NEs with the efficient delivery capacity of LNPs, as depicted in Figure 1. We investigated the use of different lengths of PEGylated lipids to ensure the highest transfection efficiency while maintaining low toxicity levels *in vitro*. Furthermore, an assessment of cytotoxicity profiles and transfection efficiency was performed in cellular models of neurons, microglia, and astrocytes. To validate our hypothesis regarding the enhanced diffusivity of iNEs, animal studies were conducted, involving inta-dentate gyrus administration of iNE containing miR-132 in an Alzheimer's disease model. Diffusivity was also assessed in healthy rats following intra-parenchymal administration of iNE encapsulating mRNA encoding

for the green fluorescent protein (mGFP), intended to elucidate the specific CNS cells where the reported GFP was selectively expressed, as well as the diffusion profile of the iNEs.

2. MATERIALS AND METHODS

2.1. MATERIALS

C12-200, HCl salt (1,1′-((2-(4-(2-((2-(bis(2-hydroxydodecyl)amino)ethyl)(2-hydroxydodecyl) amino)ethyl)piperazin-1-yl)ethyl)azanediyl)bis(dodecan-2-ol) and DMG-PEG_{2000} ((*R*)-methoxy-polyethyleneglycol-2000-carbamoyl-di-O-myristyl-sn-glyceride) were kindly gifted by Muthiah Manoharan, from Anylam Pharmaceuticals (MA, USA). DOPE (1,2-dioleoyl-sn-glycero-3-phosphoethanolamine) was purchased from Avanti Polar Lipids (AL, USA). Vitamin E (Vit E) (D, L-α-tocopherol) was obtained from BASF (Mannheim, Germany). Tween 80 was acquired from Merck Millipore (MA, USA).

Different types of oligonucleotides were explored. Messenger RNA (mRNA) encoding green fluorescence protein (mGFP, CleanCap EGFP mRNA) was purchased from TrikLink Biotechnologies (CA, USA). Silencing RNA (siRNA) anti-GFP (siGFP) was acquired from BioSpring GmbH (Frankfurt, Germany). MiRADIAN microRNA Human hsa-miR-132—3p mimic (miR-132 mimic, or miR-132) and negative control (scrambled miRNA, or miR-control) were procured by GE Healthcare Dharmacon Inc. (CO, USA).

2.2. PRODUCTION OF IONIZABLE NANOEMULSIONS

Ionizable nanoemulsions (iNE) were prepared in a single step using a micromixer NanoAssemblr™ bench-top instrument, Precision NanoSystem Inc. (Vancouver, Canada), following a solvent displacement technique [33]. Formation of the iNE and complexation of the oligonucleotide cargo occurred simultaneously. In summary, 0.2 mL of the organic phase (12.8 mg/mL of C12-200, 3.7 mg/mL of DOPE, 6 mg/mL of Vitamin E, and 2 mg/mL DMG-PEG_{2000} in EtOH, leading to molar ratios 35: 16: 46.5: 2.5) were mixed with 1 mL of the aqueous phase (containing 0.24 mg/mL of RNA diluted in citrate buffer, pH 4, 10 mM).

The nitrogen-to-phosphate ratio (between the amine group of C12-200 and the phosphate group of the RNA) was maintained at 15:1. The Flow Ratio, implying the volume-to-volume ratio between the different phases, was 1:5 (organic to aqueous phase). The Total Flow Rate was maintained at 12 mL/min. The resulting iNE-RNA formulations presented a theoretical RNA concentration of 0.2 mg/mL. Samples were set aside for stabilization for 10 minutes before physicochemical characterization.

iNEs containing Tween 80 were prepared by bulk mixing, in a single step. Briefly, 0.2 mL of the organic phase (12.8 mg/mL of C12-200, 3.7 mg/mL of DOPE, 6 mg/mL of Vitamin E, and 1 mg/mL of Tween 80 in EtOH, leading to molar ratios 35: 16: 46.5: 2.5) were added over 1 mL of the aqueous phase (containing 0.24 mg/mL of RNA diluted in citrate buffer 10 mM, pH 4). The aqueous phase was under stirring at 1400 rpm, and the resulting solution was kept under agitation for 5 seconds, and set aside for stabilization for 10 minutes before physicochemical characterization.

2.3. CHARACTERIZATION OF IONIZABLE NANOEMULSIONS

2.3.1. Characterization of the size, polydispersity index and ζ-potential of nanoemulsions and nanocapsules

Hydrodynamic diameter and polydispersity index (PDI) were characterized by dynamic light scattering (Zetasizer® Nano ZS, Malvern Instruments, Malvern, UK). ζ-potential was measured in terms of mean electrophoretic mobility values, measured by laser Doppler electrophoresis with the same equipment.

Particle size and PDI measurements were performed after diluting the samples 10 x in PBS, pH 7. ζ-potential characterization was obtained after dilution of samples 20 x in RNase-free water.

2.3.2. Characterization of encapsulation efficiency and RNA concentration

Encapsulation efficiency (EE%) and RNA concentration were assessed following different methodologies. In all cases, iNE-RNA formulations were diluted in a 1:1 (v/v) ratio with Triton X or heparin solutions, prepared at 50 mg/mL in RNase-free water. Incubation with Triton X (Triton-X-100, Sigma-Aldrich, MO, USA) induced the disruption of the nanocarrier, while heparin (Sigma-Aldrich, MO, USA) led to the displacement of the RNA from the nanoparticle.

2.3.2.1. Agarose gel electrophoresis

To qualitatively assess the amount of RNA encapsulated onto iNE-RNA formulations, samples containing 1-3 µg of RNA were loaded in an agarose gel at 1% w/v in Tris Acetate-EDTA buffer (Sigma-Aldrich, MO, USA) before and after incubation with Triton X and heparin. Samples were diluted with equal volumes of loading mix, containing 1x SYBR® Gold nucleic acid strain (Invitrogen, CA, USA). Free RNA was included as a control. Gels were run for 30 minutes at 90 V in a Sub-Cell GT cell 96/192 (Bio-Rad Laboratories, CA, USA), and evaluated with a UV transilluminator imagining system (Molecular Imager® Gel Doc™ XR, Bio-Rad Laboratories, CA, USA).

2.3.2.2. RiboGreen assay

Quant-iT RiboGreen RNA assay kit (Invitrogen, MA, USA) was used to quantitatively determine the EE% and the RNA concentration of iNE-RNA formulations. Briefly, samples were diluted 50-fold in TE buffer (1x), followed by a 2-fold dilution with Triton X and incubation at 37 °C for 30 minutes. Subsequently, samples were diluted 10-fold with TE buffer (1x). The standard curve was prepared using RNA at concentrations between 0.1 to 1 µg/mL, in the presence of Triton X. Following manufacturer instruction, RiboGreen reagent was diluted 200-fold in TE buffer (1x), and added to an equal volume of sample, leading to a final volume of 200 µL. Samples and the standard curve were transferred to a 96-black polystyrene microplate (Croning®, NY, USA). Fluorescence intensity was assessed using a microplate reader (Synergy H1, BioTek Instruments, VT, USA), using excitation at 485 nm and emission at 530 nm. The standard curve ($r^2 \geq 0.99$) was used for determining the RNA concentration of the sample. The encapsulation efficiency of RNA was calculated according to the following Equation 1.

$$Encapsulation\ efficiency\ (EE\%) = \frac{[RNA]_{disrupted}}{[RNA]_{theoretical}}$$

Where $[RNA]_{disrupted}$ is the RNA concentration determined after treating the nanosystems with the disrupting agent. $[RNA]_{theoretical}$ is the theoretical total RNA concentration of the nanosystem.

Equation 1. Calculation of encapsulation efficiency (EE%)

2.4. CONCENTRATION OF IONIZABLE NANOEMULSIONS

Aiming to significantly increase the RNA concentrations, without altering the resulting physicochemical properties, iNE-RNA formulations were concentrated using Amicon® Ultra 0.5 mL Centrifugal Filters Ultracel® -100K (Merck Millipore, MA, USA). In summary, all samples were concentrated at 14000 g during a variable amount of time, dependent on desired RNA concentration (usually, between 5 to 20 minutes). This process allowed the 7- to 12-fold concentration of the iNE-RNA formulations, leading to a final RNA concentration of 1.5 to 2.2 mg/mL. Samples were characterized as described in section 2.2. before and after the concentration process.

2.5. COLLOIDAL STABILITY OF IONIZABLE NANOEMULSIONS

The colloidal stability of iNE-RNA was evaluated upon incubation of 10% of formulations with 90% of PBS supplemented with 10% FBS, at 37 ºC. At different time points, physicochemical characterization of the iNE-RNA samples was assessed by DLS, as indicated in section 2.3.1.

In all cases, samples were subjected to gentle horizontal shaking during the incubation process (300 rpm, Heidolph Titramax/Inkubator 1000, Heidolph Instrument, Schwabach, Germany).

2.6. IN VITRO ASSESSMENT OF TRANSFECTION EFFICIENCY AND CYTOTOXICITY WITH IONIZABLE NANOEMULSIONS

2.6.1. In vitro siGFP and mGFP transfection efficiency and cytotoxicity in HeLa cells

Assessment of cytotoxicity and transfection efficiency was performed in HeLa cells expressing GFP (in the case of iNE-siRNA) and HeLa cells (in the case of iNE-mRNA). In both cases, a total of 10,000 cells were seeded per well in a flat bottom 96-well plate and allowed to adhere for 24 hours. Cells were treated with iNE-RNA formulations for 4 hours, in Opti-MEM™ (Gibco™, Thermo Fisher, MA, USA) at different oligonucleotide concentrations. In the case of siRNA, concentration ranged from 250 to 10 nM per well; whereas for mRNA, concentrations ranged from 200 and 25 ng per well. Nanocarriers were then removed, and replaced with a complete medium and the cells were incubated for another 20 hours. Cell viability was measured by resazurin assay, following manufacturer recommendations [34]. Briefly, cells were incubated with resazurin reagent (Resazurin sodium salt, Sigma-Aldrich, MO, USA) supplemented complete media for 45 minutes, and the resulting fluorescence was measured in a plate reader at 544/590 nm. Cells were then trypsinized, harvested, and fixed with 1% (w/v) formaldehyde in PBS, for flow cytometry analysis in terms of the percentage of

GFP-negative (in the case of siRNA) and -positive cells (in the case of mRNA), and mean fluorescence intensity.

2.6.2. In vitro mGFP transfection efficiency and cytotoxicity in neuron, astrocyte, and microglia model

In vitro cytotoxicity and transfection efficiency were also evaluated in human neurons (SH-SY5Y cells), rat astrocytes (C6 cell), and human microglia (CHME-3 cells) models. For that, a total of 10,000 cells were seeded per well in a flat bottom 96-well plate, and allowed to adhere for 24 hours. Cells were treated with iNE-mGFP for 4 hours, in Opti-MEM™ (Gibco™, Thermo Fisher, MA, USA) at a concentration of 500 ng per well. Nanocarriers were then removed, and replaced with a complete medium and the cells were incubated for another 20 hours.

Cell viability was measured by MTT assay (Sigma-Aldrich, MO, USA). Briefly, cells were incubated with MTT reagent (1 mg/mL) for 4h at 37 ºC. After removing the MTT reagent, the resulting formazan crystals were dissolved in acidic isopropanol and quantified in a plate reader at 544/590 nm. For transfection efficiency, cells were then trypsinized, harvested, and fixed with 1% (w/v) formaldehyde in PBS. The percentage of GFP-positive cells and mean fluorescence intensity were analyzed by flow cytometry.

2.7. ANIMAL STUDIES

All animal studies procedures were performed in compliance with relevant laws and institutional guidelines and the appropriate institutional committee(s) have approved them.

2.8. IN VIVO ASSESSMENT OF DIFFUSION OF IONIZABLE NANOEMULSIONS IN THE BRAIN

2.8.1. Intra-dentate gyrus administration of miR-132-loaded ionizable nanoemulsions

Alzheimer's disease mouse model APP_{NL-G-F} was used, consisting of an β-amyloid precursor protein (APP) knock-in model that expresses three human APP mutations: APP KM670/671NL (Swedish), APP I716F (Iberian), APP E693G (Artic). Mice start developing amyloid plaques at age 2-3 months, leading to memory deficit at 6 months of age.

Animals were directly injected in the hippocampal subregion of the dentate gyrus (DG) (A/P: -2.1 mm; M/L: 1.9 mm; D/V: 2.2 mm) with 2 µL of iNE-miR-132 or iNE-miR-control, at doses of 300 pmol and 75 pmol of miR per mouse. Administration speed was 200 nL/min. After 48 hours post-injection, animals were sacrificed and the DG and cornu ammonius (CA, adjacent regions of the hippocampus) were microdissected and frozen for further processing. RNA extraction was performed using miRVana Paris Kit (Life Technologies, Belgium), following the instructions of the manufacturer. Next, reverse transcription was performed using miRCURY LNA RT Kit (Exiqon, QIAGEN, Denmark); and real-time semi-quantitative PCR was performed using Sybr Green mastermix and LNA primers (Exiqon, QIAGEN, Denmark).

2.8.2. Intra-parenchymal administration of mGFP-loaded ionizable nanoemulsions

Intra-parenchymal administration was evaluated in Sprague-Dawley rats (3 animals in the iNE group, and 1 animal in the control group). Animals were injected with 15 ng of mGFP encapsulated onto iNE nanocarrier, in a total volume of 3 µL. The solution was injected using a 5-µL Hamilton syringe, coupled to a motorized injection (Stoelting), at a rate of 0.5 µL/min. Stereotaxic coordinates were A/P: 0.8 mm, M/L: 3.0 mm and D/V: 5.0 mm. The cannula used for the administration was left in situ 2 minutes after injection. After 24 hours, the animals were stunned with carbon dioxide and sacrificed by decapitation. Brains were removed, cryoprotected, and cut into coronal tissue sections using a sliding microtome. Sections were processed with immunofluorescence labeled.

Free-floating tissue sections were pre-incubated in KPBS-1% BSA with 5% regular donkey serum (Sigma-Aldrich, MO, USA) and 0.03% Triton X for 60 minutes at room temperature. Initially, single immunofluorescence was performed to identify cells capable of expressing GFP after mGFP transfection. The different brain cell types were labeled with primary antibodies against class III β-tubulin (β III-tubulin, Sigma-Aldrich, MO, USA) as a neuronal maker, or glial fibrillary acidic protein (GFAP, Merk Millipore, MA, USA) as an astrocytic marker, or ionized calcium-binding adaptor molecule 1 (Iba-1, Wako Chemicals, Neuss, Germany) as a microglial maker. Cell nuclei were marked with the DNA-binding dye Hoechst 33 342 (Sigma-Aldrich, MO, USA). The immunoreaction was visualized with the fluorescence secondary antibody Alexa Fluor 568-conjugated donkey anti-rabbit IgG (Molecular Probes, OR, USA) or Alexa Fluor 488-conjugated donkey anti-mouse IgG (Molecular Probes, OR, USA). Sections were mounted on gelatin-coated slides and cover-slipped with Immumount (Thermo-Shandon). Co-localization of these markers was assessed by confocal laser microscopy (AOBS-SP5X; Leica Microsystems Heidelberg GmbH, Mannheim, Germany).

Then, considering the auto-green fluorescence depicted by neurons, the decision was made to perform a double immunofluorescence against GFP (anti-GFP, Molecular Probes, OR, USA) and β III-tubulin, followed by the incubation with fluorescence secondary antibodies already mentioned. Then, the preparation of the section was performed as previously described.

3. RESULTS AND DISCUSSION

To achieve the full potential of gene therapies, the nanocarriers used to protect and deliver the RNA cargo must also facilitate diffusion across the targeted tissue, a characteristic that is currently absent in LNPs. With the aim of developing nanosystems with enhanced diffusivity properties, we investigated the combination of classical lipids of LNPs with oily cores of NEs were explored in the context of the CNS. The primary objective of these studies was to design a nanocarrier with the capacity to diffuse extensively in the brain, thereby ensuring the delivery and transfection of different types of RNA.

3.1. DEVELOPMENT OF IONIZABLE NANOEMULSIONS

To design a NE with a high diffusivity profile throughout the brain, we opted for a Vitamin E core in combination with an ionizable lipid, C12-200 [35]. C12-200 is a multi-tailed ionizable lipidoid known for its ability to adopt a cone-shaped structure, enhancing its capacity to disrupt endosomes [10]. Like other ionizable lipids, C12-200 becomes protonated upon cellular uptake in acidic endosomes, where it interacts with the endosomal phospholipids. This interaction triggers a phase change from a bilayer structure to an inverted hexagonal H_{II} phase, disrupting the endosomal membrane and facilitating the release of the oligonucleotide cargo into the cytosol [36]. Ideally, the combination of an oily core with a lipid capable of enhancing endosomal escape holds promise for achieving adequate brain diffusion and effective modulation of CNS genes.

To demonstrate the versatility of the developed nanosystem, different types of oligonucleotides were encapsulated onto the iNE. The physicochemical properties of the resulting iNEs are summarized in Table 1. Notable differences were not observed in terms of particle diameter, polydispersity index, and surface charge. These findings prove the robustness of the iNE for the delivery of different types of oligonucleotides.

Table 1. Physicochemical properties of iNE developed, containing C12-200, DOPE, Vitamin E, and DMG-PEG, in combination with siGFP, mGFP, and miR-132

Typer of RNA	Size (nm)	PDI	ζ-Potential (mV)	Encapsulation efficiency (%)
siGFP	64 ± 7	0.23 ± 0.03	-2 ± 1	80-90
miR-132	60 ± 7	0.2 ± 0.05	-1 ± 1	80-90
mGFP	72 ± 9	0.17 ± 0.07	-4 ± 2	80-90

Encapsulation efficiency was measured by agarose gel, and values were corroborated by RiboGreen assay. **Abbreviations:** GFP: green fluorescence protein. mGFP: mRNA encoding GFP. miR-132: miRNA-132 mimic. PDI: polydispersity index. siGFP: siRNA anti-GFP. Values represent the mean ± standard deviation (n ≥ 3).

Furthermore, encapsulation efficiency was determined by agarose gel electrophoresis (Figure 2). Different buffers were employed to assess the behavior of the iNE-RNA after exposure to varying pH levels upon cellular uptake. C12-200 is positively charged at acidic pH, enabling the condensation of RNA, and becomes neutrally charged at physiological pH, ensuring RNA entrapment while minimizing toxicity. In principle, RNA molecules should be entrapped in the iNE at endosomal pH (ranging between 6 and 4.5, considering both early and late endosomes), and should be protected at physiological pH (around pH 7-7.4, whether in the bloodstream or the brain) [37–39]. Irrespective of the type of RNA used, nearly complete complexation was achieved at pH 4 (citrate buffer or CB condition). However, different behavior was observed at pH 7.4 (PBS condition). In the case of siGFP and mGFP, most of the RNA molecules remained complex within the iNE, and complete release was only achieved through Triton X disruption. Conversely, iNE encapsulating miR-132 showed a minor release in PBS; this behavior was further confirmed through Ribogreen assay in PBS, leading to an encapsulation efficiency of 80.6 ± 6%.

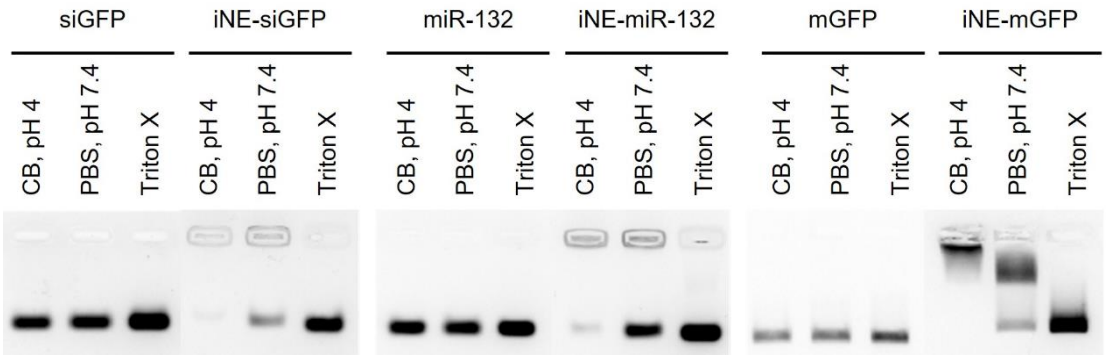

Figure 2. Encapsulation efficiency of siGFP (left), miR-132 (center), and mGFP (right) loaded iNE. Samples were treated with CB (pH 4), PBS (pH 7.4), and Triton X (for iNE disruption)

Abbreviations: CB: citrate buffer. GFP: green fluorescence protein. iNE: ionizable nanoemulsion. mGFP: mRNA encoding GFP. miR-132: miRNA-132 mimic. PBS: phosphate-buffered saline. siGFP: siRNA anti-GFP.

A variation of the iNE nanocarrier containing Tween 80 instead of DMG-PEG_{2000} was prepared by bulk mixing (Supplementary Table 1). Regardless of the type of oligonucleotide, particle size significantly increased, emphasizing the importance of the mixing process and the PEGylation length in determining the resulting physicochemical properties.

3.1.1. Concentration of ionizable nanoemulsions

Concentration of iNE-miR-132 was performed to increase the oligonucleotide concentration without altering its physicochemical properties (Table 2). The centrifugation process for concentrating the nanocarrier did not affect the particle diameter, polydispersity, surface charge, or encapsulation efficiency. Overall, miR-132 concentration increased 9.3-fold. The concentration of iNE-miR-control was also performed (Supplementary Table 2), maintaining the physicochemical properties.

Table 2. Physicochemical properties of iNE-miR-132 before and after the concentration process

Concentration	Size (nm)	PDI	ζ-Potential (mV)	Encapsulation efficiency (%)	miR-132 concentration (mg/mL)
Before	64 ± 4	0.23 ± 0.04	-0.4 ± 0.5	80.6 ± 5.8	0.2 ± 0.02
After	67 ± 4	0.18 ± 0.02	-0.5 ± 0.8	74.7 ± 8	1.84 ± .48

Encapsulation efficiency was measured by RiboGreen assay. **Abbreviations:** PDI: polydispersity index. Values represent the mean ± standard deviation (n ≥ 3).

3.1.2. Stability of ionizable nanoemulsions in relevant simulated media

The stability of miR-132-loaded iNE was assessed in a biological-mimicking media to detect any changes in the physicochemical properties (Figure 3). iNE-miR-132 maintained its particle diameter for up to 24 hours in PBS supplemented with 10% FBS. A slight size increase (30 nm) was observed immediately after dilution in the supplemented PBS, which might be due to the formation of the protein corona around the iNE-miR-132. On the other hand, derived

count rate (DCR), a relative parameter used to compare variations in the concentration of nanocarriers, also remained stable, supporting the hypothesis that iNE-miR-132 is stable in relevant simulated media for at least 24 hours.

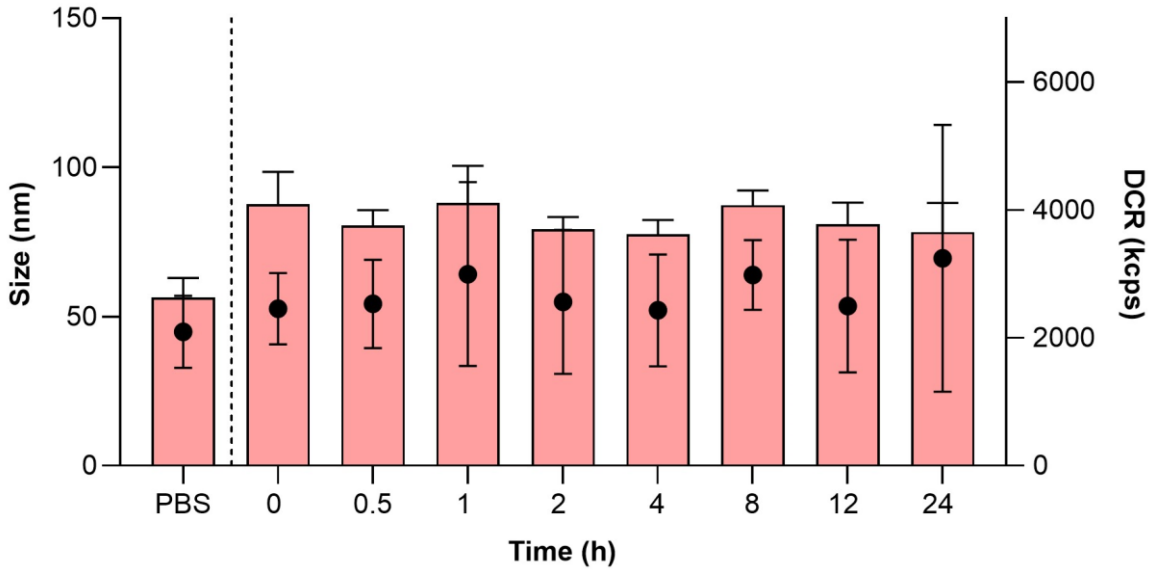

Figure 3. Stability of iNE-miR-132 in relevant simulated biological media (PBS supplemented with 10% FBS)

Abbreviations: DCR: derived count rate. FBS: fetal bovine serum. PBS: phosphate-buffered saline. Values represent the mean ± standard deviation (n ≥ 3).

In conclusion, the developed iNE exhibits the desired physicochemical properties, colloidal stability, and the ability to concentrate, making it a suitable candidate for RNA delivery in the brain.

3.2. IN VITRO CYTOTOXICITY AND TRANSFECTION EFFICIENCY IN DIFFERENT CELL LINES

3.2.1. Cytotoxicity and transfection efficiency in HeLa cells

In vitro experiments were conducted using HeLa cells to evaluate cytotoxicity and transfection efficiency, using both siGFP (Figure 4) and mGFP as model RNA molecules (Supplementary Figure 1). In the case of siGFP, the comparison was made between iNE formulations containing Tween 80 (prepared by bulk mixing) and DMG-PEG_{2000} (prepared by microfluidic mixing). Regarding cellular cytotoxicity (Figure 4, top), iNE-DMG-PEG_{2000} appeared less toxic than iNE-Tween 80 at the highest concentrations (250 and 100 nM), exhibiting similar behavior at lower concentrations (50 and 10 nM). However, both iNEs exhibited similar transfection efficiency in terms of the percentage of transfected cells and fluorescence intensity at all concentrations tested (Figure 4, bottom).

Considering these results, together with its smaller particle size, iNE containing DMG-PEG_{2000}, prepared by microfluidic mixing, was selected as the most promising candidate for

delivery and transfection of oligonucleotides, due to its extended cellular viability at high concentrations and adequate transfection efficiency at all concentrations tested.

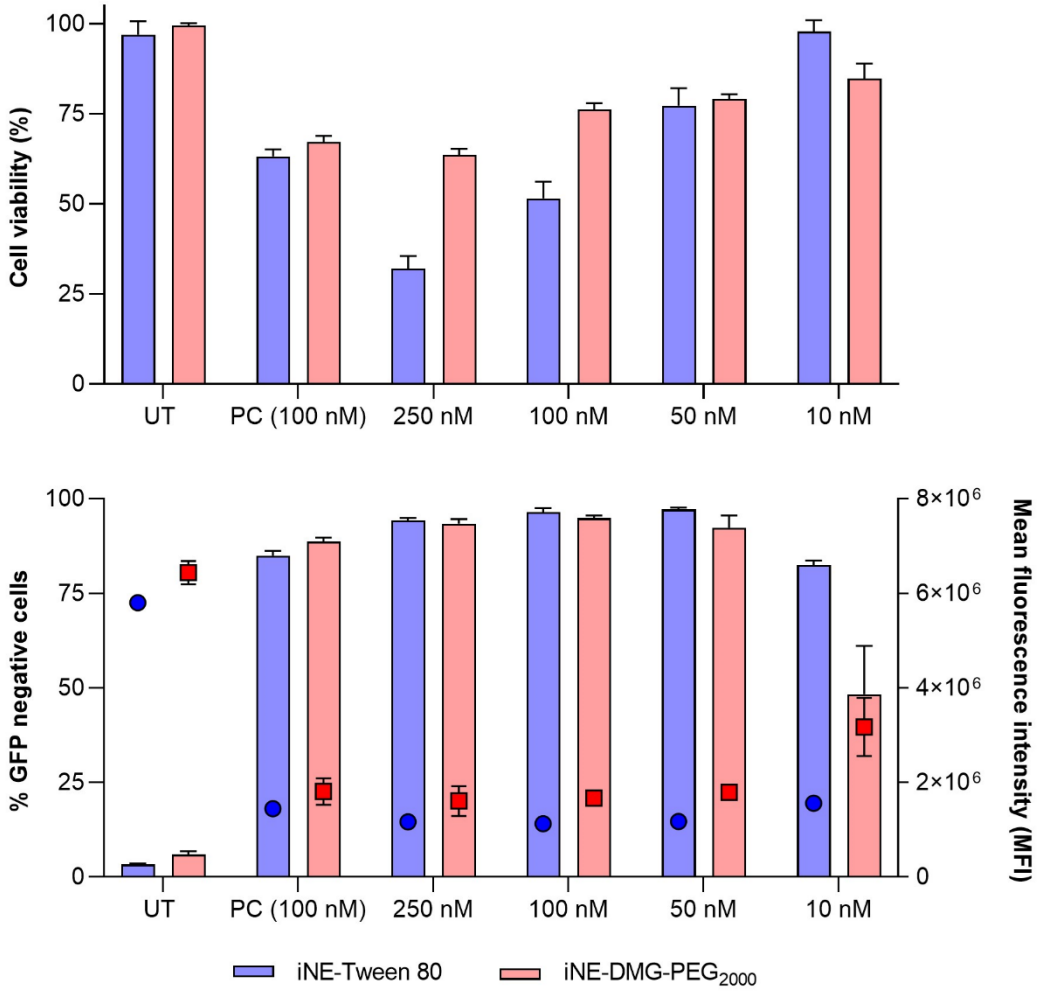

Figure 4. Cytotoxicity (top) and GFP silencing effect (bottom) of iNE-Tween 80 (blue) and iNE-DMG-PEG$_{2000}$ (red) containing siGFP, in HeLa cells expressing GFP. The silencing effect was determined in terms of the percentage of GFP negative cells (bottom, left axis, bars) and mean fluorescence intensity (bottom, right axis, symbols)

Abbreviations: DMG-PEG$_{2000}$: (*R*)-methoxy-polyethyleneglycol-2000-carbamoyl-di-O-myristyl-sn-glyceride. GFP: green fluorescence protein. iNE: ionizable nanoemulsion. MFI: mean fluorescence intensity. PC: positive control, lipofectamine. siGFP: siRNA anti-GFP. UT: untreated. Values represent the mean ± standard deviation (n ≥ 3).

Further transfection efficiency was assessed in HeLa cells using mGFP entrapped into iNE-Tween 80 (Supplementary Figure 1). A decrease in cell viability was only observed at the highest concentrations (200 and 100 ng) (Supplementary Figure 1, left). Moreover, all concentration levels showed a high percentage of GFP-positive, comparable to those obtained with lipofectamine (Supplementary Figure 1, right). Notably, no significant differences in mean fluorescence intensity (MFI) were observed at any of the tested concentrations.

3.2.2. Cytotoxicity and transfection efficiency in neuron, astrocyte, and microglia cellular models

To assess the potency of iNE nanosystems to deliver oligonucleotides in the brain, *in vitro* studies were conducted in a human neuron (SH-SY5Y), rat astrocyte (C6), and human microglia (CHME-3) cell model (Figure 5), using mGFP as a model oligonucleotide.

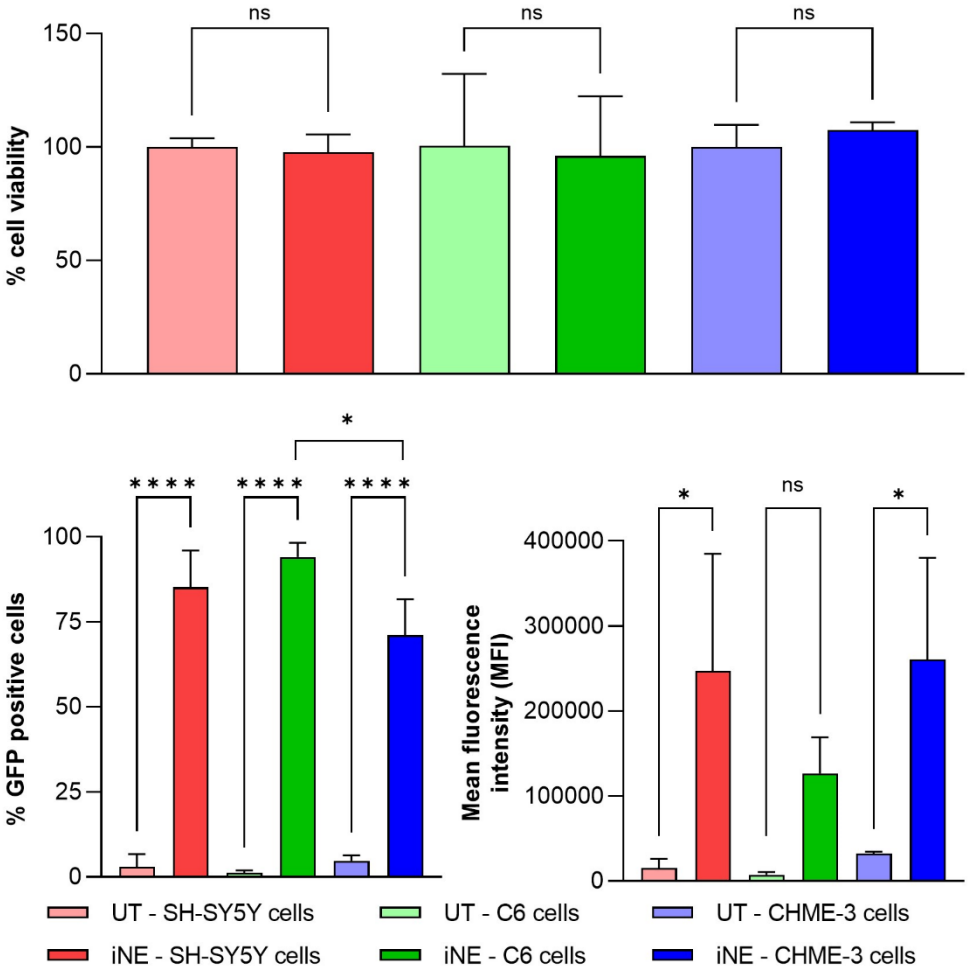

Figure 5. Cytotoxicity (top) and GFP transfection efficiency (bottom) of iNE-mGFP (bright color) in a neuron (red), astrocyte (green), and microglia (blue) cellular models. Transfection efficiency was determined in terms of the percentage of GFP-positive cells (bottom, left) and mean fluorescence intensity (bottom, right). Comparison was made with untreated cells (pale color).

Abbreviations: GFP: green fluorescence protein. iNE: ionizable nanoemulsion. MFI: mean fluorescence intensity. mGFP: mRNA encoding GFP. UT: untreated. A significant comparison was performed using an ordinary one-way ANOVA followed by Tukey's multiple comparison tests between groups. *p*-values < 0.05 were considered statistically significant (*). Also, (****) if *p*-value < 0.0001. ns: not significative. Values represent the mean ± standard deviation (n ≥ 3).

No toxicity was observed in any of the tested cell models (Figure 5, top) when compared to untreated cells. In terms of transfection efficiency, significant levels of GFP-transfected cells were detected in all three cellular models compared to the untreated groups, with all cases

showing over 70% of GFP-positive cells (Figure 5, left). Moreover, slightly greater levels of transfection were found in C6 cells, as compared to CHME-3 cells. However, in terms of fluorescence intensity (Figure 5, right), iNE-mGFP did not result in significantly increased levels of fluorescence in C6 cells, whereas this behavior was observed for both SH-SY5Y and CHME-3 cells, as compared with the untreated groups. A possible explanation for this difference in performance would be that while iNE-mGFP is capable of being uptake by all three cellular models and translating mGFP into the reported protein, the efficacy of this process is significantly more efficient for SH-SY5Y and CHME-3 cells than C6 cells.

No comparison was made with positive control (Lipofectamine) since unexpectedly high toxicity was observed when cells were transfected at the same concentration used for iNE-mGFP carriers. This led to misleading negative transfection results for the positive control. Considering the relatively high concentration of mGFP used in these studies, further experiments are needed with the positive control, reducing the mGFP concentration to reach a non-toxic level that allows a valid comparison with iNE-mGFP.

3.3. In vivo assessment of diffusion of ionizable nanoemulsions in the brain

3.3.1. Intra-dentate gyrus administration of miR-132-loaded ionizable nanoemulsions

Direct intracranial administration of iNE-miR-132 and iNE-miR-control was performed at the dentate gyrus (DG) region of the hippocampus. Levels of miR-132 were determined in both the injection site and the adjacent Cornu ammonis (CA) regions to assess the diffusion of the iNE and the RNA payload in the hippocampus (Figure 6). Moreover, miR-control was used intended to discriminate unspecific modulation of the miR-132 levels, due to the complexity of the pathways in which miR-132 is involved.

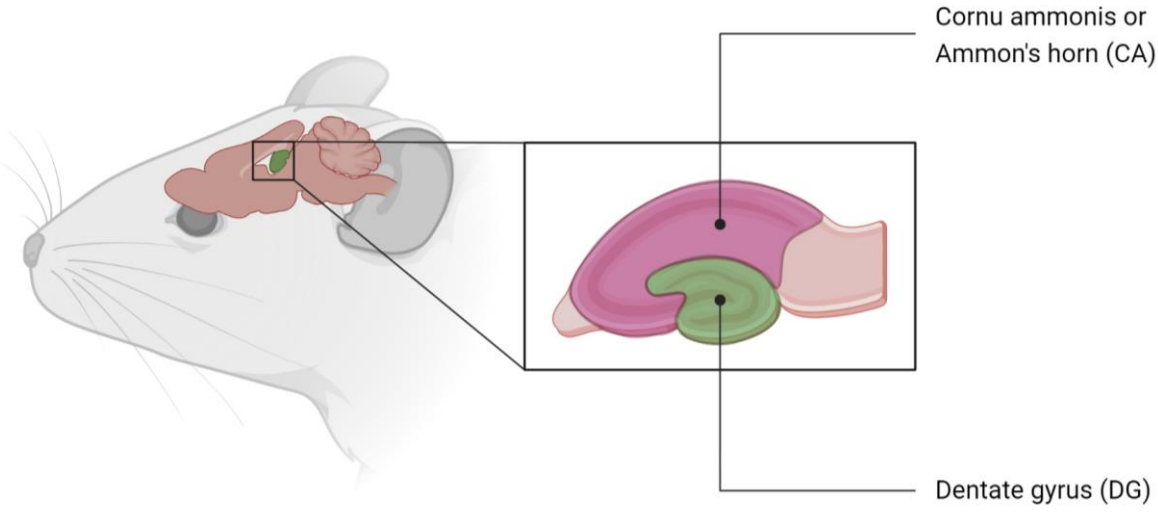

Figure 6. Schematic representation of the different regions of the hippocampus under study
Created with https://biorender.com.

After administration, miR-132 levels were determined in these two regions at two different iNE-miRNA doses: 300 pmol (Figure 7, red) and 75 pmol (Figure 7, blue). Classical LNPs (composition of patisiran, also known as Ompattro®, being considered the most established nanocarrier for siRNA delivery) were used as a positive control (Figure 7, green) to compare their diffusivity with the novel iNE [40,41]. In this case, the dose administered was 160 pmol per animal, which is considered sufficient to depict the silencing effect. A comparison between the three groups was made after being loaded with miR-132 (Figure 7, bright color) and miR-control (Figure 7, pale color).

As observed, increased levels of miR-132 were found in both DG and CA for iNE-miR-132 and LNPs-miR-132. In contrast, when nanocarriers were loaded with miR-control, no significant responses were elicited, demonstrating a specific modulation of the miR-132 levels. Notably, iNE-miR-132 reported significantly higher levels of miR-132 than LNP-miR-132, even when a considerably lower dose of miR-132 was used, a fact that might be related to the enhanced diffusion of iNE-miR-132.

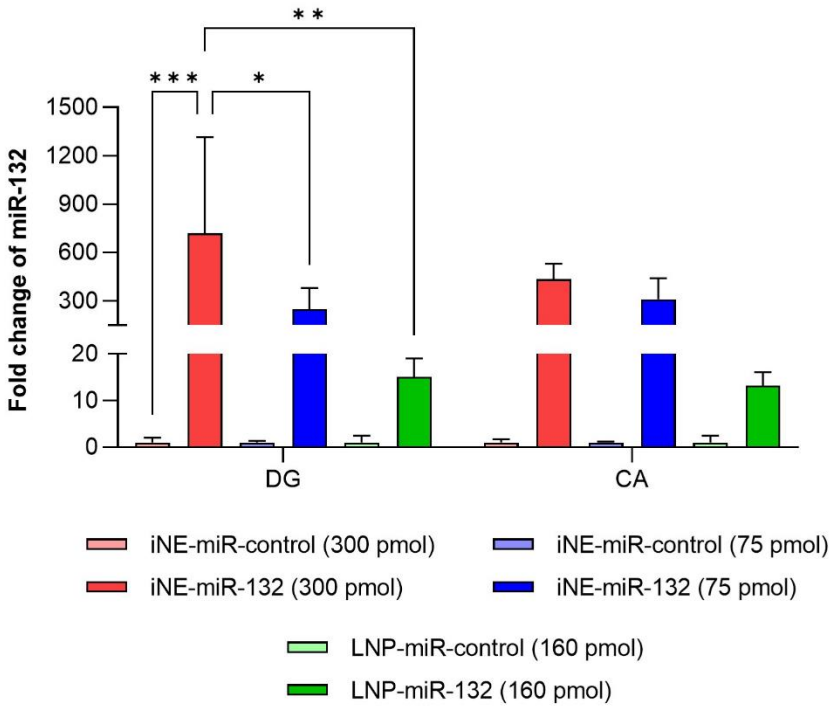

Figure 7. Semi-quantitative real-time PCR of miR-132 levels in the DG and surrounding CA regions in the hippocampus, 48 hours post-injection of iNE (at a dose of 300 pmol in red, and 75 pmol in blue) and LNPs (green), loaded with miR-132 (bright color) or miR-control (pale color)

Abbreviations: iNE: ionizable nanoemulsions. LNP: lipid nanoparticle. miR-132: miRNA-132 mimic. A significant comparison was performed using two-way ANOVA followed by Tukey's multiple comparison tests between groups. *p*-values < 0.05 were considered statistically significant (*). Also, (**) if *p*-value < 0.01, (***) if *p*-value < 0.001. Values represent the mean ± standard deviation (n ≥ 3).

On the other hand, to evaluate the possible CNS toxicity induced by the nanocarriers, levels of different inflammation makers were determined (Figure 8). A dose-dependent toxicity

profile was observed. Despite no significant differences being found, iNE-miR-132 at the highest dose (300 pmol) resulted in slightly higher toxic makers than the lower dose (75 pmol) and the LNP-miR-132 (160 pmol). In the particular case of iNE-miR-control (300 pmol), significantly higher toxicity levels were found in comparison to iNE-miR-132. These toxicity levels could be explained due to interferon responses related to the miR-132 or miR-control themselves, or the inherent toxicity of the nanocarriers. Further dose-dependent studies must be performed to elucidate the behavior of these nanosystems at non-toxic concentrations.

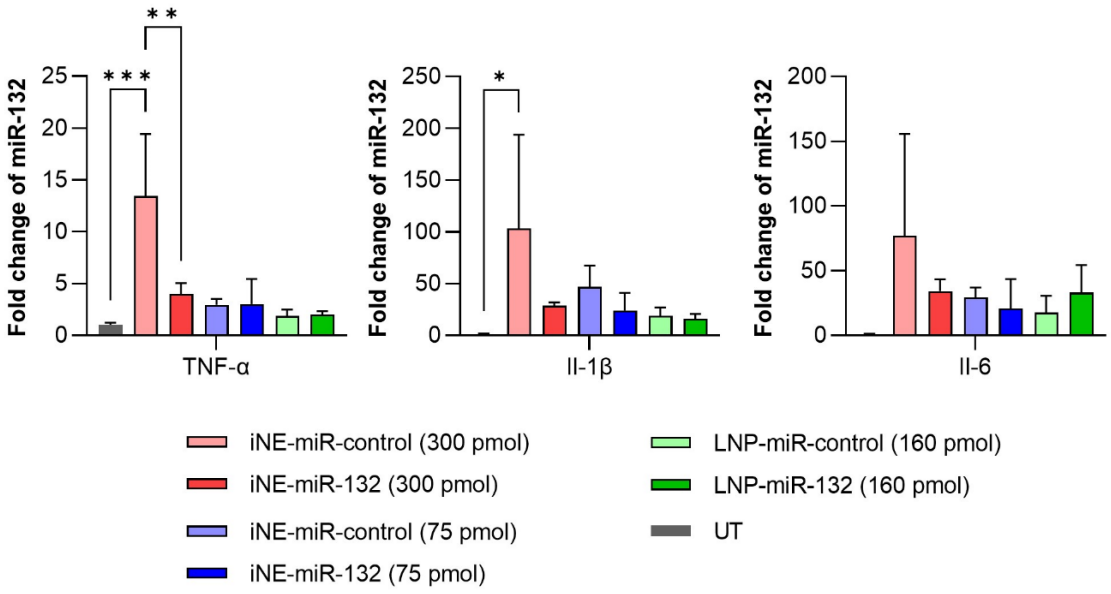

Figure 8. Semi-quantitative real-time PCR of inflammation marker gene levels in DG 48 hours post administration of iNE (at a dose of 300 pmol in red, and 75 pmol in blue) and LNPs (green), loaded with miR-132 (bright color) or miR-control (pale color)

Abbreviations: Il-1ß: interleukin-1ß. Il-6: interleukin-6. iNE: ionizable nanoemulsions. LNP: lipid nanoparticle. miR-132: miRNA-132 mimic. TNF-α: tumor necrosis factor-α. A significant comparison was performed using an ordinary one-way ANOVA followed by Tukey's multiple comparison tests between groups. *p*-values < 0.05 were considered statistically significant (*). Also, (**) if *p*-value < 0.01, (***) if *p*-value < 0.001. Values represent the mean ± standard deviation (n ≥ 3).

To assess the functionality of the delivered oligonucleotide cargo, levels of different miR-132-targeted mRNAs were evaluated (Supplementary Figure 2). Five miR-132 targets (*Btg2*, *p250Gap*, *Sall1*, *Dpysl3*, and *Dixdc1*) were assessed (Supplementary Figure 2, top), and the average change of their combined expression levels was evaluated as a miR-132 functional signature (Supplementary Figure 2, bottom). Only LNP-miR-132 resulted in a significant decrease in the mRNA target levels. One possible explanation for the lack of effect on target mRNA levels of iNE-miR-132 could be the high miR-132 overexpression, which might saturate the endogenous miRNA machinery, leading to a lower reduction of the mRNA target levels or even induce other toxicity effects [42,43].

Overall, iNE-miR-132 showed preliminary evidence of enhanced diffusion, as compared with LNP-miR-132 at lower doses. However, no changes were observed in the targeted mRNA levels studied. Further optimization or assessment of this behavior must be performed, aimed

at elucidating the cause and finding an efficient solution that allows not only the diffusion of the RNA cargo but also its adequate transfection.

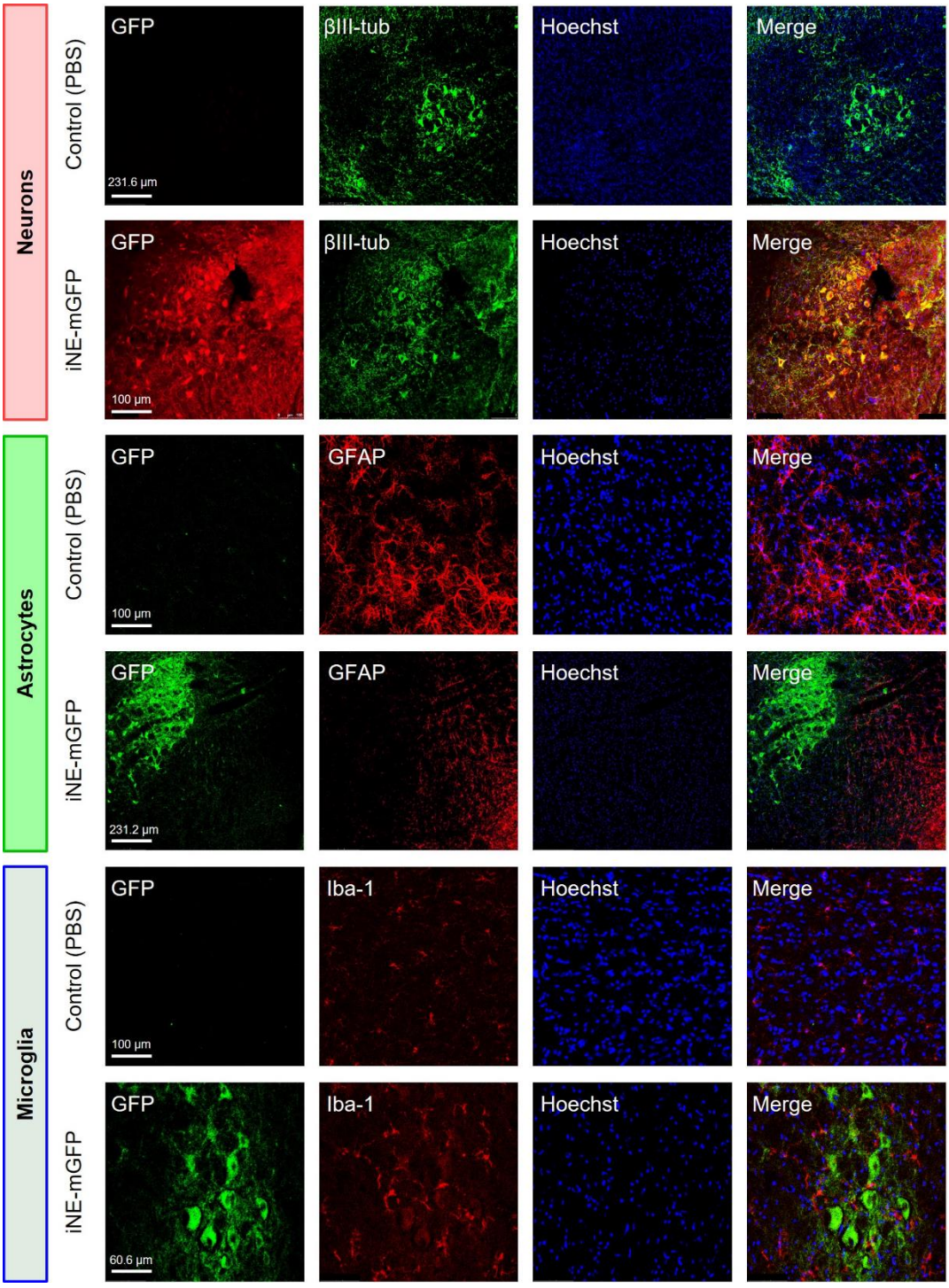

Figure 9. Immunolabelling for GFP in neurons (labeled with ßIII-tubulin), astrocytes (labeled with GFAP), and microglia (labeled with Iba-1) cells in rats after intraparenchymal administration of control (PBS) or iNE-mGFP. Hoechst was used as nuclei marker

Abbreviations: ßIII-tubulin: class III ß-tubulin. GFAP: glial fibrillary acidic protein. GFP: green fluorescence protein. Iba-1: ionized calcium-binding adaptor molecule 1. iNE: ionizable nanoemulsion. mGFP: mRNA GFP.

3.3.2. Intra-parenchymal administration of mGFP-loaded ionizable nanoemulsions

Direct intra-parenchymal administration of iNEs loaded with mGFP was performed to further determine simultaneously their diffusivity and functional performance.

After 24h, animals were sacrificed and immunolabelling was performed to determine the transfection of neurons, astrocytes, and microglia (Figure 9). Neuron analysis needed a double immunolabelling process due to the inherent fluorescence found in neurons (Supplementary Figure 3). The images showed clear GFP signals in neurons and microglia, thus indicating the uptake of the ionizable nanocarriers by these cellular types and the subsequent translation of the reporter protein. Interestingly, this behavior was not observed in astrocytes, in consonance with the fluorescence intensity results obtained *in vitro* (Figure 5, bottom right). This result suggests the specificity of iNE for microglia and, to a greater extent, neurons. Such behavior highlights the potential of this nanocarrier for neuron-specific diseases, such as amyotrophic lateral sclerosis (ALS), or conditions related to microglia malfunction, such as Alzheimer's or Parkinson's disease [44,45]. Nevertheless, this conclusion should be taken cautiously as biodistribution may be highly influenced by the disease conditions.

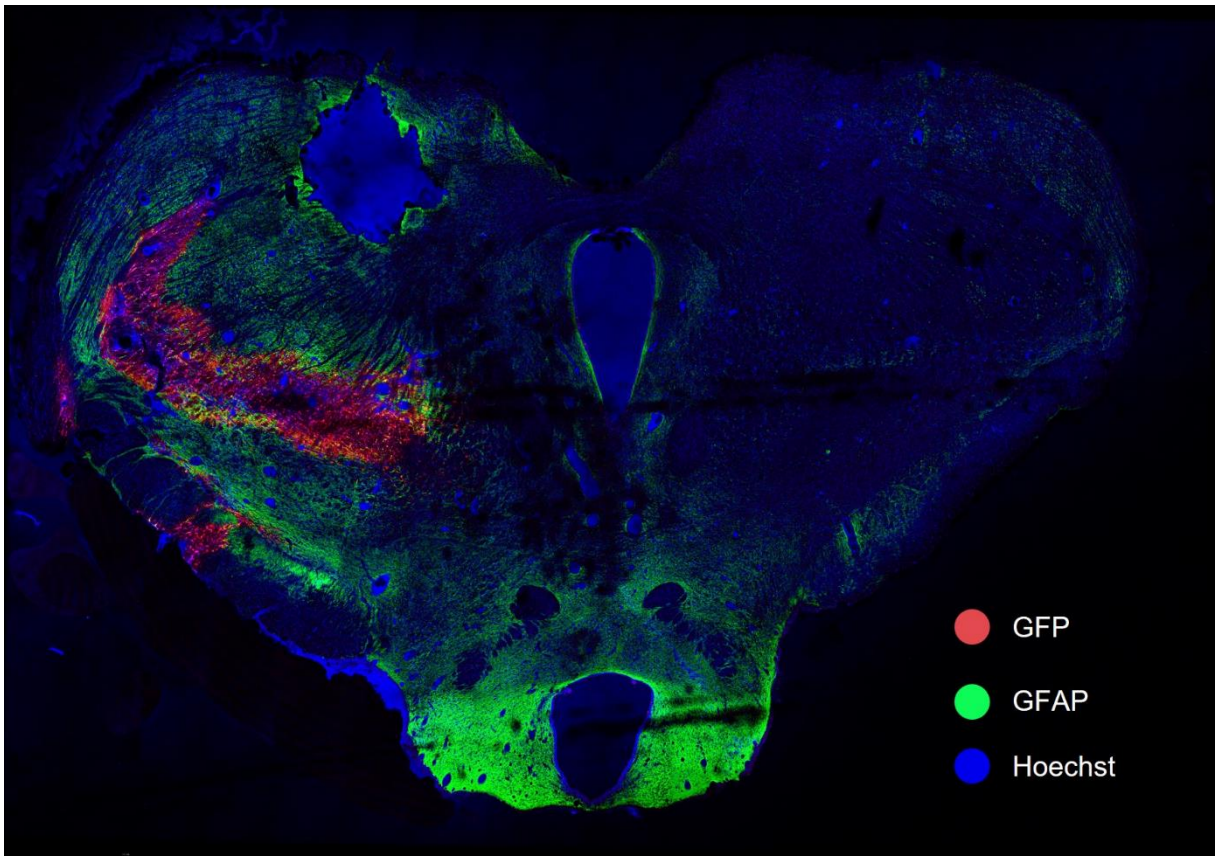

Figure 10. Double immunolabeling in the whole brain for GFP (red) and astrocytes (labeled with GFAP, green), after intraparenchymal administration of iNE-mGFP. Hoechst was used as nuclei marker (blue)

Abbreviations: GFAP: glial fibrillary acidic protein. GFP: green fluorescence protein. iNE: ionizable nanoemulsion. mGFP: mRNA encoding GFP.

Once the transfection efficiency of the iNE was confirmed, the diffusivity of the nanocarriers was assessed in the entire brain of the animals (Figure 10). Considerable diffusion was observed from the injection site, indicated by a GFP signal (in red), to more distant areas in the same hemisphere. Moreover, close-up images confirmed the colocalization of the fluorescence protein in the neurons (Supplementary Figure 4). The specificity of the signal was corroborated by the lack of fluorescence observed upon administration of PBS (Supplementary Figure 5). We hypothesize that the distribution profile observed could be attributed to diverse factors present in our iNEs. Firstly, diffusivity could be driven by the oily core of the iNEs of the nanocarrier. Previous work developed in our group with polyaminoacid nanocapsules (containing an oily core) resulted in tissular diffusivity upon subcutaneous administration, which was attributed to a combination of the particle diameter (around 100 nm) and the composition of the nanocarrier [46,47]. Moreover, the PEGylated surface of iNEs could also facilitate the diffusivity capacity, as it has been proven the positive influence of PEGylated components in NPs to enhance the diffusivity in both mucus and the brain [23,24].

These findings prove the potential of iNE to diffuse to various brain areas and efficiently transfect mRNA into neurons and microglia, with further confirmation of the transduction of the desired model protein. These results suggest that iNE can facilitate the delivery of genetic cargo to different brain regions after a single administration.

4. CONCLUSIONS

In this work, we have explored the potential to enhance the diffusivity of the current gold standard for RNA delivery, namely LNPs, by incorporating ionizable lipids into traditional NEs, leading to the development of a novel class of nanocarriers termed iNEs. The resulting nanocarrier presented the desired physicochemical properties, including a size smaller than 100 nm, a neutral surface charge, and exceptional RNA entrapment capabilities, making it a promising candidate for the delivery of RNA to the brain. Furthermore, *in vitro* assessment conducted in HeLa, SH-SY5Y, C6, and CHME cells revealed high cell viability levels at the concentrations tested, along with a favorable transfection profile.

In terms of direct *in vivo* brain administration, iNE loaded with miR-132 demonstrated substantial cargo accumulation not only at the administration site but also in adjacent regions. These findings prompted further investigation into the diffusion pattern of the formulation, as well as the identification of the specific CNS cells targeted by our nanocarrier. Using iNEs containing mGFP, we observed extraordinary diffusion from the injection site, with a particular preferential transfection of neurons and microglia.

In brief, this chapter describes the development of a novel class of ionizable nanocarriers designed for RNA delivery to the brain, with a promising diffusion pattern and specific targeting capability for neurons and microglia. Such nanocarriers hold great promise for the treatment of different CNS diseases, such as ALS, Alzheimer’s, or Parkinson’s diseases.

5. SUPPLEMENTARY INFORMATION

Supplementary Table 1. Physicochemical properties of variations of iNE with different Tween 80 and different types of oligonucleotides

Type or RNA	Size (nm)	PDI	ζ-Potential (mV)	Encapsulation efficiency (%)
siGFP (n = 1)	171	0.02	+21	80-90
mGFP (n = 2)	159 ± 2	0.09 ± 0.01	+20 ± 2	80-90

ζ-Potential was measured upon dilution in water for the formulations containing Tween 80. Encapsulation efficiency was measured by agarose gel, and values were corroborated by RiboGreen assay. **Abbreviations:** GFP: green fluorescence protein. mGFP: mRNA encoding GFP. miR-control: scrambled miRNA. PDI: polydispersity index. siGFP: siRNA anti-GFP. Values represent the mean ± standard deviation.

Supplementary Table 2. Physicochemical properties of iNE-miR-control before and after the concentration process

Concentration	Size (nm)	PDI	ζ-Potential (mV)	Encapsulation efficiency (%)	miR-control concentration (mg/mL)
Before	61 ± 5	0.18 ± 0.06	-1.1 ± 0.1	82 ± 3.5	0.2 ± 0.03
After	68 ± 12	0.2 ± 0.05	-0.8 ± 1.1	77 ± 9.1	1.9 ± 0.4

Encapsulation efficiency was measured by RiboGreen assay. **Abbreviations:** PDI: polydispersity index. Values represent the mean ± standard deviation (n ≥ 2).

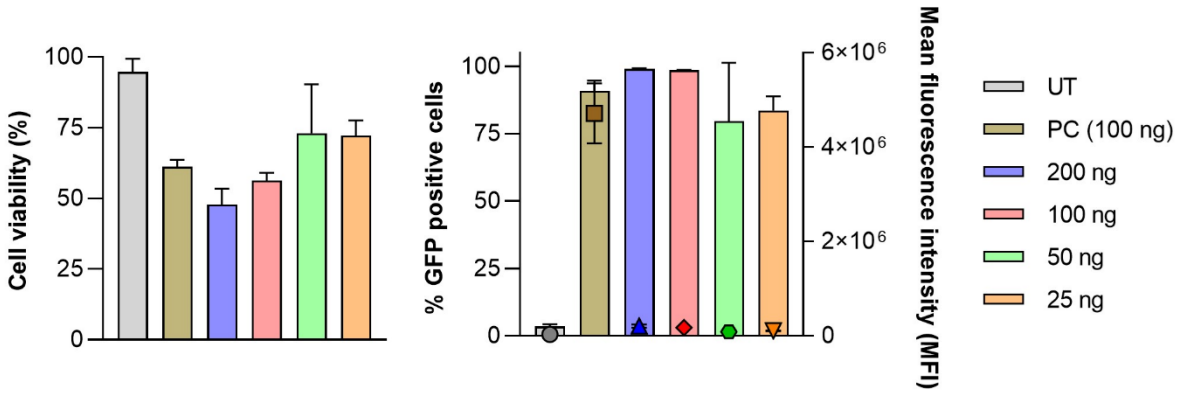

Supplementary Figure 1. Cytotoxicity (left) and GFP transfection effect (right) of iNE-DMG-Tween 80 containing mGFP at different concentrations, in HeLa cells. Transfection efficiency was determined in terms of the percentage of GFP-positive cells (right, left axis, bars) and mean fluorescence intensity (right, right axis, symbols)

Abbreviations: GFP: green fluorescence protein. iNE: ionizable nanoemulsion. MFI: mean fluorescence intensity. mGFP: mRNA encoding GFP. PC: positive control, lipofectamine. UT: untreated. Values represent the mean ± standard deviation (n ≥ 3).

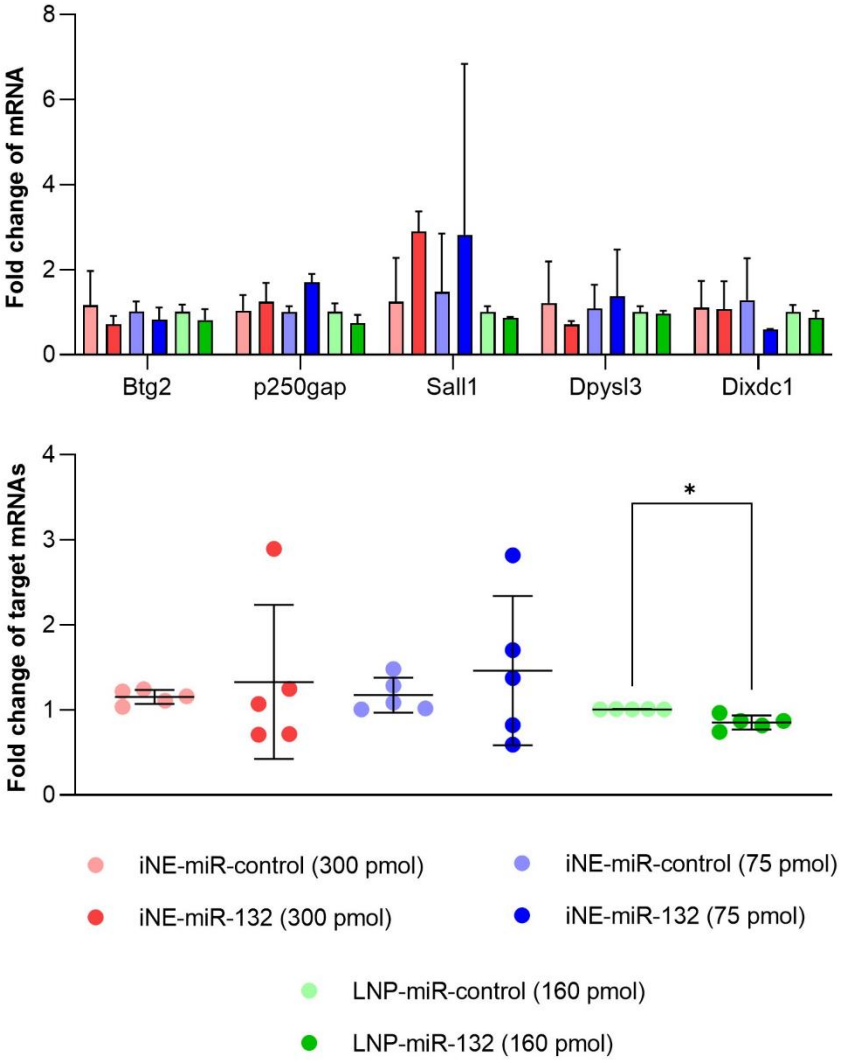

Supplementary Figure 2. Semi-quantitative real-time PCR of different miR-132 mRNA targets (*Btg2*, *p250Gap*, *Sall1*, *Dpysl3*, and *Dixdc1*) (top) and the functional signature of miR-132 represented by the average fold change of the predicted miR-132 mRNA targets (bottom). Comparison was made between iNE (at a dose of 300 pmol in red, and 75 pmol in blue) and LNPs (green), loaded with miR-132 (bright color) or miR-control (pale color)

Abbreviations: iNE: ionizable nanoemulsions. LNP: lipid nanoparticle. miR-132: miRNA-132 mimic. A significant comparison was performed using a multiple unpaired t-test with Welch correction. *p*-values < 0.05 were considered statistically significant (*). Values represent the mean ± standard deviation (n ≥ 3).

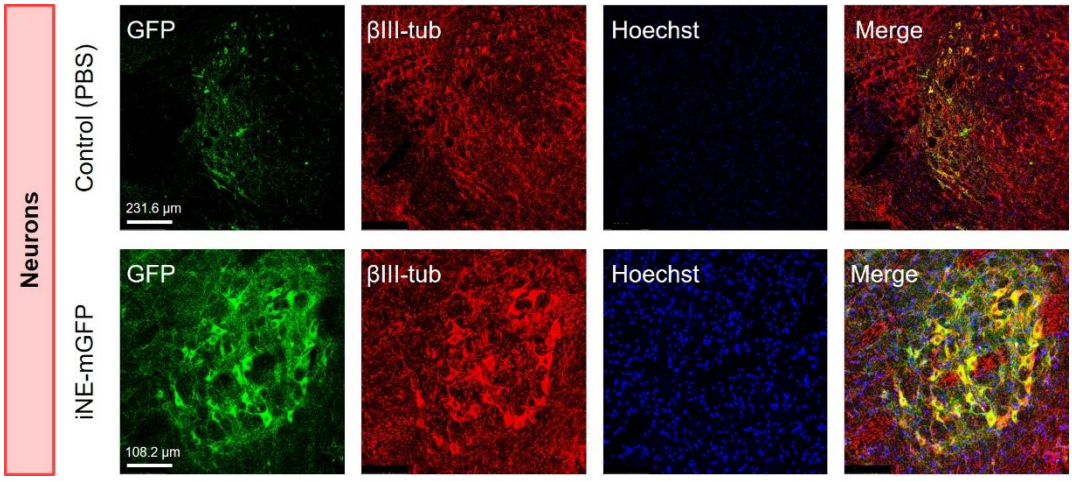

Supplementary Figure 3. Double immunolabelling for GFP in neurons (labeled with ßIII-tubulin) cells in rats after intraparenchymal administration of control or iNE-mGFP. Hoechst was used as nuclei marker

Abbreviations: ßIII-tubulin: class III ß-tubulin. GFP: green fluorescence protein. iNE: ionizable nanoemulsion. mGFP: mRNA encoding GFP.

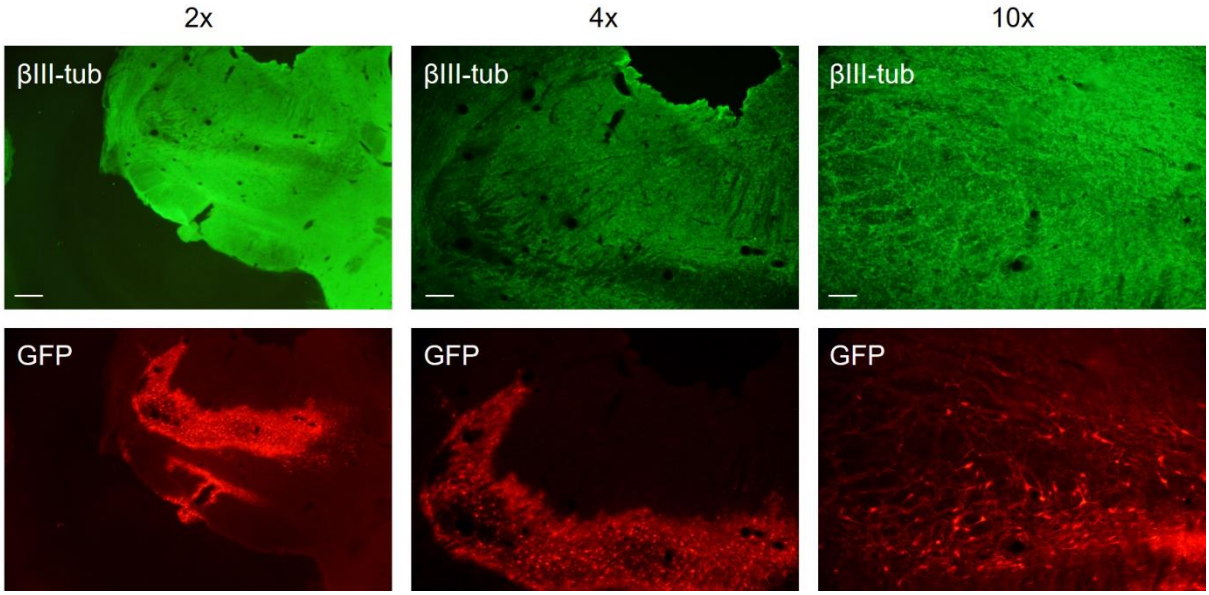

Supplementary Figure 4. Double immunolabelling of the injection site in a rat administered with iNE-mGFP, at different magnification levels (2x, 4x, and 10x). Labeling was performed for GFP (red) in neurons (labeled with ßIII-tubulin, green)

Abbreviations: ßIII-tubulin: class III ß-tubulin. GFP: green fluorescence protein. iNE: ionizable nanoemulsion. mGFP: mRNA encoding GFP.

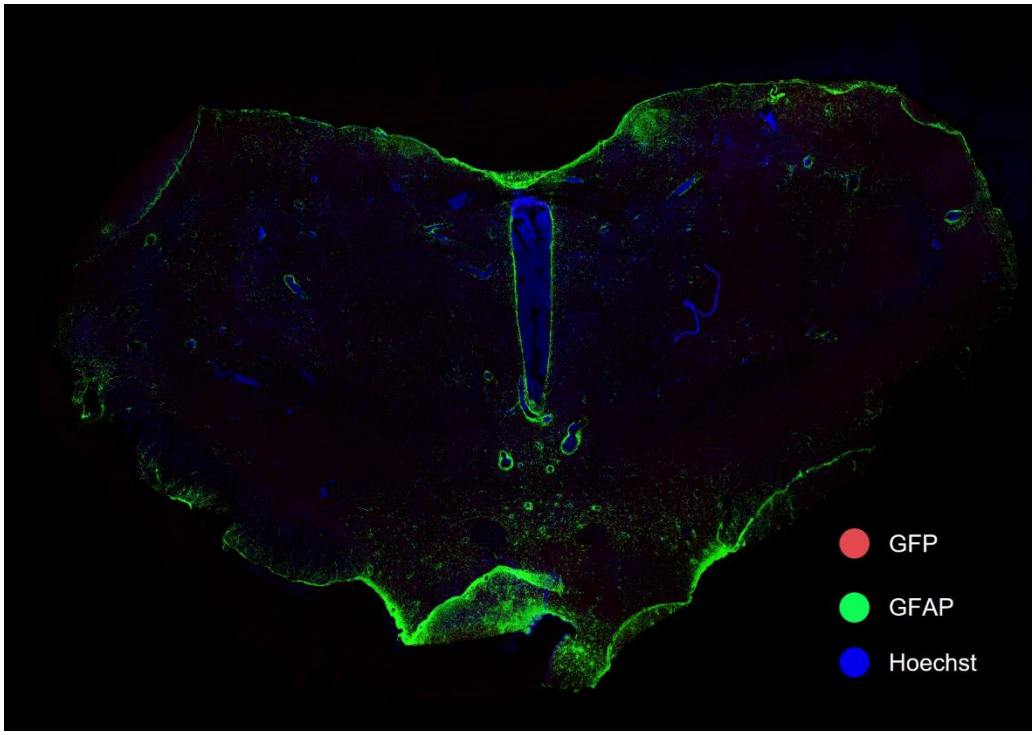

Supplementary Figure 5. Double immunolabeling in the whole brain for GFP (red) and astrocytes (marked with GFAP, green), after intraparenchymal administration of control (PBS). Hoechst was used as nuclei marker (blue)

Abbreviations: GFAP: glial fibrillary acidic protein. GFP: green fluorescence protein. mGFP: mRNA encoding GFP.

6. ACKNOWLEDGMENTS

This work was supported by the B-SMART project, funded by the European Union's Horizon 2020 research and innovation program, under grant agreement No 721058. Mireya L. Borrajo acknowledges the financial support by Instituto de Salud Carlos III, through the "Contratos i-PFIS: Doctorados ISS-empresa en Ciencias y Tecnologías de la Salud" grant.

In vitro cytotoxicity and transfection efficacy studies in HeLa cells were performed in collaboration with David Moreira, Ph.D, and Prof. Mabel Loza from BioFarma Research Group, CiMUS (Spain). *In vivo* assessment of intro-dentate gyrus administration of iNE was performed in collaboration with Hannah Walgrave, Ph.D, from the Vlaams Instituut voor Biotechnologie (Belgium). *In vitro* cytotoxicity and transfection efficacy studies in neuron, astrocyte, and microglia models, as well as *in vivo* assessment of intra-parenchymal administration of iNE was performed in collaboration with Aloia Quijano, MSc, Rita Valenzuela, Ph.D, and Prof. José Labandeira, from Molecular Neurobiology and Parkinson's disease Group, CiMUS (Spain).

7. REFERENCES

[1] M. Verma, I. Ozer, W. Xie, R. Gallagher, A. Teixeira, M. Choy, The landscape for lipid-nanoparticle-based genomic medicines, Nat. Rev. Drug Discov. 22 (2023) 349–350. https://doi.org/10.1038/d41573-023-00002-2.

[2] S.M. Hoy, Patisiran: First Global Approval, Drugs. 78 (2018) 1625–1631. https://doi.org/10.1007/s40265-018-0983-6.

[3] T. Fiolet, Y. Kherabi, C.-J. MacDonald, J. Ghosn, N. Peiffer-Smadja, Comparing COVID-19 vaccines for their characteristics, efficacy and effectiveness against SARS-CoV-2 and variants of concern: a narrative review, Clin. Microbiol. Infect. 28 (2022) 202–221. https://doi.org/10.1016/j.cmi.2021.10.005.

[4] J. Kim, Y. Eygeris, M. Gupta, G. Sahay, Self-assembled mRNA vaccines, Adv. Drug Deliv. Rev. 170 (2021) 83–112. https://doi.org/10.1016/j.addr.2020.12.014.

[5] P.R. Cullis, M.J. Hope, Lipid Nanoparticle Systems for Enabling Gene Therapies, Mol. Ther. 25 (2017) 1467–1475. https://doi.org/10.1016/j.ymthe.2017.03.013.

[6] G. Sahay, D.Y. Alakhova, A. V. Kabanov, Endocytosis of nanomedicines, J. Control. Release. 145 (2010) 182–195. https://doi.org/10.1016/j.jconrel.2010.01.036.

[7] S. Patel, J. Kim, M. Herrera, A. Mukherjee, A. V. Kabanov, G. Sahay, Brief update on endocytosis of nanomedicines, Adv. Drug Deliv. Rev. 144 (2019) 90–111. https://doi.org/10.1016/j.addr.2019.08.004.

[8] J. Heyes, L. Palmer, K. Bremner, I. MacLachlan, Cationic lipid saturation influences intracellular delivery of encapsulated nucleic acids, J. Control. Release. 107 (2005) 276–287. https://doi.org/10.1016/j.jconrel.2005.06.014.

[9] M. Jayaraman, S.M. Ansell, B.L. Mui, Y.K. Tam, J. Chen, X. Du, D. Butler, L. Eltepu, S. Matsuda, J.K. Narayanannair, K.G. Rajeev, I.M. Hafez, A. Akinc, M.A. Maier, M.A. Tracy, P.R. Cullis, T.D. Madden, M. Manoharan, M.J. Hope, Maximizing the Potency of siRNA Lipid Nanoparticles for Hepatic Gene Silencing In Vivo, Angew. Chemie Int. Ed. 51 (2012) 8529–8533. https://doi.org/10.1002/anie.201203263.

[10] X. Han, H. Zhang, K. Butowska, K.L. Swingle, M.G. Alameh, D. Weissman, M.J. Mitchell, An ionizable lipid toolbox for RNA delivery, Nat. Commun. 12 (2021) 8–13. https://doi.org/10.1038/s41467-021-27493-0.

[11] A.M. Reichmuth, M.A. Oberli, A. Jaklenec, R. Langer, D. Blankschtein, mRNA vaccine delivery using lipid nanoparticles, Ther. Deliv. 7 (2016) 319–334. https://doi.org/10.4155/tde-2016-0006.

[12] S.-T. Yang, A.J.B. Kreutzberger, J. Lee, V. Kiessling, L.K. Tamm, The role of cholesterol in membrane fusion, Chem. Phys. Lipids. 199 (2016) 136–143. https://doi.org/10.1016/j.chemphyslip.2016.05.003.

[13] J.A. Kulkarni, D. Witzigmann, J. Leung, Y.Y.C. Tam, P.R. Cullis, On the role of helper lipids in lipid nanoparticle formulations of siRNA, Nanoscale. 11 (2019) 21733–21739. https://doi.org/10.1039/c9nr09347h.

[14] P. Harvie, F.M.P. Wong, M.B. Bally, Use of Poly(ethylene glycol)–Lipid Conjugates to Regulate

the Surface Attributes and Transfection Activity of Lipid–DNA Particles, J. Pharm. Sci. 89 (2000) 652–663. https://doi.org/10.1002/(SICI)1520-6017(200005)89:5<652::AID-JPS11>3.0.CO;2-H.

[15] J.A. Kulkarni, D. Witzigmann, J. Leung, R. van der Meel, J. Zaifman, M.M. Darjuan, H.M. Grisch-Chan, B. Thöny, Y.Y.C. Tam, P.R. Cullis, Fusion-dependent formation of lipid nanoparticles containing macromolecular payloads, Nanoscale. 11 (2019) 9023–9031. https://doi.org/10.1039/C9NR02004G.

[16] R.L. Rungta, H.B. Choi, P.J. Lin, R.W. Ko, D. Ashby, J. Nair, M. Manoharan, P.R. Cullis, B.A. MacVicar, Lipid Nanoparticle Delivery of siRNA to Silence Neuronal Gene Expression in the Brain, Mol. Ther. Acids. 2 (2013) e136. https://doi.org/10.1038/mtna.2013.65.

[17] L.E. Waggoner, K.F. Miyasaki, E.J. Kwon, Analysis of PEG-lipid anchor length on lipid nanoparticle pharmacokinetics and activity in a mouse model of traumatic brain injury, Biomater. Sci. (2023) 4238–4253. https://doi.org/10.1039/d2bm01846b.

[18] H. Tanaka, T. Nakatani, T. Furihata, K. Tange, Y. Nakai, H. Yoshioka, H. Harashima, H. Akita, In Vivo Introduction of mRNA Encapsulated in Lipid Nanoparticles to Brain Neuronal Cells and Astrocytes via Intracerebroventricular Administration, Mol. Pharm. 15 (2018) 2060–2067. https://doi.org/10.1021/acs.molpharmaceut.7b01084.

[19] S. Liu, J. Liu, H. Li, K. Mao, H. Wang, X. Meng, J. Wang, C. Wu, H. Chen, X. Wang, X. Cong, Y. Hou, Y. Wang, M. Wang, Y.-G. Yang, T. Sun, An optimized ionizable cationic lipid for brain tumor-targeted siRNA delivery and glioblastoma immunotherapy, Biomaterials. 287 (2022) 121645. https://doi.org/10.1016/j.biomaterials.2022.121645.

[20] Y. Eygeris, S. Patel, A. Jozic, G. Sahay, Deconvoluting Lipid Nanoparticle Structure for Messenger RNA Delivery, Nano Lett. 20 (2020) 4543–4549. https://doi.org/10.1021/acs.nanolett.0c01386.

[21] A.B. Etame, R.J. Diaz, M.A. O'Reilly, C.A. Smith, T.G. Mainprize, K. Hynynen, J.T. Rutka, Enhanced delivery of gold nanoparticles with therapeutic potential into the brain using MRI-guided focused ultrasound, Nanomedicine Nanotechnology, Biol. Med. 8 (2012) 1133–1142. https://doi.org/10.1016/j.nano.2012.02.003.

[22] S. Pan, P.H. Yang, D. DeFreitas, S. Ramagiri, P.O. Bayguinov, C.D. Hacker, A.Z. Snyder, J. Wilborn, H. Huang, G.M. Koller, D.K. Raval, G.L. Halupnik, S. Sviben, S. Achilefu, R. Tang, G. Haller, J.D. Quirk, J.A.J. Fitzpatrick, P. Esakky, J.M. Strahle, Gold nanoparticle-enhanced X-ray microtomography of the rodent reveals region-specific cerebrospinal fluid circulation in the brain, Nat. Commun. 14 (2023) 453. https://doi.org/10.1038/s41467-023-36083-1.

[23] S.K. Lai, D.E. O'Hanlon, S. Harrold, S.T. Man, Y.-Y. Wang, R. Cone, J. Hanes, Rapid transport of large polymeric nanoparticles in fresh undiluted human mucus, Proc. Natl. Acad. Sci. 104 (2007) 1482–1487. https://doi.org/10.1073/pnas.0608611104.

[24] E.A. Nance, G.F. Woodworth, K.A. Sailor, T.-Y. Shih, Q. Xu, G. Swaminathan, D. Xiang, C. Eberhart, J. Hanes, A Dense Poly(Ethylene Glycol) Coating Improves Penetration of Large Polymeric Nanoparticles Within Brain Tissue, Sci. Transl. Med. 4 (2012) 1–7. https://doi.org/10.1126/scitranslmed.3003594.

[25] A.A. Date, N. Desai, R. Dixit, M. Nagarsenker, Self-nanoemulsifying drug delivery systems: formulation insights, applications and advances, Nanomedicine. 5 (2010) 1595–1616.

https://doi.org/10.2217/nnm.10.126.

[26] M.R. Patel, R.B. Patel, S.D. Thakore, Nanoemulsion in drug delivery, in: Appl. Nanocomposite Mater. Drug Deliv., Elsevier, 2018: pp. 667–700. https://doi.org/10.1016/B978-0-12-813741-3.00030-3.

[27] K.B. Sutradhar, M.L. Amin, Nanoemulsions: increasing possibilities in drug delivery, Eur. J. Nanomedicine. 5 (2013). https://doi.org/10.1515/ejnm-2013-0001.

[28] L.A. Brito, M. Chan, C.A. Shaw, A. Hekele, T. Carsillo, M. Schaefer, J. Archer, A. Seubert, G.R. Otten, C.W. Beard, A.K. Dey, A. Lilja, N.M. Valiante, P.W. Mason, C.W. Mandl, S.W. Barnett, P.R. Dormitzer, J.B. Ulmer, M. Singh, D.T. O'Hagan, A.J. Geall, A Cationic Nanoemulsion for the Delivery of Next-generation RNA Vaccines, Mol. Ther. 22 (2014) 2118–2129. https://doi.org/10.1038/mt.2014.133.

[29] W.M. Bogers, H. Oostermeijer, P. Mooij, G. Koopman, E.J. Verschoor, D. Davis, J.B. Ulmer, L.A. Brito, Y. Cu, K. Banerjee, G.R. Otten, B. Burke, A. Dey, J.L. Heeney, X. Shen, G.D. Tomaras, C. Labranche, D.C. Montefiori, H.-X. Liao, B. Haynes, A.J. Geall, S.W. Barnett, Potent Immune Responses in Rhesus Macaques Induced by Nonviral Delivery of a Self-amplifying RNA Vaccine Expressing HIV Type 1 Envelope With a Cationic Nanoemulsion, J. Infect. Dis. 211 (2015) 947–955. https://doi.org/10.1093/infdis/jiu522.

[30] P.T. Wong, P.H. Goff, R.J. Sun, M.J. Ruge, M.E. Ermler, A. Sebring, J.J. O'Konek, J.J. Landers, K.W. Janczak, W. Sun, J.R. Baker, Combined Intranasal Nanoemulsion and RIG-I Activating RNA Adjuvants Enhance Mucosal, Humoral, and Cellular Immunity to Influenza Virus, Mol. Pharm. 18 (2021) 679–698. https://doi.org/10.1021/acs.molpharmaceut.0c00315.

[31] S. Yadav, S.K. Gandham, R. Panicucci, M.M. Amiji, Intranasal brain delivery of cationic nanoemulsion-encapsulated TNFα siRNA in prevention of experimental neuroinflammation, Elsevier Inc., 2016. https://doi.org/10.1016/j.nano.2015.12.374.

[32] J.H. Azambuja, R.S. Schuh, L.R. Michels, N.E. Gelsleichter, L.R. Beckenkamp, I.C. Iser, G.S. Lenz, F.H. de Oliveira, G. Venturin, S. Greggio, J.C. DaCosta, M.R. Wink, J. Sevigny, M.A. Stefani, A.M.O. Battastini, H.F. Teixeira, E. Braganhol, Nasal Administration of Cationic Nanoemulsions as CD73-siRNA Delivery System for Glioblastoma Treatment: a New Therapeutical Approach, Mol. Neurobiol. 57 (2020) 635–649. https://doi.org/10.1007/s12035-019-01730-6.

[33] P. Calvo, C. Remuñán-López, J.L. Vila-Jato, M.J. Alonso, Development of positively charged colloidal drug carriers: Chitosan-coated polyester nanocapsules and submicron-emulsions, Colloid Polym. Sci. 275 (1997) 46–53. https://doi.org/10.1007/s003960050050.

[34] D.P. Ivanov, A.M. Grabowska, M.C. Garnett, High-throughput spheroid screens using volume, resazurin reduction, and acid phosphatase activity, Methods Mol. Biol. 1601 (2017) 43–59. https://doi.org/10.1007/978-1-4939-6960-9_4.

[35] A.K. Blakney, P.F. McKay, B.I. Yus, Y. Aldon, R.J. Shattock, Inside out: optimization of lipid nanoparticle formulations for exterior complexation and in vivo delivery of saRNA, Gene Ther. 26 (2019) 363–372. https://doi.org/10.1038/s41434-019-0095-2.

[36] S.C. Semple, A. Akinc, J. Chen, A.P. Sandhu, B.L. Mui, C.K. Cho, D.W.Y. Sah, D. Stebbing, E.J. Crosley, E. Yaworski, I.M. Hafez, J.R. Dorkin, J. Qin, K. Lam, K.G. Rajeev, K.F. Wong, L.B. Jeffs, L. Nechev, M.L. Eisenhardt, M. Jayaraman, M. Kazem, M.A. Maier, M. Srinivasulu,

M.J. Weinstein, Q. Chen, R. Alvarez, S.A. Barros, S. De, S.K. Klimuk, T. Borland, V. Kosovrasti, W.L. Cantley, Y.K. Tam, M. Manoharan, M.A. Ciufolini, M.A. Tracy, A. De Fougerolles, I. MacLachlan, P.R. Cullis, T.D. Madden, M.J. Hope, Rational design of cationic lipids for siRNA delivery, Nat. Biotechnol. 28 (2010) 172–176. https://doi.org/10.1038/nbt.1602.

[37] L.M. Bareford, P.W. Swaan, Endocytic mechanisms for targeted drug delivery, Adv. Drug Deliv. Rev. 59 (2007) 748–758. https://doi.org/10.1016/j.addr.2007.06.008.

[38] J.R. Casey, S. Grinstein, J. Orlowski, Sensors and regulators of intracellular pH, Nat. Rev. Mol. Cell Biol. 11 (2010) 50–61. https://doi.org/10.1038/nrm2820.

[39] I. Canton, G. Battaglia, Endocytosis at the nanoscale, Chem. Soc. Rev. 41 (2012) 2718. https://doi.org/10.1039/c2cs15309b.

[40] D. Adams, A. Gonzalez-Duarte, W.D. O'Riordan, C.-C. Yang, M. Ueda, A. V. Kristen, I. Tournev, H.H. Schmidt, T. Coelho, J.L. Berk, K.-P. Lin, G. Vita, S. Attarian, V. Planté-Bordeneuve, M.M. Mezei, J.M. Campistol, J. Buades, T.H. Brannagan, B.J. Kim, J. Oh, Y. Parman, Y. Sekijima, P.N. Hawkins, S.D. Solomon, M. Polydefkis, P.J. Dyck, P.J. Gandhi, S. Goyal, J. Chen, A.L. Strahs, S. V. Nochur, M.T. Sweetser, P.P. Garg, A.K. Vaishnaw, J.A. Gollob, O.B. Suhr, Patisiran, an RNAi Therapeutic, for Hereditary Transthyretin Amyloidosis, N. Engl. J. Med. 379 (2018) 11–21. https://doi.org/10.1056/NEJMoa1716153.

[41] J.A. Kulkarni, D. Witzigmann, S. Chen, P.R. Cullis, R. van der Meel, Lipid Nanoparticle Technology for Clinical Translation of siRNA Therapeutics, Acc. Chem. Res. 52 (2019) 2435–2444. https://doi.org/10.1021/acs.accounts.9b00368.

[42] A.A. Khan, D. Betel, M.L. Miller, C. Sander, C.S. Leslie, D.S. Marks, Transfection of small RNAs globally perturbs gene regulation by endogenous microRNAs, Nat. Biotechnol. 27 (2009) 549–555. https://doi.org/10.1038/nbt.1543.

[43] S. Mockly, H. Seitz, Inconsistencies and Limitations of Current MicroRNA Target Identification Methods, in: MicroRNA Target Identif., 2019: pp. 291–314. https://doi.org/10.1007/978-1-4939-9207-2_16.

[44] M. Miceli, C. Exertier, M. Cavaglià, E. Gugole, M. Boccardo, R.R. Casaluci, N. Ceccarelli, A. De Maio, B. Vallone, M.A. Deriu, ALS2-Related Motor Neuron Diseases: From Symptoms to Molecules, Biology (Basel). 11 (2022) 77. https://doi.org/10.3390/biology11010077.

[45] S. Bachiller, I. Jiménez-Ferrer, A. Paulus, Y. Yang, M. Swanberg, T. Deierborg, A. Boza-Serrano, Microglia in Neurological Diseases: A Road Map to Brain-Disease Dependent-Inflammatory Response, Front. Cell. Neurosci. 12 (2018). https://doi.org/10.3389/fncel.2018.00488.

[46] R. Abellan-Pose, C. Teijeiro-Valiño, M.J. Santander-Ortega, E. Borrajo, A. Vidal, M. Garcia-Fuentes, N. Csaba, M.J. Alonso, Polyaminoacid nanocapsules for drug delivery to the lymphatic system: Effect of the particle size, Int. J. Pharm. 509 (2016) 107–117. https://doi.org/10.1016/j.ijpharm.2016.05.034.

[47] R. Abellan-Pose, M. Rodríguez-Évora, S. Vicente, N. Csaba, C. Évora, M.J. Alonso, A. Delgado, Biodistribution of radiolabeled polyglutamic acid and PEG-polyglutamic acid nanocapsules, Eur. J. Pharm. Biopharm. 112 (2017) 155–163. https://doi.org/10.1016/j.ejpb.2016.11.015.

CHAPTER 2

Nanoemulsions and polymeric nanocapsules for nose-to-brain and intracerebro-ventricular delivery of siRNA

Chapter 2: Nanoemulsions and polymeric nanocapsules for nose-to-brain and intracerebroventricular delivery of siRNA*

This work has been done in collaboration with Eli Lilly & Company (Indianapolis, USA) under a collaboration agreement.

*The introduction of this chapter has been partially adapted from the published review: M. L. Borrajo[a], M. J. Alonso[a,b]. Using nanotechnology to deliver biomolecules from nose to brain – peptides, proteins, monoclonal antibodies and RNA. *Drug Delivery and Translational Research*. 12, 862-880. (2022). doi: 10.1007/s13346-021-01086-2. ISSN: 2190393X, 21903948.[1]

[a] Center for Research in Molecular Medicine and Chronic Diseases (CiMUS), Universidade de Santiago de Compostela, Santiago de Compostela, 15782, Spain.
[b] Department of Pharmacology, Pharmacy and Pharmaceutical Technology, School of Pharmacy, Universidade de Santiago de Compostela, Santiago de Compostela, 15782, Spain.

ABSTRACT

Among the many difficulties in developing an efficient genetic therapy for the central nervous system (CNS), one of the most challenging hurdles is the presence of multiple protective layers in the brain, notably the blood-brain barrier (BBB). Various administration pathways have been explored to directly access the CNS, such as the nose-to-brain (N-to-B) route. However, gaining access to the brain does not always correlate with the successful delivery of the cargo to the desired CNS areas, mainly due to the lack of diffusivity of the used nanocarriers.

The objective of this work was to develop a library of nanoemulsions (NEs) and polymeric nanocapsules (NCs), capable of entrapping small interference RNA (siRNA), to be delivered to different brain areas through N-to-B or direct intracerebroventricular (ICV) administration. This library of nanocarriers featured sizes below 100 nm, cationic to anionic surface charges, and adequate long-term stability at 4 ºC. One selected NE, named NE-2, was functionalized with the rabies virus glycoprotein (RVG) to facilitate its penetration into the CNS.

In vitro results in a neuroblastoma cellular model revealed a low toxicity profile and a dose-dependent transfection efficiency of the nanocarriers. At the highest concentration tested, 100 nM/well, the nanocarriers exhibited a silencing effect of approximately 50% of the targeted gene. *In vivo* N-to-B administration enabled direct access of the nanocarriers to the brain, with modest distribution to various brain areas. However, the functionalization of the selected NE with RVG did not result in an enhancement in brain uptake. Direct ICV injection of one selected NCs, NC-1, demonstrated an outstanding silencing effect in the frontal cortex, striatum, hippocampus, brain stem, and dorsal root ganglion (DRG), reducing targeted mRNA levels by 50-80%, depending on the region. Moreover, based on the RNAscope results, it was concluded that this NC exhibited a remarkable capacity to diffuse throughout the brain.

Overall, this work allowed us to identify a promising candidate for the delivery of siRNA to the CNS, due to its extensive diffusion across multiple brain regions and its specific knockdown effect on the targeted mRNA.

GRAPHICAL ABSTRACT

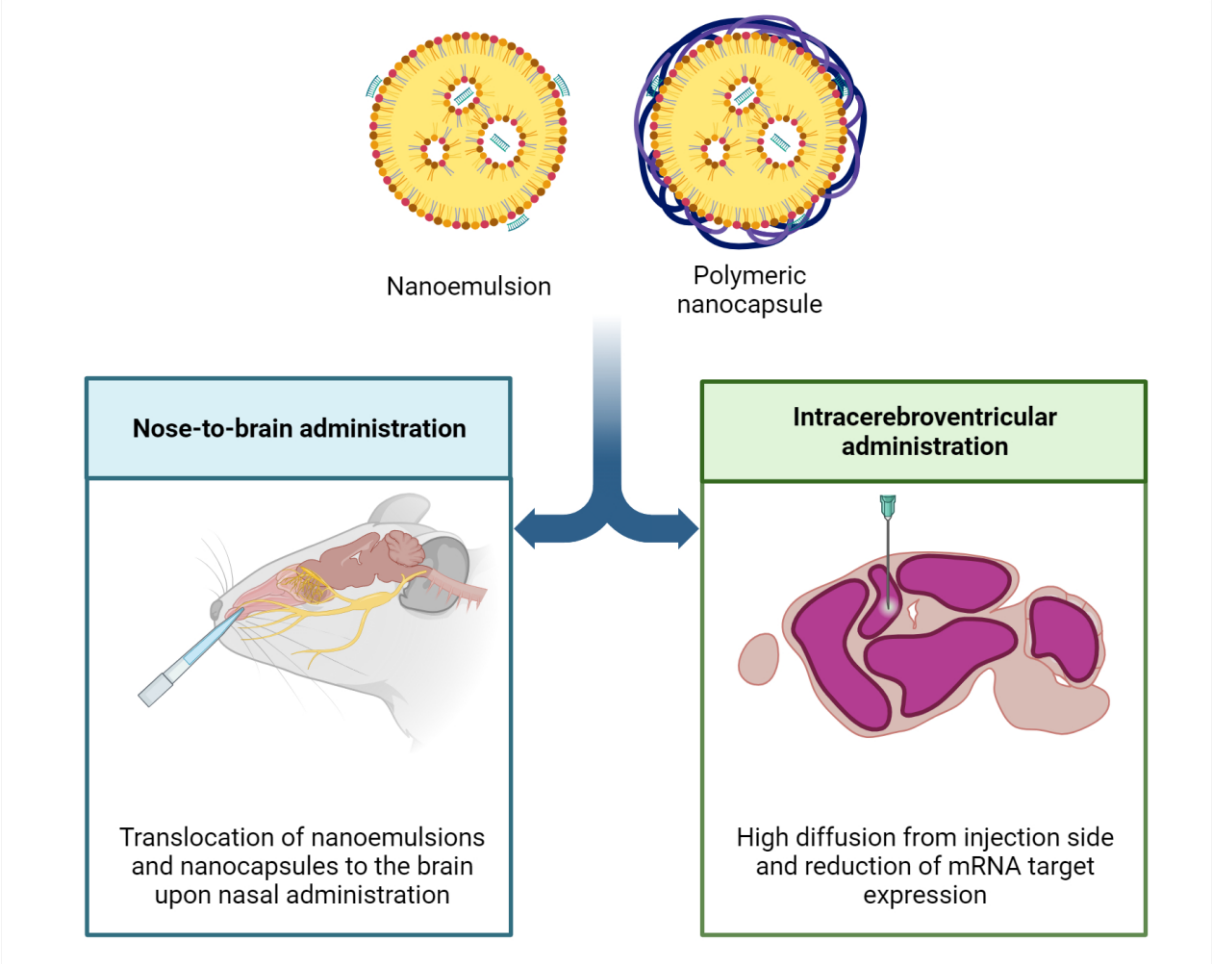

Created with https://biorender.com.

1. INTRODUCTION

In recent decades, central nervous system (CNS)-related disorders have been positioned as the second leading cause of mortality worldwide [2]. In just 20 years, from 1990 to 2019, mortality and prevalence due to neurological disorders have dramatically increased, and it is expected that 103 million people will be affected by these disorders in 2030 [3,4]. Unfortunately, the need for treatment of neurological diseases remains unmet, due to the limited efficacy of conventional therapies [5,6]. Within this frame, gene therapies are expected to play a key role in reversing or correcting the genetic cause underlying CNS diseases [7–9].

Among the different gene therapies, small interference RNAs (siRNA) have shown potential for long-term mRNA knockdown, and several siRNAs have been identified to regulate the biology in the CNS [9–11]. Regardless of their potential to inhibit therapeutic targets in the brain, siRNA molecules have inherent limitations, including fast clearance, degradation, and difficulties in overcoming biological barriers to reach their targets [12–16]. Recent work suggests that these challenges might be addressed using nanotechnology. This is based on the fact that the association of siRNA molecules with specific nanocarriers enables their protection from degradation and facilitates their access to certain organs [17].

The major barrier to the access of siRNA molecules to the brain is the blood-brain barrier (BBB) [18,19]. This barrier is fundamental for maintaining the homeostasis of the CNS and controlling the entry of potentially toxic compounds; however, it also prevents the transport of drugs into the brain [18–21]. As shown in Figure 1, the cerebral blood vessels are surrounded by endothelial cells closely connected by tight junctions [22]. These endothelial cells are covered by a continuous basal lamina, pericytes, and astrocytes, forming a highly restrictive barrier [23]. Due to the complexity of the BBB, researchers have explored various technological approaches to facilitate transport across it, making it one of the most ambitious challenges in CNS disease therapy [24,25].

Because of the difficulties for the access of RNA molecules to the brain, the only approach that has reached the clinic involves intrathecal administration [26–28]. An example of this is Spinraza® (nusinersen), an FDA-approved antisense oligonucleotide for the treatment of spinal muscular atrophy, administered via intrathecal injection [29,30]. However, this invasive technique is not suitable for long-term therapies [31]. Consequently, less invasive strategies are being explored, including the transient disruption of the BBB through ultrasounds or the use of nanocarriers with the capacity to cross the BBB. Moreover, the nose-to-brain (N-to-B) route is currently being investigated as an option for brain access [1,32,33].

The first study aimed to investigate the N-to-B transport of a dye was performed in 1937, using a rabbit model [34]. Since then, N-to-B pathways to access the brain have been elucidated, and it is known that molecules deposited on the olfactory mucosa of the nose can be directly delivered into the brain though the olfactory and trigeminal nerves, or they can diffuse across the olfactory epithelium in the case of small, hydrophobic molecules [35,36]. In fact, numerous clinical trials involving N-to-B delivery are being conducted for the treatment of various conditions, such as glioblastoma, Alzheimer's disease, and different psychiatric disorders [37,38].

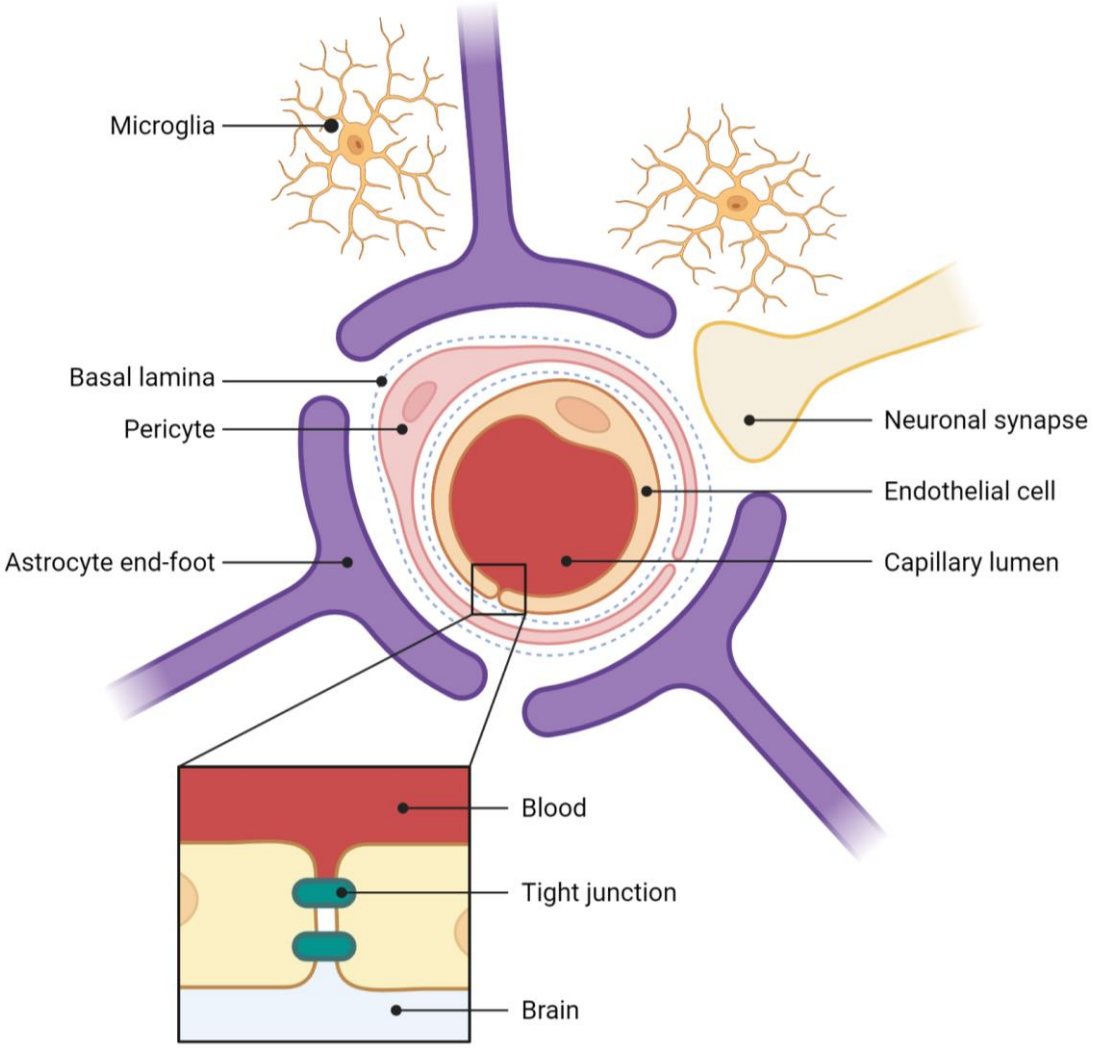

Figure 1. Schematic representation of the structure of the blood-brain barrier

The capillary or vascular lumen interacts with the continuous layer of endothelial cells that are tightly connected by tight junctions. These endothelial cells are supported by various cellular elements, including pericytes, basal lamina, neurons, astrocytes, and microglia. Created with https://biorender.com.

As shown in Figure 2, after intranasal administration, drug molecules may have direct access to the brain by crossing the olfactory epithelium, which is innervated by olfactory and trigeminal nerves [39,40]. This may occur through different mechanisms: direct internalization into the olfactory nerve, followed by axonal transport; paracellular transport between epithelial cells and channels near the olfactory nerves; and transcellular transport across the cells of the olfactory epithelium [41,42]. After crossing this barrier, the drug molecules reach the olfactory bulb, from where they can be distributed into different brain regions [43,44]. Moreover, axonal transport through the trigeminal nerves from the nasal cavity is possible, which synapses at the trigeminal ganglion, gaining access to the brain stem and the caudal and rostral regions of the brain [45,46].

Considering the obvious limitations of the delivery of oligonucleotides, various nanocarriers have been designed to efficiently transport siRNA via the N-to-B route. For example, a decade ago, trans-activator of transcription protein (Tat) -modified polyethylene glycol-poly(ε-

caprolactone) (PEG-PCL) nanomicelles, sized between 50-160 nm and possessing a positive surface charge (+10 mV) were found to effectively facilitate the transfer of fluorescein amidite (FAM) -siRNA into the olfactory and trigeminal nerves [47]. Subsequent research with this nanosystem involved the encapsulation of siRNA targeting serine-threonine kinase 1 (Raf-1) and camptothecin for the treatment of glioblastoma [48]. A modified version of this nanocarrier, siRNA targeting tumor necrosis factor-α (TNF-α) -loaded Tat-modified PEG-PCL nanomicelles (62 nm and +19 mV) were intranasally administered into an ischemic stroke mouse model, resulting in a reduction of the infracted brain area [49]. Similarly, siRNA against galectin-1 (Gal-1) -loaded chitosan nanoparticles (NPs) (140 nm and a surface charge of +30 mV) were administered intranasally for the treatment of glioblastoma in a mouse model. Combining siRNA-loaded chitosan nanocarriers with temozolomide or a programmed cell death protein 1 (PD-1) blocking agent led to an increase in survival rates [50,51]. A different carrier consisting of hyaluronic acid-coated nanocomplexes of DP7-C (a cholesterol-modified version of the DP7 cell-penetrating peptide) and siRNA targeting vascular endothelial growth factor (VEGF) or siRNA against polo-like kinase 1 (PLK1) (particle size of 105 nm and a surface charge of -25 mV) resulted in a decrease in the tumor volume and an extended lifespan of the animals in a glioblastoma mouse model [52]. A similar approach was followed with siRNA slit 2, which was encapsulated onto T7-C nanocomplexes (a cholesterol-modified T7, which is a targeting ligand for transferrin receptor), with a size of 60 nm and a surface charge of +23 mV. The results showed a prolonged survival rate in a glioma mouse model, with a significantly smaller tumor area and increased levels of immune cells detected in the tumor microenvironment [53].

siRNA-loaded NPs were also explored for the treatment of neurodegenerative diseases, such as Huntington's disease. Different versions of anti-huntingtin siRNA were associated with chitosan nanocarriers and intranasally administered into a Huntington's disease model. The encapsulation of this modified siRNA onto chitosan NPs led to a reduction in huntingtin mRNA and protein levels [54]. The N-to-B route has also been investigated in the context of Alzheimer's disease. Specifically, siRNA β-secretase 1 (BACE-1), in combination with rapamycin, both entrapped into a PEGylated poly-L-lysine (PLL) NPs functionalized with a lectin and a β-amyloid-binding peptide (130 nm, neutral surface charge), were administered intranasally. As a result, BACE1 mRNA levels and Aβ plaques in the brain were reduced, and these biological changes were translated into an improvement in the learning and memory capacity of the animals [55]. In the context of Alzheimer's disease, our group developed octaarginine-lauric acid (r8-C12) nanocomplexes enveloped with PEG-polyglutamic acid (PGA) for the N-to-B delivery of miRNA-132. This nanocarrier (96 nm and neutral surface charge) resulted in a significant modulation of the mRNA targets in the olfactory bulb and the hippocampus [56].

Despite the potential of the N-to-B pathway, once molecules, and especially NPs, get access to the CNS, their diffusion to the targeted brain areas could be a highly limiting step [57,58]. For example, it has been reported that PEGylated polymeric NPs diffuse less than 20 µm after crossing the BBB [59]. The best approach to investigate this diffusion process is following intracerebroventricular (ICV) administration. This route of administration consists of a surgical procedure and a well-defined cannulation process that allows the direct injection of the drugs into the cerebrospinal fluid (CSF) [26,60]. *In vivo* studies comprising ICV administration of siRNA associated were initially performed with naked siRNA and, more recently, with the conjugation of siRNA with chemical modification agents or encapsulated onto nanocarriers [61–63]. For example, polyethylamine nanocomplexes containing siRNA α-

synuclein (90 nm, positive surface charge), which were used in a Parkinson's disease mice model, resulted in a ~ 50% reduction in α-synuclein expression in the striatum, without signs of toxicity [64,65]. Other studies focused on determining the diffusion of the nanocarriers from the injection site. For example, following ICV administration, LNPs loaded with siRNA glutamate *N*-mehtyl-D-aspartic acid receptor subunit zeta-1 (GRIN1) or siRNA phosphatase and tensin homolog 1 (PTEN) (60 nm and neutral surface charge) were observed to only diffuse up to 4 mm from the site of injection [66].

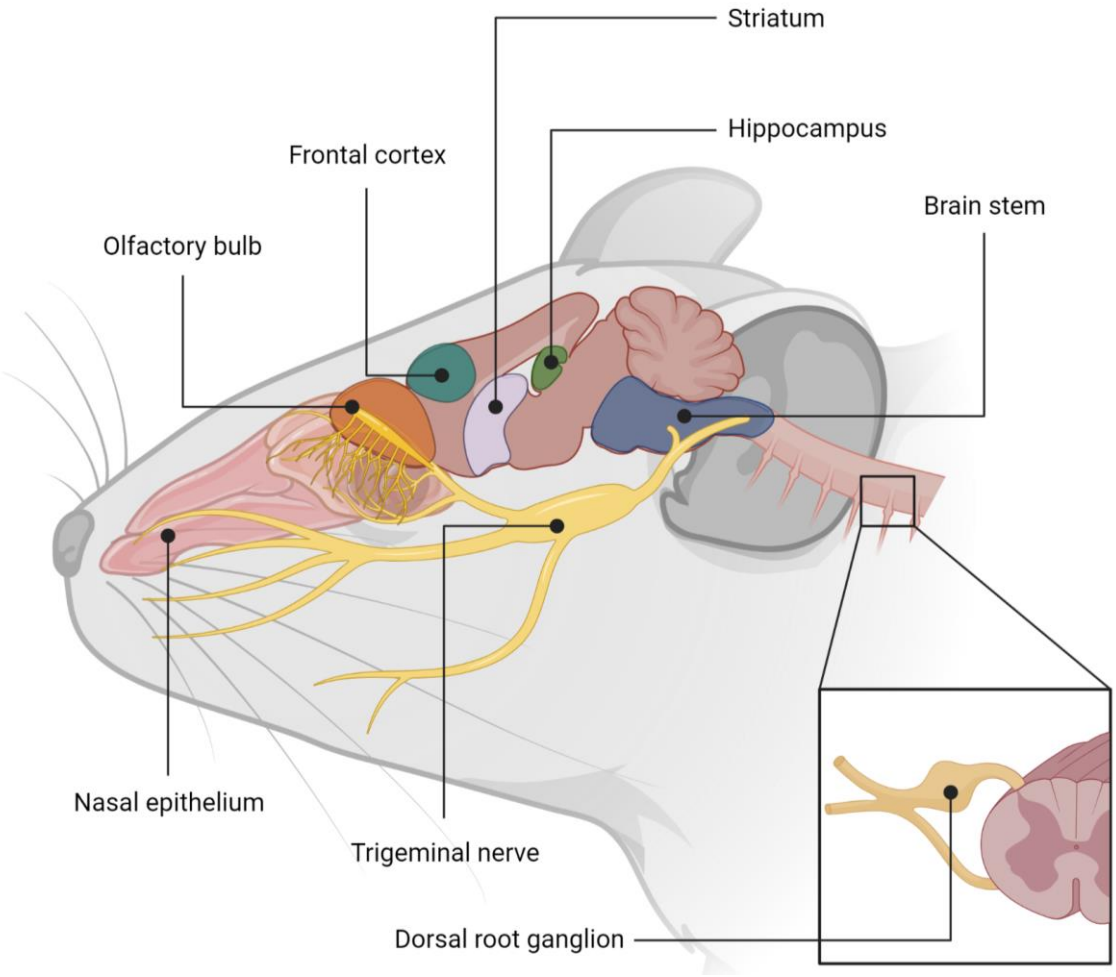

Figure 2. Schematic representation of the brain areas involved in the nose-to-brain and intracerebroventricular administration modalities

Upon nasal administration, nanocarriers would reach the olfactory or trigeminal nerves, allowing access to various areas of the CNS, such as the olfactory bulb or the brain stem. In the case of intracerebroventricular administration, the injection site is situated between the frontal cortex, the striatum, and the hippocampus, where the administered systems are expected to be located and produce effects. Other areas, such as the brain stem or dorsal root ganglion, would require greater diffusion from the injection site. Created with https://biorender.com.

Based on this background information, the primary objective of this work was the development of a library of nanoemulsions (NEs) and polymeric nanocapsules (NCs) and their evaluation of their capacity to encapsulate, protect, and deliver siRNA to the CNS. We

hypothesized that the liquid nature of the proposed nanocarriers would facilitate their brain distribution. Different oils and surfactants were selected for the screening of this library, to fulfill the following requirements: (A) reproducible and scalable production; (B) particle size close to 100 nm in diameter; (C) different surface chargers, including neutral, positive, and negative; (D) final siRNA concentration of at least 0.25 mg/mL; and (E) at least one-month stability at 4 °C. Modifications on the surface charge and composition of the nanocarriers were assessed by different types of polymeric coating, intended to facilitate the permeation properties of the systems, as well as to enhance their stability in biological environments. Selected formulations were evaluated in terms of their capability of disrupting 3-dimensional barriers *in vitro*, cellular toxicity, and transfection efficiency. Finally, selected nanocarriers were administered by the N-to-B and ICV routes to evaluate their capacity to access the brain and diffuse to different CNS areas, respectively.

2. MATERIALS AND METHODS

2.1. MATERIALS

DOTAP (1,2-dioleoyl-3-trimethylammonium-propane, chloride salt), DSPC (1,2-distearoyl-sn-glycero-3-phosphocholine), and DSPE-PEG$_{2000}$-maleimide (1,2-distearoyl-sn-glycero-3-phosphoethanolamine-N-[maleimide(polyethylene glycol)-2000], ammonium salt) were purchased from Avanti Polar Lipids (AL, USA). Vitamin E (Vit E) (D, L-α-tocopherol) and K-HS15® (Kolliphor® HS15) were obtained from BASF (Mannheim, Germany). Castor oil was purchased from Acofarma (Madrid, Spain). Oleic acid (super-refined oleic acid) and SPAN 80 (Span 80-LQ-(MV)) were obtained from Croda International (Snaith, UK). Labrafac™ (Labrafac™ Lipophile, WL 1349, medium chain triglycerides of caprylic and capric acids) and Labrasol® (PEG-8 (MW 400) mono- and diesters of caprylic and capric acids) were purchased from Gattefossé (Saint-Priest, France). Tween 80 was acquired from Merck Millipore (Darmstadt, Germany). Inulin (Inutec® SL1) was obtained from CreaChem (Tienen, Belgium).

PEG-PGA (PEG (5 kDa)-b-PGA (10) [Na]) (polyethylene glycol (5 kDa)-block-poly(α-glumatic acid) (10u)sodium salt) was obtained from Polypeptide Therapeutic Solutions (Valencia, Spain). HA (hyaluronic acid, 40 kDa) was acquired from Lehmann & Voss & Co. KG (Hamburg, Germany). PSA (polysialic acid, 30 kDa) was obtained from Serum Institute of India (PUNE, India). CS (chitosan) was purchased from Heppe Medical Chitosan GmbH (Saale, Germany). C-PEG3-RVG peptide (C-PEG3-rabies virus glycoprotein derived peptide, sequence: C-PEG3-YTIWMPENPRPGTPCDIFTNSRGKRASNG, purity = 89.85%) was purchased from ChinaPeptides (Shanghai, China).

siRNA-1 and siRNA-2 were manufactured and provided by Eli Lilly and Company (IN, USA).

2.2. PRODUCTION OF NANOEMULSIONS AND NANOCAPSULES

2.2.1. Selection of the nanoemulsion core

Different nanoemulsion (NE) cores were prepared using DOTAP in combination with four different oils (Vitamin E, oleic acid, Labrafac™, and castor oil) and four different surfactants (DSPC, SPAN 80, Tween 80, and Kolliphor HS15). In all cases, NEs were prepared by solvent-displacement technique, maintaining the mass ratio 25.6: 61.6: 12.8 (DOTAP: oil: surfactant). Briefly, an organic phase was prepared by dissolving DOTAP, oil, and surfactant in ethanol. This resulting solution (0.15 mL, containing 32 mg/mL DOTAP, 77.2 mg/mL oil, and 16.1 mg/mL surfactant) was added over an aqueous phase (1 mL, RNase-free water), under magnetic stirring (1400 rpm), leading to the formulation of the blank NEs. The solution was kept under stirring for 5 minutes and set aside for stability for 5 minutes.

Evaporation under vacuum (Heidolph Hei-VAP Advantage; Schwabach, Germany) was used to eliminate organic solvents and to concentrate the resulting blank NEs up to a final DOTAP concentration of 8.47 mg/mL, for further complexation with siRNA.

2.2.1.1. Complexation of siRNA onto nanoemulsions

Complexation of siRNA-1 (named siRNA for the rest of section 2.2) onto the cationic surface of blank NEs was performed following two different strategies. The first approach consisted of bulk mixing, in which complexation occurred upon mixing of siRNA solution (at different concentrations, including 0.5, 1, 1.5, and 2 mg/mL in RNase-free water) with the blank NE solution. Briefly, blank NEs were diluted in RNase-free water to a final volume of 0.1 mL, aiming for a DOTAP concentration of 1.06, 2.12, 3.18, and 4.23 mg/mL (depending on the concentration of the siRNA solution). This NE solution was added to 0.1 mL of siRNA solution, under magnetic stirring at 700 rpm for 10 seconds. The volume/volume (v/v) ratio between the different solutions was kept constant at 1:1. Formulations were allowed to stabilize for 30 minutes. In all cases, the nitrogen to phosphate (N/P) ratio was maintained as 2:1. Resulting NE-siRNA formulations presented a final siRNA concentration of 0.25, 0.5, 0.75, and 1 mg/mL.

The second strategy consisted of microfluidic mixing, in which the blank NEs and the siRNA solution were injected using a micromixer NanoAssemblr™ bench-top instrument, Precision NanoSystem Inc. (Vancouver, Canada). Similarly, as in the bulk mixing approach, v/v ratios of 1:1 of blank NEs (at DOTAP concentration of 4.23 mg/mL) and siRNA solution (at a concentration of 2 mg/mL) were mixed inside the microfluidic cartridge. Different Total Flow Rates were explored, and N/P ratio was kept at 2:1.

2.2.2. Preparation of siRNA-loaded nanoemulsions

siRNA-loaded NEs (NE-siRNA) were produced using the micromixer instrument described in section 2.2.1.1. In this case, the formation of the NE and the complexation of the siRNA occurred simultaneously. In summary, 0.2 mL of the organic phase (consisting of DOTAP at a concentration of 19.05 mg/mL and oil, dissolved in EtOH) were mixed with 1 mL of the aqueous phase (containing siRNA and the selected surfactant diluted in RNase-free water, at a concentration of 0.9 mg/mL). The N/P ratio was kept constant at 2:1. The mixing process was performed on a microfluidic cartridge, using a v/v ratio of 1:5 (organic to aqueous phase).

Different Total Flow Rates were tested, aiming to obtain the desired physicochemical properties. The resulting NE-siRNA formulation presented a theoretical siRNA concentration of 0.75 mg/mL.

For some of the selected NE cores, as Labrafac^{TM}-based NEs, different molar ratios (mol%) were explored, including 46: 35: 18.5 and 25: 56.5: 18.5 (DOTAP: oil: surfactant), aiming to obtain more desirable physicochemical properties.

2.2.3. Preparation of siRNA-loaded nanocapsules

After formulation of NE-siRNA, nanocapsules (NC-siRNA) were prepared by adding a polymeric solution (at concentrations dependent on the weight to weight (w/w) or mol to mol (mol/mol) ratio between the polymer and the siRNA, and the type of polymer used) over the preformed NE-siRNA system. In summary, 0.2 mL of the polymeric solution were added over 1 mL of the pre-formed NE-siRNA (at a siRNA concentration of 0.75 mg/mL), and the resulting solution was maintained under magnetic stirring at 700 rpm for 10 seconds, allowing the proper mixing between the phases and enhancing the electrostatic complexation of the polymer over the cationic surface of the NE-siRNA. In all cases, the v/v ratio was kept constant at 1:5 (polymer to siRNA). The resulting formulations were stabilized for 10 minutes.

Multi-layer NC-siRNA (MNC-siRNA) systems were prepared by mixing a cationic polymer with a preformed anionic NC-siRNA. Briefly, 0.2 mL of the cationic polymeric solution were added over the 1 mL of the pre-formed NC-siRNA (at a siRNA concentration of 0.625 mg/mL). The resulting solution was maintained under stirring at 700 rpm for 10 seconds, followed by a stabilization of 10 minutes. In all cases, the v/v ratio was kept constant at 1:5 (cationic polymer to anionic NC-siRNA). Different w/w ratios between the cationic polymer and the siRNA were explored.

2.3. FUNCTIONALIZATION OF SELECTED NANOEMULSIONS

2.3.1. Synthesis of DSPE-PEG$_{2000}$-maleimide-RVG

1 molar equivalent of DSPE-PEG$_{2000}$-mal at 1 mg/mL in 60% ethanol was incubated with 1.5 molar equivalents of C-PEG3-RVG at 40 mg/mL in 60% ethanol. The appropriate amount of C-PEG3-RVG peptide was added over DSPE-PEG$_{2000}$-mal solution, followed by the addition of 1M MES/triethylamine (TEA) buffer (pH 6.5) to achieve a final concentration of 25 mM MES buffer. The resulting mixture was incubated at room temperature for 1 hour, and at 4 °C for 20 hours. Following incubation, the mixture was placed inside a 100,000 MW cut-off dialysis membrane and subjected to an initial dialysis against 0.9% NaCl and to three subsequent cycles against endotoxin-free ultrapure water, each cycle lasting at least 4 hours, to remove unconjugated C-PEG3-RVG peptide.

For the calculation of the encapsulation efficiency, 500 µL of 2 mg/mL of DSPE-PEG$_{2000}$-mal-C-PEG3-RVG (DSPE-PEG-RVG) solution in DMSO-d_6 were placed inside a 5-mm nuclear magnetic resonance (NMR) tube and analyzed by a ^{1}H NMR of 500 MHz in a Bruker DRX-500 spectrometer, under a magnetic field strength of 11.74 T (MA, USA), without presaturation. ^{1}H NMR spectrum was analyzed with MestReNova 14.2.2. The areas under the curve (AUC) corresponding with DSPE-PEG$_{2000}$-mal and C-PEG3-RVG were recorded and

used to calculate the conjugation efficiency. $AUC_{0.86\ ppm}$ corresponds with the area under the curve of the six hydrogens of the terminal methyl groups of the alkyl chains of DSPE-PEG_{2000}-mal, with a chemical shift of 0.85 ppm. Regarding C-PEG3-RVG, the average value was calculated using three distinct peaks: $AUC_{10.78\ ppm}$, $AUC_{6.62\ ppm}$, and $AUC_{0.76\text{-}0.63\ ppm}$. $AUC_{10.78\ ppm}$ is the area under the curve of the hydrogen present in the tryptophan secondary amine, with a chemical shift of 10.78 ppm. $AUC_{6.62\ ppm}$ corresponds with the area under the curve of the two hydrogens of the tyrosine's benzene ring, with a chemical shift of 6.62 ppm. $AUC_{0.76\text{-}0.63\ ppm}$ is the area under the curve of twelve hydrogens present on the four methyl groups of the isoleucine, with a chemical shift of 0.76 to 0.63 ppm.

2.3.2. Formulation of siRNA-loaded NE-RVG

Modification of NE-siRNA-1 (named NE-siRNA for the rest of section 2.3) with DSPE-PEG-RVG was performed on NE containing DOTAP, Vitamin E, and Tween 80 (19.4: 75.4: 5.2 mol%). Two different approaches were explored: incorporation of DSPE-PEG_{2000}-maleimide and further functionalization with RVG; and direct incorporation of already modified DSPE-PEG-RVG.

The first strategy consisted of adding 0.1 mol% of DSPE-PEG_{2000}-maleimide to the formulation, leading to a lower Vitamin E content (from 75.4 to 75.3 mol%), and procedure with the formulation of the NE-siRNA depicted in section 2.2.2. In a second step, 0.75 mL of the previously formed NE-siRNA (containing 0.07 mg/mL of DSPE- PEG_{2000}-maleimide) were mixed with different volumes of C-PEG3-RVG solution (1 mg/mL in HEPES, 10 mM, pH 7). The volume of the RVG peptide solution added is dependent on the molar ratios between DSPE-PEG_{2000}-maleimide and C-PEG3-RVG. Both solutions were combined by pipette mixing, and incubated overnight at 4 °C.

The second strategy consisted of the direct formulation of the NE-siRNA as depicted in section 2.2.2., using 0.1 mol% of DSPE-PEG-RVG, synthesized as described in section 2.3.1. In both cases, intended to eliminate unreacted peptides, samples were filtered using Amicon® Ultra 0.5 mL Centrifugal Filters Ultracel® -100K (Merck Millipore, MA, USA).

2.4. CHARACTERIZATION OF NANOEMULSIONS AND NANOCAPSULES

2.4.1. Characterization of the size, polydispersity index and ζ-potential of nanoemulsions and nanocapsules

Hydrodynamic diameter and polydispersity index (PDI) were characterized by dynamic light scattering (Zetasizer® Nano ZS, Malvern Instruments, Malvern, UK). ζ-potential was measured in terms of mean electrophoretic mobility values, measured by laser Doppler electrophoresis with the same equipment.

Particle size and PDI measurements were performed after diluting the samples 10 x in RNase-free water. ζ-potential characterization was obtained after dilution of samples 20 x in RNase-free water.

2.4.2. Characterization of encapsulation efficiency and siRNA concentration

Encapsulation efficiency (EE%) and siRNA-1 (named siRNA in the rest of section 2.4) concentration were assessed following different methodologies. In all cases, NE-siRNA and NC-siRNA formulations were diluted in a 1:1 (v/v) ratio with Triton X or heparin solutions, prepared at 50 mg/mL in RNase-free water. Incubation with Triton X (Triton-X-100, Sigma-Aldrich, MO, USA) induced the disruption of the nanocarrier, while heparin (Sigma-Aldrich, MO, USA) led to the displacement of the siRNA from the NP.

2.4.2.1. Agarose gel electrophoresis

To qualitatively assess the amount of siRNA encapsulated onto NE-siRNA and NC-siRNA formulations, samples containing 1-3 µg of siRNA were loaded in an agarose gel at 1% w/v in Tris Acetate-EDTA buffer (Sigma-Aldrich, MO, USA) before and after incubation with Triton X and heparin. Samples were diluted with equal volumes of loading mix, containing 1x SYBR® Gold nucleic acid strain (Invitrogen, CA, USA). Free siRNA was included as a control. Gels were run for 30 minutes at 90 V in a Sub-Cell GT cell 96/192 (Bio-Rad Laboratories, CA, USA), and evaluated with a UV transilluminator imagining system (Molecular Imager® Gel Doc™ XR, Bio-Rad Laboratories, CA, USA).

2.4.2.2. RiboGreen assay

Quant-iT RiboGreen RNA assay kit (Invitrogen, MA, USA) was used to quantitatively determine the EE% and the siRNA concentration of NE-siRNA and NC-siRNA formulations. Briefly, samples were diluted 50-fold in TE buffer (1x), followed by a 2-fold dilution with Triton X and incubation at 37 °C for 30 minutes. Subsequently, samples were diluted 10-fold with TE buffer (1x). The standard curve was prepared using siRNA at concentrations between 0.1 to 1 µg/mL, in the presence of Triton X. Following manufacturer instruction, RiboGreen reagent was diluted 200-fold in TE buffer (1x), and added to an equal volume of sample, leading to a final volume of 200 µL. Samples and the standard curve were transferred to a 96-black polystyrene microplate (Croning®, NY, USA). Fluorescence intensity was assessed using a microplate reader (Synergy H1, BioTek Instruments, VT, USA), using excitation at 485 nm and emission at 530 nm. The standard curve ($r^2 \geq 0.99$) was used for determining the siRNA concentration of the sample. The encapsulation efficiency of siRNA was calculated according to the following Equation 1.

$$Encapsulation\ efficiency\ (EE\%) = \frac{[siRNA]_{disrupted}}{[siRNA]_{theoretical}}$$

Where $[siRNA]_{disrupted}$ is the siRNA concentration determined after treating the nanosystems with the disrupting agent. $[siRNA]_{theoretical}$ is the theoretical total siRNA concentration of the nanosystem.

Equation 1. Calculation of encapsulation efficiency (EE%)

2.4.2.3. Ultra Performance Liquid Chromatography

Intended to obtain more reliable encapsulation efficiency and siRNA concentration values, NE-siRNA and NC-siRNA formulations were analyzed by Ultra Performance Liquid Chromatography (UPLC) on an Acquity H-UPLC Class system with a UV detector at 260 nm (Waters Corporation, MA, USA), equipped with an ACQUITY UPLC BEH Amide Column, 130Å, 1.7 µm, 3 mm x 50 mm (Waters Corporation, MA, USA). Mobile phase A consisted of 25 mM of ammonium acetate in 80:20 acetonitrile HPLC grade: water (v/v), and phase B of 25 mM of ammonium acetate in 40:60 acetonitrile HPLC grade: water (v/v). The column temperature was set at 40 °C, and 3 µL of the sample were injected at a flow rate of 0.5 mL/min, setting the sample temperature as 20 °C. The chromatography method consisted of a linear gradient from 0% to 100% of phase B in 10 minutes, followed by a gradient from 100% to 0% in 1 minute, and stabilization at 0% of phase B for 6 minutes.

In the case of the NE-siRNA containing DOTAP, Vitamin E, and Tween 80 (with and without DSPE-PEG-RVG functionalization), the chromatography method was adapted to obtain a more distinctive peak for siRNA. In this case, the method consisted of a linear gradient from 0% to 100% of phase B in 18 minutes, followed by a gradient from 100% to 0% in 1 minute, and stabilization at 0% of phase B for 6 minutes.

Regardless of the chromatographic method used, the amount of siRNA in each sample was calculated using a standard curve generated with known concentrations of the siRNA (4-320 µg/mL – $r^2 \geq 0.99$). The encapsulation efficiency of siRNA was calculated according to the following Equation 1. Each analysis was done at least in duplicate.

2.5. CONCENTRATION AND SCALE-UP OF NANOCAPSULES

To achieve the targeted siRNA-1 (named siRNA in the rest of section 2.5) concentrations, NE-siRNA and NC-siRNA formulations were concentrated using Amicon® Ultra 0.5 mL Centrifugal Filters Ultracel® -100K (Merck Millipore, MA, USA). In summary, all samples were concentrated at 14000 g during a variable amount of time, dependent on the formulation (usually, between 5 to 20 minutes). This process allowed the 5-fold concentration of the formulations, leading to a final volume of around 0.1 mL and a final siRNA concentration of 3-3.75 mg/mL. Samples were characterized as described in section 2.4. before and after the concentration process.

To meet the requirements for functional evaluation of the nanocarriers, the preparation and concentration of selected NE-siRNA and NC-siRNA formulations were scaled up. For the preparation of NE-siRNA samples, 2 mL of the organic phase were mixed with 10 mL of the aqueous phase, maintaining the parameters optimized in section 2.2.2. This step constituted a 10-fold increase in the production volume, leading to a final volume of 12 mL and a siRNA concentration of 0.75 mg/mL. These NE-siRNA formulations were used for the scale-up of the NC-siRNA. Briefly, 2 mL of the polymer solution were added over 10 mL of the previously formed NE-siRNA solution. The rest of the parameters optimized in section 2.2.3. were maintained. This adaptation constituted a 10-fold increase in the production volume, leading to a final volume of 12 mL and a siRNA concentration of 0.625 mg/mL.

The concentration process was also scaled up by using Amicon® Ultra-15 Centrifugal Filters Ultracel® -100K (Merck Millipore, MA, USA), allowing a 5-fold concentration. This

optimization constituted a 20-fold improvement in the production volume, leading to a final volume of approximately 2 mL and a siRNA concentration of around 3-3.75 mg/mL.

2.6. STABILITY OF NANOEMULSIONS AND NANOCAPSULES

The experiments described in this section were performed using siRNA-1, named siRNA in the rest of section 2.6. The colloidal stability of the NE-siRNA and NC-siRNA samples was assessed upon storage at 4 °C for up to 1 month. Besides visual inspection of the samples, to identify macroscopic changes in their appearance, color, or the presence of aggregates, measurements of particle size, PDI, ζ-potential, and siRNA association efficiency were performed, as described in section 2.4. The sample in solution would be considered stable if the change in the average diameter is inferior to 10%, as compared with the initial sample.

2.7. PRELIMINARY *IN VITRO* EVALUATION OF NANOCARRIERS

The experiments described in this section were performed using siRNA-1, named siRNA in the rest of section 2.7.

2.7.1. Barrier function assessment

Barrier function, tissue viability, and siRNA permeability of different nanocarriers were evaluated in an EpiAirway™ tissue model (MatTek Corporation, MA, USA). Barrier function was evaluated by transepithelial electrical resistance (TEER), while viability was assessed by lactate dehydrogenase (LDH) assay. NE-siRNA and NC-siRNA were applied to the apical surface of the tissues. Different controls were used, including untreated tissue, vehicle control (PBS), and two positive controls (Triton X, and LY-06D, an internal positive control provided by Eli Lilly). All samples were applied for 4 hours, during which tissues were transferred to fresh media at different time points (including 5, 60, 120, and 240 minutes) to assess permeability. Samples were removed and tissues were rinsed to eliminate any remaining formulation and incubated for an additional 20 hours. At each point, an LDH assay was performed. In summary, basolateral media samples were collected and incubated with LDH reagent, at room temperature for 30 minutes, protected from light. After that time, a stop solution was added, and absorbance of the samples was measured in a plate reader at 490 nm.

The barrier function was evaluated by TEER before exposure and after 4- and 24-hours post-treatment. Briefly, after rinsing the tissues, TEER buffer was added to the apical surface of the tissue, which was then transferred into the culture cup. There, ohms measurement was performed using an EVOM2 voltohmmeter.

The permeability of the nanocarriers was evaluated by hybridization enzyme-linked immunosorbent assay (hELISA) (protocol is detailed in section 2.8).

2.7.2. Transfection efficiency and cytotoxicity in BE(2)-C cells

A total of 10,000 BE(2)-C cells were seeded per well in a flat bottom 96-well plate and allowed to adhere for 24 hours. Cells were treated with nanocarriers containing siRNA for 24 hours, in Opti-MEM™ (Gibco™, Thermo Fisher, MA, USA) with 1% FBS, at concentrations

ranging from 100 to 0.1 nM. Then, nanocarriers were removed and replaced with a complete medium, and cells were incubated for another 20 hours.

Cell viability was measured using CytoTox 96® Non-Radioactive Cytotoxicity Assay (Promega, WI, USA), following manufacturer recommendations. Briefly, cells were lysed and incubated with the cytotoxicity reagent for 30 minutes in the absence of light. A stop solution was added and cytotoxicity was measured in a plate reader, at 490 nm.

Transfection efficiency was measured using SYBR™ Green Fast Advanced Cell-to-CT™ kit (Thermo Fisher, MA, USA), followed by a quantitative real-time PCR (qPCR). In summary, cells were lysed, and reverse transcription (RT) was performed by adding the RT reaction master mix (containing SYBR™ RT mix and the RT enzyme mix) and performing a thermal cycle of 1 hour at 37 ºC, 5 minutes at 95 ºC, and hold at 4 ºC. cDNA samples obtained from this process were incubated with the corresponding target probes, and TaqMan™ Fast Advanced Master Mix (Thermo Fisher, MA, USA). Analysis was performed in a QuantStudio™ qPCR system (Applied Biosystem, Thermo Fisher, MA, USA), following one cycle of 15 minutes at 50 ºC, one cycle of 1 minute at 95 ºC, 44 cycles of 40 seconds (10 seconds at 95 ºC and 30 seconds at 60 ºC), one cycle of 10 seconds at 95 ºC, one cycle of 5 seconds at 65 ºC, and a final dissociation curve.

2.8. ANIMAL STUDIES

All animal studies procedures were performed in compliance with relevant laws and institutional guidelines and the appropriate institutional committee(s) have approved them. Two different modalities of administration were investigated.

2.8.1. NOSE-TO-BRAIN (N-TO-B) ADMINISTRATION

The administration was performed on Sprague-Dawley rats, having 5 animals per group.

Animals were anesthetized and placed in a supine position. Size polyethylene (PE10) flexible catheter tubing was carefully inserted 2 cm deep into the right dorsal nasal cavity and attached to a syringe pump infusion. The nose-to-brain direction was titled towards the ground to improve the administration by gravity force. A total of 0.32 mL were administered over 60 minutes of intranasal infusion. Nanocarriers were administered at a total siRNA-1 concentration of 3.68, 3.57, and 4.1 mg/mL for NE-2, NE-2-RVG, and NC-5, respectively. Internal positive control (LY-06D) was used for comparison and was administered at a siRNA-1 concentration of 6.25 mg/mL. During administration, an oximeter was used along with oxygen flow near the nose to maintain appropriate oxygen saturation. Once completion of the administration session, animals were kept in a supine position until woken up.

After 4.5h post-administration, animals were sacrificed, and different brain areas were harvested (including the olfactory bulb, trigeminal nerve, and frontal cortex); nasal epithelium was also collected. hELISA was performed, after homogenizing the tissues and treating the samples with Triton X to fully release siRNA-1.

For that, tissues were initially homogenized, and samples were treated with Triton X, aiming to break the remaining nanocarriers and release the siRNA-1. A standard curve with free siRNA-1 was also prepared in the presence and absence of Triton X. Then, samples and

controls were incubated with the hybridization buffer (containing the sense or antisense probes), followed by a thermal cycle for hybridization (90 ºC for 5 minutes, 40 ºC for 30 minutes, and a hold stage at 12 ºC). Then, all samples were transferred to a pre-blocked streptavidin-coated plate, and incubated for 1 hour while shaking (250 rpm). The plate was washed (at least 4 times), and incubation with conjugate antibody in blocking buffer was performed for 1 hour while shaking (250 rpm). This process was followed by a final wash, and incubation with the substrate solution, preventing light exposure, for 15 minutes at room temperature. Finally, detection was performed on a plate reader, at 450 nm.

2.9. INTRACEREBROVENTRICULAR (ICV) ADMINISTRATION

The administration was performed on C57Bl/6 mice, having 6 animals per group. The selected formulation to be explored was NC-1, containing siRNA-2 at a concentration of 2 mg/mL. Different controls were added, including a vehicle control (PBS), a positive control (internal positive control provided by Eli Lilly, containing siRNA-2 at a concentration of 3 mg/mL), and free siRNA-2 (at a concentration of 2 mg/mL).

ICV administration was performed using a stereotaxic-guided Hamilton syringe and infusion system (Harvard Apparatus). A single infusion of 10 µL of the material was performed into the right ventricle (AP = -0.3 mm; ML = +1.0 mm; DV: -2.4 mm), using a 25 µL Hamilton syringe with a 30-gauge needle. After 14 days, animals were euthanized and tissue was collected from the left hemisphere, including the frontal cortex, striatum, hippocampus, brain stem, and dorsal root ganglion (DRG). These tissues were homogenized, and Cell-to-CT and qPCR process was performed as summarized in section 2.7.1., with specific probes for quantification of the mRNA target of siRNA-2.

The right hemisphere was fixed with neutral buffered formalin, and sagittal slides were sectioning, of around 5 µm thickness. Samples were used to perform RNAscope, aiming to visualize the siRNA-2 diffusion in the brain.

3. RESULTS AND DISCUSSION

In the context of CNS disorders, siRNA-based therapies offer promising alternatives to conventional therapies. They have the potential to address the root causes of diseases rather than merely alleviating symptoms. However, their clinical application faces challenges, primarily related to accessing the CNS and the necessity for invasive administration techniques. Additionally, the development of suitable delivery systems is crucial to protect and ensure the effective delivery of siRNA to the targeted cells. Aiming to explore the potential of nanotechnology for various modalities of administration, including N-to-B and ICV, a library of NEs and polymeric NCs was developed and fully characterized. The selection of these delivery technologies, which are well established in our laboratory, was based on their versatility, flexibility, small size, and adjustable surface composition and surface charge.

3.1. DEVELOPMENT OF A LIBRARY OF NANOEMULSIONS AND NANOCAPSULES

3.1.1. Selection of the core of nanoemulsions

A library of different NEs and NCs was developed, aiming to fulfill the mentioned target product profile. Specifically, the selected nanocarriers needed to be reproducible, with a particle diameter less than or approximately 100 nm, and exhibit different surface charges (including neutral, positive, and negative). Additionally, their production had to be scalable and ensure at least one-month stability at 4ºC.

To determine the composition of the NEs, an initial screening was performed using DOTAP, a cationic lipid capable of interacting with siRNA. It was combined with four different oils (Vitamin E, oleic acid, Labrafac™, and castor oil), and four different surfactants (DSPC, SPAN 80, Tween 80, and K-HS15®). The combinations of specific oils and surfactants were expected to influence the stability of the NEs in biological fluids and their brain uptake [67,68]. The results of this screening (Supplementary Table 1) indicate that, overall, the smallest sizes were achieved with NE combining DOTAP and Vitamin E, followed by the combination of DOTAP and Labrafac™. In these two combinations, the use of the surfactants K-HS15® and Tween 80 also yielded more favorable physicochemical properties in terms of particle size and polydispersity.

The combination of DOTAP with the oils Vitamin E and Labrafac™, along with K-HS15® and Tween 80, were selected for further optimization. Initially, blank NEs were prepared and concentrated using vacuum evaporation, resulting in a final DOTAP concentration of 8.47 mg/mL (Supplementary Table 2). Subsequently, a screening was conducted using different concentrations of blank NEs and siRNA, aiming to achieve a final siRNA concentration in the range of 0.25 to 1 mg/mL. In all cases, the N/P ratio was maintained as 2:1, to ensure complete complexation of siRNA. As shown in Supplementary Table 3, Vitamin E-based NEs exhibited smaller sizes than the Labrafac™-based NEs, with no significant differences found among the surfactants used. The complexation of siRNA, as determined by the agarose gel technique, was optimal for Vitamin E-based NEs, with no siRNA displacement in the presence of heparin (Supplementary Figure 1). The band corresponding with free siRNA was only observed after the disruption of the nanocarriers with Triton X.

In the final step of this initial screening, NE production was performed using a microfluidic system to further reduce the particle size [69]. As a part of this exploratory assay, a NE containing Vitamin E and K-HS15® was mixed with the siRNA solution, resulting in a final siRNA concentration of 0.75 mg/mL. Two different total flow rates were explored, and as reported in Supplementary Table 4, higher flow rates led to smaller particle sizes and reduced polydispersity index. Additionally, no changes in encapsulation efficiency were found at different total flow rates, indicating that all siRNA was entrapped within the nanocarrier and fully released after treatment with Triton X, as shown in Supplementary Figure 2.

This initial screening enabled the identification of a combination of oils and surfactants for the formulation of blank NEs that meet the desired physicochemical properties. Furthermore, microfluidic mixing has been shown to reduce the polydispersity of the formulation upon the complexation of siRNA.

3.1.2. Development of siRNA-loaded nanoemulsions

NEs were produced by microfluidics mixing of an organic phase containing the cationic lipid and the oil, and an aqueous phase with the siRNA and surfactant solutions. Various combinations of oils (Vitamin E and Labrafac™) and surfactants (Tween 80, K-HS15®, Labrasol®, and Inulin) were explored to increase the compositional variability of our library. The ratios among the different components were optimized to achieve a particle size smaller than 100 nm, a positive surface charge, and a final siRNA concentration of 0.75 mg/mL, as required by the TPP.

The production of small NE-siRNA shown in Table 1 required optimization. Specifically, NE-3 (DOTAP: Labrafac™: Tween 80) was optimized, as reported in Supplementary Table 5. Initially, a high content of oil was used (16.8: 81.4: 1.8), resulting in considerably larger size and polydispersity. By reducing the oily content and increasing both cationic lipid and surfactant molar percentages (46: 35.5: 18.5), the polydispersity index and particle diameter were reduced accordingly. To further reduce the particle size, adjustments were made to slightly reduce the cationic lipid and increase the amount of oil (25: 56.5: 18.5). Moreover, different total flow rates were explored, concluding that high rates (14 mL/min) resulted in smaller particle sizes. In summary, the molar ratio selected for the formulation of NE-3 was 25: 56.5: 18.5 (DOTAP: Labrafac™: Tween 80), using a total flow rate of 14 mL/min, and a final siRNA concentration of 0.75 mg/mL.

Table 1. Physicochemical properties of siRNA-loaded NE-1, NE-2, NE-3, NE-4 and NE-5

	NE-1	NE-2	NE-3	NE-4	NE-5
Composition (DOTAP:oil: surfactant)	DOTAP: Vit E: K-HS15®	DOTAP: Vit E: Tween 80	DOTAP: Lab™: Tween 80	DOTAP: Vit E: Labrasol®	DOTAP: Vit E: Inulin
Molar ratio (mol%)	16.9:65.8:17.3	19.4:75.4:5.2	25:56.5:18.5	19.4:75.4:5.2	19.4:75.4:5.2
Particle diameter (nm)	90 ± 16	73 ± 10	86 ± 10	100 ± 8	68 ± 5
PDI	0.20 ± 0.04	0.20 ± 0.04	0.24 ± 0.03	0.18 ± 0.01	0.26 ± 0.03
ζ-Potential (mV)	+51 ± 3	+47 ± 4	+38 ± 6	+50 ± 3	+48 ± 2
Encapsulation efficiency (%)	100	100	100	100	100

Encapsulation efficiency was measured by agarose gel, and values were corroborated by RiboGreen assay and/or UPLC analysis. **Abbreviations:** DOTAP: 1,2-dioleoyl-3-trimethylammonium propane. K-HS15®: Kolliphor® HS15. Lab™: Labrafac™ Lipophile, WL 1349. NE: nanoemulsion. PDI: polydispersity index. Vit E: D, L-α-tocopherol. Values represent the mean ± standard deviation (n ≥ 3).

On the other hand, the optimization of NEs containing DOTAP, Labrafac™, and K-HS15® can be found in Supplementary Table 6. The initial molar ratio explored (16: 77.5: 6.5), regardless of the total flow rate used for their microfluidic production or the final siRNA concentration, resulted in sizes exceeding the desirable limits. The reduction of the oily content of the NEs led to a reduction in particle diameters and an increase in the polydispersity index. Considering the physicochemical properties obtained, this combination of materials was discarded.

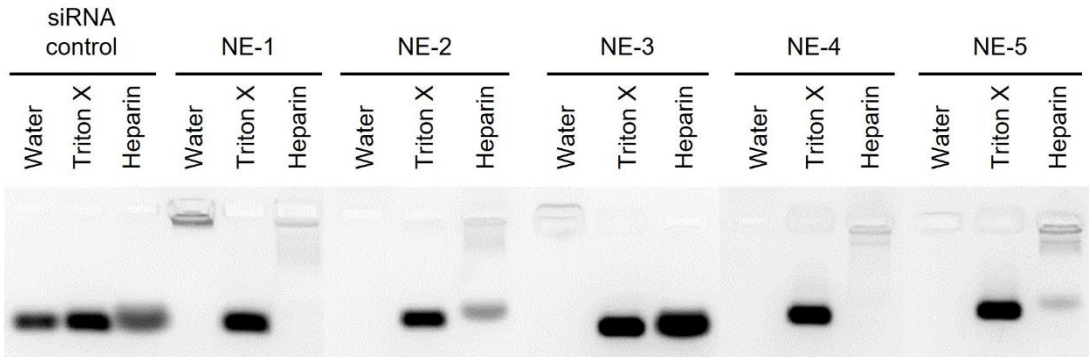

Figure 3. Encapsulation efficiency of siRNA-loaded NE-1, NE-2, NE-3, NE-4 and NE-4. Samples were treated with Triton X or heparin for nanoemulsion disruption or siRNA displacement, respectively

Abbreviations: NE: nanoemulsion. Triton X: Triton-X-100.

According to the agarose gel, and further confirmed by Ribogreen assay and UPLC analysis, all siRNA was associated with the NEs (Figure 3). Treatment with Triton X led to disruption of NE-siRNA systems, allowing the release and detection of the free siRNA. However, displacement by heparin was only observed for NE-3. In the case of NE-2 and NE-5, partial displacement was observed after heparin treatment, while no displacement was detected in NE-1 and NE-4. These distinct behaviors indicate differences in the interactions between siRNA and the cationic component of the NE-siRNA. A possible explanation would be the type of surfactant used, as NE-2, NE-4, and NE-3 contain the same components at the same molar ratios, except for the surfactant.

3.1.3. Development of siRNA-loaded nanocapsules

The complexation of different polymers over pre-formed NE-siRNA systems led to the formation of siRNA-loaded NCs (NC-siRNA) with different physicochemical and surface properties. Polymers used to form the capsule shell include polyethylene glycol-polyglutamic acid (PEG-PGA), hyaluronic acid (HA), polysialic acid (PSA), and chitosan (CS). Their selection was based on their solubility in water, safety profile, and variety of net charges (neutral, from PEG-PGA; negative, from HA and PSA; and positive, from CS). In addition, some of these polymers, CS and HA, are known for their bioadhesive properties.

Regarding the physicochemical properties that may influence the N-to-B transport, it has been reported that positively charged NPs and liposomes are retained on the negatively charged olfactory epithelium, thereby facilitating the transport of associated molecules into the brain [42,70]. This behavior has been attributed to their adhesion to the olfactory epithelium. In particular, HA and CS, have been reported to facilitate the diffusion of drugs across the olfactory epithelium [39,71–74]. However, the capacity of these nanocarriers to overcome the N-to-B barriers has not been sufficiently validated.

On the other hand, when considering the influence of the nanocarrier's charge on brain transport, results are controversial and highly affected by the nature of the studies performed. Some authors have reported that highly anionic nanocarriers have a greater chance of disrupting the BBB and diffusing across the brain than neutral NPs [75,76]. However, other reports highlight the importance of a positive surface charge for electrostatic adhesion to endothelial

cell membranes and subsequent transcytosis of these nanocarriers across the BBB and the brain [77,78]. Unfortunately, all these studies fail to understand the role of the protein corona, particularly relevant in charged particles, and their subsequent transport across the BBB and the CNS. This is a subject that still needs significant attention from the scientific community.

Table 2. Physicochemical properties of siRNA-loaded NC-1, NC-2, NC-3, NC-4, NC-5 and MNC-1

	NC-1	NC-2	NC-3	NC-4	NC-5	MNC-1
Base nanosystem	NE-2	NE-2	NE-2	NE-3	NE-3	NC-2
Base composition	DOTAP: Vit E: T80	DOTAP: Vit E: T80	DOTAP: Vit E: T80	DOTAP: Lab™: T80	DOTAP: Lab™: T80	DOTAP: Vit E: T80 + HA
Polymer coating	PEG-PGA	HA	PSA	HA	PSA	CS
siRNA: polymer ratio (mol/mol)	1:2	1:4	-	1:4	-	-
siRNA: polymer ratio (w/w)	-	-	1:2	-	1:4	1:3.8
Particle diameter (nm)	73 ± 5	87 ± 6	116 ± 3	70 ± 8	79 ± 11	100 ± 16
PDI	0.15 ± 0.03	0.15 ± 0.02	0.13 ± 0.03	0.24 ± 0.03	0.23 ± 0.02	0.18 ± 0.02
ζ-Potential (mV)	-1 ± 6	-28 ± 2	-48 ± 1	-23 ± 5	-44 ± 8	+49 ± 4
Encapsulation efficiency (%)	100	100	100	100	100	100

Encapsulation efficiency was measured by agarose gel, and values were corroborated by RiboGreen assay and/or UPLC analysis. **Abbreviations:** CS: chitosan. DOTAP: 1,2-dioleoyl-3-trimethylammonium propane. HA: hyaluronic acid (40 kDa). Lab™: Labrafac™ Lipophile, WL 1349. MNC: multi-layer nanocapsule. mol/mol: mol to mol ratio. NC: nanocapsule. NE: nanoemulsion. PEG-PGA: PEG (5 kDa)-b-PGA (10) (Na). PDI: polydispersity index. PSA: polysialic acid (30 kDa). T80: Tween 80. Vit E: D, L-α-tocopherol. w/w: weight-to-weight ratio. Values represent the mean ± standard deviation (n ≥ 3).

The polymer coating of the NCs was formed using different amounts of polymer, with varying weight-to-weight (w/w) or mol-to-mol (mol/mol) ratios between the siRNA and the polymer. In the case of CS, a double HA/CS layer was formed. Table 2 shows that the particle diameter was influenced by the type of polymer used. For example, NC-1 (DOTAP: Vitamin E: Tween 80 + PEG-PGA), NC-2 (DOTAP: Vitamin E: Tween 80 + HA), and NC-3 (DOTAP: Vitamin E: Tween 80 + PSA), with the same oily core (NE-2), presented different particle sizes due to the different polymer shell. A similar behavior was observed for NC-4 and NC-5 with the same oily core (DOTAP: Labrafac™: Tween 80), but with a HA or PSA polymer shell, respectively. Finally, MNC-1 (DOTAP: Vitamin E: Tween 80 + HA + CS) exhibited the largest size, which may be attributed to the double polymer shell. As expected, the different polymer coatings had an impact on the surface charge of the NCs. NC-1, being the only system with PEG-PGA, depicted a neutral surface charge; while MNC-1, containing CS on the outer layer, exhibited a positive charge. Overall, the coating of selected NE-siRNA with different polymers allowed the development of a diverse library of NC-siRNA, presenting differences in size and surface charge.

The RNA association efficiency was 100% in all cases, leading to a final siRNA concentration of 0.625 mg/mL (Figure 4). Interestingly, regardless of the polymeric coating, dissociation of siRNA from the NC-siRNAs was equivalent to the observed with the NE-siRNAs. Therefore, NC-siRNA derived from NE-2 (NC-1, NC-2, NC-3, and MNC-1)

completely released their siRNA content after treatment with Triton X, but not after the addition of heparin. On the other hand, NC-siRNA derived from NE-3 (NC-4 and NC-5) presented a total release of the siRNA after treatment with both disrupting reagents.

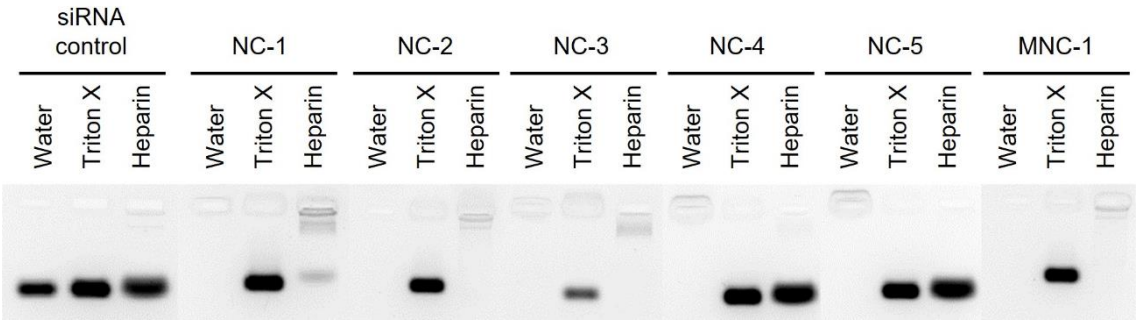

Figure 4. Encapsulation efficiency of siRNA-loaded NC-1, NC-2, NC-3, NC-4, NC-5 and MNC-1. Samples were treated with Triton X or heparin for nanoemulsion disruption or siRNA displacement, respectively

Abbreviations: MNC: multi-layer nanocapsule. NC: nanocapsule. Triton X: Triton-X-100.

For each NC-siRNA, different w/w or mol/mol ratios between siRNA and the polymers were tested, resulting in variations in the physicochemical properties of the NC-siRNA, as outlined in Supplementary Table 7. Overall, higher siRNA-to-polymer ratios, regardless of the polymer used, resulted in larger particle diameters and more significant alterations in the surface charge. Specific siRNA-to-polymer ratios were required for each polymer and NC, as summarized in Table 2. These variations may be attributed to the specific polymer used and its interactions with the cationic surface of the NEs.

3.2. FUNCTIONALIZATION OF SIRNA-LOADED NANOEMULSION WITH RVG PEPTIDE

We selected NE-2 for functionalization with a rabies virus glycoprotein (RVG). The RVG peptide, responsible for cellular entry and virus fusion, binds to the nicotinic acetylcholine receptor found in CNS cells [79]. RVG has previously been utilized as a targeting ligand for RNA delivery via the N-to-B route [80]. To achieve this, we conjugated RVG with a PEGylated surfactant, DSPE-PEG_{2000}, which has a maleimide terminal group. Two different methodologies were explored for functionalization: (i) direct conjugation of the targeting ligand onto the preformed NE-2, containing DSPE-PEG_{2000}-maleimide; or (ii) pre-conjugation, involving the functionalization of RVG onto DSPE-PEG_{2000}-maleimide, followed by the formulation of the nanosystem in presence of the modified lipid. In both strategies, RVG was conjugated to the maleimide group using thiol-maleimide click chemistry.

As illustrated in Figure 5 (top left), RVG was modified to present a Cys on the N-terminus, intended to facilitate the interaction with the maleimide group. According to the modeling of the RVG sequence, both Cys residues (highlighted in yellow) are accessible for their interaction with the maleimide group. The results obtained by ^{1}H NMR allowed the assessment of the peptide conjugation reaction and its yield. Both RVG peptide and DSPE-PEG_{2000}-maleimide were analyzed separately (top right and bottom left, respectively) to identify characteristic peaks. These peaks were observed on the spectrum obtained after the conjugation process

(bottom right), indicating the successful reaction between the RVG and the maleimide group of the PEGylated lipid. The conjugation efficiency was calculated as 95%, and the yield or recovery percentage of the reaction was estimated at 73.6%.

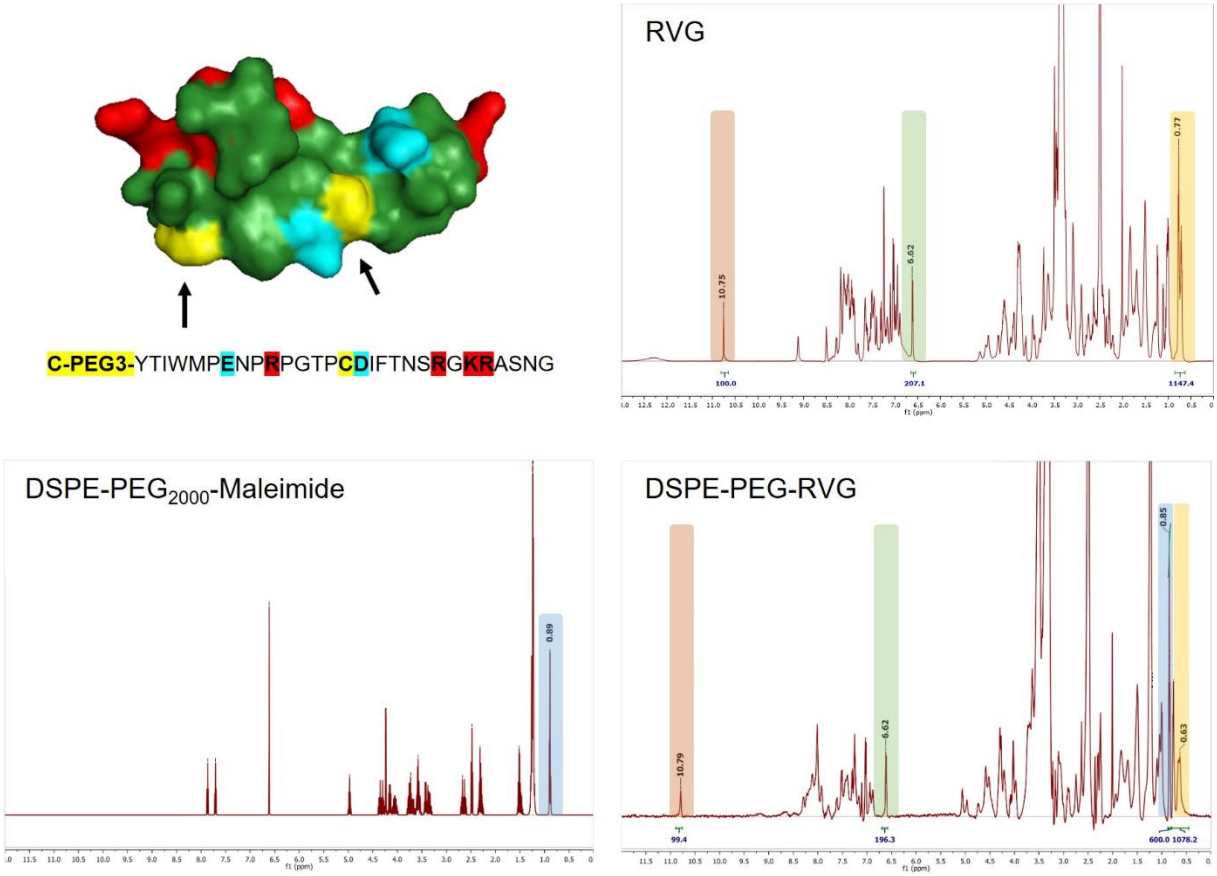

Figure 5. RVG functionalization onto DSPE-PEG$_{2000}$-maleimide

Structure of C-PEG3-RVG, predicted using PEP-FOLD 3 online tool. The 3D-surface of the peptide was generated by PyMOL Molecular Graphics Systems, Version 1.4.7.5 Edu, Schrodinger, LLC. Black arrows indicate the theoretical location of the cysteine (C) residues on the folded peptide (top left). ^{1}H NMR spectrum of RVG (top right), DSPE-PEG$_{2000}$-maleimide (bottom left), and DSPE-PEG-RVG (bottom right). The orange box indicates the signal from the NH group in the indole ring of the tryptophan (W) residue (10.78 ppm, 1 hydrogen); the green box corresponds with the signal of the OH group of the tyrosine (Y) residue (8.99 ppm, 4 hydrogens); the yellow box indicates the signal of four methyl groups of the isoleucine (I) residue (0.76-0.63 ppm, 12 hydrogens); all provided by the RVG peptide. The blue box indicates the signal from two CH3 groups, from the terminal methyl groups of alkyl chains of DSPE-PEG$_{2000}$-maleimide (0.85 ppm, 6 hydrogens).

Both conjugation strategies, pre- and post-insertion onto the NE, resulted in significant differences in terms of physicochemical characterization, as presented in Table 3. Direct conjugation of RVG peptide onto preformed NE-2-siRNA, containing 0.1% mol of DSPE-PEG$_{2000}$-maleimide, was explored with two different mol/mol ratios between maleimide and the targeting ligand. The second strategy involved the formulation of NE-2-RVG in a single step by adding 0.1% mol of pre-conjugated DSPE-PEG-RVG. Due to differences in particle size, the second strategy was selected for further studies.

Table 3. Physicochemical properties of NE-2 functionalized with RVG peptide, following two different conjugation strategies

Strategy	Condition	Ratio Mal:RVG (mol/mol)	Particle diameter (nm)	PDI	ζ-Potential (mV)	EE (%)
Direct conjugation	NE-2-Mal		61	0.24	+48	100
	NE-2-RVG	1:1	75	0.24	+60	100
		1:2	70	0.22	+55	100
Pre-conjugation	NE-2-RVG	-	84 ± 37	0.25 ± 0.01	+57 ± 6	100

Encapsulation efficiency was measured by agarose gel, and values were corroborated by RiboGreen assay and/or UPLC analysis. **Abbreviations:** EE: encapsulation efficiency. Mal: maleimide. mol/mol: mol to mol ratio. NE: nanoemulsion. PDI: polydispersity index. RVG: rabies virus glycoprotein. Values represent the mean ± standard deviation (n ≥ 3, unless no standard deviation is reported).

3.3. CONCENTRATION, SCALE-UP, AND STABILITY OF NANOEMULSIONS AND NANOCAPSULES

The formulations developed were concentrated using Amicon® Ultra 0.5 mL Centrifugal Filters Ultracel® -100K (Merck Millipore, MA, USA). As presented in Table 4, selected NE-siRNA (NE-1, NE-2, NE-3, NE-4, and NE-5) and NC-siRNA (NC-1, NC-4, NC-5, and MNC-1) were concentrated to achieve siRNA concentrations of at least 3 mg/mL.

Table 4. Physicochemical properties of selected NE-siRNA and NC-siRNA after concentration using centrifugal filters

Nanosystem	Speed (g)	Time (min)	$[siRNA]_{final}$ (mg/mL)	Particle diameter (nm)	PDI	ζ-Potential (mV)	EE (%)
NE-1	14000	5	4.1 ± 0.1	95 ± 2	0.21 ± 0.01	+52 ± 1	100
NE-2	14000	5	3.5 ± 0.3	69 ± 4	0.22 ± 0.02	+60 ± 3	100
NE-3	14000	5	4.3 ± 0.6	88 ± 1	0.23 ± 0.01	+47 ± 1	100
NE-4	14000	10	3.2 ± 0.5*	107 ± 2	0.24 ± 0.02	+55 ± 5	100
NE-5 (n = 2)	14000	5	3.4 ± 0.1*	81 ± 1	0.26 ± 0.01	+49 ± 1	100
NC-1 (n = 2)	14000	15	2.9 ± 0.8	73 ± 1	0.09 ± 0.02	+0.3 ± 1	100
NC-4 (n = 2)	14000	10	4 ± 1.1	84 ± 11	0.20 ± 0.02	-25 ± 1	100
NC-5 (n = 2)	14000	10	3.8 ± 0.9	83 ± 2	0.19 ± 0.01	-44 ± 2	100
MNC-1	14000	10	3.4 ± 0.1	95 ± 2	0.13 ± 0.02	+66 ± 4	100

Final concentrations of siRNA were determined by RiboGreen assay or UPLC analysis (indicated as *). Encapsulation efficiency was measured by agarose gel, and values were corroborated by RiboGreen assay and/or UPLC analysis. **Abbreviations:** EE: encapsulation efficiency. MNC: multi-layer nanocapsule. NC: nanocapsule NE: nanoemulsion. PDI: polydispersity index. Values represent the mean ± standard deviation (n ≥ 3, unless no standard deviation is reported, or indicated otherwise).

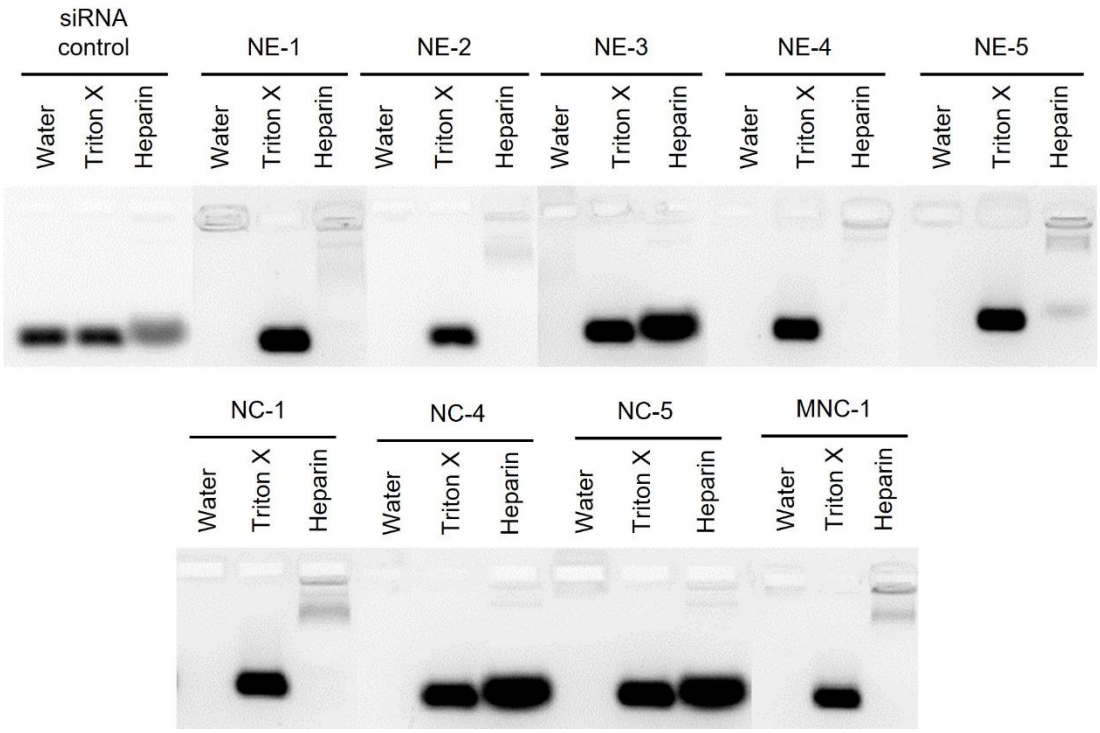

Figure 6. Encapsulation efficiency of selected NE-siRNA and NC-siRNA after concentration using centrifugal filters. Samples were treated with Triton X or heparin for nanosystem disruption or siRNA displacement, respectively

Abbreviations: MNC: multi-layer nanocapsule. NC: nanocapsule. NE: nanoemulsion. Triton X: Triton-X-100.

Table 5. Physicochemical properties of selected nanosystems after the scale-up of formulation and concentration processes

Nanosystem	Process	$[siRNA]_{final}$ (mg/mL)	Particle diameter (nm)	PDI	ζ-Potential (mV)	EE (%)
NE-2	Formulation	-	61 ± 5	0.22 ± 0.2	+49 ± 5	-
	Concentration 5000 g | 20 min	3.8 ± 0.3	69 ± 2	0.25 ± 0.01	+59 ± 2	100
NE-3	Formulation	-	68 ± 3	0.25 ± 0.01	+46 ± 5	-
NE-2-RVG	Formulation	-	57 ± 3	0.25 ± 0.01	+54 ± 8	-
	Concentration 5000 g | 20 min	3.6 ± 0.1	64 ± 3	0.26 ± 0.01	+58 ± 4	100
NC-1 (n = 2)	Formulation	-	68 ± 2	0.15 ± 0.03	+2 ± 8	-
	Concentration 7000 g | 15 min	3 ± 0.1	71 ± 2	0.13 ± 0.01	+4 ± 13	100
NC-5	Formulation	-	65 ± 3	0.22 ± 0.01	-46 ± 4	-
	Concentration 5000 g | 20 min	4.6 ± 0.5	70 ± 4	0.21 ± 0.01	-52 ± 3	100

Final concentration of siRNA and encapsulation efficiency were determined by UPLC analysis. **Abbreviations:** EE: encapsulation efficiency. NC: nanocapsule NE: nanoemulsion. PDI: polydispersity index. RVG: rabies virus glycoprotein. Values represent the mean ± standard deviation (n ≥ 3, unless indicated otherwise).

The physicochemical characteristics of the concentrated carriers remained unmodified after concentration. The agarose gel exhibited complete entrapment of siRNA in all the nanocarriers prepared, as disclosed in Figure 6. Moreover, total release was achieved after treatment with Triton X; while heparin displacement, similar to the non-concentrated nanosystems, was only accomplished on formulations containing Labrafac^{TM} as the oily core. The difference may be attributed to their surface properties and the presence of certain surfactants and polymeric coatings. Some nanocarriers, such as NC-2, could not be concentrated, due to aggregation and poor encapsulation efficiency after the concentration process.

Considering that the ultimate goal of these formulations was their administration into an animal model, a scale-up from the original batch (1.2 mL) to a more suitable size was performed. Thus, the scale-up of the formulations and concentration processes was assessed. The formulation of NE-siRNA was performed on a microfluidic system, adjusting the process to reach a final volume of 12 mL. Both scaled-up NE-siRNA and NC-siRNA nanocarriers were concentrated on a larger scale, using Amicon® Ultra-15 Centrifugal Filters Ultracel® -100K (Merck Millipore, MA, USA), resulting in greater final volumes (2 mL) and similar final siRNA concentrations. As reported in Table 5, physicochemical properties after the scale-up process were similar to those prepared on a smaller scale, successfully validating the method.

Table 6. Physicochemical properties of NE-siRNA and NC-siRNA nanosystems after 1 month at 4 °C, before and after concentration

Nanosystem	Particle diameter (nm)	PDI	ζ-Potential (mV)	EE (%)
NE-1	102 ± 16	0.19 ± 0.04	+49 ± 2	100
NE-1 concentrated	107 ± 9	0.19 ± 0.03	+53 ± 3	-
NE-2	79 ± 9	0.19 ± 0.02	+55 ± 8	100
NE-2 concentrated	80 ± 6	0.23 ± 0.02	+54 ± 3	-
NE-3	98 ± 8	0.27 ± 0.08	+60 ± 4	100
NE-3 concentrated	104 ± 4	0.27 ± 0.03	+51 ± 1	-
NE-4	115 ± 6	0.15 ± 0.01	+49 ± 4	100
NE-4 concentrated (n = 2)	116 ± 5	0.21 ± 0.02	+54 ± 5	-
NE-5 (n = 1)	73	0.22	+43	100
NE-5 concentrated (n = 2)	86 ± 1	0.3 ± 0.01	+54 ± 1	-
NE-2-RVG (n = 2)	131 ± 1	0.19 ± 0.02	+59 ± 1	-
NC-1	76 ± 6	0.16 ± 0.04	-6 ± 1	100
NC-1 concentrated (n = 2)	77 ± 1	0.15 ± 0.01	-3 ± 1	-
NC-2	90 ± 7	0.14 ± 0.04	-31 ± 5	100
NC-3 (n = 1)	122	0.21	-49	100
NC-4	86 ± 12	0.29 ± 0.09	-27 ± 3	100
NC-4 concentrated (n = 2)	92 ± 8	0.22 ± 0.04	-25 ± 1	-
NC-5	81 ± 8	0.23 ± 0.01	-45 ± 4	100
NC-5 concentrated (n = 2)	90 ± 5	0.26 ± 0.06	-47 ± 1	-
MNC-1	110 ± 21	0.17 ± 0.02	+37 ± 8	100
MNC-1 concentrated	100 ± 2	0.13 ± 0.02	+57 ± 6	-

Final concentrations of siRNA were determined by RiboGreen assay or UPLC analysis (*). Encapsulation efficiency was measured by agarose gel. **Abbreviations:** EE: encapsulation efficiency. MNC: multi-layer nanocapsule. NC: nanocapsule NE: nanoemulsion. PDI: polydispersity index. RVG: rabies virus glycoprotein. Values represent the mean ± standard deviation (n ≥ 3, unless indicated otherwise).

The stability of the nanoformulations was assessed after their storage at 4 ºC for one month, both before and after their concentration, as reported in Table 6. The results showed that all NE-siRNA and NC-siRNA explored were stable, with differences in particle diameter size smaller than 20%. According to Figure 7, all siRNA remained associated to the different nanocarriers, and the release patterns were similar to those found on freshly prepared NEs. Therefore, it can be concluded that the developed nanocarriers are highly stable at 4 ºC for at least one month.

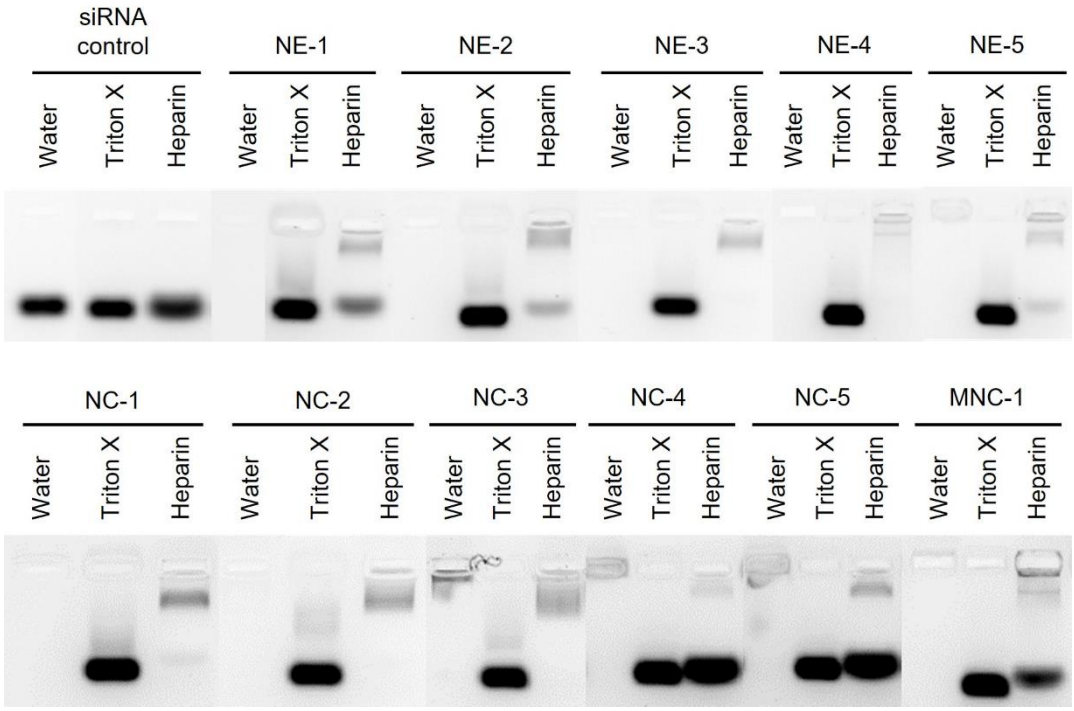

Figure 7. Encapsulation efficiency of NE-siRNA and NC-siRNA nanosystems after 1 month at 4 ºC, before and after concentration. Samples were treated with Triton X or heparin for nanosystem disruption or siRNA displacement, respectively

Abbreviations: MNC: multi-layer nanocapsule. NC: nanocapsule. NE: nanoemulsion. Triton X: Triton-X-100.

3.4. PRELIMINARY IN VITRO EVALUATION OF NANOCARRIERS

Selected NEs and NCs were evaluated in different *in vitro* studies intended to assess the transfection potency, cytotoxicity, and barrier-crossing abilities of selected NEs and NCs (Table 7). In all cases, *in vitro* studies were performed using siRNA-1.

Table 7. Summary of the nanocarriers used for *in vitro* evaluation

Nanosystem	Composition	Barrier crossing capacity	Transfection efficiency and cytotoxicity
NE-1	DOTAP: Vit E: K-HS15®	✓	
NE-2	DOTAP: Vit E: Tween 80	✓	
NE-2-RVG	DOTAP: Vit E: Tween 80: DSPE-PEG_{2000}-RVG	✓	
NE-3	DOTAP: Lab™: Tween 80	✓	
NC-1	DOTAP: Vit E: Tween 80 + PEG-PGA	✓	✓
NC-2	DOTAP: Vit E: Tween 80 + HA	✓	✓
NE-3	DOTAP: Vit E: Tween 80 + PSA		✓
NE-4	DOTPA: Lab™: Tween 80 + HA	✓	✓
NC-5	DOTAP: Lab™: Tween 80 + PSA	✓	✓

Abbreviations: DOTAP: 1,2-dioleoyl-3-trimethylammonium propane. HA: hyaluronic acid (40 kDa). K-HS15®: Kolliphor® HS15. Lab™: Labrafac™ Lipophile, WL 1349. NC: nanocapsule NE: nanoemulsion. PEG-PGA: PEG (5 kDa)-b-PGA (10) (Na). PSA: polysialic acid (30 kDa). RVG: rabies virus glycoprotein. Vit E: D, L-α-tocopherol.

3.4.1. Evaluation of the capacity of nanocarriers to cross an *in vitro* epithelium model

We conducted a study to investigate the interaction and toxicity of selected nanocarriers using the EpiAirway™ model. EpiAirway™ is a 3-dimensional model of highly differentiated primary human tracheal and bronchial epithelial cells, which exhibit uniform thickness and *in vivo*-like barrier properties. The selection of the nanocarriers was based on their differences in composition and physicochemical properties, and the aim was to compare their capacity to cross this barrier. The transendothelial electrical resistance (TEER) was used as a quantitative technique to assess the integrity and permeability of tight junctions in this co-culture model of endothelial and epithelial cells. TEER involves measuring electrical resistance across a cellular monolayer, indicating its integrity [81,82].

Four NEs (NE-1, NE-2, NE-2-RVG, and NE-3) and four NCs (NC-1, NC-2, NC-4, and NC-5) were incubated in the *in vitro* epithelium model, and their TEER values were measured at two different time points (Figure 8, top). Controls used included Triton X (as a positive control, or PC), untreated conditions (UT), PBS (or vehicle control, VC), and LY-06-D (an internal control provided by Eli Lilly). PC and LY-06D resulted in a complete loss of barrier integrity at both time points analyzed, with no recovery after 24 hours. In contrast, PBS (VC) exhibited reduced TEER values after 4 hours, followed by full recovery after 24 hours, indicating a temporary loosening of tight junctions.

As depicted in Figure 8, both NEs and NCs displayed a similar TEER profile, which closely resembled that of PBS (VC). This profile involved a temporary loss of barrier integrity followed by a complete recovery. In all cases, TEER values of the nanocarriers exceeded those of the UT condition, suggesting an overgrowth of the cells in the *in vitro* model. However, there were some subtle trends observed among the different nanocarriers. Overall, NEs exhibited slightly lower TEER values than NCs, possibly due to their positive surface charge, which may influence their interaction with the negatively charged endothelial surface [83]. Furthermore, the type of polymer shell also appeared to influence the TEER values. Specifically, formulation NC-5, which contained PSA as a polymer shell, exhibited the highest reduction in TEER. Nevertheless, these findings should be interpreted with caution, as no significant differences were found after statistical analysis.

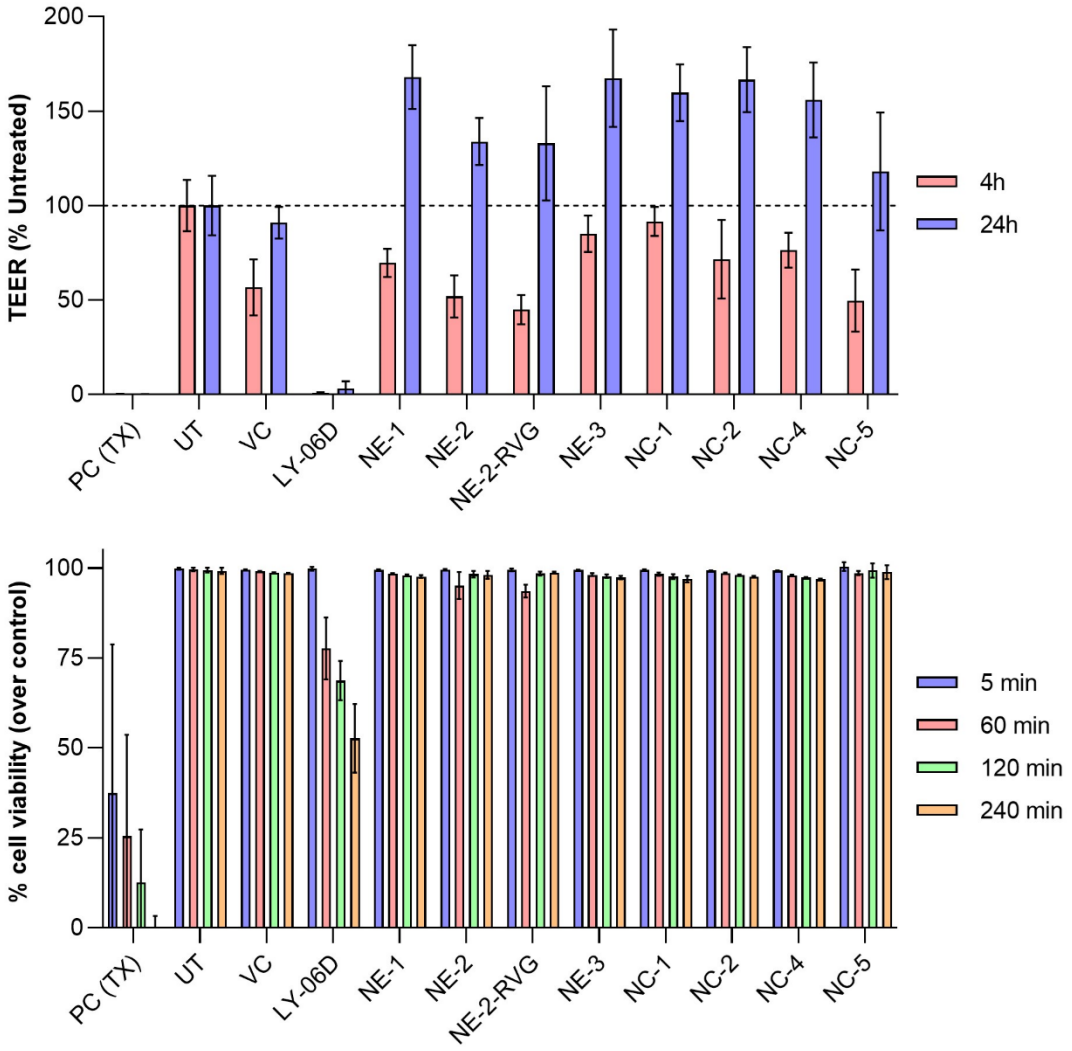

Figure 8. TEER measurement of different NEs and NCs, on a full-thickness epithelium *in vitro* model (top), and their cellular viability at different time points (bottom)

Abbreviations: LY-06D: positive control (internal control from Eli Lilly & Company). NC: nanocapsule. NE: nanoemulsion. PC: positive control. RVG: rabies virus glycoprotein. TEER: transendothelial electrical resistance. TX: Triton X. UT: untreated. VC: vehicle control (PBS). Values represent the mean ± standard deviation (n ≥ 3).

Cellular cytotoxicity was also assessed at different time points (Figure 8, bottom). Both positive controls (PC and LY-06D) displayed time-dependent cytotoxicity; while none of the nanoformulations tested induced any cellular toxicity at any of the time points evaluated. This supports the hypothesis of a temporal loosening on the cellular barrier model, unrelated to cytotoxicity, and which recovers over time.

Samples collected at different time points were treated to disrupt the nanocarriers and release the siRNA cargo. Subsequently, hELISA was performed to determine the permeability coefficient (Supplementary Figure 3, top) and the percentage of nanocarrier permeated (Supplementary Figure 3, bottom). Notably, significant differences were observed compared to the internal LY-06D positive control, as none of the nanocarriers showed significant permeation across the model barrier.

3.4.2. Silencing efficacy and cytotoxicity assessment

The *in vitro* behavior of the NC prototypes was assessed in a neuroblastoma cell model (BE(2)-C cells) in a dose-dependent manner, with concentrations ranging from 100 to 10 nM (Figure 9). Both silencing efficacy and cytotoxicity responses were compared to those of free siRNA and two positive controls (PC). PC (LNP) corresponds to a classical LNP used for the delivery of partisiran [84,85]; whereas PC (LP) corresponds with Lipofectamine. PC (LNP) was tested at different concentrations, ranging from 100 to 0.1 nM; whereas PC (LP) contained a final siRNA concentration of 10 mM.

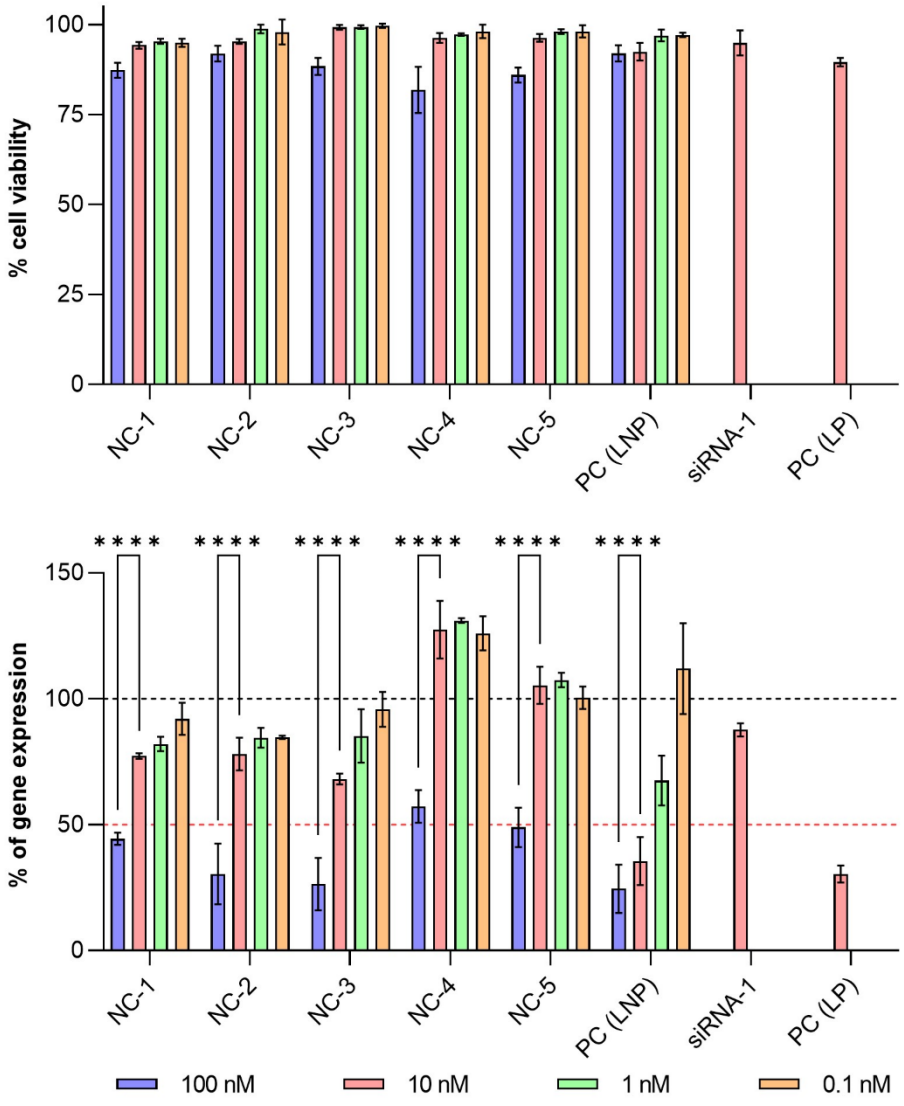

Figure 9. Cytotoxicity (top) and quantitative real-time PCR of the silencing effect of siRNA-1 (bottom), after the administration of NC-1, NC-2, NC-3, NC-4, and NC-5 in BE(2)-C cells. The comparison was made with free siRNA-1 (siRNA-1), an optimized LNP formulation (PC (LNP)), and Lipofectamine (PC (LP))

Abbreviations: LNP: lipid nanoparticle. LP: Lipofectamine. NC: nanocapsule. PC: positive control. A significant comparison was performed using two-way ANOVA followed by Tukey's multiple comparison tests of each formulation at the different concentrations tested. *p*-values < 0.0001 were considered statistically significant (****). Values represent the mean ± standard deviation (n ≥ 3).

None of the explored NC formulations exhibited significant cellular toxicity at the tested concentration, similar to the results obtained with free siRNA and both positive controls (Figure 9, top). Small differences among the formulations were found in terms of silencing efficiency (Figure 9, bottom). All of them exhibited a significant dose-dependent silencing effect, with over a 50% reduction at a concentration of 100 nM. Interestingly, no significant differences were found among the NCs containing Vitamin E and low amounts of Tween 80 (NC-1, NC-2, and NC-3), compared to PC (LNP) at the different concentrations tested. This indicates that these formulations were able to transfect the neuron cellular model as efficiently as the current gold standard in terms of RNA delivery (Supplementary Figure 4).

In contrast, formulations containing Labrafac^{TM} and a high amount of Tween 80 (NC-4 and NC-5) resulted in significantly reduced transfection efficiency compared to PC (LNP). These findings suggest that the choice of the oil and the amount of surfactant present on the NE significantly influence cellular uptake. Moreover, considering that NCs with the same coating (such as NC-2 and NC-4, both coated with HA) resulted in different gene silencing effects, it becomes clear that the *in vitro* transfection ability of these NCs is primarily determined by the core itself rather than the coating shell. Overall, this behavior further supports our initial hypothesis that the core of the nanocarriers plays a fundamental role in the overall performance of the delivery system.

3.5. NOSE-TO-BRAIN DELIVERY OF NANOCARRIERS

Selected nanocarriers (NE-2, NE-2-RVG, and NC-5), containing siRNA-1, were administered intranasally to assess their capacity to reach different brain areas (Figure 10). In all cases, the internal positive control LY-06D was included.

Most studies reporting N-to-B delivery of RNA focus on analyzing responses rather than assessing the biodistribution of the NPs in the brain [49,51,54,80]. The few authors who examine brain distribution simply rely on fluorescence analysis or quantitative evaluation of the entire brain [47,48,80,86]. In our study, we determined the distribution of siRNA-1 in the nasal epithelium, olfactory bulb, trigeminal nerve, and frontal cortex to understand the pathways followed by the nanocarriers when they access the brain.

After intranasal administration, a clear accumulation was observed in the nasal epithelium (Figure 10, top left), with higher levels seen for the NCs, compared to the positive control. This improved interaction with the olfactory epithelium might increase the possibility of accessing the brain through both the olfactory and the trigeminal nerve routes. Regarding the olfactory nerve route, both NE-2-RVG and NC-5 showed greater presence in the olfactory bulb compared to the positive control (Figure 10, top right). Additionally, some minor accumulation was observed in the trigeminal nerve (Figure 10, bottom left) and frontal cortex (Figure 10, bottom right). However, these results should be interpreted cautiously due to the high experimental variability.

On the other hand, despite the similar accumulation observed in the nasal epithelium for both NE-2 and NE-2-RVG, only NE-2-RVG was capable of reaching the olfactory bulb. This result suggests that the NEs are unable to access the olfactory bulb on their own, without the assistance of a targeting ligand. One possible explanation could be the electrostatic interaction between the positive charge of the NE and the negative charge of the nasal cavity mucus, which hinders NEs movement. Consequently, targeting ligands (as in NE-2-RVG) or negative surface

charges (as in NC-5) resulted in a greater enhancement of the delivery to the olfactory bulb. Despite the limited transport, significant entrapment of the nasal epithelium was observed for all three nanocarriers tested.

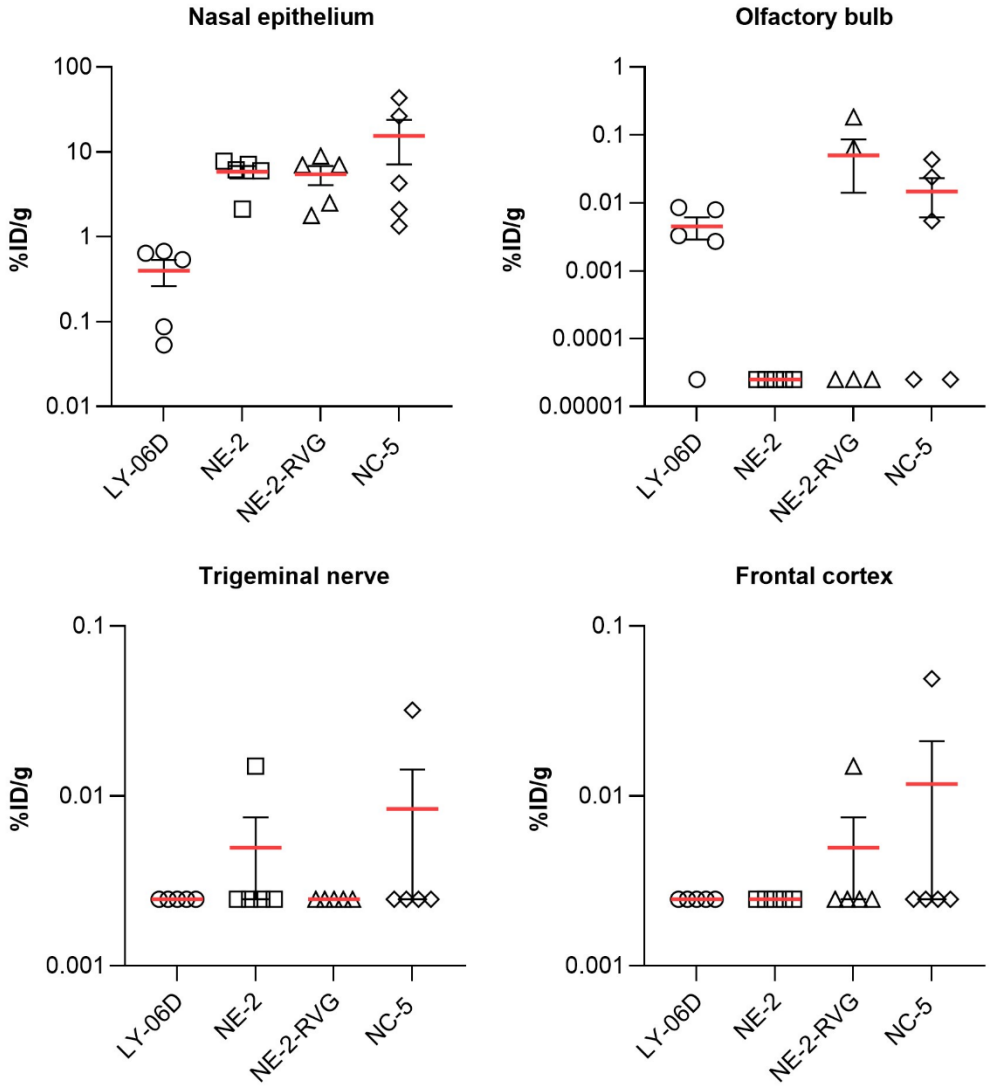

Figure 10. Mean percentage injected dose of siRNA-1 per gram (%ID/g) in different nasal and brain regions, including nasal epithelium (top, left), olfactory bulb (top, right), trigeminal nerve (bottom, left), and frontal cortex (bottom, right)

Abbreviations: LY-06D: internal positive control. NC: nanocapsule. NE: nanoemulsion. RVG: rabies virus glycoprotein. Values represent the mean ± standard deviation (n ≥ 3).

3.6. INTRACEREBROVENTRICULAR DELIVERY OF NANOCARRIERS

Based on the adequate physicochemical properties of NC-1 (particle size of 73 nm, neutral surface charge) and the promising results obtained in our group with neutral, PEGylated nanocarriers for RNA delivery in the brain [56], NC-1 was selected as our most promising

candidate for efficient siRNA delivery and diffusivity in the brain. NC-1 was administered directly to the brain via ICV injection. After 14 days, animals were sacrificed, and their brains were collected and processed. Levels of targeted mRNA were determined to assess the silencing effectiveness of siRNA-2. Additionally, different brain areas were studied to determine the diffusion capacity of NC-1.

As shown in Figure 11, NC-1 containing siRNA-2 successfully reduced the levels of targeted mRNA in the frontal cortex, striatum, hippocampus, and brain stem, as compared with the free siRNA-2 group. The comparison was also made with an internal positive control (PC), which contained siRNA-2 at a slightly higher concentration than NC-1 (3 mg/mL and 2 mg/mL, respectively). A similar knockdown effect was observed for the PC and NC-1, both compared with the free siRNA-2 group. More details about the specific behavior of NC-1 and all the controls used in each specific tissue can be found in Supplementary Figure 5. Overall, the performance of NC-1 resulted in a reduction of targeted mRNA levels of over 50% in all the brain areas analyzed. The highest silencing effect was found in the areas surrounding the injection site, particularly in the striatum (80% silencing effect) and hippocampus (73% silencing effect). Moreover, considerably distant areas also reported outstanding silencing values, such as in the frontal cortex (70% silencing effect), brain stem (67% silencing effect), and the DRGs (50% silencing effect).

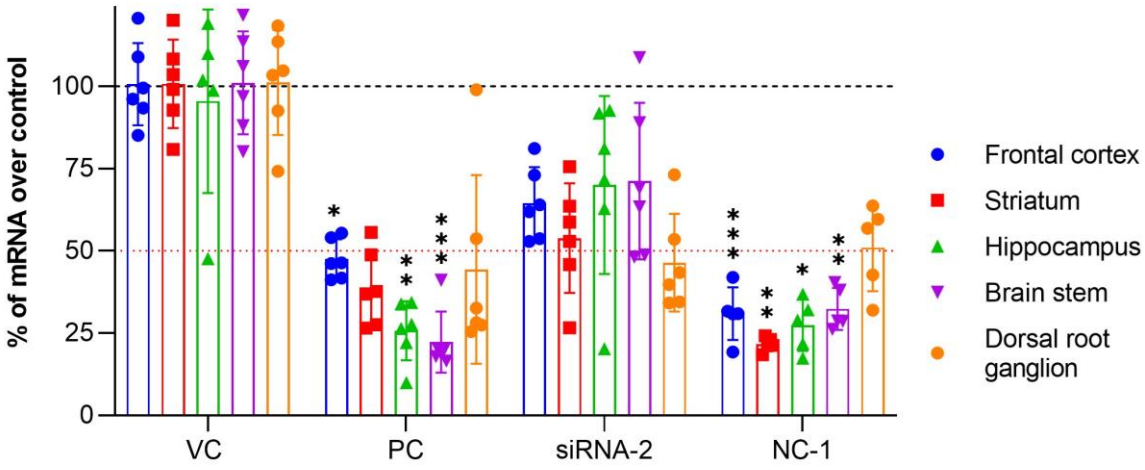

Figure 11. Quantitative qPCR of levels of targeted mRNA upon ICV administration of NC-1 encapsulating siRNA-2, in different brain areas, including the frontal cortex, striatum, hippocampus, brain stem, and dorsal root ganglion. Results were normalized using a housekeeping gene

Abbreviations: NC: nanocapsule. PC: internal positive control. VC: vehicle control (PBS). A significant comparison was performed using an ordinary one-way ANOVA followed by Tukey's multiple comparison tests of PC and NC-1 *vs*. siRNA-2. *p*-values < 0.05 were considered statistically significant (*). Also, (**) if *p*-value < 0.01, (***) if *p*-value < 0.001. Values represent the mean ± standard deviation (n ≥ 3).

These results are especially promising when considering previous reports in the literature. Similar knockdown effects were previously reported using LNPs for the treatment of glioblastoma, leading to an 80% reduction of the targeted mRNA in the tumor after intratumoral administration [87]. Other authors used LNPs for ICV administration, resulting in a target mRNA reduction of 50% in the striatum and 56% in the hippocampus [66]. However, none of

these studies analyzed the mRNA levels in areas other than the injection site and their immediate surrounding areas. To our knowledge, this is the first time that extensive silencing effects across the entire brain have been reported, demonstrating the diffusivity and silencing potential of a nanocarrier.

Moreover, the observation of siRNA-2 diffusion and distribution in the brain was confirmed by RNAscope (Figure 12). The whole-brain examination (Figure 12, top left) indicated that siRNA-2 was present in almost all regions of the brain. Interestingly, the diffusion observed across the brain for NC-1 outreaches the current gold standard for RNA delivery, LNPs, which have been reported to poorly diffuse (up to 4 mm) from the administration site [66]. A close-up observation of different brain areas highlighted the degree of diffusion achieved, as seen in the frontal cortex (Figure 12, top right), the striatum (Figure 12, bottom left), and the brain stem (Figure 12, bottom right). More images and close-up observations of the frontal cortex can be found in Supplementary Figure 6). Greater diffusion was observed in areas close to the administration site, such as the striatum and frontal cortex; interestingly, this observation correlates with the results obtained by PCR analysis (Figure 11).

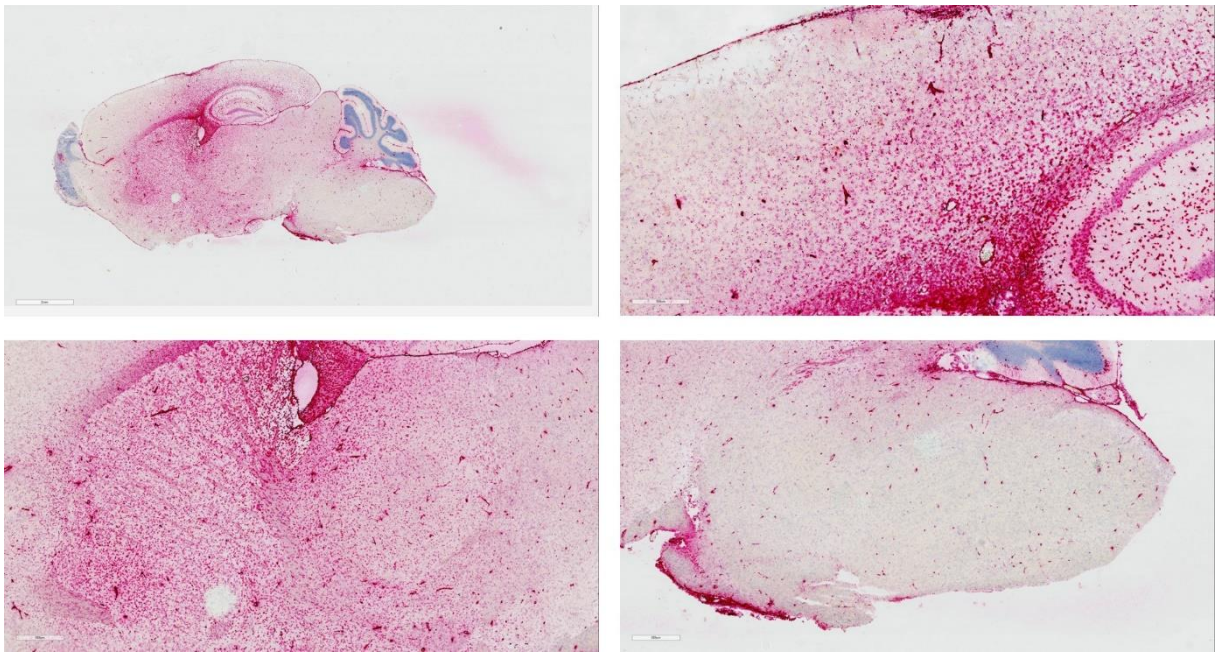

Figure 12. Detection of siRNA-2 in the brain after ICV administration of NC-1. Images were obtained for the complete brain (top, left), and close-up of the frontal cortex (top, right), the hippocampus (bottom, left), and the brain stem (bottom, right)

This finding suggests that not only does NC-1 diffuse to these areas, but it also enhances the transfection efficiency and silencing effect of siRNA-2. Considering these results, we hypothesize that the diffusion observed by NC-1 is mainly due to the combined effect of the small particle size of the nanocarrier, its hydrophilic surface, and the flexibility conferred by the oily core. Overall, the results of this functional biodistribution study indicate not only the ability of NC-1 to diffuse to different brain areas but also its potency in terms of silencing the targeted mRNA.

4. CONCLUSIONS

In the present study, we designed and developed a library of multiple NE-siRNA and NC-siRNA nanocarriers, with a particle size smaller than 100 nm in diameter, a range of surface charges, capability for reproducible and scalable production, high siRNA encapsulation efficiency, and adequate stability at 4 ºC. Furthermore, one of the NE-siRNA produced, NE-2-siRNA, served as a model NE for the functionalization with a brain penetration enhancer, RVG. The *in vitro* evaluation of these nanocarriers in a human glioblastoma cell model demonstrated a remarkable transfection profile at non-toxic concentration.

Moving forward to N-to-B administration, specific formulations (namely, NE-2, NE-2-RVG, and NC-5) exhibited greater accumulation within the nasal cavity compared to the internal positive control. Meanwhile, upon ICV administration, it was observed the exceptional diffusivity of NC-1. This nanocarrier showcased the ability to access multiple brain areas (including the frontal cortex, striatum, hippocampus, brain stem, and DRG), where it achieved a substantial reduction in mRNA target levels, lowering them below the 50% threshold.

Collectively, we have developed a highly promising nanocarrier for efficient siRNA diffusion and transfection within the brain. This finding holds significant potential for the treatment of different CNS conditions, contributing to advancement in the field of RNA-based therapeutics.

5. SUPPLEMENTARY INFORMATION

Supplementary Table 1. Physicochemical properties of nanoemulsions, screening different oils and surfactants in combination with DOTAP

Nanoemulsion core		Particle diameter (nm)	PDI	ζ-Potential (mV)
DOTAP | Vitamin E	K-HS15®	75	0.26	+77
	Tween 80	76	0.27	+51
	SPAN 80	145	0.13	+66
	DSPC	180	0.34	+54
DOTAP | Castor oil	K-HS15®	157	0.15	-
	Tween 80	166	0.16	-
	SPAN 80	186	0.20	-
	DSPC	141	0.16	-
DOTAP | Oleic acid	K-HS15®	174	0.58	-
	Tween 80	180	0.51	-
	SPAN 80	175	0.49	-
	DSPC	150	0.27	-
DOTAP | Labrafac™	K-HS15®	114	0.12	+62
	Tween 80	116	0.11	+66
	SPAN 80	162	0.12	-
	DSPC	130	0.08	+65

Abbreviations: DOTAP: 1,2-dioleoyl-3-trimethylammonium propane. DSPC: 14,2-stearoyl-sn-glycerol-3-phosphocholine. K-HS15®: Kolliphor® HS15. Labrafac™: Labrafac™ Lipophile, WL 1349. SPAN 80: Span 80-LQ-(MV). Vitamin E: D, L-α-tocopherol. (n = 1).

Supplementary Table 2. Physicochemical properties of nanoemulsions before and after the evaporation under vacuum process

Nanoemulsion	Evaporation	Particle diameter (nm)	PDI	ζ-Potential (mV)
DOTAP | Vitamin E | K-HS15®	Before	86	0.23	+66
	After	62	0.25	-67
DOTAP | Vitamin E | Tween 80	Before	75	0.19	-
	After	53	0.3	+67
DOTAP | Labrafac™ | K-HS15®	Before	136	0.19	+71
	After	138	0.13	+71
DOTAP | Labrafac™ | Tween 80	Before	150	0.14	+66
	After	125	0.14	+70

Abbreviations: DOTAP: 1,2-dioleoyl-3-trimethylammonium propane. K-HS15®: Kolliphor® HS15. Labrafac™: Labrafac™ Lipophile, WL 1349. PDI: polydispersity index. Vitamin E: D, L-α-tocopherol. (n = 1).

Supplementary Table 3. Physicochemical properties of nanoemulsions after complexation with different siRNA concentrations

Nanoemulsion	$[siRNA]_{final}$ (mg/mL)	Particle diameter (nm)	PDI	ζ-Potential (mV)
DOTAP | Vitamin E | K-HS15®	0.25	57	0.37	+62
	0.5	158	0.08	+47
	0.75	153	0.08	+50
	1	172	0.13	+51
DOTAP | Vitamin E | Tween 80	0.25	58	0.41	+50
	0.5	156	0.06	+46
	0.75	154	0.09	+47
	1	167	0.09	+47
DOTAP | Labrafac™ | K-HS15®	0.25	124	0.19	+62
	0.5	182	0.18	+45
	0.75	189	0.25	+46
DOTAP | Labrafac™ | Tween 80	0.25	136	0.19	-
	0.5	231	0.27	+36
	0.75	245	0.39	+40

Abbreviations: DOTAP: 1,2-dioleoyl-3-trimethylammonium propane. K-HS15®: Kolliphor® HS15. Labrafac™: Labrafac™ Lipophile, WL 1349. PDI: polydispersity index. Vitamin E: D, L-α-tocopherol. (n = 1).

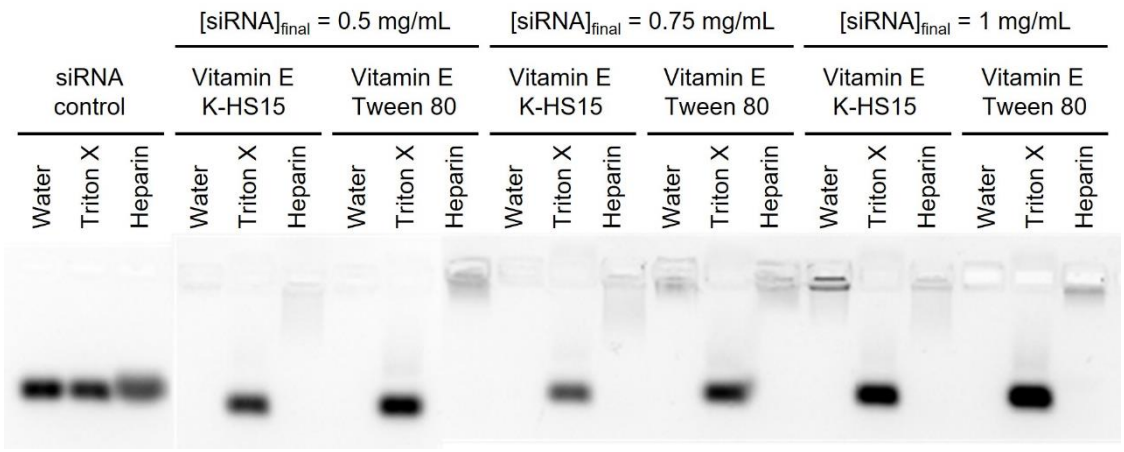

Supplementary Figure 1. Encapsulation efficiency of siRNA onto nanoemulsions containing Vitamin E and K-HS15® or Tween 80, upon bulk mixing. Samples were treated with Triton X or heparin for nanoemulsion disruption or siRNA displacement, respectively. Different siRNA final concentrations were explored

Abbreviations: K-HS15®: Kolliphor® HS15. Labrafac™: Labrafac™ Lipophile, WL 1349. Triton X: Triton-X-100. Vitamin E: D, L-α-tocopherol.

Supplementary Table 4. Physicochemical properties of nanoemulsion containing Vitamin E and K-HS15® after complexation with siRNA by bulk and microfluidic mixing, at different total flow rates

Type of method for siRNA complexation	Particle diameter (nm)	PDI	ζ-Potential (mV)
Bulk mixing	76	0.24	+69
Microfluidic mixing – TFR = 12 mL/min	120	0.16	+52
Microfluidic mixing – TFR = 14 mL/min	103	0.14	+47

Abbreviations: PDI: polydispersity index. TFR: total flow rate. (n = 1).

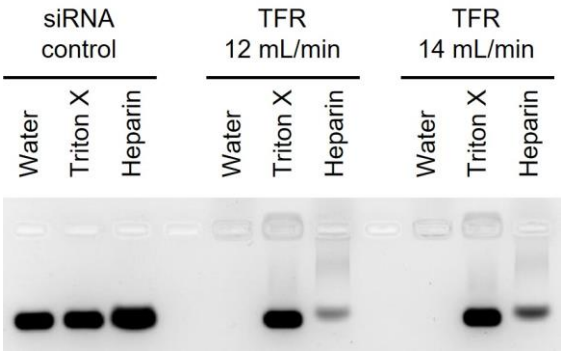

Supplementary Figure 2. Encapsulation efficiency of siRNA onto nanoemulsions containing Vitamin E and K-HS15®, prepared by microfluidic mixing of blank nanoemulsions and the siRNA solution at different total flow rates

Abbreviations: TFR: total flow rate.

Supplementary Table 5. Physicochemical properties of NE-3 (DOTAP: Labrafac™: Tween 80) at different molar ratios, total flow rates, and siRNA final concentrations

Molar ratio (%)	TFR (mL/min)	$[siRNA]_{final}$ (mg/mL)	Particle diameter (nm)	PDI	ζ-Potential (mV)	EE (%)
16.8:81.4:1.8	10	0.75	146 ± 17	0.34 ± 0.1	+50 ± 4	-
	12	0.75	198	0.40	+40	-
		0.5	127	0.35	-	-
46:35.5:18.5	12	0.5	123	0.20	+21	
	14	0.5	111 ± 4	0.24 ± 0.01	+45 ± 1	100
25:56.5:18.5	12	0.75	121	0.25	+29	-
	14	0.5	99 ± 13	0.26 ± 0.04	+33 ± 1	100
		0.75	97 ± 6	0.21 ± 0.02	+36 ± 2	100

Encapsulation efficiency was measured by agarose gel, and values were corroborated by RiboGreen assay and/or UPLC analysis. **Abbreviations:** EE: encapsulation efficiency. PDI: polydispersity index. Values represent the mean ± standard deviation (n = 2, unless no standard deviation is reported).

Supplementary Table 6. Physicochemical properties of siRNA-NE containing DOTAP: Labrafac™: K-HS15®, at different molar ratios, total flow rates, and siRNA final concentrations

Molar ratio (%)	TFR (mL/min)	$[siRNA]_{final}$ (mg/mL)	Particle diameter (nm)	PDI	ζ-Potential (mV)	EE (%)
16:77.5:6.5	10	0.75	110 ± 16	0.25 ± 0.03	+49 ± 1	100
	12	0.75	142 ± 53	0.23 ± 0.02	+50 ± 1	-
		0.5	119	0.3	+50	-
		0.4	175	0.26	+43	-
	14	0.75	89	0.33	+53	-
46:35.5:18.5	12	0.5	87	0.50	+51	-
25:56.5:18.5	12	0.5	197	0.21	+40	-

Encapsulation efficiency was measured by agarose gel, and values were corroborated by RiboGreen assay and/or UPLC analysis. **Abbreviations:** EE: encapsulation efficiency. PDI: polydispersity index. Values represent the mean ± standard deviation (n = 2, unless no standard deviation is reported).

Supplementary Table 7. Physicochemical properties of NC-1, NC-2, NC-3, NC-4, NC-5 and MNC-1, exploring different ratios between siRNA and polymers

NC	Ratio siRNA: polymer	Particle diameter (nm)	PDI	ζ-Potential (mV)	EE (%)
NC-1	1:2 mol/mol	75 ± 2	0.14 ± 0.02	+1 ± 2	100
	1:4 mol/mol	74	0.18	-15	100
	1:8 mol/mol	92	0.25	-18	100
NC-2	1:2 mol/mol	> 1 µm	0.09 ± 0.01	-4 ± 12	100
	1:4 mol/mol	88 ± 4	0.15 ± 0.02	-27 ± 3	100
	1:8 mol/mol	91 ± 4	0.14 ± 0.01	-32 ± 1	100
NC-3	1:2 w/w	113	0.11	-49	100
	1:4 w/w	107	0.12	-52	100
	1:8 w/w	108	0.10	-56	100
NC-4	1:2 mol/mol	77	0.25	-23	100
	1:4 mol/mol	88 ± 15	0.22 ± 0.01	-28 ± 2	100
	1:8 mol/mol	89	0.23	-31	100
NC-5	1:2 w/w	81	0.28	-44	100
	1:4 w/w	89 ± 8	0.22 ± 0.02	-42 ± 3	100
	1:8 w/w	79	0.20	-44	100
MNC-1	1:3.8 w/w	94 ± 1	0.19 ± 0.01	+47 ± 2	100
	1:7.7 w/w	140	0.22	+59	-
	1: 15.4 w/w	147	0.23	+58	-

Encapsulation efficiency was measured by agarose gel, and values were corroborated by RiboGreen assay and/or UPLC analysis. **Abbreviations:** MNC: multi-layer nanocapsule. mol/mol: mol to mol ratio. NC: nanocapsule. EE: encapsulation efficiency. PDI: polydispersity index. w/w: weight-to-weight ratio. Values represent the mean ± standard deviation (n = 2, unless no standard deviation is reported).

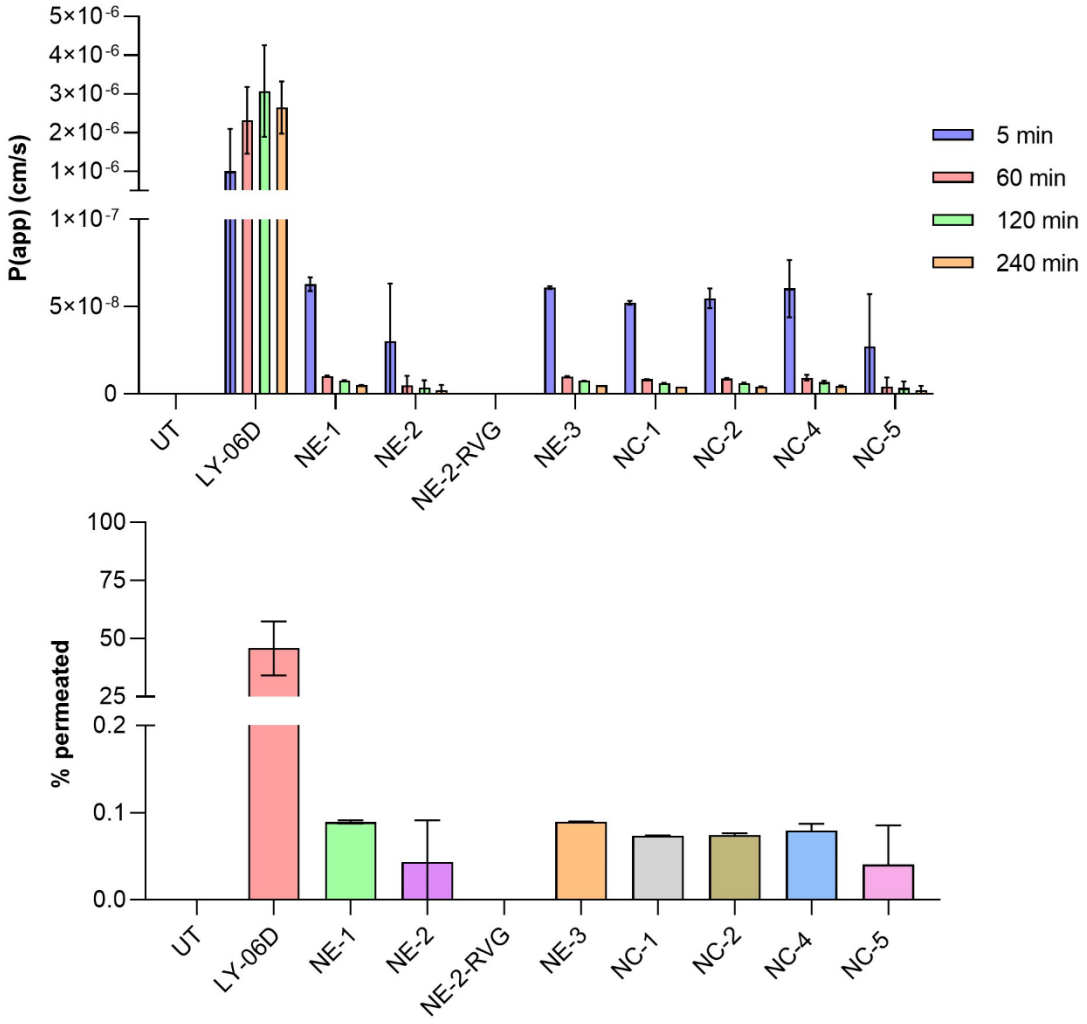

Supplementary Figure 3. Permeation coefficient (top) and percentage of nanocarrier permeated for different NEs and NCs

Abbreviations: LY-06D: positive control (internal control from Eli Lilly & Company). NC: nanocapsule. NE: nanoemulsion. RVG: rabies virus glycoprotein. UT: untreated. Values represent the mean ± standard deviation (n ≥ 3).

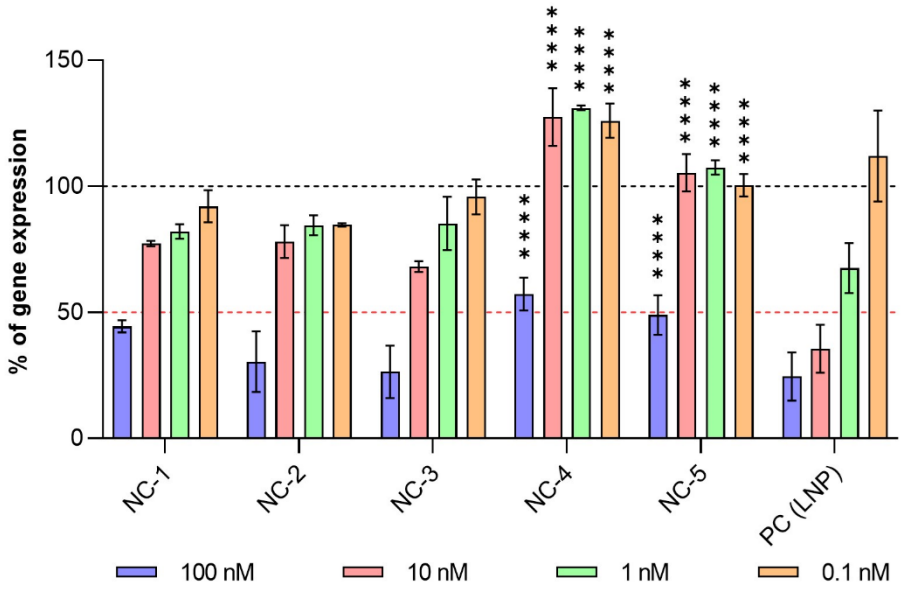

Supplementary Figure 4. Quantitative real-time PCR of the silencing effect of siRNA-1, after the administration of NC-1, NC-2, NC-3, NC-4, and NC-5 in BE(2)-C cells. The comparison was made with an optimized LNP formulation (PC (LNP))

Abbreviations: LNP: lipid nanoparticle. NC: nanocapsule. PC: positive control. A significant comparison was performed using two-way ANOVA followed by Tukey's multiple comparison tests of each formulation at the different concentrations tested vs PC (LNP). *p*-values < 0.0001 were considered statistically significant (****). Values represent the mean ± standard deviation (n ≥ 3).

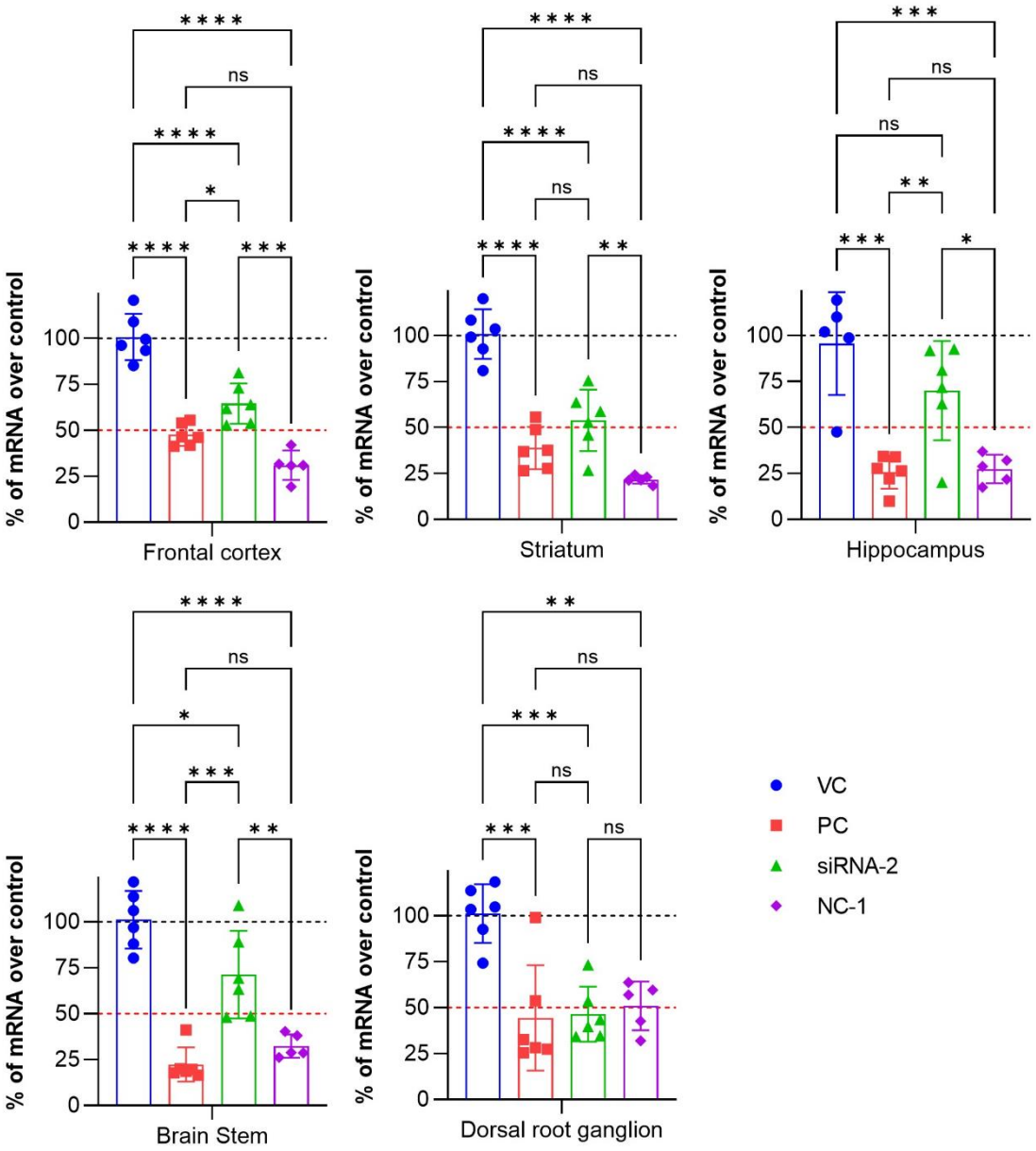

Supplementary Figure 5. Quantitative qPCR of levels of targeted mRNA upon ICV administration of NC-1 encapsulating siRNA-2, in different brain areas, including the frontal cortex (top, left), striatum (top, middle), hippocampus (top, right), brain stem (bottom, left), and dorsal root ganglion (bottom, middle)

Abbreviations: DRG: dorsal root ganglion. NC: nanocapsule. PC: internal positive control. VC: vehicle control (PBS). A significant comparison was performed using one-way ANOVA followed by Tukey's multiple comparison tests between groups. *p*-values < 0.05 were considered statistically significant (*). Also, (**) if *p*-value < 0.01, (***) if *p*-value < 0.001, (****) if *p*-value < 0.0001, and ns if *p*-value > 0.05. Values represent the mean ± standard deviation (n ≥ 3).

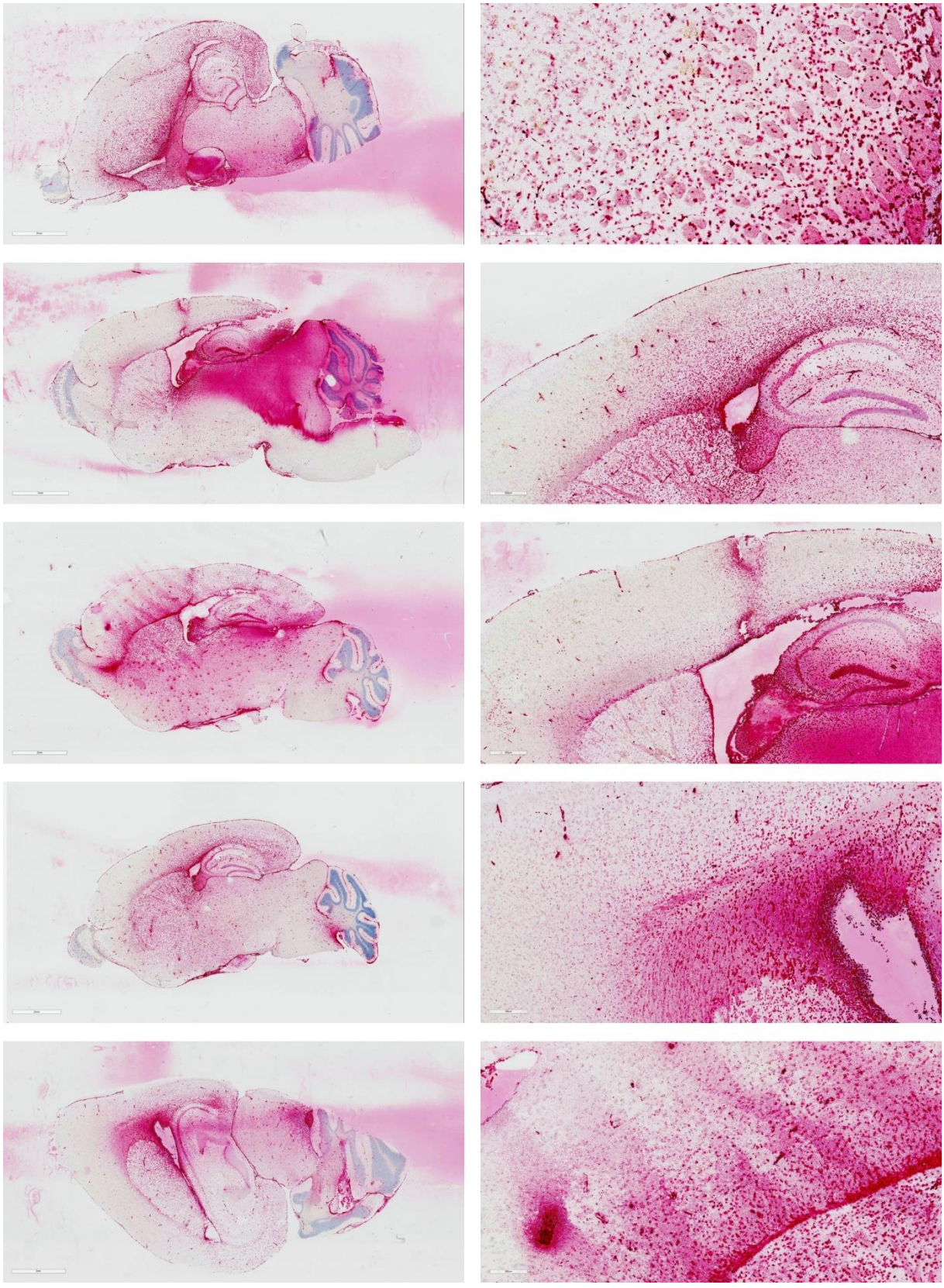

Supplementary Figure 6. Detection of siRNA-2 in the brain after ICV administration of NC-1. Images were obtained for the complete brain (left), and a close-up of the frontal cortex (right)

6. ACKNOWLEDGMENTS

This work was supported by Eli Lilly and Company, under a collaboration agreement between Eli Lilly and Company and Universidade de Santiago de Compostela. Mireya L. Borrajo acknowledges the financial support by Instituto de Salud Carlos III, through the "Contratos i-PFIS: Doctorados ISS-empresa en Ciencias y Tecnologías de la Salud" grant.

Functionalization of nanoemulsions with RVG peptide was carried out in collaboration with Subaash Anthiya, PhD, from Universidade de Santiago de Compostela.

In vitro and *in vivo* assessments were performed at Eli Lilly and Company (IL, USA), in collaboration with Samantha Sarett, PhD, Zhefeng (Eddie) Li, PhD, Sean K. Bedingfield, PhD, and Hao-Cheng (Toby) Chueh, MSc.

7. REFERENCES

[1] M.L. Borrajo, M.J. Alonso, Using nanotechnology to deliver biomolecules from nose to brain — peptides, proteins, monoclonal antibodies and RNA, Drug Deliv. Transl. Res. 12 (2022) 862–880. https://doi.org/10.1007/s13346-021-01086-2.

[2] V.L. Feigin, A.A. Abajobir, K.H. Abate, F. Abd-Allah, A.M. Abdulle, S.F. Abera, G.Y. Abyu, M.B. Ahmed, A.N. Aichour, I. Aichour, M.T.E. Aichour, R.O. Akinyemi, S. Alabed, R. Al-Raddadi, N. Alvis-Guzman, J.R. Zunt, C.J.L. Murray, T. Vos, Global, regional, and national burden of neurological disorders during 1990–2015: a systematic analysis for the Global Burden of Disease Study 2015, Lancet Neurol. 16 (2017) 877–897. https://doi.org/10.1016/S1474-4422(17)30299-5.

[3] C. Ding, Y. Wu, X. Chen, Y. Chen, Z. Wu, Z. Lin, D. Kang, W. Fang, F. Chen, Global, regional, and national burden and attributable risk factors of neurological disorders: The Global Burden of Disease study 1990–2019, Front. Public Heal. 10 (2022). https://doi.org/10.3389/fpubh.2022.952161.

[4] World Health Organization, Neurological disorders: public health challenges, Geneva, (2006).

[5] S. Ingusci, G. Verlengia, M. Soukupova, S. Zucchini, M. Simonato, Gene Therapy Tools for Brain Diseases, Front. Pharmacol. 10 (2019) 1–19. https://doi.org/10.3389/fphar.2019.00724.

[6] S.A. Pena, R. Iyengar, R.S. Eshraghi, N. Bencie, J. Mittal, A. Aljohani, R. Mittal, A.A. Eshraghi, Gene therapy for neurological disorders: challenges and recent advancements, J. Drug Target. 28 (2020) 111–128. https://doi.org/10.1080/1061186X.2019.1630415.

[7] R.L. Setten, J.J. Rossi, S. ping Han, The current state and future directions of RNAi-based therapeutics, Nat. Rev. Drug Discov. 18 (2019) 421–446. https://doi.org/10.1038/s41573-019-0017-4.

[8] J. Sun, S. Roy, Gene-based therapies for neurodegenerative diseases, Nat. Neurosci. 24 (2021) 297–311. https://doi.org/10.1038/s41593-020-00778-1.

[9] M. Luo, L.K.C. Lee, B. Peng, C.H.J. Choi, W.Y. Tong, N.H. Voelcker, Delivering the Promise of Gene Therapy with Nanomedicines in Treating Central Nervous System Diseases, Adv. Sci. 9 (2022) 1–41. https://doi.org/10.1002/advs.202201740.

[10] N.R. Smalheiser, G. Lugli, J. Thimmapuram, E.H. Cook, J. Larson, Endogenous siRNAs and noncoding RNA-derived small RNAs are expressed in adult mouse hippocampus and are up-regulated in olfactory discrimination training, RNA. 17 (2011) 166–181. https://doi.org/10.1261/rna.2123811.

[11] N.R. Smalheiser, The Search for Endogenous siRNA in the Mammalian Brain, Exp. Neurol. 235 (2012) 455–463. https://doi.org/10.1016/j.expneurol.2011.10.015.

[12] A. Daka, D. Peer, RNAi-based nanomedicines for targeted personalized therapy, Adv. Drug Deliv. Rev. 64 (2012) 1508–1521. https://doi.org/10.1016/j.addr.2012.08.014.

[13] R. Kanasty, J.R. Dorkin, A. Vegas, D. Anderson, Delivery materials for siRNA therapeutics, Nat. Mater. 12 (2013) 967–977. https://doi.org/10.1038/nmat3765.

[14] P. Neuberg, A. Kichler, Recent developments in nucleic acid delivery with polyethylenimines, Elsevier, 2014. https://doi.org/10.1016/B978-0-12-800148-6.00009-2.

[15] H.J. Kim, A. Kim, K. Miyata, K. Kataoka, Recent progress in development of siRNA delivery vehicles for cancer therapy, Adv. Drug Deliv. Rev. 104 (2016) 61–77. https://doi.org/10.1016/j.addr.2016.06.011.

[16] R. García, R. Pérez, Dynamic atomic force microscopy methods, Surf. Sci. Rep. 47 (2002) 197–301. https://doi.org/10.1016/S0167-5729(02)00077-8.

[17] B.B. Mendes, J. Conniot, A. Avital, D. Yao, X. Jiang, X. Zhou, N. Sharf-Pauker, Y. Xiao, O. Adir, H. Liang, J. Shi, A. Schroeder, J. Conde, Nanodelivery of nucleic acids, Nat. Rev. Methods Prim. 2 (2022). https://doi.org/10.1038/s43586-022-00104-y.

[18] D.J. Begley, Delivery of therapeutic agents to the central nervous system: The problems and the possibilities, Pharmacol. Ther. 104 (2004) 29–45. https://doi.org/10.1016/j.pharmthera.2004.08.001.

[19] B. Obermeier, R. Daneman, R.M. Ransohoff, Development, maintenance and disruption of blood-brain barrier, Nat. Med. 19 (2013) 1584–1596. https://doi.org/10.1038/nm.3407.Development.

[20] B. Engelhardt, L. Sorokin, The blood-brain and the blood-cerebrospinal fluid barriers: function and dysfunction, Semin. Immunopathol. 31 (2009) 497–511. https://doi.org/10.1007/s00281-009-0177-0.

[21] J.J. Lochhead, R.G. Thorne, Intranasal delivery of biologics to the central nervous system, Adv. Drug Deliv. Rev. 64 (2012) 614–628. https://doi.org/10.1016/j.addr.2011.11.002.

[22] S. Ayloo, C. Gu, Transcytosis at the blood – brain barrier, Curr. Opin. Neurobiol. 57 (2019) 32–38. https://doi.org/10.1016/j.conb.2018.12.013.

[23] G.C. Terstappen, A.H. Meyer, R.D. Bell, W. Zhang, Strategies for delivering therapeutics across the blood–brain barrier, Nat. Rev. Drug Discov. 20 (2021) 362–383. https://doi.org/10.1038/s41573-021-00139-y.

[24] D.S. Hersh, A.S. Wadajkar, N. Roberts, J.G. Perez, N.P. Connolly, V. Frenkel, J.A. Winkles, G.F. Woodworth, A.J. Kim, Evolving Drug Delivery Strategies to Overcome the Blood Brain Barrier., Curr. Pharm. Des. 22 (2016) 1177–1193.

[25] D. Furtado, M. Björnmalm, S. Ayton, A.I. Bush, K. Kempe, F. Caruso, Overcoming the Blood–Brain Barrier: The Role of Nanomaterials in Treating Neurological Diseases, Adv. Mater. 30 (2018). https://doi.org/10.1002/adma.201801362.

[26] M.J. Fowler, J.D. Cotter, B.E. Knight, E.M. Sevick-Muraca, D.I. Sandberg, R.W. Sirianni, Intrathecal drug delivery in the era of nanomedicine, 2020. https://doi.org/10.1016/j.addr.2020.02.006.

[27] J. Gurke, T.E. Naegele, S. Hilton, R. Pezone, V.F. Curto, D.G. Barone, E.J.W. List-Kratochvil, A. Carnicer-Lombarte, G.G. Malliaras, Hybrid fabrication of multimodal intracranial implants for electrophysiology and local drug delivery, Mater. Horizons. 9 (2022) 1727–1734. https://doi.org/10.1039/D1MH01855H.

[28] R.R. Lonser, M. Sarntinoranont, P.F. Morrison, E.H. Oldfield, Convection-enhanced delivery to the central nervous system, J. Neurosurg. 122 (2015) 697–706. https://doi.org/10.3171/2014.10.JNS14229.

[29] C.A. Chiriboga, Nusinersen for the treatment of spinal muscular atrophy, Expert Rev. Neurother. 17 (2017) 955–962. https://doi.org/10.1080/14737175.2017.1364159.

[30] J. Erdos, C. Wild, Mid- and long-term (at least 12 months) follow-up of patients with spinal muscular atrophy (SMA) treated with nusinersen, onasemnogene abeparvovec, risdiplam or combination therapies: A systematic review of real-world study data, Eur. J. Paediatr. Neurol. 39 (2022) 1–10. https://doi.org/10.1016/j.ejpn.2022.04.006.

[31] D. Wu, Q. Chen, X. Chen, F. Han, Z. Chen, Y. Wang, The blood–brain barrier: structure, regulation, and drug delivery, Signal Transduct. Target. Ther. 8 (2023) 217. https://doi.org/10.1038/s41392-023-01481-w.

[32] C.M. Gorick, V.R. Breza, K.M. Nowak, V.W.T. Cheng, D.G. Fisher, A.C. Debski, M.R. Hoch, Z.E.F. Demir, N.M. Tran, M.R. Schwartz, N.D. Sheybani, R.J. Price, Applications of focused ultrasound-mediated blood-brain barrier opening, Adv. Drug Deliv. Rev. 191 (2022) 114583. https://doi.org/10.1016/j.addr.2022.114583.

[33] B. Nabi, S. Rehman, S. Khan, S. Baboota, J. Ali, Ligand conjugation: An emerging platform for enhanced brain drug delivery, Brain Res. Bull. 142 (2018) 384–393. https://doi.org/10.1016/j.brainresbull.2018.08.003.

[34] W.M. Faber, The nasal mucosa and the subarachnoid space, Am. J. Anat. 62 (1937) 121–148.

[35] H. Wu, K. Hu, X. Jiang, From nose to brain: understanding transport capacity and transport rate of drugs, Expert Opin. Drug Deliv. 5 (2008) 1159–1168. https://doi.org/10.1517/17425247.5.10.1159.

[36] P.G. Djupesland, J.C. Messina, R.A. Mahmoud, The nasal approach to delivering treatment for brain diseases: An anatomic, physiologic, and delivery technology overview, Ther. Deliv. 5 (2014) 709–733. https://doi.org/10.4155/tde.14.41.

[37] F.A. Bruinsmann, G.R. Vaz, A. De Cristo Soares Alves, T. Aguirre, A.R. Pohlmann, S.S.

Guterres, F. Sonvico, Nasal drug delivery of anticancer drugs for the treatment of glioblastoma: Preclinical and clinical trials, Molecules. 24 (2019). https://doi.org/10.3390/molecules24234312.

[38] D.A. Martins, N. Mazibuko, F. Zelaya, S. Vasilakopoulou, J. Loveridge, A. Oates, S. Maltezos, M. Mehta, S. Wastling, M. Howard, G. McAlonan, D. Murphy, S.C.R. Williams, A. Fotopoulou, U. Schuschnig, Y. Paloyelis, Effects of route of administration on oxytocin-induced changes in regional cerebral blood flow in humans, Nat. Commun. 11 (2020) 1–16. https://doi.org/10.1038/s41467-020-14845-5.

[39] M.S. Landis, T. Boyden, S. Pegg, Nasal-to-CNS drug delivery: Where are we now and where are we heading? An industrial perspective, Ther. Deliv. 3 (2012) 195–208. https://doi.org/10.4155/tde.11.149.

[40] S. Gizurarson, Anatomical and Histological Factors Affecting Intranasal Drug and Vaccine Delivery, Curr. Drug Deliv. 9 (2012) 566–582.

[41] L.R. Hanson, W.H. Frey, Intranasal delivery bypasses the blood-brain barrier to target therapeutic agents to the central nervous system and treat neurodegenerative disease, BMC Neurosci. 9 (2008) 1–4. https://doi.org/10.1186/1471-2202-9-S2-S5.

[42] A. Mistry, S.Z. Glud, J. Kjems, J. Randel, K.A. Howard, S. Stolnik, L. Illum, Effect of physicochemical properties on intranasal nanoparticle transit into murine olfactory epithelium, J. Drug Target. 17 (2009) 543–552. https://doi.org/10.1080/10611860903055470.

[43] A. Mistry, S. Stolnik, L. Illum, Nose-to-Brain delivery: investigation of the transport of nanoparticles with different surface characteristics and sizes in excised porcine olfactory epithelium, Mol. Pharm. 12 (2015) 2755–2766. https://doi.org/10.1021/acs.molpharmaceut.5b00088.

[44] K. Selvaraj, K. Gowthamarajan, V.V.S.R. Karri, Nose to brain transport pathways an overview: potential of nanostructured lipid carriers in nose to brain targeting, Artif. Cells, Nanomedicine Biotechnol. 46 (2018) 2088–2095. https://doi.org/10.1080/21691401.2017.1420073.

[45] N.J. Johnson, L.R. Hanson, W.H. Frey, Trigeminal pathways deliver a low molecular weight drug from the nose to the brain and orofacial structures, Mol. Pharm. 7 (2010) 884–893. https://doi.org/10.1021/mp100029t.

[46] A.R. Khan, M. Liu, M.W. Khan, G. Zhai, Progress in brain targeting drug delivery system by nasal route, J. Control. Release. 268 (2017) 364–389. https://doi.org/10.1016/j.jconrel.2017.09.001.

[47] T. Kanazawa, F. Akiyama, S. Kakizaki, Y. Takashima, Y. Seta, Delivery of siRNA to the brain using a combination of nose-to-brain delivery and cell-penetrating peptide-modified nano-micelles, Biomaterials. 34 (2013) 9220–9226. https://doi.org/10.1016/j.biomaterials.2013.08.036.

[48] T. Kanazawa, K. Morisaki, S. Suzuki, Y. Takashima, Prolongation of life in rats with malignant glioma by intranasal siRNA/drug codelivery to the brain with cell-penetrating peptide-modified micelles, Mol. Pharm. 11 (2014) 1471–1478. https://doi.org/10.1021/mp400644e.

[49] T. Kanazawa, T. Kurano, H. Ibaraki, Y. Takashima, T. Suzuki, Y. Seta, Therapeutic effects in a transient middle cerebral artery occlusion rat model by nose-to-brain delivery of anti-tnf-alpha sirna with cell-penetrating peptide-modified polymer micelles. (pharmaceutics, (2019), 11(9),

478, 10.3390/pharmaceutics11090478), Pharmaceutics. 11 (2019) 478. https://doi.org/10.3390/pharmaceutics11120689.

[50] M. Van Woensel, T. Mathivet, N. Wauthoz, R. Rosière, A.D. Garg, P. Agostinis, V. Mathieu, R. Kiss, F. Lefranc, L. Boon, J. Belmans, S.W. Van Gool, H. Gerhardt, K. Amighi, S. De Vleeschouwer, Sensitization of glioblastoma tumor micro-environment to chemo- and immunotherapy by Galectin-1 intranasal knock-down strategy, Sci. Rep. 7 (2017) 1217. https://doi.org/10.1038/s41598-017-01279-1.

[51] M. Van Woensel, N. Wauthoz, R. Rosière, V. Mathieu, R. Kiss, F. Lefranc, B. Steelant, E. Dilissen, S.W. Van Gool, T. Mathivet, H. Gerhardt, K. Amighi, S. De Vleeschouwer, Development of siRNA-loaded chitosan nanoparticles targeting Galectin-1 for the treatment of glioblastoma multiforme via intranasal administration, J. Control. Release. 227 (2016) 71–81. https://doi.org/10.1016/j.jconrel.2016.02.032.

[52] Y. Yang, X. Zhang, S. Wu, R. Zhang, B. Zhou, X. Zhang, L. Tang, Y. Tian, K. Men, L. Yang, Enhanced nose-to-brain delivery of siRNA using hyaluronan-enveloped nanomicelles for glioma therapy, J. Control. Release. 342 (2022) 66–80. https://doi.org/10.1016/j.jconrel.2021.12.034.

[53] L. Tang, R. Zhang, Y. Wang, X. Zhang, Y. Yang, B. Zhao, L. Yang, A simple self-assembly nanomicelle based on brain tumor-targeting peptide-mediated siRNA delivery for glioma immunotherapy via intranasal administration, Acta Biomater. 155 (2023) 521–537. https://doi.org/10.1016/j.actbio.2022.11.013.

[54] V. Sava, O. Fihurka, A. Khvorova, J. Sanchez-Ramos, Enriched chitosan nanoparticles loaded with siRNA are effective in lowering Huntington's disease gene expression following intranasal administration, Nanomedicine Nanotechnology, Biol. Med. 24 (2020) 102119. https://doi.org/10.1016/j.nano.2019.102119.

[55] X. Yang, W. Yang, X. Xia, T. Lei, Z. Yang, W. Jia, Y. Zhou, G. Cheng, H. Gao, Intranasal Delivery of BACE1 siRNA and Rapamycin by Dual Targets Modified Nanoparticles for Alzheimer's Disease Therapy, Small. 18 (2022) 2203182. https://doi.org/10.1002/smll.202203182.

[56] E. Samaridou, H. Walgrave, E. Salta, D.M. Álvarez, V. Castro-López, M. Loza, M.J. Alonso, Nose-to-brain delivery of enveloped RNA - cell permeating peptide nanocomplexes for the treatment of neurodegenerative diseases, Biomaterials. 230 (2020) 119657. https://doi.org/10.1016/j.biomaterials.2019.119657.

[57] A. Kumar, A.N. Pandey, S.K. Jain, Nasal-nanotechnology: Revolution for efficient therapeutics delivery, Drug Deliv. 23 (2016) 681–693. https://doi.org/10.3109/10717544.2014.920431.

[58] L.A. Keller, O. Merkel, A. Popp, Intranasal drug delivery: opportunities and toxicologic challenges during drug development, Drug Deliv. Transl. Res. (2021). https://doi.org/10.1007/s13346-020-00891-5.

[59] E.A. Nance, G.F. Woodworth, K.A. Sailor, T.-Y. Shih, Q. Xu, G. Swaminathan, D. Xiang, C. Eberhart, J. Hanes, A Dense Poly(Ethylene Glycol) Coating Improves Penetration of Large Polymeric Nanoparticles Within Brain Tissue, Sci. Transl. Med. 4 (2012) 1–7. https://doi.org/10.1126/scitranslmed.3003594.

[60] W.M. Pardridge, Drug transport in brain via the cerebrospinal fluid, Fluids Barriers CNS. 8 (2011) 2–5. https://doi.org/10.1186/2045-8118-8-7.

[61] J. Huang, W. Liu, D.M. Doycheva, M. Gamdzyk, W. Lu, J. Tang, J.H. Zhang, Ghrelin attenuates oxidative stress and neuronal apoptosis via GHSR-1α/AMPK/Sirt1/PGC-1α/UCP2 pathway in a rat model of neonatal HIE, Free Radic. Biol. Med. 141 (2019) 322–337. https://doi.org/10.1016/j.freeradbiomed.2019.07.001.

[62] P. Xu, C. Tao, Y. Zhu, G. Wang, L. Kong, W. Li, R. Li, J. Li, C. Zhang, L. Wang, X. Liu, W. Sun, W. Hu, TAK1 mediates neuronal pyroptosis in early brain injury after subarachnoid hemorrhage, J. Neuroinflammation. 18 (2021) 188. https://doi.org/10.1186/s12974-021-02226-8.

[63] K.M. Brown, J.K. Nair, M.M. Janas, Y.I. Anglero-Rodriguez, L.T.H. Dang, H. Peng, C.S. Theile, E. Castellanos-Rizaldos, C. Brown, D. Foster, J. Kurz, J. Allen, R. Maganti, J. Li, S. Matsuda, M. Stricos, T. Chickering, M. Jung, K. Wassarman, J. Rollins, L. Woods, A. Kelin, D.C. Guenther, M.W. Mobley, J. Petrulis, R. McDougall, T. Racie, J. Bombardier, D. Cha, S. Agarwal, L. Johnson, Y. Jiang, S. Lentini, J. Gilbert, T. Nguyen, S. Chigas, S. LeBlanc, U. Poreci, A. Kasper, A.B. Rogers, S. Chong, W. Davis, J.E. Sutherland, A. Castoreno, S. Milstein, M.K. Schlegel, I. Zlatev, K. Charisse, M. Keating, M. Manoharan, K. Fitzgerald, J.-T. Wu, M.A. Maier, V. Jadhav, Expanding RNAi therapeutics to extrahepatic tissues with lipophilic conjugates, Nat. Biotechnol. 40 (2022) 1500–1508. https://doi.org/10.1038/s41587-022-01334-x.

[64] S. Werth, B. Urban-Klein, L. Dai, S. Höbel, M. Grzelinski, U. Bakowsky, F. Czubayko, A. Aigner, A low molecular weight fraction of polyethylenimine (PEI) displays increased transfection efficiency of DNA and siRNA in fresh or lyophilized complexes, J. Control. Release. 112 (2006) 257–270. https://doi.org/10.1016/j.jconrel.2006.02.009.

[65] C. Helmschrodt, S. Höbel, S. Schöniger, A. Bauer, J. Bonicelli, M. Gringmuth, S.A. Fietz, A. Aigner, A. Richter, F. Richter, Polyethylenimine Nanoparticle-Mediated siRNA Delivery to Reduce α-Synuclein Expression in a Model of Parkinson's Disease, Mol. Ther. - Nucleic Acids. 9 (2017) 57–68. https://doi.org/10.1016/j.omtn.2017.08.013.

[66] R.L. Rungta, H.B. Choi, P.J. Lin, R.W. Ko, D. Ashby, J. Nair, M. Manoharan, P.R. Cullis, B.A. MacVicar, Lipid Nanoparticle Delivery of siRNA to Silence Neuronal Gene Expression in the Brain, Mol. Ther. Acids. 2 (2013) e136. https://doi.org/10.1038/mtna.2013.65.

[67] N. Voigt, P. Henrich-Noack, S. Kockentiedt, W. Hintz, J. Tomas, B.A. Sabel, Surfactants, not size or zeta-potential influence blood-brain barrier passage of polymeric nanoparticles, Eur. J. Pharm. Biopharm. 87 (2014) 19–29. https://doi.org/10.1016/j.ejpb.2014.02.013.

[68] A. Joseph, G.M. Simo, T. Gao, N. Alhindi, N. Xu, D.J. Graham, L.J. Gamble, E. Nance, Surfactants influence polymer nanoparticle fate within the brain, Biomaterials. 277 (2021) 121086. https://doi.org/10.1016/j.biomaterials.2021.121086.

[69] Y. Liu, G. Yang, Y. Hui, S. Ranaweera, C.X. Zhao, Microfluidic Nanoparticles for Drug Delivery, Small. 18 (2022) 1–33. https://doi.org/10.1002/smll.202106580.

[70] S.L. Law, K.J. Huang, H.Y. Chou, Preparation of desmopressin-containing liposomes for intranasal delivery, J. Control. Release. 70 (2001) 375–382. https://doi.org/10.1016/S0168-3659(00)00369-2.

[71] M.I. Ugwoke, R.U. Agu, N. Verbeke, R. Kinget, Nasal mucoadhesive drug delivery: Background, applications, trends and future perspectives, Adv. Drug Deliv. Rev. 57 (2005) 1640–1665. https://doi.org/10.1016/j.addr.2005.07.009.

[72] D. Vllasaliu, R. Exposito-Harris, A. Heras, L. Casettari, M. Garnett, L. Illum, S. Stolnik, Tight junction modulation by chitosan nanoparticles: Comparison with chitosan solution, Int. J. Pharm. 400 (2010) 183–193. https://doi.org/10.1016/j.ijpharm.2010.08.020.

[73] L. Casettari, L. Illum, Chitosan in nasal delivery systems for therapeutic drugs, J. Control. Release. 190 (2014) 189–200. https://doi.org/10.1016/j.jconrel.2014.05.003.

[74] Z.N. Warnken, H.D.C. Smyth, A.B. Watts, S. Weitman, J.G. Kuhn, R.O. Williams, Formulation and device design to increase nose to brain drug delivery, J. Drug Deliv. Sci. Technol. 35 (2016) 213–222. https://doi.org/10.1016/j.jddst.2016.05.003.

[75] P.R. Lockman, J.M. Koziara, R.J. Mumper, D.D. Allen, Nanoparticle Surface Charges Alter Blood–Brain Barrier Integrity and Permeability, J. Drug Target. 12 (2004) 635–641. https://doi.org/10.1080/10611860400015936.

[76] T. Yuan, L. Gao, W. Zhan, D. Dini, Effect of Particle Size and Surface Charge on Nanoparticles Diffusion in the Brain White Matter, Pharm. Res. 39 (2022) 767–781. https://doi.org/10.1007/s11095-022-03222-0.

[77] M.M.B. Ribeiro, M.M. Domingues, J.M. Freire, N.C. Santos, M.A.R.B. Castanho, Translocating the blood-brain barrier using electrostatics, Front. Cell. Neurosci. 6 (2012) 1–14. https://doi.org/10.3389/fncel.2012.00044.

[78] L. Zhang, J. Fan, G. Li, Z. Yin, B.M. Fu, Transcellular Model for Neutral and Charged Nanoparticles Across an In Vitro Blood–Brain Barrier, Cardiovasc. Eng. Technol. 11 (2020) 607–620. https://doi.org/10.1007/s13239-020-00496-6.

[79] M. Oswald, S. Geissler, A. Goepferich, Targeting the Central Nervous System (CNS): A Review of Rabies Virus-Targeting Strategies, Mol. Pharm. 14 (2017) 2177–2196. https://doi.org/10.1021/acs.molpharmaceut.7b00158.

[80] R. Hao, B. Sun, L. Yang, C. Ma, S. Li, RVG29-modified microRNA-loaded nanoparticles improve ischemic brain injury by nasal delivery, Drug Deliv. 27 (2020) 772–781. https://doi.org/10.1080/10717544.2020.1760960.

[81] B. Srinivasan, A.R. Kolli, M.B. Esch, H.E. Abaci, M.L. Shuler, J.J. Hickman, TEER Measurement Techniques for In Vitro Barrier Model Systems, SLAS Technol. 20 (2015) 107–126. https://doi.org/10.1177/2211068214561025.

[82] W. Zhang, A. Mehta, Z. Tong, L. Esser, N.H. Voelcker, Development of Polymeric Nanoparticles for Blood–Brain Barrier Transfer—Strategies and Challenges, Adv. Sci. 8 (2021) 1–32. https://doi.org/10.1002/advs.202003937.

[83] F.R. Walter, A.R. Santa-Maria, M. Mészáros, S. Veszelka, A. Dér, M.A. Deli, Surface charge, glycocalyx, and blood-brain barrier function, Tissue Barriers. 9 (2021). https://doi.org/10.1080/21688370.2021.1904773.

[84] D. Adams, A. Gonzalez-Duarte, W.D. O'Riordan, C.-C. Yang, M. Ueda, A. V. Kristen, I. Tournev, H.H. Schmidt, T. Coelho, J.L. Berk, K.-P. Lin, G. Vita, S. Attarian, V. Planté-Bordeneuve, M.M. Mezei, J.M. Campistol, J. Buades, T.H. Brannagan, B.J. Kim, J. Oh, Y. Parman, Y. Sekijima, P.N. Hawkins, S.D. Solomon, M. Polydefkis, P.J. Dyck, P.J. Gandhi, S. Goyal, J. Chen, A.L. Strahs, S. V. Nochur, M.T. Sweetser, P.P. Garg, A.K. Vaishnaw, J.A. Gollob, O.B. Suhr, Patisiran, an RNAi Therapeutic, for Hereditary Transthyretin Amyloidosis,

N. Engl. J. Med. 379 (2018) 11–21. https://doi.org/10.1056/NEJMoa1716153.

[85] J.A. Kulkarni, D. Witzigmann, S. Chen, P.R. Cullis, R. van der Meel, Lipid Nanoparticle Technology for Clinical Translation of siRNA Therapeutics, Acc. Chem. Res. 52 (2019) 2435–2444. https://doi.org/10.1021/acs.accounts.9b00368.

[86] Y. Su, B. Sun, X. Gao, X. Dong, L. Fu, Y. Zhang, Z. Li, Y. Wang, H. Jiang, B. Han, Intranasal Delivery of Targeted Nanoparticles Loaded With miR-132 to Brain for the Treatment of Neurodegenerative Diseases, Front. Pharmacol. 11 (2020). https://doi.org/10.3389/fphar.2020.01165.

[87] Z.R. Cohen, S. Ramishetti, N. Peshes-Yaloz, M. Goldsmith, A. Wohl, Z. Zibly, D. Peer, Localized RNAi Therapeutics of Chemoresistant Grade IV Glioma Using Hyaluronan-Grafted Lipid-Based Nanoparticles, ACS Nano. 9 (2015) 1581–1591. https://doi.org/10.1021/nn506248s.

CHAPTER 3

Nanoemulsions and polymeric nanocapsules as SARS-CoV-2 vaccines

Chapter 3: Nanoemulsions and polymeric nanocapsules as SARS-CoV-2 vaccines

This work has been done in collaboration with the National Center of Biotechnology, Spanish National Research Council (CNB-CSIC) (Madrid, Spain), the BioFarma Research Group, Center for Research in Molecular Medicine and Chronic Diseases (CiMUS), University of Santiago de Compostela (Santiago de Compostela, Spain), the Laboratory for Molecular and Cellular Therapy, Vrije University Brussel (Brussel, Belgium), the August Pi i Sunyer Biomedical Research Institute (IDIBAPS) (Barcelona, Spain), the Barcelona Supercomputing Center (Barcelona, Spain), the Department of Medicine and Life Sciences, Faculty of Health and Life Sciences, University Pompeu Fabra (Barcelona, Spain), the Institute for Research in Biomedicine (Barcelona, Spain), and the Hospital Clinic of Barcelona (Barcelona, Spain).

ABSTRACT

The global coronavirus disease 2019 (COVID-19) emergency resulted in worldwide efforts to develop vaccines for protection against severe acute respiratory syndrome coronavirus 2 (SARS-CoV-2). Our contribution to this international effort has involved the development of a diverse library of nanocarriers, including nanoemulsions (NEs) and nanocapsules (NCs), with the primary objective of protecting and delivering messenger ribonucleic acid (mRNA) vaccines derived from SARS-CoV-2.

Through *in vitro* and *in vivo* experiments using model mRNAs, a promising nanocarrier candidate was successfully identified, capable of transfecting various mRNA reporters while eliciting moderate immune responses. This candidate consisted of dextran sulfate NC with a specific core composition (NC-4-DX). The results of the *in vivo* evaluation of NC-4-DX loaded with SARS-CoV-2 derived mRNAs, either as single mRNA or in combination with different mRNAs, indicated a significant increase in the levels of cytokines secreted by $CD8^+$ T immune cells. These findings highlight the potential of polymeric NCs in advancing mRNA vaccine development for combating infectious diseases.

GRAPHICAL ABSTRACT

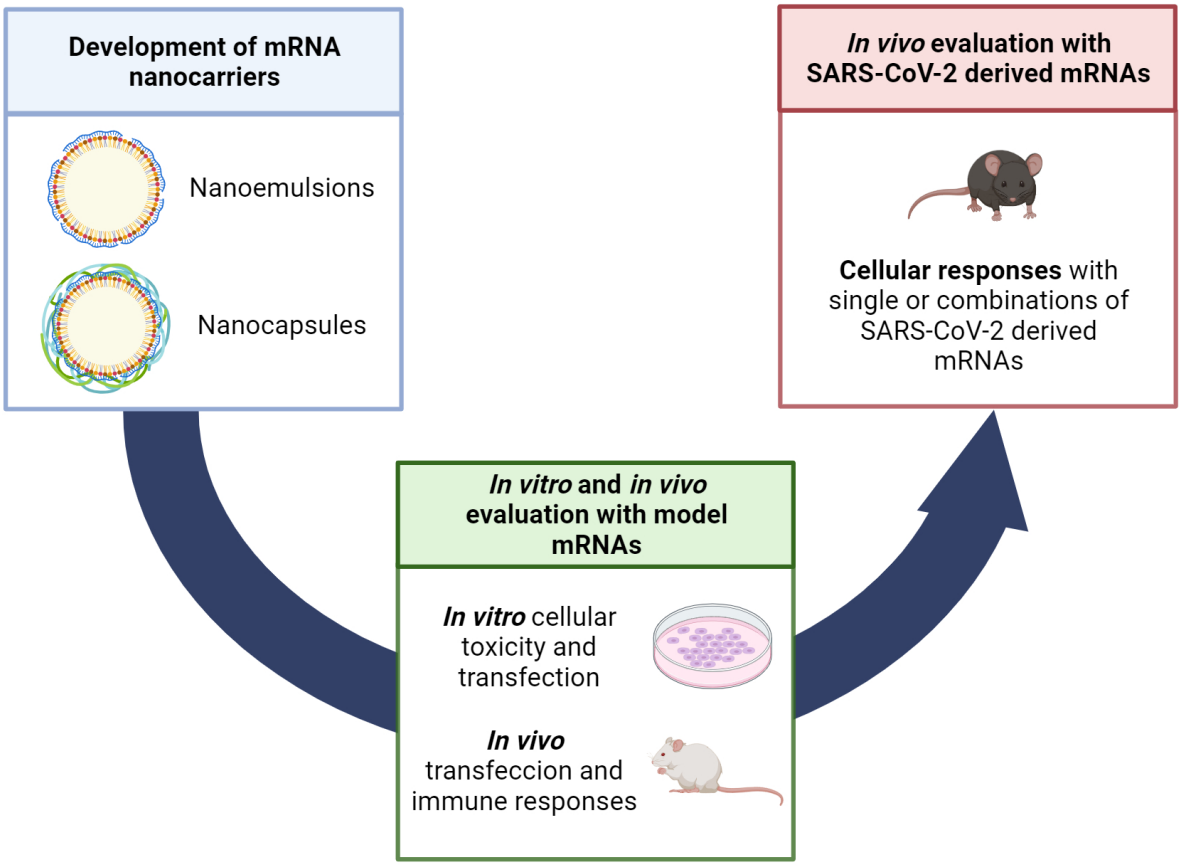

Created with https://biorender.com.

1. INTRODUCTION

On March 11, 2020, the World Health Organization (WHO) declared the coronavirus disease 2019 (COVID-19) outbreak as a global pandemic [1]. COVID-19 is caused by the highly contagious, pathogenic, and mutagenic severe acute respiratory syndrome coronavirus 2 (SARS-CoV-2), resulting in over 760 million confirmed cases, and nearly 7 million deaths worldwide [2–4]. Intended to stop the spread of the virus, and reduce the severity of COVID-19, research on messenger ribonucleic acid (mRNA) vaccines gained importance [5]. Notably, the first two vaccines authorized by the European Medicines Agency (EMA) and the US Food and Drug Administration (FDA) were mRNA vaccines from BioNTech/Pfizer and Moderna, demonstrating over 90% protective efficacy against symptomatic SARS-CoV-2 infection in phase III clinical trials [6,7].

The success of mRNA vaccines relied not only on their rapid design and development processes, but mainly on their high-efficiency immune responses, and overall safety [8]. mRNA constructs can be designed within days, allowing for fast production and scaling-up processes [9,10]. Moreover, mRNA vaccines are safer than live viruses and they do not need to access the nucleus to depict their function, unlike deoxyribonucleic acid (DNA) vaccines [11].

In April 2020, our laboratory joined the COVARNA consortium, an ambitious team of scientists from Spain and Belgium encompassing immunologists, pharmacologists, computer scientists, and molecular experts. Within this consortium, different mRNAs intended to induce responses against the receptor binding domain (RBD) of the surface spike glycoprotein of the SARS-CoV-2 were developed [12]. In addition, different mRNAs intended to enhance T and B cell responses were also produced.

Our approach consisted of taking advantage of all our knowledge of nanocarriers for nucleic acid delivery and nanovaccines to develop a library of potential candidates for the delivery of mRNA [13–21]. Ideally, our nanocarriers aimed not only to protect the mRNA but also to enhance the overall immunogenic profile of the vaccine without compromising its safety. Figure 1 represents the efforts of our laboratory to develop a vaccine against SARS-CoV-2. In our attempt to move away from LNPs, we selected nanoemulsions (NEs) and nanocapsules (NCs) as mRNA carriers. Within this context, different lipids, surfactants, oils, and polymers were investigated to increase the variability of our library of nanocarriers. Around 100 different prototypes were developed, with diverse properties and compositions.

To narrow down our candidates, we implemented a target product profile (TPP), considering criteria such as (A) particle size below or around 200 nm; (B) uniform particle size distribution; (C) high mRNA association capacity; (D) stability or lyophilization potential; and (E) alignment with regulatory requirements (eg. low ethanol content, or the use of compounds already approved). The candidates fulfilling these criteria underwent *in vitro* and *in vivo* assessments of their transfection efficiency using model mRNAs. *In vitro* cytotoxicity and transfection efficiency were evaluated in both HeLa cells and human dendritic cells; while *in vivo* studies included transfection efficiency evaluation and preliminary immunity assessment. These studies enabled us to identify a candidate for further evaluations using various SARS-CoV-2 derived mRNAs and to determine their cellular immune responses, both individually or in combination with different mRNAs.

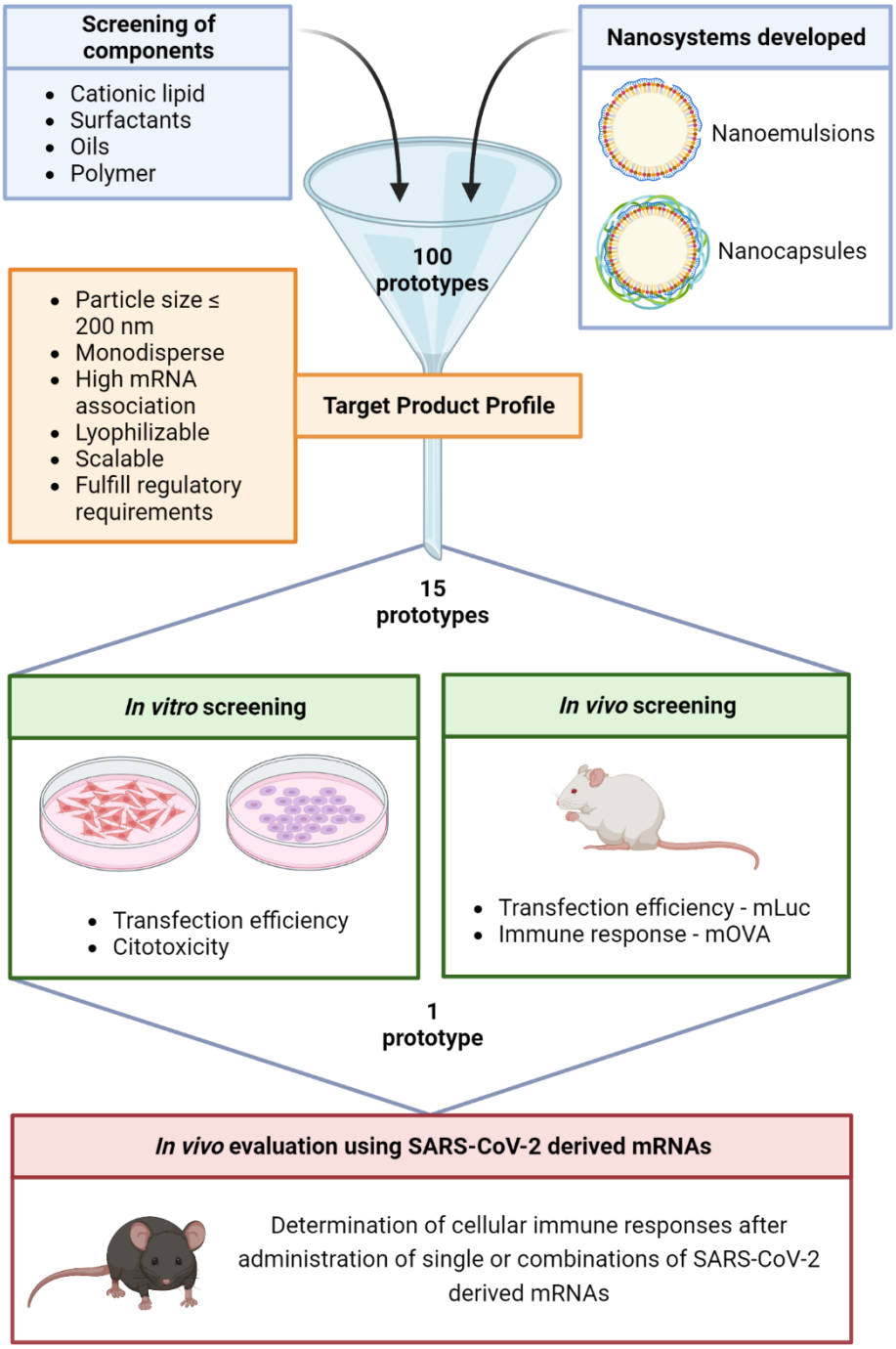

Figure 1. Schematic representation of the prototype development process

Different NEs and NCs, containing lipids, surfactant oils, and polymers were prepared. The selection process was based on their ability to fulfill the target product profile criteria. Out of these formulations, 15 prototypes were selected for comprehensive studies, evaluating their transfection efficiency and immune potential in both *in vitro* and *in vivo* settings. One particular prototype was selected for the formulation of multiple SARS-CoV-2-derived mRNAs, and their cellular immune responses were assessed.

Created with https://biorender.com.

2. MATERIALS AND METHODS

2.1. MATERIALS

DOTAP (1,2-dioleoyl-3-trimethylammonium propane, chloride salt) and DOPE (1,2-dioleoyl-sn-glycero-3-phosphoethanolamine) were purchased from Avanti Polar Lipids (AL, USA). Vitamin E (Vit E) (D, L-α-tocopherol) and K-HS15® (Kolliphor® HS15) were obtained from BASF (Mannheim, Germany). Tween 80 and sucrose were purchased from Merck Millipore (Darmstadt, Germany). LAE (LAE®, ethyl lauroyl arginate HCl) was acquired from Vedeqsa (Barcelona, Spain). Benzethonium chloride (BZT) was obtained from Spectrum Chemical MFG Corp (NJ, USA). Glycocholic acid, sodium salt (sodium glycocholate, SG) was acquired from Dextra Laboratories Ltd (Reading, UK). Inulin (Inutec® SL1) was obtained from CreaChem (Tienen, Belgium).

Dextran sulfate (DX) (sodium salt), DEAE-dextran hydrochloride (DEAE-DX, diethylaminoethyl-dextran hydrochloride), and spermine were purchased from Sigma-Aldrich SAFC© (MO, USA). Chitosan (CS) (poly (D-glucosamide) hydrochloride salt) was obtained from HMC$^+$ (Halle, Germany). PEG-PGA (PEG (5 kDa)-b-PGA (10) [Na]) (poly(ethylene glycol)-block-poly(l-glumatic acid sodium salt) and PArg (poly-L-arginine) were obtained from Polypeptide Therapeutic Solutions (Valencia, Spain). Hyaluronic acid (HA, 40 kDa) was acquired from Lehmann & Voss & Co. KG (Hamburg, Germany). Protamine (PRT) (Protamine Sulphate EP) was purchased from Yuki Gosei Kogyo Co. Ltd (Tokyo, Japan).

Transfer Ribonucleic acid (tRNA) from baker's yeast (S. cerevisiae) was purchased from Sigma-Aldrich (MO, USA). Three model mRNAs were used for the evaluation of the nanocarriers to evaluate their transfection and immunogenic capabilities: mRNA encoding green fluorescence protein (mGFP) (CleanCap EGFP mRNA, TriLink Biotechnologies, CA, USA), mRNA encoding luciferase (mLuc), and mRNA encoding ovalbumin protein (mOVA).

Four different mRNA immunogens against SARS-CoV-2 were designed and provided for this project: mRNA intended to trigger a T cell response (SARS-CoV-2-T cells mRNA or mT), mRNA intended to trigger a B cell response (SARS-CoV-2-B cells mRNA or mB), mRNA encoding for RBD domain of the virus (SARS-CoV-2-RBD mRNA or mRBD) and mRNA encoding a highly immunogenic motif from the RBD domain (SARS-CoV-2-RBD$_{epi}$ mRNA or mRBD$_{epi}$). All these mRNA constructs were synthesized by Prof. Thielemans's Lab (Vrije Universiteit Brussels, Brussels, Belgium).

2.2. PRODUCTION OF NANOEMULSIONS AND NANOCAPSULES

Two different approaches were used for the preparation of nanoemulsions (NEs): bulk production of blank NEs followed by the electrostatic adsorption of mRNA onto the surface in a second step; or microfluidic production of NEs in the presence of mRNA, in a single process using a microfluidic mixer system. The preparation of nanocapsules (NCs) consisted of a separate procedure, comprising the polymeric coating of pre-formed NE-mRNA.

2.2.1. Preparation of mRNA-nanoemulsions by bulk process

2.2.1.1. Preparation of blank nanoemulsions

The preparation method for blank NEs consisted of a solvent-displacement technique [22]. Briefly, an organic phase was prepared by dissolving different lipids (including DOTAP, DOPE, Vitamin E, or Tween 80) in ethanol. The resulting organic solution (0.3 mL, containing the concentrations described in Table 1) was added over an aqueous phase (2 mL, RNase-free water), under magnetic stirring (1400 rpm), and further incubated under stirring for 5 minutes. The solution was set aside for stability for 5 minutes.

Evaporation under vacuum (Heidolph Hei-VAP Advantage; Schwabach, Germany) was used to eliminate organic solvents from blank NE-4. The eliminated volume was supplemented with RNase-free water, aiming for a theoretical ethanol percentage lower than 10%.

Table 1. Concentration of different lipidic components of the organic phase for the preparation of blank nanoemulsions

	DOTAP (mg/mL)	DOPE (mg/mL)	Vitamin E (mg/mL)	Tween 80 (mg/mL)
NE-1	19.2	19.4	46	-
NE-2	65.2	19.2	46	-
NE-3	65.2	19.2	46	19.2
NE-4	32.6	16.3	78	16.3

Abbreviations: DOPE: 1,2-dioleoyl-sn-glycero-3-phosphoethanolamine. DOTAP: 1,2-dioleoyl-3-trimethylammonium propane. NE: nanoemulsion. Vitamin E: D, L-α-tocopherol.

2.2.1.2. Complexation of mRNA onto nanoemulsions

Complexation of mRNA onto pre-formed blank NEs was performed by bulk mixing. A solution containing mRNA (at different concentrations, depending on the needed final mRNA concentration) was added over the previously formed blank NE solution. Briefly, blank NE was diluted in RNase-free water, leading to the desired DOTAP concentration depending on the nitrogen-to-phosphate (N/P) ratio explored and the desired final mRNA concentration. Solution containing mRNA was added over the blank NE solution, under magnetic stirring at 700 rpm for 10 seconds. Formulations were allowed to stabilize for 30 minutes.

Different N/P ratios were explored, from 0.64:1 to 4:1, leading to different physicochemical properties. Volume/volume (v/v) ratio used for the formation of NE-mRNA was kept as 4:1 (mRNA solution to blank NE solution) for all N/P ratios, except for N/P ratio 4:1, in which solutions were mixed at 1.1:1 v/v ratio.

2.2.2. Preparation of mRNA-nanoemulsions by microfluidic process

Microfluidic mixing comprises the simultaneous formation of the NE and the complexation of the mRNA onto a micromixer NanoAssmblr^{TM} bench-top instrument, Precision NanoSystem Inc. (Vancouver, Canada). In summary, 0.4 mL of the organic phase (consisting of DOTAP, DOPE, Vitamin E, or Tween 80 diluted in ethanol, as described in Table 2) were mixed with 2

mL of the aqueous phase (containing mRNA at a concentration of 0.288 mg/mL, and Tween 80 solution in the case of NE-5, diluted in RNase-free water).

Table 2. Concentration of different lipidic components of the organic phase for the preparation of mRNA-NEs by microfluidic process

	DOTAP (mg/mL)	DOPE (mg/mL)	Vitamin E (mg/mL)	Tween 80 (mg/mL)
NE-4	16.3	8.1	39	8
NE-5	16.3	3.4	7	0.9*

(*) Tween 80 is included in the aqueous phase in this particular case. **Abbreviations:** DOPE: 1,2-dioleoyl-sn-glycero-3-phosphoethanolamine. DOTAP: 1,2-dioleoyl-3-trimethylammonium propane. NE: nanoemulsion. Vitamin E: D, L-α-tocopherol.

The N/P ratio was kept constant at 4:1. The mixing process was performed using a v/v ratio of 1:5 (organic to aqueous phase). The Total Flow Rate was kept at 12 mL/min.

2.2.3. Preparation of mRNA-nanocapsules

After the preparation of NE-mRNA nanosystems, NC (NC-mRNA) were produced by adding a polymeric solution (at concentrations dependent on the weight to weight (w/w) and the type of polymer used) over the preformed NE-mRNA carrier. In all cases, 0.2 mL of the polymeric solution was added over 1 mL of the preformed NE-mRNA nanosystem, and the resulting solution was kept under magnetic stirring at 700 rpm for 10 seconds. Regardless of the polymer used, the v/v ratio was constant at 1:5 (polymer to mRNA). The resulting NC-mRNA carriers were stabilized for 10 minutes.

2.3. CHARACTERIZATION OF NANOEMULSIONS AND NANOCAPSULES

2.3.1. Characterization of the size, polydispersity index and ζ-potential of nanoemulsions and nanocapsules

Hydrodynamic diameter and polydispersity index (PDI) were characterized by dynamic light scattering (Zetasizer® Nano ZS, Malvern Instruments, Malvern, UK). ζ-potential was measured in terms of mean electrophoretic mobility values, measured by laser Doppler electrophoresis with the same equipment.

Particle size and PDI measurements were performed after diluting the samples 10x in RNase-free water. ζ-potential characterization was obtained after dilution of samples 20x in RNase-free water.

2.3.2. Characterization of encapsulation efficiency of mRNA

Encapsulation efficiency (EE%) was determined by agarose gel electrophoresis. Both NE-mRNA and NC-mRNA formulations were diluted in a 1:1 (v/v) ratio with a solution of heparin (Sigma-Aldrich, MO, USA) or Triton X (Triton-X-100, Sigma-Aldrich, MO, USA), prepared at 50 mg/mL in RNase-free water, intended to displace the mRNA from the nanoparticle.

Agarose gel electrophoresis allows the qualitative quantification of the amount of mRNA associated with the NE-mRNA and NC-mRNA carriers. For that, samples containing 1-3 µg of mRNA were loaded in an agarose gel at 1% w/v in Tris Acetate-EDTA buffer (Sigma-Aldrich, MO, USA) before and after incubation with heparin or Triton X solution. Samples were diluted with equal volumes of loading mix, containing 1x SYBR® Gold nucleic acid strain (Invitrogen, CA, USA). Free mRNA was included as a control. Gels were run for 30 minutes at 90 V in a Sub-Cell GT cell 96/192 (Bio-Rad Laboratories, CA, USA), and evaluated with a UV transilluminator imagining system (Molecular Imager® Gel Doc™ XR, Bio-Rad Laboratories, CA, USA).

2.4. FREEZE-DRYING OF SELECTED NANOEMULSIONS AND NANOCAPSULES

Selected NE-mRNA and NC-mRNA formulations were frozen in the presence of cryoprotectants (including sucrose and trehalose) at -40 °C for at least 1 hour, then freeze-dried (Genesis™ 25 EL, S.P Industries, PA, USA). Samples were initially left freeze-dried at -65 °C for 1 hour with a vacuum of 200 mTorr, to ensure that formulations were completely frozen. The first drying phase was performed at a temperature ranging from -40 °C to 15 °C, under a progressive vacuum to 20 mTorr for 20 hours. The second drying phase was done for 1 hour at 20 °C and 20 mTorr. After this process, formulations were stored at 4 °C until resuspension in RNase-free water, and their physicochemical properties were determined as described in section 2.3.

2.5. IN VITRO ASSESSMENT OF MRNA TRANSFECTION EFFICIENCY AND CYTOTOXICITY

2.5.1. In vitro mGFP transfection efficiency and cytotoxicity in HeLa cells

A total of 10,000 HeLa cells were seeded per well in a flat bottom 96-well plate and allowed to adhere for 24 hours. Cells were treated with NE- and NC-mRNA GFP formulations for 4 hours, in Opti-MEM™ (Gibco™, Thermo Fisher, MA, USA) at mGFP concentrations ranging from 200 to 25 ng per well. Nanocarriers were then removed, and replaced with a complete medium and the cells were incubated for another 20 hours. Cell viability was measured by resazurin assay, following manufacturer recommendations [23]. Briefly, cells were incubated with resazurin reagent (Resazurin sodium salt, Sigma-Aldrich, MO, USA) supplemented complete media for 45 minutes, and the resulting fluorescence was measured in a plate reader at 544/590 nm. Cells were then trypsinized, harvested, and fixed with 1% (w/v) formaldehyde in PBS, for flow cytometry analysis in terms of the percentage of GFP-positive cells and mean fluorescence intensity.

In other experiments, 60,000 HeLa cells per well were seeded in 24-well plates. In these experiments, mGFP concentrations of up to 1000 ng per well were used.

2.5.2. In vitro mRBD transfection efficiency and cytotoxicity in human dendritic cells

Human monocyte-derived dendritic cells (hMDDCs or hDCs) were obtained from blood monocytes from healthy donors, as previously reported [24]. hDCs were harvested from a 96-well plate (1,000,000 cells per well) and transfected with NE-mRBD and NC-mRBD nanocarriers at concentrations ranging from 10 µg to 3 µg per well. After 3 hours, cells were

washed, and a medium containing a maturation cocktail (IL-6, IL-1β, PGE2, and TNFα) was added. At different time points after transfection, cells were collected and RBD expression was analyzed by flow cytometer. Cell cytotoxicity was also evaluated using the LIVE/DEAD^{TM} Fixable Near IR Reagent (Invitrogen, MA, USA).

2.6. ANIMAL STUDIES

All animal studies procedures were performed in compliance with relevant laws and institutional guidelines and the appropriate institutional committee(s) have approved them.

2.7. IN VIVO TRANSFECTION EFFICIENCY WITH MRNA MODELS

2.7.1. Intramuscular administration of nanocarriers with mLuc

BALB/c and Swiss mice (each strain used in different studies, evaluating formulations prepared by bulk mixing process and microfluidic mixing preparation, respectively) were administered with two intramuscular injections (one in each thigh muscle), in a single administration session, with 10 µg of mLuc, encapsulated in different NE-mLuc and NC-mLuc. The total volume administered was 50 µL per leg. This led to a total volume of 100 µL with a total dose of 20 µg per animal. At different time points, including 6, 24, and 48 hours, animals were intraperitoneally administered 100 µL of D-luciferin, and whole-body fluorescence was visualized in an *in vivo* imaging system (IVIS).

2.7.2. Intramuscular administration of nanocarriers with mOVA

C57BL/6J mice were administered with a single intramuscular injection (right thigh muscle), on two different administration sessions (day 0 and day 7), with 10 µg of mOVA encapsulated in NC-4-DX per injection. The total volume administered was 50 µL per animal per injection. On day 7, prior second administration, 100 µL of blood were collected for flow cytometer analysis. On day 10, animals were euthanized, the spleen was harvested, and single-cell suspension was generated. Splenocytes were used for ELISpot and flow cytometer analysis.

For flow cytometer analysis, blood and splenocytes samples were stained with MHC Dextramer® staining (Immudex, Copenhague, Denmark) following manufacturer recommendations. In the case of IFN-γ ELIspot (Diaclone, Besançon, France), immunoassay was performed following manufacturer recommendations.

2.8. IN VIVO EVALUATION OF CELLULAR IMMUNE RESPONSES WITH SARS-COV-2 DERIVED MRNAS

C57BL/6J mice were administered with two intramuscular injections on the thigh muscles, on two different administration sessions (day 0 and day 21), with different doses of SARS-CoV-2 derived mRNAs encapsulated in NC-4-DX per injection. Administration consisted of a single mRNA or combinations of two different mRNAs, which determined if the dose administered was 10 or 20 µg, respectively. The total volume administered was 50 µL per

animal per injection, leading to a total volume of 100 µL. On day 36, animals were sacrificed, and humoral and cellular responses were determined from splenocytes.

Cellular responses were studied by flow cytometer, after stimulation of splenocytes with different SARS-CoV-2 S1 and S2 peptide pools representing the S antigen, in combination with SARS-CoV-2 S protein. Non-stimulated samples were used as a control.

3. RESULTS AND DISCUSSION

3.1. SCREENING OF NANOEMULSIONS AND NANOCAPSULES

As indicated in the introduction of this chapter, our first experimental objective was the production of a library of NEs and polymeric NCs. To explore a wide range of components that could enhance immune responses elicited by the developed nanocarriers, different combinations of cationic and anionic lipids, surfactants, and polymers were explored. Based on our previous experience, the selected oil was Vitamin E, due to its versatility in forming NEs for RNA delivery. As surfactants, we considered multiple candidates capable of entrapping RNA while facilitating the formation of small and stable nanocarriers, such as ethyl lauroyl arginate (LAE), benzethonium chloride (BZT), Kolliphor® HS15 (K-HS15®), 1,2-dioleoyl-3-trimethylammonium propane (DOTAP), 1,2-dioleoyl-sn-glycero-3-phosphoethanolamine (DOPE) or Tween 80, among others.

These components were combined at different molar ratios to increase variability in the physicochemical properties of the resulting nanocarriers. Additionally, we explored various volume-to-volume (v/v) ratios between the aqueous phase and the organic phase; and weight-to-weight (w/w) ratios between the polymer and the mRNA. Notably, we observed that greater v/v ratios led to smaller particle sizes while increasing the polydispersity of the NEs. This highlighted the importance of carefully tuning this parameter to achieve smaller diameters without compromising the stability of the resulting NEs. Moreover, higher w/w ratios between the polymer and the mRNA resulted in more significant alterations in the surface properties of the resulting NCs. These formulations underwent characterization for physicochemical properties, storage stability, or alignment with regulatory requirements. Selected prototypes were screened based on their *in vitro* cytotoxicity profile and mRNA transfection efficiency potency.

As outlined in Table 3, more than 80 NE and NCs were discarded during this process. The primary reasons for exclusion included inadequate particle size and polydispersity, instability or poor storage capacity, high ethanol content, substantial *in vitro* toxicity, or complete inability to achieve *in vitro* transfection.

Table 3. Summary of nanocarriers developed during this project that failed to fulfill the target product profile

#	Nanosystem	Composition	Molar ratio (%)	v/v ratio	Polymer	w/w ratio
1	NE	LAE: Vit E	35.9: 64.1	3.2: 1		
2	NE	LAE: Vit E	35.9: 64.1	19.8: 1		
3	NE	LAE: Vit E	35.9: 64.1	19: 1		
4	NE	LAE: Vit E	35.9: 64.2	9: 1		
5	NE	LAE: Vit E	35.9: 64.1	3.6: 1		
6	NE	BZT: Vit E	60.8: 39.2	3.2: 1		
7	NE	BZT: Vit E	52.7: 47.3	3.2: 1		
8	NE	BZT: Vit E	31.7: 68.3	3.2: 1		
9	NC	BZT: Vit E	31.7: 68.3	3.2: 1	SPM	0.32: 1
10	NC	BZT: Vit E	31.7: 68.3	3.2: 1	PRT	0.5: 1
11	NC	BZT: Vit E	31.7: 68.3	3.2: 1	PRT	1: 1
12	NC	BZT: Vit E	31.7: 68.3	3.2: 1	PRT	2: 1
13	NC	BZT: Vit E	31.7: 68.3	3.2: 1	PRT	4: 1
14	NE	BZT: Vit E	23.6: 76.4	3.2: 1		
15	NE	BZT: Vit E	52.8: 47.2	3.2: 1		
16	NE	BZT: Vit E	35.8: 64.2	3.2: 1		
17	NE	BZT: Vit E	32: 68	3.2: 1		
18	NC	BZT: Vit E	32: 68	3.2: 1	SPM	0.32: 1
19	NC	BZT: Vit E	32: 68	3.2: 1	SPM	0.43: 1
20	NC	BZT: Vit E	32: 68	3.2: 1	SPM	2: 1
21	NC	BZT: Vit E	32: 68	3.2: 1	SPM	5: 1
22	NC	BZT: Vit E	32: 68	3.2: 1	SPM	10: 1
23	NC	BZT: Vit E	32: 68	3.2: 1	SPM	20: 1
24	NC	BZT: Vit E	32: 68	3.2: 1	SPM | HA	0.32: 1 | 0.6: 1
25	NC	BZT: Vit E	32: 68	3.2: 1	SPM | HA	0.32: 1 | 6: 1
26	NC	BZT: Vit E	32: 68	3.2: 1	SPM | HA	0.43: 1| 8: 1
27	NE	BZT: Vit E	23.4: 76.6	3.2: 1		
28	NE	BZT: Vit E	13.4: 86.6	3.2: 1		
29	NE	BZT: Vit E	5.8: 94.2	3.2: 1		
30	NE	Inulin: Vit E: SG	3: 75.5: 21.5	3.2: 1		
31	NE	K-HS15®: Vit E: SG	73.8: 20.4: 5.8	3.2: 1		
32	NE	K-HS15®: Vit E: SG	65.3: 27: 7.7	3.2: 1		
33	NE	K-HS15®: Vit E: SG	48.5: 40.1: 11.4	3.2: 1		
34	NE	K-HS15®: Vit E: SG	32: 52.9: 15.1	3.2: 1		
35	NC	K-HS15®: Vit E: SG	32: 52.9: 15.1	3.2: 1	PRT	0.125: 1
36	NC	K-HS15®: Vit E: SG	32: 52.9: 15.1	3.2: 1	PRT	0.25: 1
37	NC	K-HS15®: Vit E: SG	32: 52.9: 15.1	3.2: 1	PRT	0.5: 1
38	NC	K-HS15®: Vit E: SG	32: 52.9: 15.1	3.2: 1	PRT	1: 1

Abbreviations: BZT: benzethonium chloride. HA: hyaluronic acid. Inulin: Inutec® SL1. K-HS15: Kolliphor® HS15. LAE: ethyl lauroyl arginate. NC: nanocapsule NE: nanoemulsion. PRT: protamine sulphate EP. SG: sodium glycocholate. SPM: spermine. Vit E: D, L-α-tocopherol. v/v ratio: volume-to-volume ratio between aqueous and organic phases. w/w ratio: weight-to-weight ratio between polymer and mRNA content.

Table 3. Summary of nanocarriers developed during this project that failed to fulfill the target product profile (continuation)

#	Nanosystem	Composition	Molar ratio (%)	v/v ratio	Polymer	w/w ratio
39	NE	K-HS15®: Vit E: SG	26.6: 68.7: 4.7	3.2: 1		
40	NC	K-HS15®: Vit E: SG	26.6: 68.7: 4.7	3.2: 1	PARG	0.4: 1
41	NC	K-HS15®: Vit E: SG	26.6: 68.7: 4.7	3.2: 1	PARG	0.8: 1
42	NC	K-HS15®: Vit E: SG	26.6: 68.7: 4.7	3.2: 1	PARG	1.6: 1
43	NC	K-HS15®: Vit E: SG	26.6: 68.7: 4.7	3.2: 1	PARG	4: 1
44	NE	DOTAP: DOPE: Vit E	18.9: 5.2: 75.9	6.7: 1		
45	NE	DOTAP: DOPE: Vit E	25.8: 7.1: 67.1	6.7: 1		
46	NE	DOTAP: DOPE: Vit E	18.2: 8.5: 73.3	6.7: 1		
47	NE	DOTAP: DOPE: Vit E	25.5: 14.1: 60.4	6.7: 1		
48	NC	DOTAP: DOPE: Vit E	16.8: 49.3: 33.8	6.7: 1	PRT	0.2: 1
49	NC	DOTAP: DOPE: Vit E	16.8: 49.3: 33.8	6.7: 1	PRT	0.4: 1
50	NC	DOTAP: DOPE: Vit E	16.8: 49.3: 33.8	6.7: 1	PRT	0.5: 1
51	NC	DOTAP: DOPE: Vit E	16.8: 49.3: 33.8	6.7: 1	PRT	0.5: 1
52	NC	DOTAP: DOPE: Vit E	16.8: 49.3: 33.8	6.7: 1	SPM	0.08: 1
53	NC	DOTAP: DOPE: Vit E	16.8: 49.3: 33.8	6.7: 1	SPM	0.22: 1
54	NC	DOTAP: DOPE: Vit E	16.8: 49.3: 33.8	6.7: 1	SPM	0.32: 1
55	NC	DOTAP: DOPE: Vit E	16.8: 49.3: 33.8	6.7: 1	SPM	0.44: 1
56	NC	DOTAP: DOPE: Vit E	16.8: 49.3: 33.8	6.7: 1	SPM	0.66: 1
57	NC	DOTAP: DOPE: Vit E	16.8: 49.3: 33.8	6.7: 1	DEAEDX	1: 1
58	NC	DOTAP: DOPE: Vit E	16.8: 49.3: 33.8	6.7: 1	DEAEDX	2: 1
59	NC	DOTAP: DOPE: Vit E	16.8: 49.3: 33.8	6.7: 1	DEAEDX	3: 1
60	NC	DOTAP: DOPE: Vit E	16.8: 49.3: 33.8	6.7: 1	SPM	0.22: 1
61	NC	DOTAP: DOPE: Vit E	16.8: 49.3: 33.8	6.7: 1	SPM	0.44: 1
62	NC	DOTAP: DOPE: Vit E	16.8: 49.3: 33.8	6.7: 1	SPM	0.66: 1
63	NE	DOTAP: Vit E: T80	18.8: 75.8: 5.4	6.7: 1		
64	NE	DOTAP: Vit E: T80	27: 63.9: 9	6.7: 1		
65	NE	DOTAP: DOPE: Vit E: T80	33.1: 9.1: 52.2: 5.5	6.7:1		
66	NE	DOTAP: DOPE: Vit E: T80	30.1: 12.1: 50.5: 7.3	6.7: 1		
67	NE	DOTAP: DOPE: Vit E: T80	35.9: 9.9: 51.2: 3	6.7: 1		
68	NE	DOTAP: DOPE: Vit E: T80	32.4: 15.2: 51.5: 0.9	6.7: 1		
69	NE	DOTAP: DOPE: Vit E: T80	50: 10: 38.5: 1.5	6.7: 1		
70	NE	DOTAP: DOPE: Vit E: T80	50: 10: 38.5: 1.5	1.1: 1		
71	NE	DOTAP: DOPE: Vit E: T80	29.9: 8.8: 53: 8.3	1.1:1		

Abbreviations: DEAEDX: DEAE-dextran hydrochloride. DOPE: 1,2-dioleoyl-sn-glycero-3-phosphoethanolamine. DOTAP: 1,2-dioleoyl-3-trimethylammonium propane. K-HS15: Kolliphor® HS15. NC: nanocapsule. NE: nanoemulsion. PARG: poly-L-arginine. PRT: protamine sulphate EP. SG: sodium glycocholate. SPM: spermine. T80: Tween 80. Vit E: D, L-α-tocopherol. v/v ratio: volume-to-volume ratio between aqueous and organic phases. w/w ratio: weight-to-weight ratio between polymer and mRNA content.

Table 3. Summary of nanocarriers developed during this project that failed to fulfill the target product profile (continuation)

#	Nanosystem	Composition	Molar ratio (%)	v/v ratio	Polymer	w/w ratio
72	NC	DOTAP: DOPE: Vit E: T80	38.1: 10.5: 45.1: 6.4	6.7: 1	PRT	0.5: 1
73	NC	DOTAP: DOPE: Vit E: T80	38.1: 10.5: 45.1: 6.4	6.7: 1	SPM	0.44: 1
74	NC	DOTAP: DOPE: Vit E: T80	38.1: 10.5: 45.1: 6.4	6.7: 1	DEAEDX	1: 0.5
75	NC	DOTAP: DOPE: Vit E: T80	38.1: 10.5: 45.1: 6.4	6.7: 1	PARG	0.5: 1
76	NC	DOTAP: DOPE: Vit E: T80	38.1: 10.5: 45.1: 6.4	6.7: 1	CS	0.5: 1
77	NC	DOTAP: DOPE: Vit E: T80	38.1: 10.5: 45.1: 6.4	6.7: 1	CS	2: 1
78	NC	DOTAP: DOPE: Vit E: T80	38.1: 10.5: 45.1: 6.4	6.7: 1	CS	4: 1
79	NC	DOTAP: DOPE: Vit E: T80	17.3: 8.1: 69.7: 4.9	6.7: 1	CS	0.5: 1
80	NC	DOTAP: DOPE: Vit E: T80	17.3: 8.1: 69.7: 4.9	6.7: 1	CS	2: 1
81	NC	DOTAP: DOPE: Vit E: T80	17.3: 8.1: 69.7: 4.9	6.7: 1	CS	4: 1
82	NC	DOTAP: DOPE: Vit E: T80	50: 10: 38.5: 1.5	6.7: 1	DX	4: 1
83	NC	DOTAP: DOPE: Vit E: T80	46.2: 9: 35.6: 9.3	5: 1	DX	4: 1
84	NC	DOTAP: DOPE: Vit E: T80	46.2: 9: 35.6: 9.3	5: 1	PEG-PGA	2: 1
85	NC	DOTAP: DOPE: Vit E: T80	46.2: 9: 35.6: 9.3	5: 1	PEG-PGA	4: 1
86	NC	DOTAP: DOPE: Vit E: T80	46.2: 9: 35.6: 9.3	5: 1	PEG-PGA	8: 1
87	NC	DOTAP: DOPE: Vit E: T80	46.2: 9: 35.6: 9.3	5: 1	PEG-PGA	16: 1

Abbreviations: CS: chitosan. DEAEDX: DEAE-dextran hydrochloride. DOPE: 1,2-dioleoyl-sn-glycero-3-phosphoethanolamine. DOTAP: 1,2-dioleoyl-3-trimethylammonium propane. DX: dextran sulfate. NC: nanocapsule. PARG: poly-L-arginine. PEG-PGA: PEG (5 kDa)-b-PGA (10) (Na). PRT: protamine sulphate EP. SPM: spermine. T80: Tween 80. Vit E: D, L-α-tocopherol. v/v ratio: volume-to-volume ratio between aqueous and organic phases. w/w ratio: weight-to-weight ratio between polymer and mRNA content.

Regarding the physicochemical properties aligning with the TPP, several NEs and NCs met the specified requirements. As indicated in Table 4, these selected NEs consisted of a cationic lipid (DOTAP), a helper lipid (DOPE), and an oil (Vitamin E), with or without the short-PEGylated lipid Tween 80. These different lipid components were combined in varying proportions to evaluate their impact on mRNA encapsulation efficiency, particle diameter, colloidal stability, or transfection efficiency.

Table 4. Summary of the lipid compositions and molar ratios between the different components of the nanoemulsions investigated

Nanosystem	Lipid composition	Molar composition (%)
NE-1	DOTAP: DOPE: Vit E	16.8: 15.7: 67.5
NE-2	DOTAP: DOPE: Vit E	40.7: 11.2: 48.1
NE-3	DOTAP: DOPE: Vit E: Tween 80	38.1: 10.5: 45.1: 6.4
NE-4	DOTAP: DOPE: Vit E: Tween 80	17.3: 8.1: 69.7: 4.9
NE-5	DOTAP: DOPE: Vit E: T80	46.2: 9: 35.6: 9.3

Abbreviations: DOPE: 1,2-dioleoyl-sn-glycero-3-phosphoethanolamine. DOTAP: 1,2-dioleoyl-3-trimethylammonium propane. NE: nanoemulsion. Vit E: D, L-α-tocopherol.

Following mRNA entrapment, these NEs were used for the development of NC-mRNA, by adding a polymeric layer over the pre-formed NE-mRNA nanocarriers. The nomenclature for the resulting NC-mRNAs was derived from the initial NE name code, for easy identification. As detailed in Table 5, different polymers were explored, including protamine (PR), dextran sulfate (DX), chitosan (CS), and PEG-PGA (PP), aiming to modify the surface of the nanocarriers and enhance their immunogenic properties. All four polymers have previously been used as adjuvant and antigen delivery systems, capable of activating different T and B cell responses [25–29].

Table 5. Summary of the lipid and polymer compositions, and the molar and weight-to-weight ratio between the different components of the nanocapsules investigated

Nanosystem	Initial NE composition	Molar composition (%)	Polymer coating	w/w ratio
NC-1-PR	DOTAP: DOPE: Vit E	16.8: 15.7: 67.5	Protamine	1: 1
NC-3-PR	DOTAP: DOPE: Vit E: Tween 80	38.1: 10.5: 45.1: 6.4	Protamine	1: 1
NC-4-PR	DOTAP: DOPE: Vit E: Tween 80	17.3: 8.1: 69.7: 4.9	Protamine	1: 1
NC-3-DX	DOTAP: DOPE: Vit E: Tween 80	38.1: 10.5: 45.1: 6.4	Dextran Sulfate	1: 1
NC-4-DX	DOTAP: DOPE: Vit E: Tween 80	17.3: 8.1: 69.7: 4.9	Dextran Sulfate	1: 1 or 2: 1
NC-5-DX	DOTAP: DOPE: Vit E: Tween 80	46.2: 9: 35.6: 9.3	Dextran Sulfate	2: 1
NC-3-CS	DOTAP: DOPE: Vit E: Tween 80	38.1: 10.5: 45.1: 6.4	Chitosan	1: 1
NC-4-CS	DOTAP: DOPE: Vit E: Tween 80	17.3: 8.1: 69.7: 4.9	Chitosan	1: 1
NC-4-PP	DOTAP: DOPE: Vit E: Tween 80	17.3: 8.1: 69.7: 4.9	PEG-PGA	12: 1
NC-5-PP	DOTAP: DOPE: Vit E: Tween 80	46.2: 9: 35.6: 9.3	PEG-PGA	12: 1

Abbreviations: CS: chitosan. DOPE: 1,2-dioleoyl-sn-glycero-3-phosphoethanolamine. DOTAP: 1,2-dioleoyl-3-trimethylammonium propane. DX: dextran sulfate. NC: nanocapsule. PEG-PGA or PP: PEG (5 kDa)-b-PGA (10) (Na). PRT: protamine sulphate EP. Vit E: D, L-α-tocopherol. w/w ratio: weight-to-weight ratio between polymer and mRNA content.

3.1.1. Preparation and optimization of mRNA-loaded nanoemulsions

NE-mRNA nanocarriers were prepared using two distinct strategies. In the first approach, blank NEs were prepared through the solvent-displacement technique, resulting in nanoparticles with a size diameter ranging from 100 to 130 nm and a highly positive surface charge (Table 6). In the case of NE-4, organic solvents were removed by evaporation under vacuum, which did not affect its physicochemical properties. Subsequently, mRNA was

complexed over the blank NEs through electrostatic interactions between the positively charged cationic lipid and the negatively charged oligonucleotide.

Table 6. Physicochemical properties of blank NEs

Nanosystem	Particle diameter (nm)	PDI	ζ-Potential (mV)
NE-1 (n = 2)	132 ± 1	0.14 ± 0.01	+54 ± 3
NE-2 (n = 2)	101 ± 5	0.38 ± 0.01	+59 ± 1
NE-3	102 ± 13	0.40 ± 0.05	+56 ± 5
NE-4	104 ± 15	0.30 ± 0.04	+55 ± 2
$NE\text{-}4_{evaporated}$	93 ± 10	0.27 ± 0.03	+55 ± 3

Abbreviations: NE: nanoemulsion. PDI: polydispersity index. Values represent the mean ± standard deviation (n ≥ 3, unless indicated otherwise).

Table 7. Physicochemical properties of NE-1, NE-2, NE-3, NE-4, and NE-5 using different types of mRNAs and different N/P ratios

Nanosystem	mRNA	N/P ratio	Particle diameter (nm)	PDI	ζ-Potential (mV)	EE (%)
NE-1 (n = 2)	mGFP	0.64	152 ± 19	0.04 ± 0.01	-9 ± 1	50
NE-2 (n = 1)	mGFP	2	108	0.17	+40	100
NE-3	mGFP	0.9	122 ± 12	0.13 ± 0.02	-12 ± 6	50
NE-3	mGFP	2	108 ± 13	0.14 ± 0.03	+39 ± 2	100
NE-3 (n = 1)	mLuc	0.9	127	0.15	-17	70
NE-3 (n = 2)	mLuc	2	112 ± 16	0.17 ± 0.01	+35 ± 6	100
NE-3 (n = 1)	mOVA	2	99	0.16	+45	100
NE-4 (n = 2)	mGFP	0.9	128 ± 2	0.13 ± 0.04	-10 ± 1	50
NE-4	mGFP	2	127 ± 13	0.09 ± 0.03	+43 ± 4	100
NE-4	mLuc	2	138 ± 18	0.14 ± 0.06	+42 ± 2	100
NE-4 (n = 2)	mOVA	2	121 ± 9	0.10 ± 0.01	+40 ± 3	100
NE-4 (n = 2)	mLuc	4	89 ± 2	0.21 ± 0.02	+48 ± 6	100
NE-4	mT	4	108 ± 14	0.19 ± 0.03	+43 ± 3	100
NE-4	mB	4	111 ± 13	0.2 ± 0.03	+43 ± 2	100
NE-4	mRBD	4	105 ± 11	0.2 ± 0.01	+48 ± 3	100
NE-4	$mRBD_{epi}$	4	110 ± 8	0.19 ± 0.01	+49 ± 3	100
$NE\text{-}4_{microfluid}$	mLuc	4	84 ± 11	0.21 ± 0.02	+54 ± 3	100
$NE\text{-}4_{microfluid}$	mRBD	4	73 ± 13	0.23 ± 0.02	+46 ± 4	100
$NE\text{-}5_{microfluid}$ (n = 2)	mGFP	4	62 ± 13	0.24 ± 0.07	+53 ± 7	-
$NE\text{-}5_{microfluid}$ (n = 1)	mLuc	4	71	0.15	+50	100
$NE\text{-}5_{microfluid}$	mRBD	4	63 ± 3	0.23 ± 0.05	+56 ± 15	100
$NE\text{-}5_{microfluid}$ (n = 1)	$mRBD_{epi}$	4	90	0.26	+45	-

Abbreviations: EE: encapsulation efficiency. mB: SARS-CoV-2-B cells mRNA. mGFP: mRNA encoding GFP. mLuc: mRNA encoding luciferase. mOVA: mRNA encoding ovalbumin protein. mRBD: SARS-CoV-2-RBD mRNA. $mRBD_{epi}$: SARS-CoV-2-RBD_{epi}. mT: SARS-CoV-2-T cells mRNA. NE: nanoemulsion. N/P ratio: nitrogen to phosphate ratio. PDI: polydispersity index. Values represent the mean ± standard deviation (n ≥ 3, unless indicated otherwise).

On the other hand, a second strategy involved a single-step microfluidic mixing of both aqueous and organic phases, leading to the simultaneous complexation of the mRNA and the formation of NE-mRNA nanosystems. This preparation technique led to the formation of nanostructures with a smaller particle size (60-100 nm) than the simple mixing of components (100-150 nm) (Table 7). These variations suggested potential changes in the internal structure of the NEs and the organization of the mRNA molecules.

Furthermore, the incorporation of negatively charged mRNA onto the surface of the previously formed blank NEs led to alterations in the physicochemical properties, mainly evident by the reduction of the positive charge of the resulting NE-mRNAs. These surface changes were dependent on the N/P ratio used, resulting in slightly negative NE-mRNAs at low N/P ratios, and highly positive NE-mRNAs at high N/P ratios. The importance of the N/P ratio used was also highlighted on the EE%, with higher values obtained at a higher N/P ratio (Figure 2). Additionally, different types of mRNA exhibited different particle diameters and polydispersity indexes, indicating differences in the interaction between the cationic DOTAP and the specific types of mRNA.

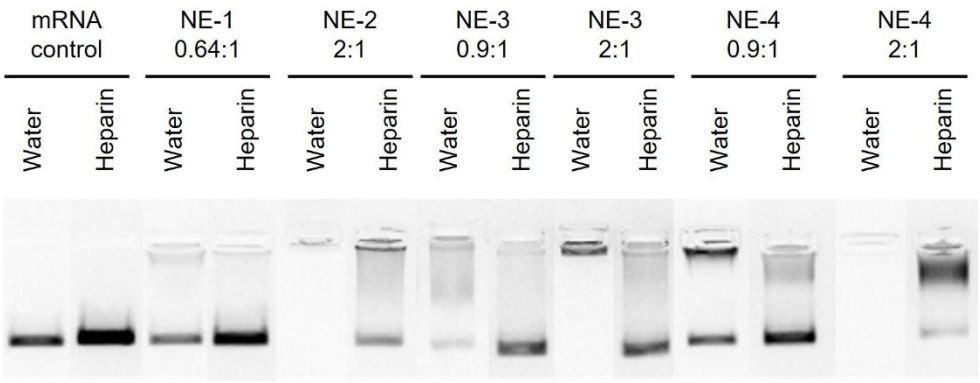

Figure 2. Encapsulation efficiency of mGFP-loaded NE-1, NE-2, NE-3, and NE-4, at different N/P ratios. Samples were treated with heparin for mGFP displacement

Abbreviations: NE: nanoemulsion.

Various N/P ratios were explored for some of the formulations, including NE-3 and NE-4, using a model transfer RNA (tRNA). As depicted in Figure 3, both NE-tRNAs present a shift in surface charge from 0.9:1 to 1.1: ratios, transitioning from a negative to a positive surface charge. In the case of NE-3-tRNA (Figure 3, top left), neutrality was achieved at 0.9:1 ratio, resulting in a significant increase in the particle size. This behavior, however, was not observed in NE-4-tRNA (Figure 3, top right), where the transition from a negative to a positive surface charge did not lead to neutral charges at the explored N/P ratio. Furthermore, encapsulation efficiency was assessed using agarose gel electrophoresis, suggesting complete complexation of the tRNA from ratios 0.9:1 for NE-3-tRNA (Figure 3, bottom left), and 0.8:1 for NE-4-tRNA (Figure 3, bottom right).

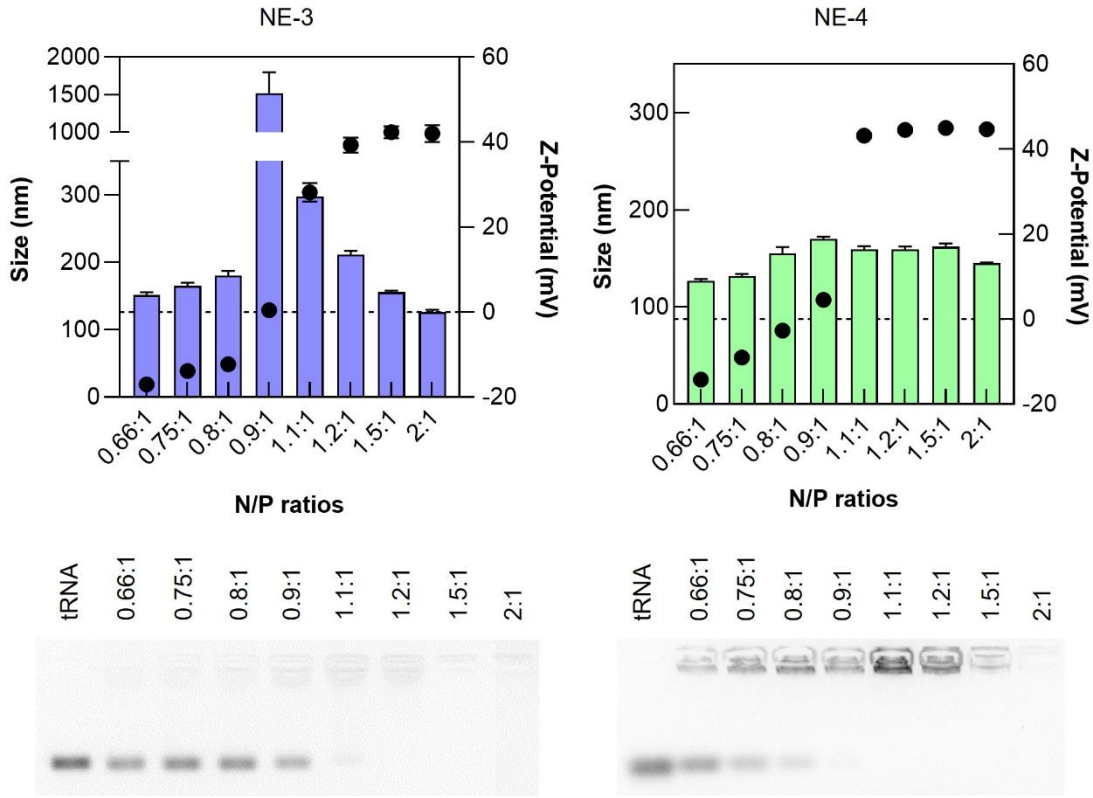

Figure 3. Physicochemical properties (top) and encapsulation efficiency (bottom) of NE-3-tRNA and NE-4 tRNA (left and right figures, respectively), at different N/P ratios between DOTAP and tRNA. Particle size corresponds with the left axis (bars), while surface charge corresponds with the right axis (dots)

Abbreviations: NE: nanoemulsion. N/P ratio: nitrogen to phosphate ratio. tRNA: transfer RNA.

3.1.2. Preparation and optimization of mRNA-loaded nanocapsules

The resulting NE-mRNAs were subsequently coated with various polymers to form a polymer shell that would modulate the surface properties of the resulting NC-mRNAs (Table 8). Different w/w ratios between the polymer and the mRNA were determined for each NC-mRNA, based on the amount of polymer required to modify the surface properties effectively while preserving particle stability. In all nanocarriers, particle diameter increased after polymer attachment compared with the initial NE-mRNA used. The final surface charge was aligned with the ionizable groups of the polymer backbone. To facilitate the attachment of the polymer shell onto the surface of the NEs, an adjustment of the N/P ratios of the NE-mRNAs was made. Consequently, all NC-PR-mRNA and NC-CS nanocarriers were prepared at a N/P ratios 0.64: 1 or 0.9: 1.

Overall, the particle diameters observed in the NC-mRNAs ranged from 100 to 235 nm, primarily dependent on the method used for the initial preparation of NE-mRNA. Significant differences were observed for various mRNA molecules.

Table 8. Physicochemical properties of NC-mRNA-PR, NC-mRNA-DX, NC-mRNA-CS, and NC-mRNA-PP using different NE-mRNAs, types of mRNAs, and w/w ratios

Nanosystem	mRNA	w/w ratio	Particle diameter (nm)	PDI	ζ-Potential (mV)	EE (%)
NC-1-PR (n =1)	mGFP	1: 1	168	0.09	+26	100
NC-3-PR	mGFP	1: 1	152 ± 9	0.12 ± 0.01	+24 ± 1	100
NC-3-PR (n =1)	mLuc	1: 1	179	0.16	+24	100
NC-4-PR	mGFP	1: 1	153 ± 16	0.11 ± 0.03	+27 ± 2	75
NC-4-PR (n = 1)	mLuc	1: 1	224	0.12	+22	100
NC-3-DX (n = 1)	mGFP	1: 1	144	0.09	-26	100
NC-4-DX (n = 1)	mGFP	1: 1	148	0.07	-14	90
NC-4-DX (n = 1)	mGFP	2: 1	113	0.09	-18	100
NC-4-DX	mLuc	1: 1	154 ± 8	0.14 ± 0.04	-14 ± 1	100
NC-4-DX	mLuc	2: 1	126 ± 3	0.11 ± 0.02	-21 ± 2	100
NC-4-DX	mOVA	2: 1	132 ± 3	0.07 ± 0.03	-16 ± 2	100
NC-4-DX	mT	2: 1	111 ± 6	0.09 ± 0.02	-15 ± 5	100
NC-4-DX	mB	2: 1	114 ± 5	0.1 ± 0.02	-13 ± 5	100
NC-4-DX	mRBD	2: 1	109 ± 6	0.11 ± 0.01	-18 ± 2	90
NC-4-DX	$mRBD_{epi}$	2: 1	113 ± 6	0.09 ± 0.01	-19 ± 3	90
NC-4-DX	mT + mB	2: 1	113 ± 3	0.10 ± 0.02	-13 ± 4	100
NC-4-DX (n = 2)	mT + mRBD	2: 1	105 ± 1	0.09 ± 0.01	-19 ± 4	90
NC-4-DX (n = 2)	mT + $mRBD_{epi}$	2: 1	106 ± 1	0.10 ± 0.01	-17 ± 4	90
$NC\text{-}4\text{-}DX_{microfluid}$ (n = 1)	mLuc	2: 1	101	0.07	-35	100
$NC\text{-}4\text{-}DX_{microfluid}$	mRBD	2:1	105 ± 5	0.12 ± 0.01	-6 ± 10	100
$NC\text{-}5\text{-}DX_{microfluid}$ (n = 2)	mGFP	2: 1	93 ± 9	0.2 ± 0.01	-6 ± 7	-
$NC\text{-}5\text{-}DX_{microfluid}$ (n = 1)	$mRBD_{epi}$	2: 2	112	0.18	-26	-
NC-3-CS (n = 1)	mGFP	1: 1	188	0.19	+30	100
NC-4-CS (n = 1)	mGFP	1: 1	167	0.15	+29	100
NC-4-CS (n = 2)	mLuc	1: 1	234 ± 31	0.22 ± 0.07	+31 ± 5	100
$NC\text{-}4\text{-}PP_{microfluid}$ (n = 1)	mLuc	12: 1	89	0.21	+16	-
$NC\text{-}4\text{-}PP_{microfluid}$	mRBD	12: 1	80 ± 20	0.21 ± 0.02	+19 ± 4	100
$NC\text{-}5\text{-}PP_{microfluid}$ (n = 2)	mGFP	12: 1	70 ± 1	0.17 ± 0.01	+13 ± 5	-
$NC\text{-}5\text{-}PP_{microfluid}$ (n = 1)	mLuc	12: 1	81	0.17	+13	-
$NC\text{-}5\text{-}PP_{microfluid}$	mRBD	12: 1	74 ± 6	0.17 ± 0.02	+14 ± 2	100

Abbreviations: CS: chitosan. DX: dextran sulfate. EE: encapsulation efficiency. mB: SARS-CoV-2-B cells mRNA. mGFP: mRNA encoding GFP. mLuc: mRNA encoding luciferase. mOVA: mRNA encoding ovalbumin protein. mRBD: SARS-CoV-2-RBD mRNA. $mRBD_{epi}$: SARS-CoV-2-RBD_{epi}. mT: SARS-CoV-2-T cells mRNA. NC: nanocapsule. PDI: polydispersity index. PEG-PGA or PP: PEG (5 kDa)-b-PGA (10) (Na). PR: protamine sulphate EP. w/w ratio: weight-to-weight ratio between polymer and mRNA content. Values represent the mean ± standard deviation (n ≥ 3, unless indicated otherwise).

Furthermore, EE% was determined using agarose gel electrophoresis (Figure 4, top), revealing that most NC-mRNA were capable of fully complexing the oligonucleotides. However, the mRNA displacement by heparin was dependent on the type of NE and polymer used, suggesting that different interactions between RNA and the polymer shell varied across different formulations. For example, heparin was unable to displace the mRNA when chitosan shells were used (namely, in the case of NC-3-CS and NC-4-CS), suggesting a strong interaction between the polymeric NC and the mRNA cargo. In the case of dextran sulfate, heparin was capable of fully displacing mRNA in NC-3-DX, whereas no displacement was found in NC-4-DX, despite using the same polymer in the coating shell. This indicates that the composition of the oily core also mediates the interactions and release of the mRNA.

Additionally, EE% was determined for NC-4-DX in combination with the different SARS-CoV-2 mRNAs developed (Figure 4, bottom). Full complexation of mRNA was achieved for mT and mB, while some free mRNA was observed in the case of mRBD and $mRBD_{epi}$. Similar behaviors were noted after combining NC-4-DX-mT with NC-4-DX-mB, -mRBD, and -$mRBD_{epi}$. A possible explanation for this behavior could be the chemical modifications applied to the SARS-CoV-2 constructs as well as the differences in length of the different sequences, as they encode for different proteins. This hypothesis needs to be further confirmed.

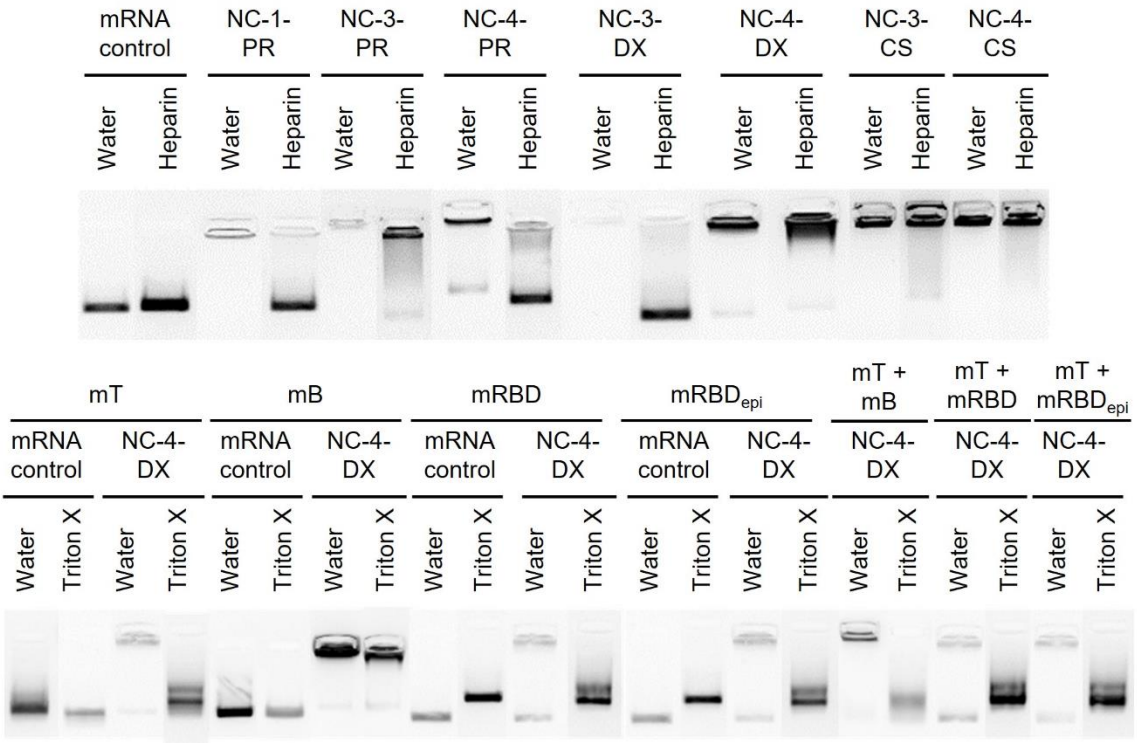

Figure 4. Encapsulation efficiency of mGFP-loaded NCs (top) and mB-, mT-, mRBD-, $mRBD_{epi}$-loaded NCs (bottom). Samples were treated with heparin for mGFP displacement (top) and Triton X for NC disruption (bottom)

Abbreviations: CS: chitosan. DX: dextran sulfate. mB: SARS-CoV-2-B cells mRNA. mGFP: mRNA encoding GFP. mRBD: SARS-CoV-2-RBD mRNA. $mRBD_{epi}$: SARS-CoV-2-RBD_{epi}. mT: SARS-CoV-2-T cells mRNA. NC: nanocapsule. PR: protamine sulphate EP.

For specific NC-mRNA nanocarriers, selected based on their promising *in vitro* performance, the ratio between the polymer and the RNA content was optimized. In the case of NC-3-DX and NC-4-DX, this optimization was performed using tRNA, exploring w/w ratios between DX and tRNA (Figure 5). Overall, no differences were found in terms of particle diameter at the different w/w ratios used for both NC-tRNA-DX, except for a small reduction in size when ratio 4:1 was used in NC-3-DX. However, a significant reduction in the surface charge, moving from positive to negative values, was observed with increasing w/w ratios between the polymer and the tRNA (Figure 5, top). In terms of EE%, no changes were observed (Figure 5, bottom), as all tRNA content was completely adsorbed onto the surface of the nanocarrier before coating with the polymer.

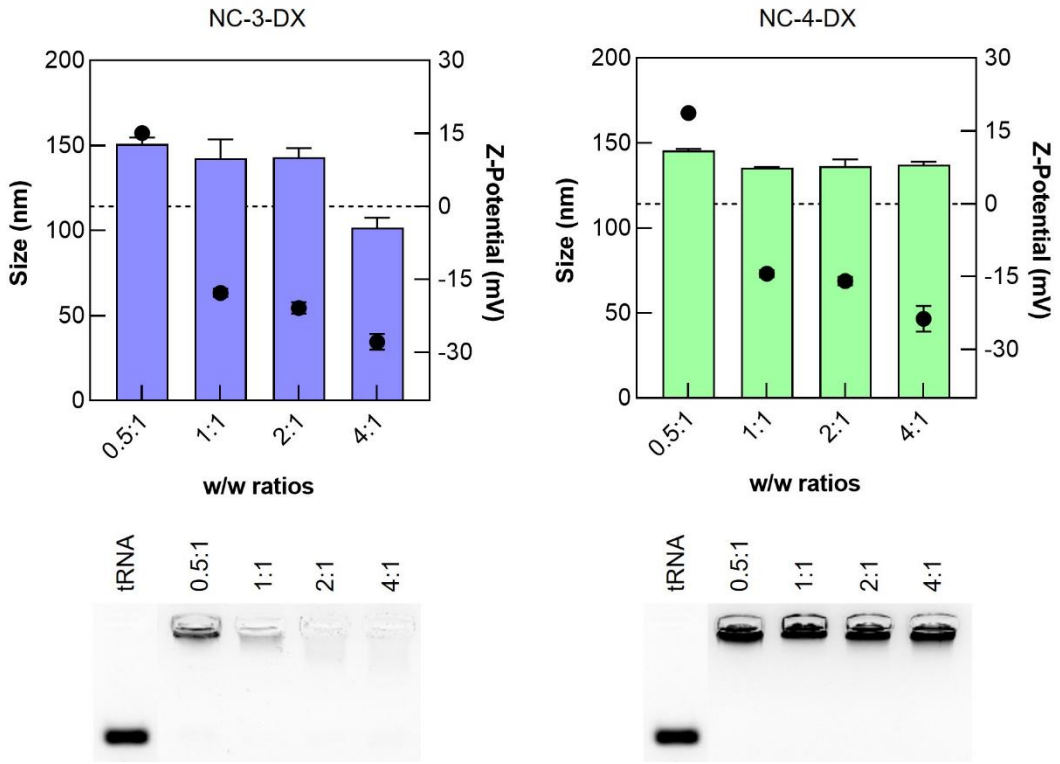

Figure 5. Physicochemical properties (top) and encapsulation efficiency (bottom) of NC-3-DX-tRNA and NC-4-DX-tRNA (left and right figures, respectively), at different w/w ratios between the DX shell and the tRNA. Particle size corresponds with the left axis (bars), while surface charge corresponds with the right axis (dots)

Abbreviations: DX: dextran sulfate. NC: nanocapsule. tRNA: transfer RNA. w/w ratio: weight-to-weight ratio between the polymer and tRNA content.

Certain NE-mRNA and NC-mRNA nanocarriers were freeze-dried to enhance the long-term stability of the different mRNA formulations (Supplementary Table 1). Various cryoprotectants were screened, including trehalose, sucrose, and glucose, to identify suitable conditions to ensure that the physicochemical characteristics of the formulations remained unaltered upon reconstitution of the free-dried powder. Interestingly, differences in the required cryoprotectant were found between different formulations, and even within the same nanocarrier when different types of mRNA were used.

3.2. IN VITRO SCREENING OF NANOEMULSIONS AND NANOCAPSULES

Before administering the nanocarriers in animals, NE-mRNAs and NC-mRNAs formulations were studied *in vitro* in different cell lines, assessing their toxicity and transfection potency.

3.2.1. Cytotoxicity and transfection efficiency in HeLa cells using mGFP

HeLa cells were selected as a model for easy transfection and evaluation of cellular toxicity. These cells have also been used in various vaccine studies in the literature [30,31]. Different NE-mGFP and NC-mGFP were incubated with HeLa cells for 4 hours, and toxicity and fluorescence transfection were assessed 24 hours after treatment.

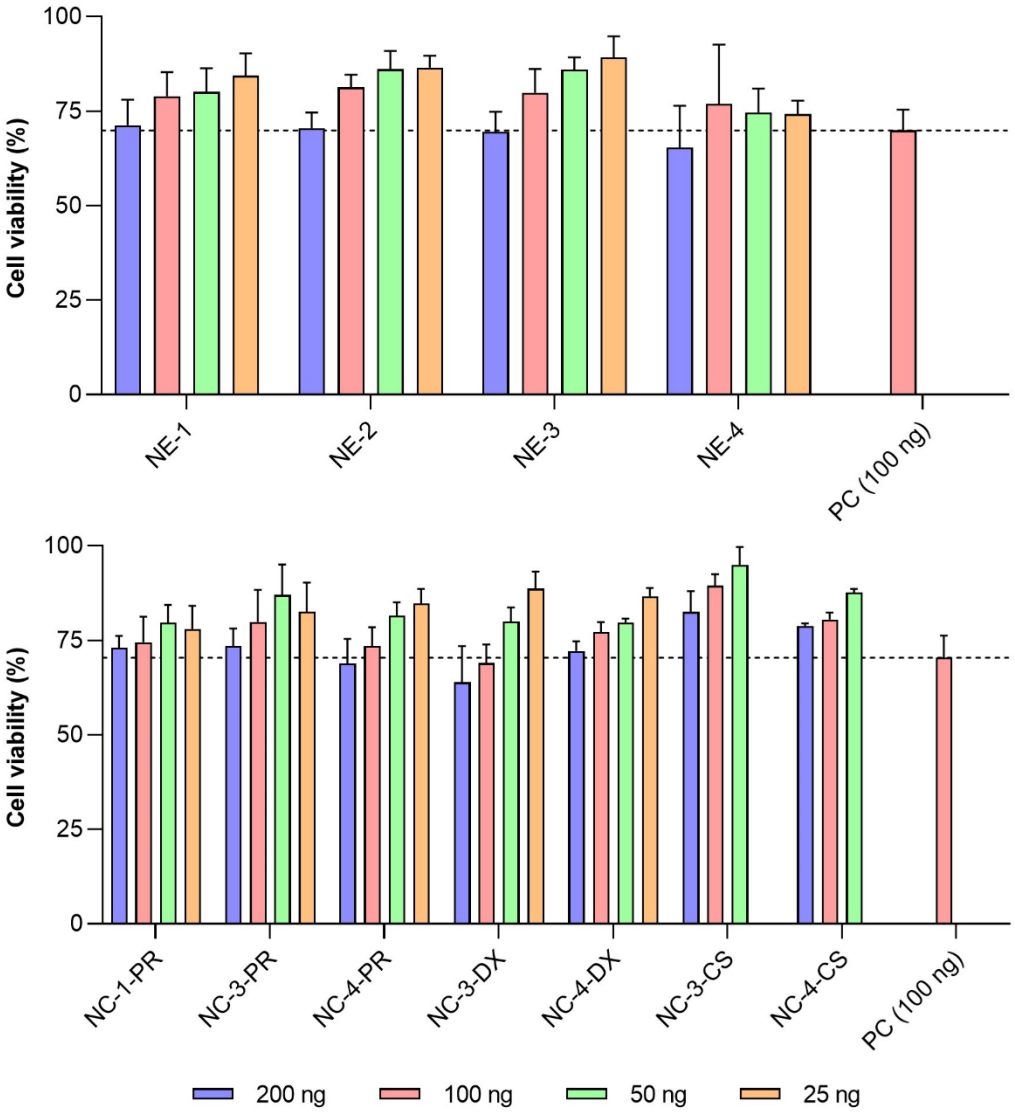

Figure 6. Cytotoxicity of NE-mGFP (top) and NC-mGFP (bottom), at different mGFP concentrations, in HeLa cells at 24 hours post-transfection

Abbreviations: CS: chitosan. DX: dextran sulfate. mGFP: mRNA encoding GFP. NE: nanoemulsion. NC: nanocapsule. PC: positive control, lipofectamine. PR: protamine sulphate EP. Values represent the mean ± standard deviation (n ≥ 3).

The results depicted in Figure 6 show minor concentration-dependent toxicity, reaching a maximum reduction in viability of 25% at the highest doses investigated (200 and 100 ng of mGFP). Interestingly, no significant differences in cell viability were found between the different NE-mGFP or NC-mGFP. However, NC-mGFP presented slightly overall lower toxicity than NE-mGFP (e.g. NC-4-PR-mGFP, NC-4-DX-mGFP, and NC-4-CS-mGFP presented better cell viability profile than NE-4-mGFP). These findings suggest that the polymer shell contributes to reducing the overall high surface charge of the NE-mGPF and that NC-mGFP with low positive or negative surface charges leads to better cell viability profiles.

To assess transfection efficiency, two measurements were considered: the percentage of GFP-positive cells, which determines the percentage of cells able to express the GFP, and mean fluorescence intensity (MFI), which evaluates the amount of fluorescence produced for those cells. Overall, NE-mGFP formulations (Figure 7, top) resulted in a higher percentage of GFP-positive cells and MFI than NC-mGFP formulations (Figure 7, bottom), regardless of the polymeric layer present on the NC-mGFP. In all cases, a significant dose-dependent transfection efficiency was found. Among the different NE-mRNAs, NE-3-mGFP and NE-4-mGFP showed the highest transfection efficiency, possibly due to the presence of Tween 80 in their composition, which can enhance the transfection potency of lipidic nanocarriers in cell studies [32].

Regarding NC-mGFP formulations, differences were observed, mainly between NC-mGFP formulations using the same NE-mGFP. For example, both NC-3-PR-mGFP and NC-3-CS-mGFP elicited better percentages of GFP-positive cells than NC-3-DX-mGFP. Moreover, notable differences among formulations using the same polymer were observed, as in the case of NC-4-DX-mGFP, which significantly exceeded the transfection efficiency of NC-3-DX-mGFP, while both of them used DX as the polymeric shell. These differences between systems were not observed when NE-3-mGFP and NE-4-mGFP were compared, suggesting that the polymeric shell can further modulate the transfection efficiency of the nanocarriers. Overall, among all the different NC-mGFP nanosystems tested, NC-4-DX-mGFP was the most efficient delivery system in terms of transfection potency.

Specific formulations, all of them prepared by microfluidic mixing, were tested in HeLa cells using a greater number of cells in 24-well plates. This would allow for testing greater concentration of the nanosystems, namely NE-5-mGFP, NC-5-DX-mGFP, and NC-5-PP-mGFP (Supplementary Figure 1). Considering the poor transfection efficiency depicted by NE-5-mGFP, it was no surprise that NC-5-mGFP derived from it would also lead to percentages of GFP-positive cells lower than 50%. However, lipofectamine control also depicted a low transfection efficiency, suggesting a possible underestimation of the results.

Selected formulations were exposed to FBS (to mimic the physiological environment in the human body) and RNase (to assess mRNA cargo protection against this enzyme), before their incubation with HeLa cells (Supplementary Figure 2). In terms of cell viability, no significant differences were observed compared to formulations not exposed to FBS or RNase. However, the transfection efficiency of NE-3-mGFP and NC-3-PR-mGFP was reduced when exposed to RNase, suggesting deficient protection of the cargo towards degradation.

Finally, some of the formulations subjected to freeze-drying were tested *in vitro* after their resuspension (Supplementary Figure 3). The sample preservation process did not impact the nanocarriers in terms of cellular cytotoxicity and transfection efficiency, confirming the potential for long-term stability of these nanosystems without reduction of their effectiveness.

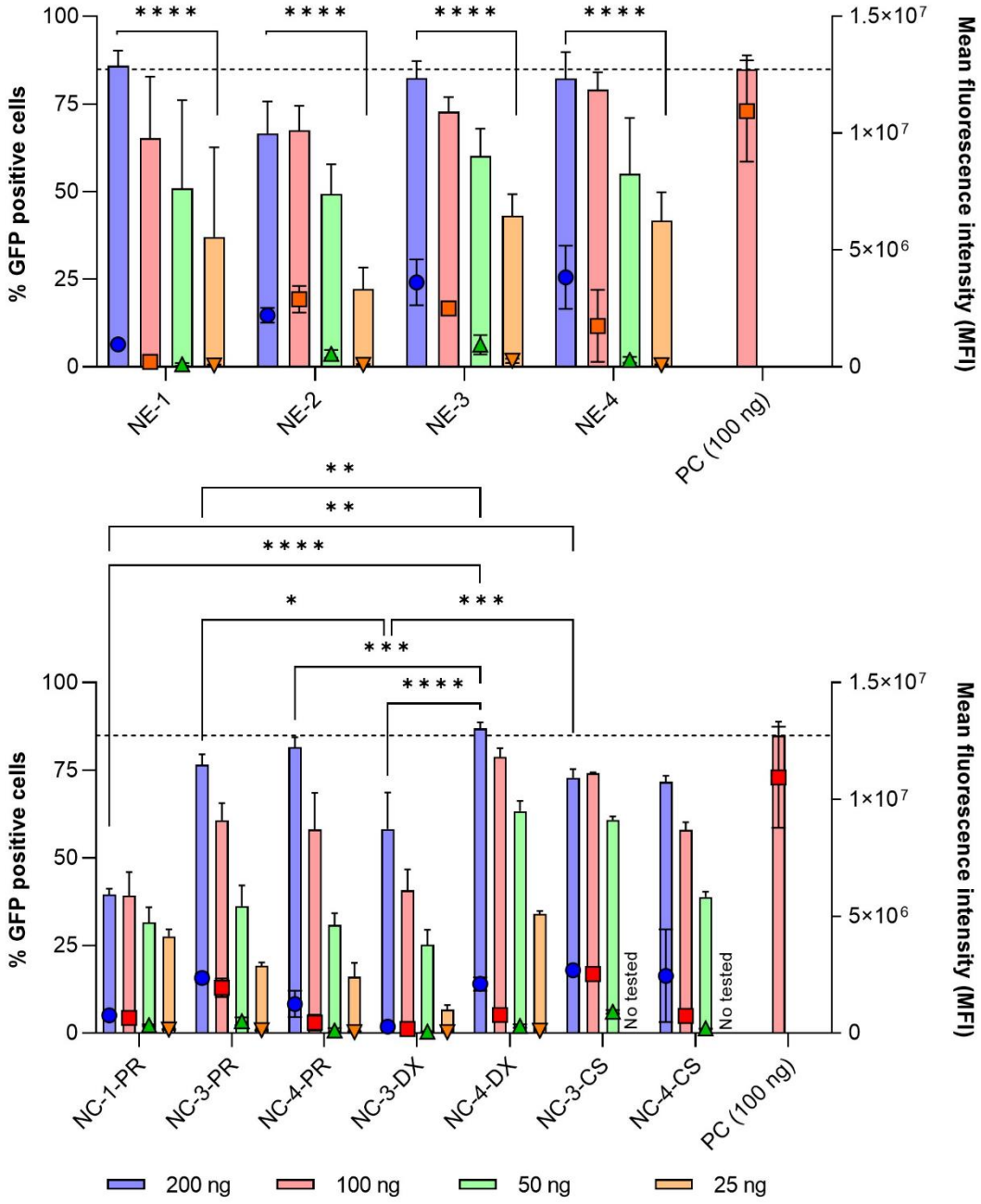

Figure 7. GFP transfection efficiency of NE-mGFP (top) and NC-mGFP (bottom) nanocarriers, at different mGFP concentrations. Percentage of GFP positive cells (left axis) and mean fluorescence intensity (right axis) in HeLa cells, 24 hours post-transfection

Abbreviations: CS: chitosan. DX: dextran sulfate. mGFP: mRNA encoding GFP. NE: nanoemulsion. NC: nanocapsule. PC: positive control, lipofectamine. PR: protamine sulphate EP. A significant comparison was performed using two-way ANOVA followed by Tukey's multiple comparison tests between the highest concentration and lower concentration (top) and between the highest concentration of each group. *p*-values < 0.05 were considered statistically significant (*). Also, (**) if *p*-value < 0.01, (***) if *p*-value < 0.001, and (****) if *p*-value < 0.0001. Values represent the mean ± standard deviation (n ≥ 3).

3.2.2. Cytotoxicity and transfection efficiency in human dendritic cells using mRBD

Based on the *in vitro* results, NE-4, NC-4-PP, and NC-5-PP containing mRBD were selected to be evaluated in human dendritic cells (hDCs), as a representative model for studying DC activation after *in vivo* administration [33]. Cell viability and percentage of cells expressing RBD were analyzed at 6 and 24 hours after treatment with the selected formulations (Figure 8). In terms of cell viability, only the lowest RNA concentration (3 µg) exhibited minor levels of cell toxicity (Figure 8, top).

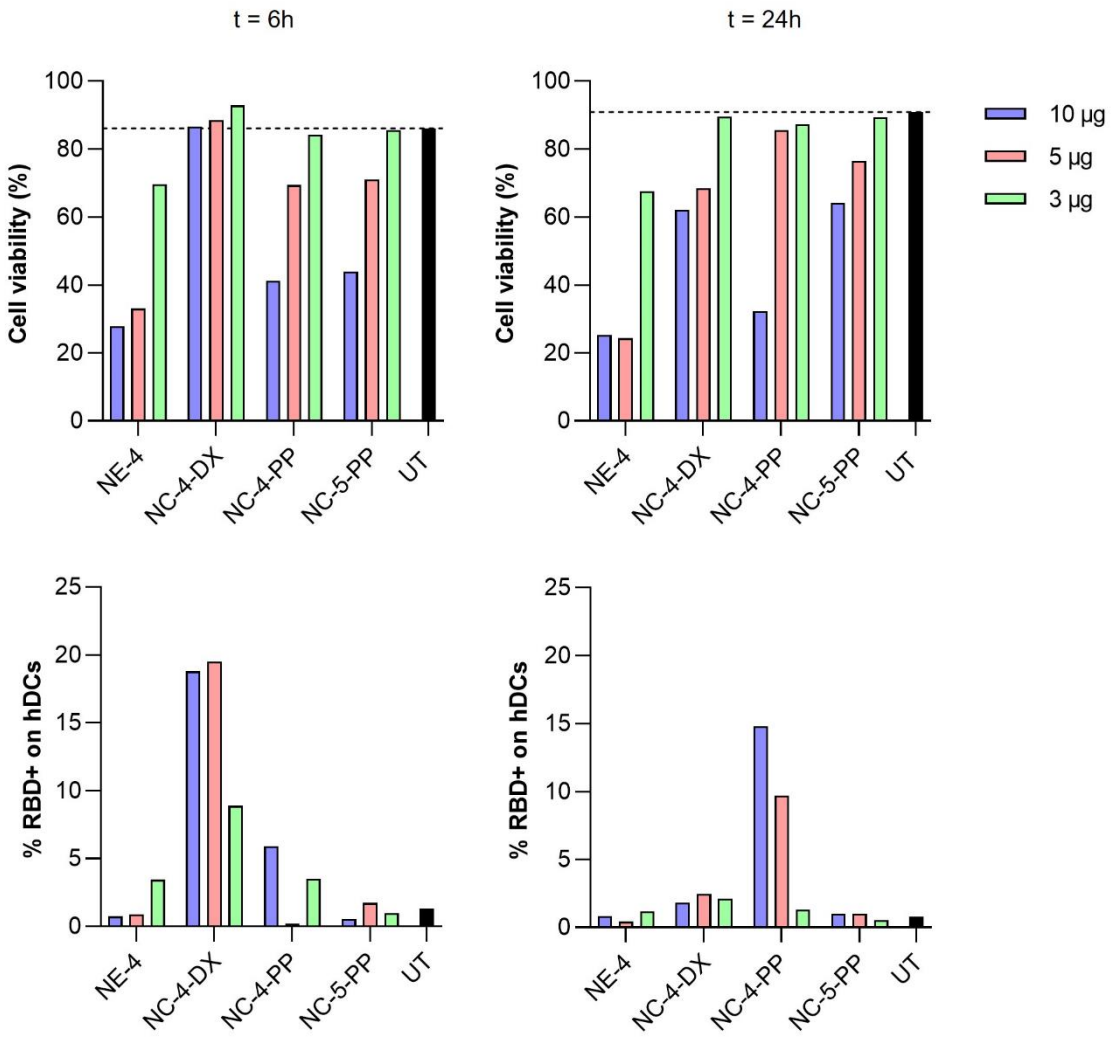

Figure 8. Cell viability (top) and percentage of hDCs able to express RBD (bottom) after 6 hours (left) and 24 hours (right) post-treatment with NE-4-mRBD, NC-4-DX-mRBD, NC-4-PP-mRBD, and NC-5-PP-mRBD, at different mRBD concentrations

Abbreviations: DX: dextran sulfate. hDCs: human-derived dendritic cells. mRBD: SARS-CoV-2 RBD. NC: nanocapsule. NE: nanoemulsion. PP: PEG-PGA (PEG (5 kDa)-b-PGA (10) (Na)). UT: untreated Values represented as n = 1.

Regarding their ability to transfect hDCs, noticeable differences were found among the formulations (Figure 8, bottom). None of the tested nanocarriers were able to achieve

expression of RBD in more than 20% of hDCs, with formulation NC-4-DX-mRBD exhibiting the highest transfection efficiency. This level of expression, although disappointing, is consistent with previous findings in the literature. Authors have reported *in vitro* transfection rates of up to 28% in bone-marrow-derived DCs (BMDCs) using an mRNA transfection reagent [34]. Other reports using LNPs to deliver mGFP into BMDCs demonstrated transfection rates ranging from 20-50%, depending on the concentration and type of ionizable lipids used [35].

These results could be attributed to the inherent difficulty of transfecting DCs, as well as distinct release and endosomal scape profiles. Our hypothesis is that NC-4-DX-mRBD could potentially facilitate faster endosomal scape compared to NC-4-PP-mRBD, resulting in higher RBD production at short time intervals (Figure 8, bottom left). At longer time points, only NC-4-PP-mRBD showed a modest RBD production, which we hypothesize may be indicative of a slower release of the mRDB cargo (Figure 8, bottom right).

3.3. *IN VIVO* SCREENING OF NANOEMULSIONS AND NANOCAPSULES USING MODEL MRNAS

In vivo evaluations of NE-mRNA and NC-mRNA were conducted using mLuc and mOVA as model mRNAs, to assess the transfection potency of the developed nanocarriers.

3.3.1. Intramuscular administration of nanocarriers with mLuc

As an initial approach to assessing the *in vivo* transfection capacity of selected formulations, mRNA encoding for luciferase (mLuc) was used as cargo. Following intramuscular administration in mice, fluorescence was measured at different times (Figure 9). In the first set of experiments, the selected formulations were prepared through bulk mixing, including NE-3-mLuc, NE-4-mLuc, NC-3-PR-mLuc, and NC-4-DX-mLuc (Figure 9, left). In all cases, N/P ratio used was 2:1. None of the nanocarriers, except for NC-4-DX, significantly improved transfection compared to free mLuc administration. Subsequently, aiming to evaluate the potential for improving the transfection efficiency of the nanosystems, formulations NE-4-mLuc, NC-4-DX-mLuc, NC-4-PP-mLuc, and NC-5-PP-mLuc were prepared with increased N/P ratios of 4:1 and using microfluidics, which resulted in a substantial reduction in particle diameter. Overall, the signal detected was significantly higher than in the first set of experiments. Some of the nanosystems, namely NE-4-mLuc and NC-4-PP-mLuc, resulted in significant differences as compared to both controls (PBS and free mLuc).

Assuming that the N/P ratio would primarily influence the transfection potency of the nanocarriers, differences in the behavior of the same NE-mLuc or NC-mLuc in the different sets of experiments could be explained by the type of production process. When prepared by bulk mixing (Figure 9, left), no significant differences were found between NE-mLuc and their derivatives NC-mLuc. However, notable differences were observed when these nanocarriers were manufactured through microfluidic mixing (Figure 9, right). For example, NE-4-mLuc and NC-4-DX-mLuc, prepared by bulk mixing, resulted in no significant differences in terms of transfection potency, but significant differences were found when prepared by microfluidic mixing. While still preliminary, these results suggest that different mixing processes influence the transfection potency of the nanocarriers, as has been previously reported for LNPs [36]. In summary, these results highlight the impact of the N/P ratio and the production process on the transfection potency of the developed mRNA nanosystem.

IVIS images corresponding to this study can be found in Supplementary Figure 4 and Supplementary Figure 5 (corresponding with Figure 9 left and right, respectively).

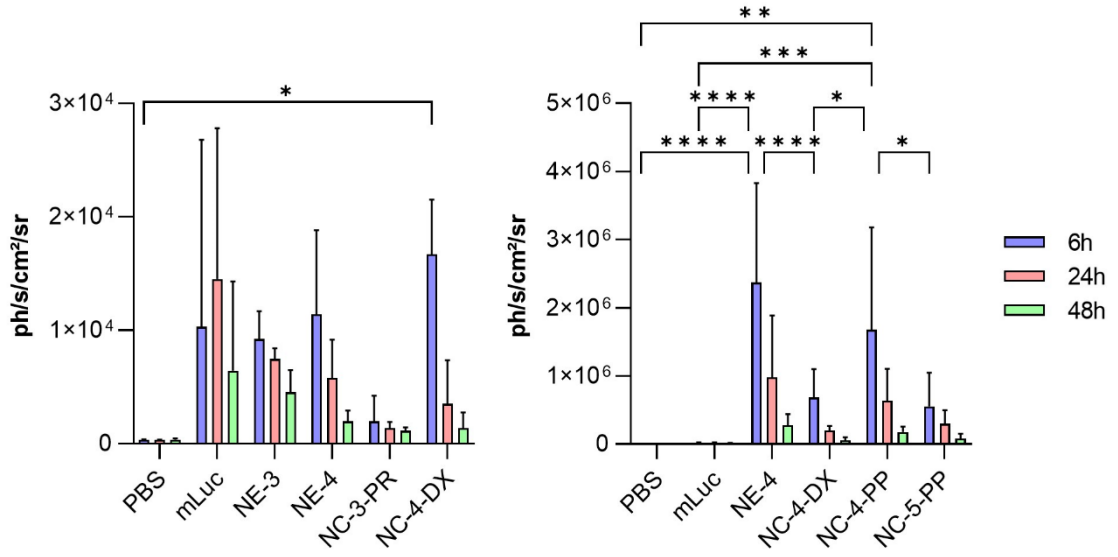

Figure 9. Normalized quantification of whole-body luciferase signal of NE-mLuc and NC-mLuc prepared by bulk mixing (left) and by microfluidic mixing (right), after intramuscular administration. Each animal was injected in both legs and imaged by IVIS at different time points (6, 24, and 48 hours)

Abbreviations: DX: dextran sulfate. mLuc: mRNA encoding luciferase. NC: nanocapsule. NE: nanoemulsion. PBS: phosphate-buffered saline. PR: protamine sulphate EP. A significant comparison was performed using two-way ANOVA followed by Tukey's multiple comparison tests between groups. *p*-values < 0.05 were considered statistically significant (*). Also, (**) if *p*-value < 0.01, (***) if *p*-value < 0.001, and (****) if *p*-value < 0.0001. Values represent the mean ± standard deviation (n ≥ 3).

3.3.2. Intramuscular administration of nanocarriers with mOVA

Based on mLuc transfection results, the most promising nanoformulation, NC-4-DX (N/P ratio 2:1), was selected for the loading of mRNA encoding the model immunology protein ovalbumin (OVA) [37].

The adaptative immune system, designed to protect us from recurring infections, can be activated through humoral responses (mainly, antibodies) or cellular responses (T cells). Cellular responses can include specialized T cells, known as cytotoxic T cells (CTLs), or clusters of differentiation 8 ($CD8^+$) T cells. Ideally, the nanosystems developed should be capable of inducing robust Major Histocompatibility Complex I (MHC-I)-mediated $CD8^+$ T cell responses [38,39]. To evaluate this, blood samples were collected on day 7, and spleen samples on day 10, following intramuscular administration of NC-4-DX-mOVA on day 0 and day 7 (Figure 10).

Dextramer staining enables the detection of MHC-I $CD8^+$ T cells, and NC-4-DX-mOVA successfully stimulated higher levels of dextramer-positive $CD8^+$ T cells in both blood and spleen compared to the free mOVA control (Figure 10, top left). Activated $CD8^+$ T cells produce interferon-gamma (IFN-γ), a cytokine involved in the immune response process [40]. The results of the quantification of IFN-γ, assessed using ELISpot assay, indicated that NC-4-DX-mOVA elicited higher levels of the cytokine compared to free mOVA (Figure 10, top right and bottom). These results showed the role of the nanocarrier in delivering mRNA immunogens to induce immune responses, as the levels of $CD8^+$ T cells and IFN-γ provoked by the administration of free mOVA are lower than those generated by NC-4-DX-mOVA.

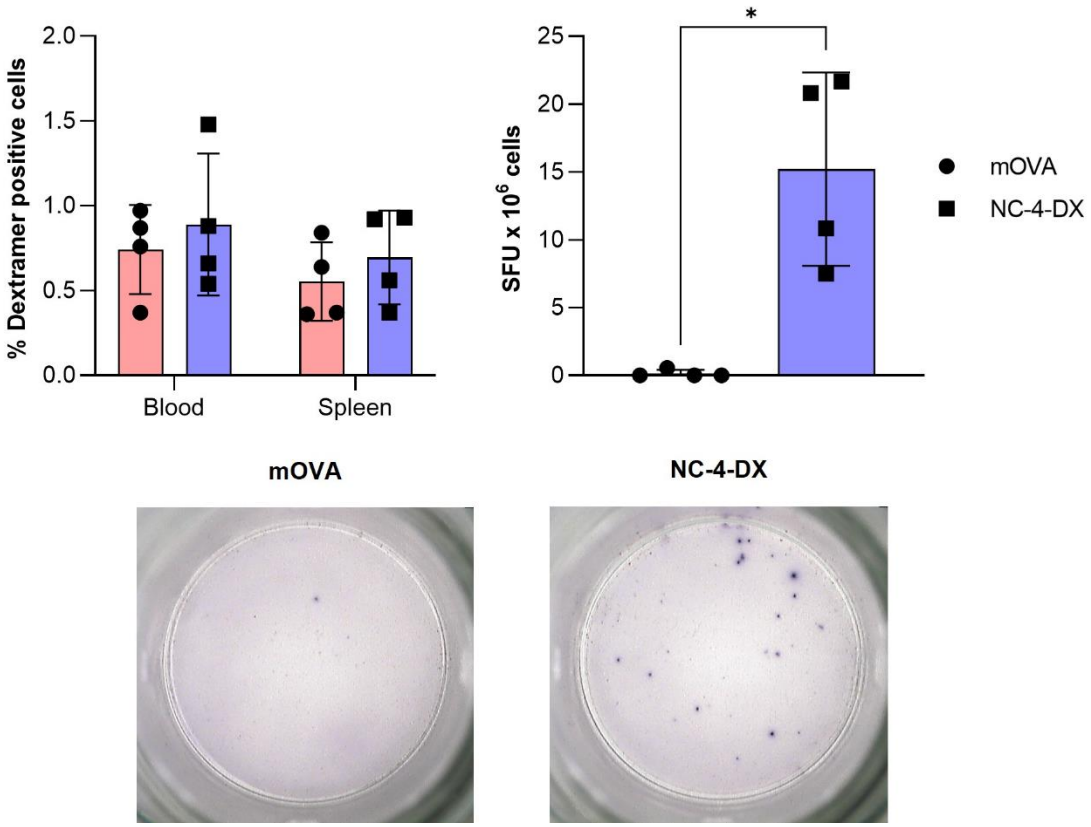

Figure 10. Percentage of dextramer-positive cells, obtained by flow cytometer, in the blood (collected on day 7 post-administration) and the spleen (collected on day 10 post-administration) (top, left), and IFN-γ-producing spot-forming units (SFU) from splenocytes, by ELISpot assay (collected in day 10-post administration) (top, right). Images of the INFγ-producing SFU of mOVA (bottom, left) and NC-4-DX (bottom, right)

Abbreviations: DX: dextran sulfate. IFN-γ: interferon gamma. mOVA: mRNA encoding ovalbumin protein. NC: nanocapsule. SFU: spot-forming units. A significant comparison was performed using multiple unpaired t-tests followed by a Welch correction. *p*-values < 0.05 were considered statistically significant (*). (n ≥ 3).

3.4. *IN VIVO* IMMUNE RESPONSE OF NANOEMULSIONS AND NANOCAPSULES CONTAINING SARS-COV-2 DERIVED MRNAS

The immune responses induced by the developed NE-mRNAs and NC-mRNAs were evaluated using various SARS-CoV-2 mRNA constructs produced by the COVARNA consortium. These mRNA sequences included mT (SARS-CoV-2-T cell mRNA, designed to trigger a T cell response), mB (SARS-CoV-2-B cell mRNA, intended to provoke B cell responses), mRBD (SARS-CoV-2-RBD mRNA, encoding for RBD domain of the virus), $mRBD_{epi}$ (SARS-CoV-2-RBD_{epi} mRNA, encoding a highly immunogenic motif from the RBD domain). The administration protocol is illustrated in Figure 11.

Figure 11. Schematic representation of the study design timeline

Created with https://biorender.com.

Both humoral and cellular immune responses were evaluated after intramuscular administration of nanocarriers with a single mRNA or combinations of different mRNAs. The results showed negligible humoral responses in the form of antibodies against SARS-CoV-2. This absence of humoral immune response was previously described in other cationic NE-mRNAs featuring different lipid compositions, which authors attributed to their endosomal escape pattern in DCs [41]. Consequently, the following results focus solely on the cellular immune responses observed.

3.4.1. Cellular responses after intramuscular administration of NC-4-DX containing a single SARS-CoV-2 derived mRNA

Three different mRNAs derived from SARS-CoV-2 (mT, mRBD, and $mRBD_{epi}$) were encapsulated onto NC-DX-4 (N/P ratio 2:1, prepared by bulk mixing). The animals received two separate injection sessions, with a 21-day interval between them. In each session, 10 µg of each mRNA was administered in a total volume of 50 µL, and each animal received injections in both legs, intramuscularly. This resulted in a total dose of 20 µg in 100 µL per animal per dose session. Two controls were used: NC-4-DX-mLuc, to assess any immune response related to the nanocarrier itself; and positive control-mT (PC-mT) consisting of an LNP encapsulating SARS-CoV-2 mT (C12-200: DOPE: Cholesterol: DMG-PEG, at molar ratios 40: 16: 42.5: 1.5), serving as a reference for a nanocarrier capable of inducing potent mRNA transfection [42–44], used to evaluate performance of NC-4-DX-mT.

As described in Figure 12, both clusters of differentiation 4 ($CD4^+$) and $CD8^+$ T cell responses were investigated. Overall responses, which combined the percentage of each type of T cell capable of secreting specific cytokines, showed higher levels of immune response than their respective controls (Figure 12, top). Specific cytokines considered for evaluating the immune response were IFN-γ and TNF-α (or tumor necrosis factor-α), both actively produced upon activation of $CD4^+$ and $CD8^+$ T cells after infection or immunization [45].

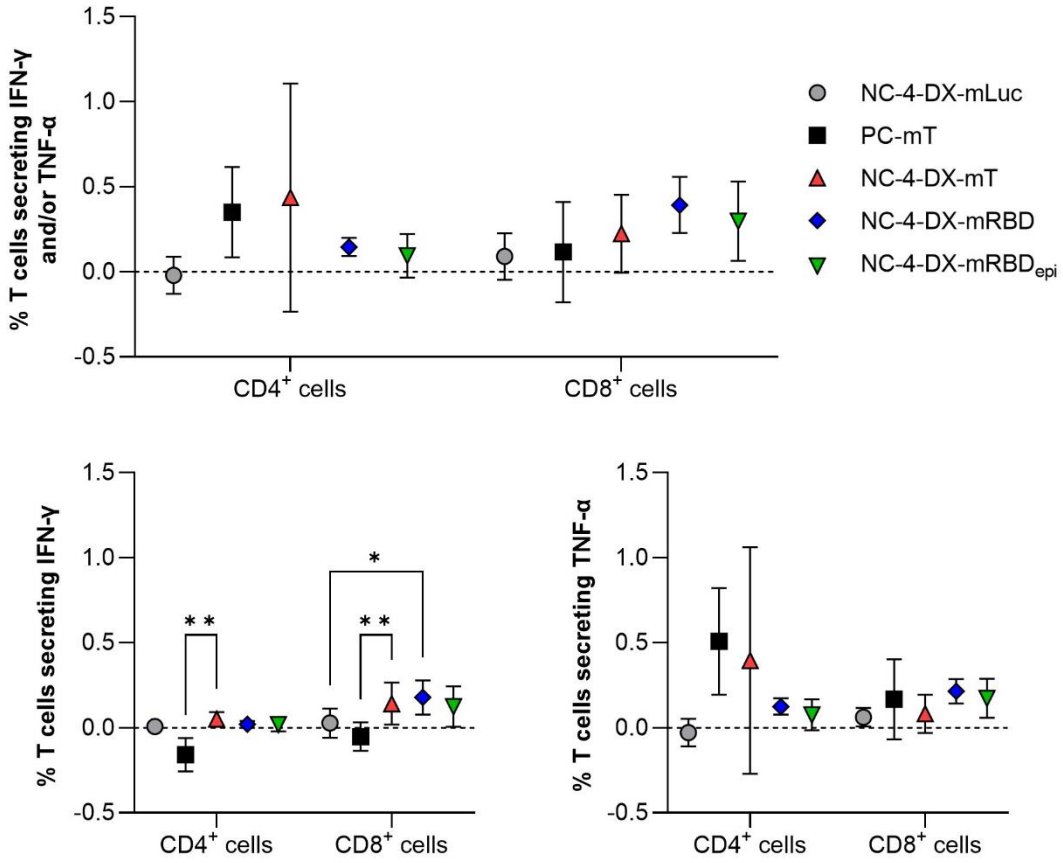

Figure 12. CD4⁺ and CD8⁺ T cell responses (top) in terms of IFN-γ (bottom, left) and TNF-α (bottom, right)

Abbreviations: DX: dextran sulfate. IFN-γ: interferon gamma. mLuc: mRNA encoding luciferase. mRBD: SARS-CoV-2-RBD mRNA. $mRBD_{epi}$: SARS-CoV-2-RBD_{epi} mRNA. mT: SARS-CoV-2-T cells mRNA. NC: nanocapsule. TNF-α: tumor necrosis factor-alpha. A significant comparison was performed using two-way ANOVA followed by Tukey's multiple comparison tests between groups. *p*-values < 0.05 were considered statistically significant (*). Also, (**) if *p*-value < 0.01. Values represent the mean ± standard deviation (n ≥ 3).

In terms of individual cytokines, significant changes were observed in the levels of IFN-γ (Figure 12, bottom left). There were significantly higher levels of IFN-γ in both $CD4^+$ and $CD8^+$ cells following the administration of NC-4-DX-mT, as well as after the administration of NC-4-DX-mRBD for $CD4^+$ cells. Regarding TNF-α, no significant differences were found when compared to the control groups; however, slight increases in this cytokine were observed in T cells (Figure 12, bottom right). Overall, all NC-4-DX-mRNAs tested exhibited higher cytokine levels than their respective controls, indicating that the immune response observed is strongly related to the type of mRNA used rather than the nanocarrier itself.

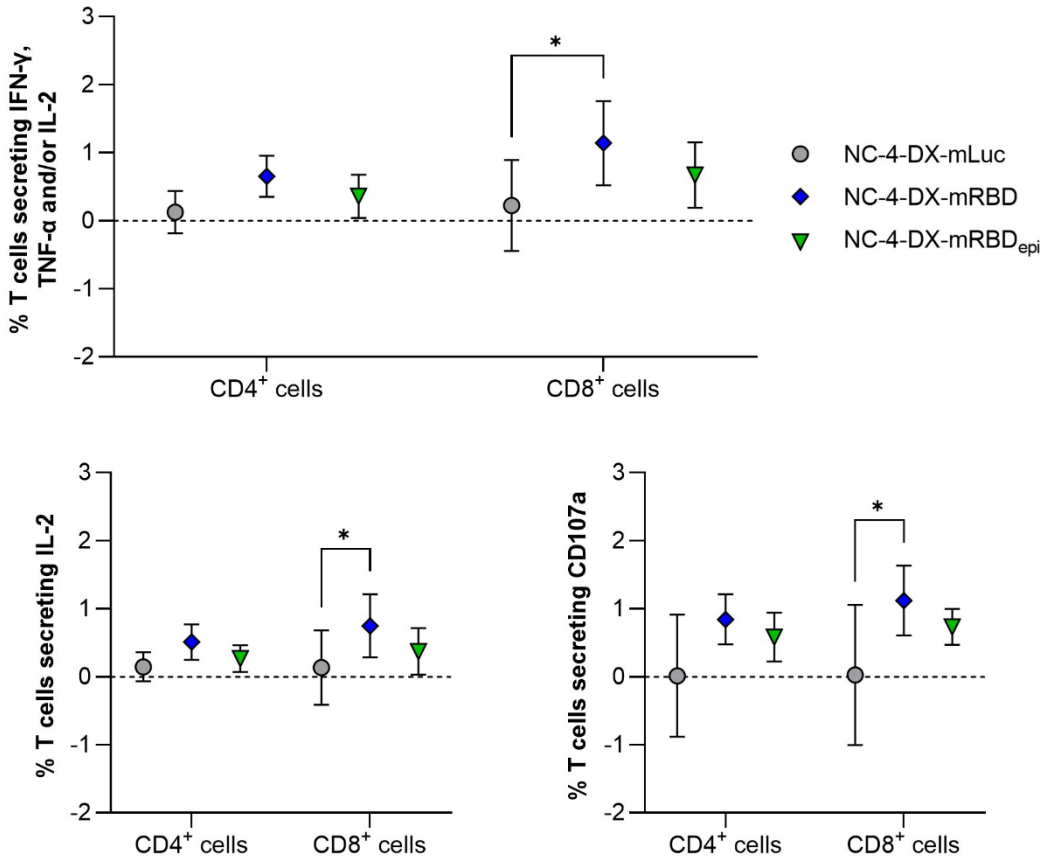

Figure 13. CD4⁺ and CD8⁺ T cell responses (top) considering IFN-γ, TNF-α, and IL-2. IL-2 (bottom, left) and C107a secretions (bottom, right) from T cells were also determined

Abbreviations: C107a: LAMP-1 or lysosomal-assocaited membrane protein-1. DX: dextran sulfate. IFN-γ: interferon gamma. IL-2: interleukin-2. mLuc: mRNA encoding luciferase. mRBD: SARS-CoV-2-RBD mRNA. $mRBD_{epi}$: SARS-CoV-2-RBD_{epi} mRNA. NC: nanocapsule. TNF-α: tumor necrosis factor-alpha. A significant comparison was performed using two-way ANOVA followed by Tukey's multiple comparison tests between groups. *p*-values < 0.05 were considered statistically significant (*). Values represent the mean ± standard deviation (n ≥ 3).

Given the similarities between mRBD and $mRBD_{epi}$, further exploration was conducted. In an effort to discern differences between these two mRNA constructs, additional cytokine responses were examined, including not only TNF-α but also interleukin-2 (IL-2), also involved in T cell responses (Figure 13, top) [45]. NC-4-DX-mRBD depicted higher levels of IL-2 produced by $CD8^+$ T cells compared to NC-4-DX-$mRBD_{epi}$ (Figure 13, bottom left), which influenced the overall $CD8^+$ T cell response (Figure 13, top). NC-4-DX-$mRBD_{epi}$ exhibited higher levels than the control group, but these differences were not statistically significant.

Moreover, levels of CD107a were determined (Figure 13, bottom right). CD107a, or LAMP-1 (lysosomal-associated membrane protein-1) is a marker of cellular immunity activation, and cytotoxic degranulation associated with natural killer (NK) cell activity [46]. Similar to the previous scenario, levels of CD107a were significantly elevated in the case of the $CD8^+$ T cell responses induced by NC-4-DX-mRBD.

In conclusion, when comparing mT, mRBD, and $mRBD_{epi}$, differences were observed depending on the type of T cell. In the case of $CD4^+$ T cell responses, it appears that NC-4-DX-

mT generated an overall higher response than the other NC-4-DX-mRNA investigated; however, variations between different animals were noted, which could lead to an inaccurate interpretation of this conclusion. Regarding $CD8^+$ T cell responses, all three mRNAs evaluated elicited immune responses greater than those observed in the control groups, although NC-4-DX-mRBD and NC-4-DX-$mRBD_{epi}$ seemed to induce higher cellular responses. When comparing mRBD and $mRBD_{epi}$, greater immune responses were observed following the administration of NC-4-DX-mRBD in both $CD4^+$ and $CD8^+$ T cells.

3.4.2. Cellular responses after intramuscular administration of NC-4-DX containing combinations SARS-CoV-2 derived mRNAs

Lastly, the immune responses of combinations of different mRNAs derived from SARS-CoV-2, associated to NC-4-DX (N/P ratio 2:1), were evaluated. The intramuscular injection schedule followed the same protocol as discussed in section 3.4.1, where 10 µg of each mRNA was administered, resulting in a total dose of 20 µg. The injections involved combinations of NC-4-DX-mT with NC-4-DX-mB, -mRBD, and -$mRBD_{epi}$, respectively. A nanocarrier control was included, represented by NC-4-DX-mLuc.

The results showed significantly superior $CD8^+$ cellular responses as compared to CD4+ responses, these differences being particularly significant in the combinations with mRBD and $mRBD_{epi}$ (Figure 14, top). In these studies, the cytokines explored were IFN-γ, TNF-α, and IL-2 (Figure 14, bottom left, center, and right, respectively). Significant increases in IFN-γ secreting levels were noted in the combination of mT with mB when compared to the nanocarrier control group and the other mRNA combinations explored (Figure 14, bottom left). Additionally, the combination of mT and mRBD resulted in significantly higher levels of IL-2 when compared to the control group (Figure 14, bottom right).

In summary, greater immune responses were elicited when combinations of mRNA were administered. However, this effect can also be attributed to the higher dose administered (10 µg of mRNA for a single mRNA versus 20 µg of mRNA for the mRNA combinations). Furthermore, predominantly observed were $CD8^+$ cellular responses, with mRBD (alone or in combination with mT) shown to induce the highest immune response among the various SARS-CoV-2 derived mRNA explored.

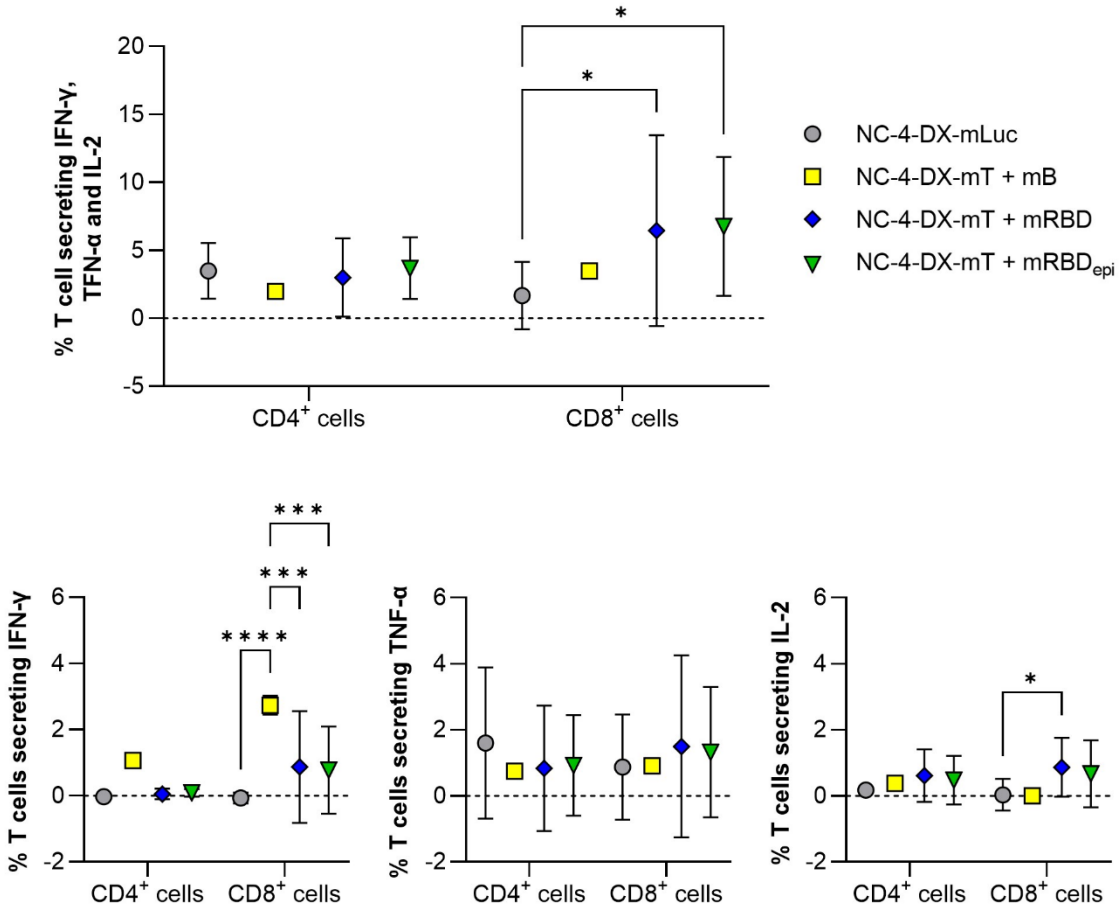

Figure 14. CD4⁺ and CD8⁺ T cell responses (top) considering IFN-γ, TNF-α, and IL-2 (bottom, left, center, and right, respectively)

Abbreviations: DX: dextran sulfate. IFN-γ: interferon gamma. IL-2: interleukin-2. mB: SARS-CoV-2-B cells mRNA. mLuc: mRNA encoding luciferase. mRBD: SARS-CoV-2-RBD mRNA. mRBD$_{epi}$: SARS-CoV-2-RBD$_{epi}$ mRNA. mT: SARS-CoV-2-T cells mRNA. NC: nanocapsule. TNF-α: tumor necrosis factor-alpha. A significant comparison was performed using two-way ANOVA followed by Tukey's multiple comparison tests between groups. *p*-values < 0.05 were considered statistically significant (*). Values represent the mean ± standard deviation (n ≥ 3).

4. CONCLUSIONS

Overall, we have developed around 100 different nanocarriers, and successfully identified several prototypes capable of encapsulating and transfecting various types of mRNA, while meeting the established TPP criteria, in terms of physicochemical properties and stability. Among them, NC-4-DX emerged as our most promising candidate, capable of inducing significant levels of specific cellular immune responses following intramuscular administration of SARS-CoV-2-derived mRNAs. We also explored combinations of different mRNAs, resulting in similar overall CD4$^+$ and CD8$^+$ cellular immune responses. These findings showcase the potential of NEs and NCs as vaccine delivery systems.

5. SUPPLEMENTARY INFORMATION

Supplementary Table 1. Physicochemical properties of developed nanoemulsions and nanocapsules, before and after the freeze-drying process, using different mRNAs

Nanosystem	mRNA	Condition	Particle diameter (nm)	PDI	ζ-Potential (mV)
NE-3	mGFP	Before FD	93	0.12	+36
		Trehalose 10%	387	0.42	+28
		Sucrose 10%	122	0.20	+34
	mLuc	Before FD (n = 2)	112 ± 16	0.17 ± 0.01	+35 ± 6
		Trehalose 10%	368	1	-
		Sucrose 10%	143	0.17	+36
		Sucrose 20%	100	0.18	+35
	mOVA	Before FD	99	0.16	+45
		Glucose 10%	162	0.22	-
		Glucose 20%	88	0.22	-
NE-4	mGFP	Before FD	128	0.11	+42
		Trehalose 10%	169	0.20	+46
		Sucrose 10%	168	0.17	+42
	mLuc	Before FD	123	0.22	+45
		Sucrose 20%	116	0.14	+44
	mOVA	Before FD	127	0.11	+42
		Sucrose 10%	190	0.11	-
		Sucrose 20%	118	0.09	-
NC-3-PR	mGFP	Before FD	154	0.11	+28
		Trehalose 10%	174	0.17	+29
		Sucrose 10%	207	0.17	+24
	mLuc	Before FD	179	0.16	+24
		Trehalose 10%	180	0.16	+24
		Sucrose 10%	213	0.20	+25
NC-4-PR	mGFP	Before FD	168	0.10	+27
		Trehalose 10%	185	0.07	+31
		Sucrose 10%	191	0.07	+31
NC-4-DX	mLuc	Before FD	139 ± 21	0.14 ± 0.05	-19 ± 4
		Sucrose 10%	162 ± 20	0.12 ± 0.07	-30 ± 11
	mOVA	Before FD (n = 2)	132 ± 3	0.07 ± 0.03	-16 ± 2
		Sucrose 10%	263	0.05	-
		Sucrose 20%	183	0.08	-32
		Glucose 20%	173	0.13	-
	mT	Before FD (n = 2)	115 ± 2	0.07 ± 0.01	-17 ± 1
		Sucrose 10%	148	0.11	-23
		Sucrose 20%	147	0.09	-21

Abbreviations: DX: dextran sulfate. FD: freeze-drying. mGFP: mRNA encoding GFP. mLuc: mRNA encoding luciferase. mOVA: mRNA encoding ovalbumin protein. mT: SARS-CoV-2-T cells mRNA. NE: nanoemulsion. NC: nanocapsule. PDI: polydispersity index. PR: protamine sulphate EP. Values represent the mean ± standard deviation (n ≥ 3, unless indicated otherwise or no standard deviation is indicated).

Supplementary Table 1. Physicochemical properties of developed nanoemulsions and nanocapsules, before and after the freeze-drying process, using different mRNAs (continuation)

Nanosystem	mRNA	Condition	Particle diameter (nm)	PDI	ζ-Potential (mV)
NC-4-DX	mRBD	Before FD (n = 2)	114 ± 5	0.11 ± 0.01	-18 ± 2
		Sucrose 10% (n = 2)	136 ± 18	0.07 ± 0.04	-16 ± 4
	$mRBD_{epi}$	Before FD (n = 2)	116 ± 2	0.08 ± 0.01	-17 ± 1
		Sucrose 10% (n = 2)	137 ± 20	0.06 ± 0.04	-20 ± 7
	mT + mB	Before FD	114 ± 1	0.09 ± 0.02	-16 ± 1
		Sucrose 10%	174 ± 30	0.14 ± 0.04	-19 ± 2
		Sucrose 20%	139 ± 10	0.12 ± 0.02	-21 ± 2
	mT + mRBD	Before FD (n = 2)	105 ± 1	0.09 ± 0.01	-19 ± 4
		Sucrose 20% (n = 2)	143 ± 9	0.05 ± 0.02	-21 ± 7
	mT + $mRBD_{epi}$	Before FD (n = 2)	106 ± 1	0.10 ± 0.01	-17 ± 4
		Sucrose 20% (n = 2)	120 ± 16	0.06 ± 0.01	-21 ± 4

Abbreviations: DX: dextran sulfate. mB: SARS-CoV-2-B cells mRNA. mRBD: SARS-CoV-2-RBD mRNA. $mRBD_{epi}$: SARS-CoV-2-RBD_{epi}. mT: SARS-CoV-2-T cells mRNA. NC: nanocapsule. PDI: polydispersity index. Values represent the mean ± standard deviation (n ≥ 3, unless indicated otherwise or no standard deviation is indicated).

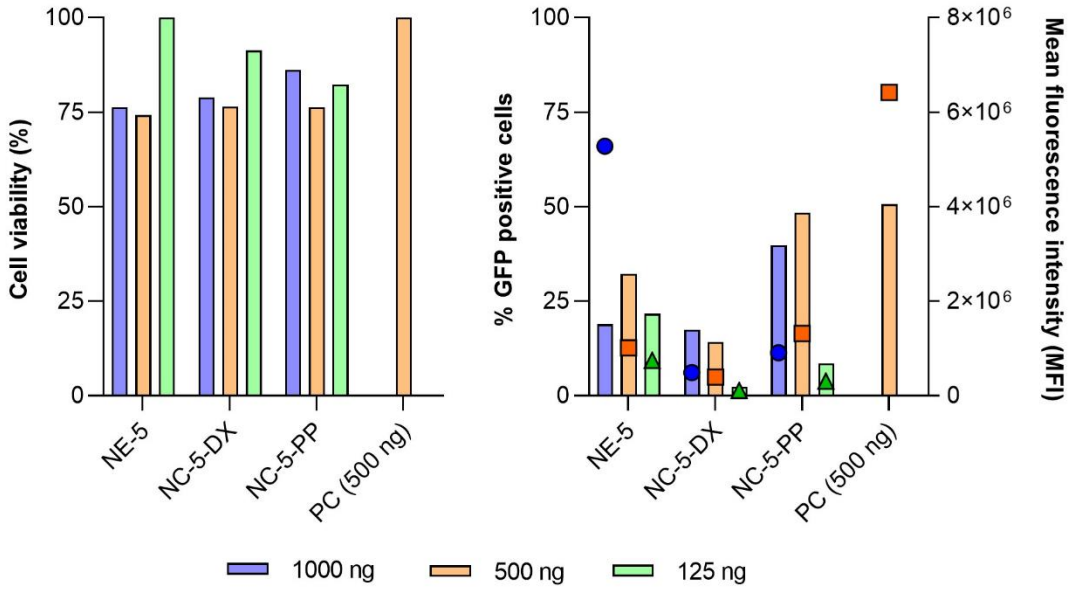

Supplementary Figure 1. Cytotoxicity (left) and GFP transfection efficiency (right) of NE-5-mGFP, NC-5-DX-mGFP, and NC-5-PP-mGFP (left), at different mGFP concentrations. Percentage of GFP positive cells (right figure, left axis) and mean fluorescence intensity (right figure, right axis) in HeLa cells, 24 hours post-transfection

Abbreviations: DX: dextran sulfate. mGFP: mRNA encoding GFP. NE: nanoemulsion. NC: nanocapsule. PC: positive control, lipofectamine. PEG-PGA or PP: PEG (5 kDa)-b-PGA (10) (Na). (n = 1).

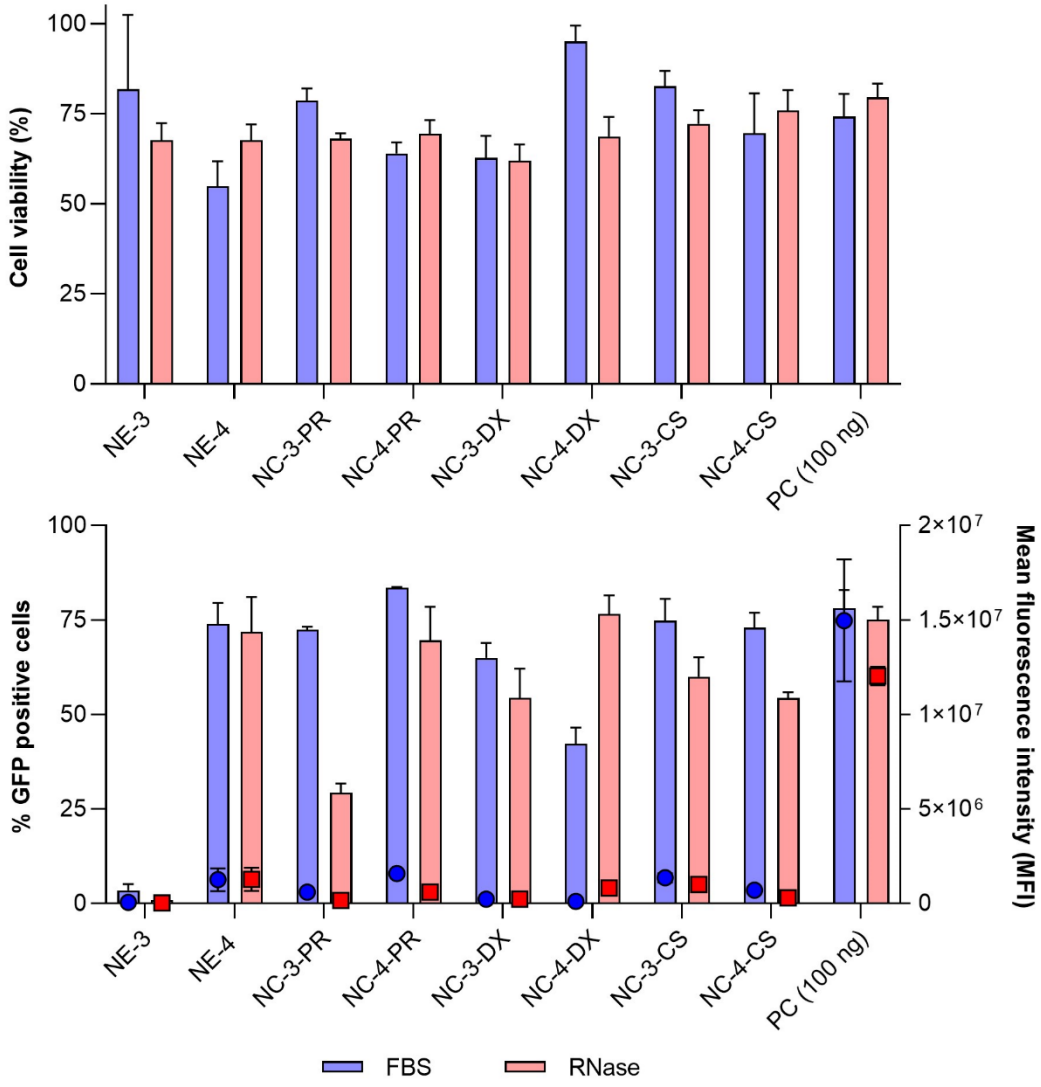

Supplementary Figure 2. Cytotoxicity (top) and GFP transfection efficiency (bottom) of NE-3-mGFP, NE-4-mGFP, NC-3-PR-mGFP, NC-4-PR-mGFP, NC-3-DX-mGFP, NC-4-DX-mGFP, NC-3-CS-mGFP, and NC-4-CS-mGFP after being treated with FBS (blue) or RNase (red). Percentage of GFP positive cells (bottom figure, left axis) and mean fluorescence intensity (bottom figure, right axis) in HeLA cells, 24 hours post-transfection

Abbreviations: CS: chitosan. DX: dextran sulfate. mGFP: mRNA encoding GFP. NE: nanoemulsion. NC: nanocapsule. PC: positive control, lipofectamine. PR: protamine sulphate EP. Values represent the mean ± standard deviation (n ≥ 3).

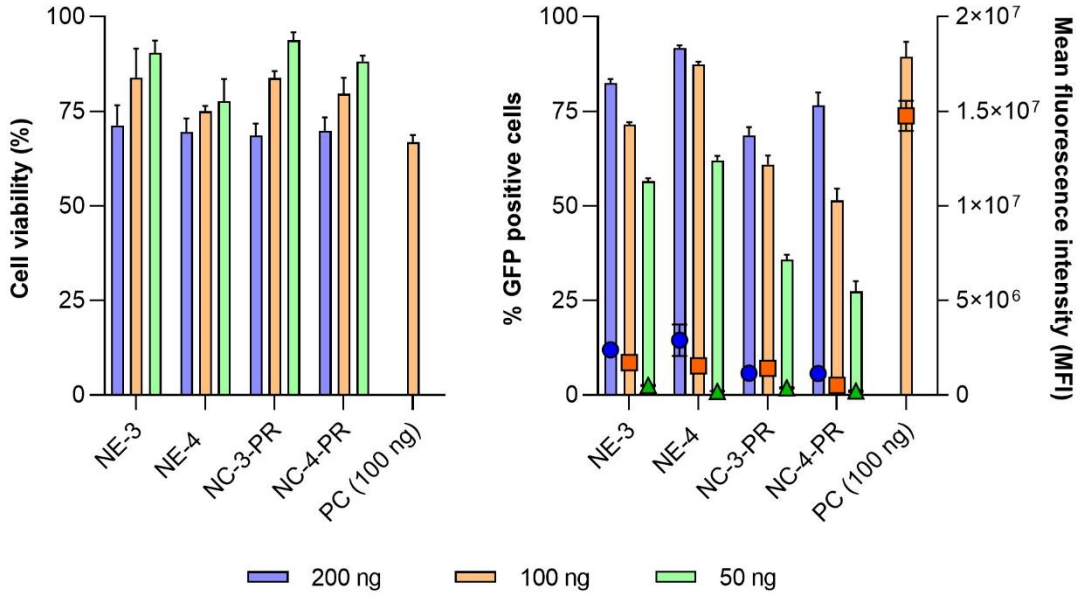

Supplementary Figure 3. Cytotoxicity (top) and GFP transfection efficiency (bottom) of NE-3-mGFP, NE-4-mGFP, NC-3-PR-mGFP, and NC-4-PR-mGFP, resuspended after the freeze-drying process. Percentage of GFP positive cells (right figure, left axis) and mean fluorescence intensity (right figure, right axis) in HeLA cells, 24 hours post-transfection

Abbreviations: mGFP: mRNA encoding GFP. NE: nanoemulsion. NC: nanocapsule. PC: positive control, lipofectamine. PR: protamine sulphate EP. Values represent the mean ± standard deviation (n ≥ 3).

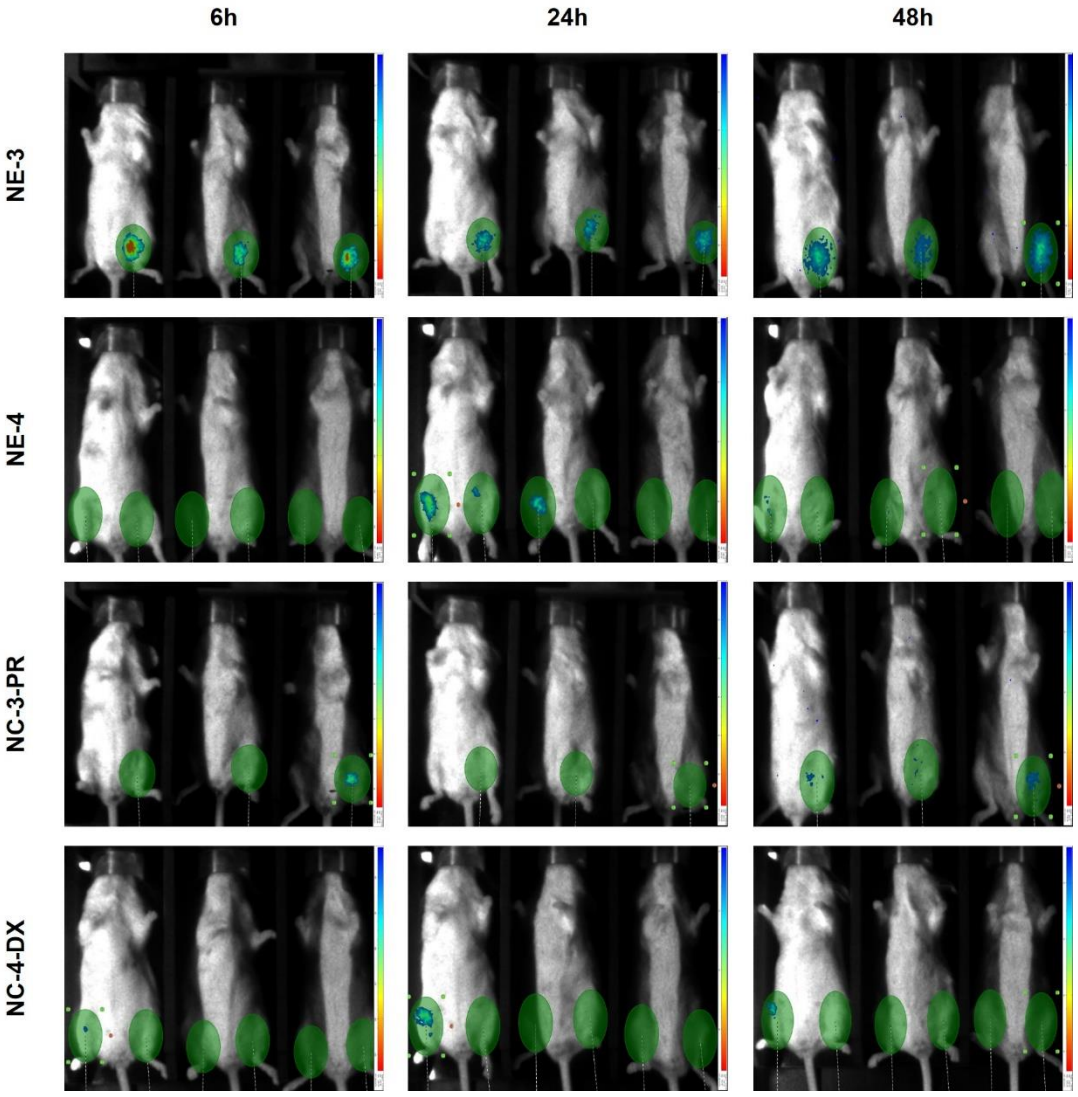

Supplementary Figure 4. Luciferase fluorescence signal detected by IVIS using NE-3mLuc, NE-4-mLuc, NC-3-PR-mLuc, and NC-4-DX-mLuc (prepared by bulk mixing), at different time points (6, 24, and 48 hours), after intramuscular administration

Abbreviations: DX: dextran sulfate. mLuc: mRNA encoding luciferase. NE: nanoemulsion. NC: nanocapsule. PR: protamine sulphate EP.

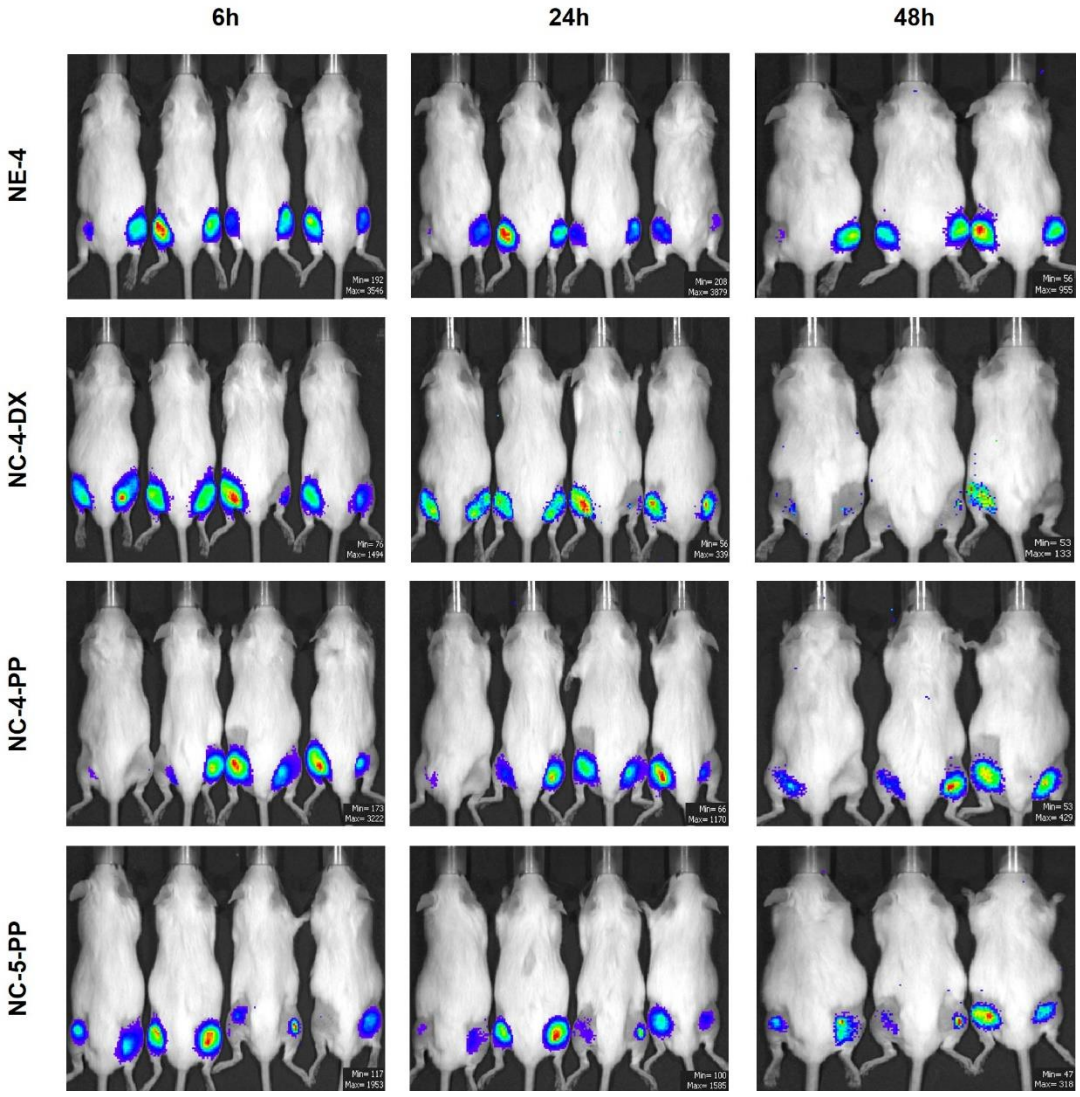

Supplementary Figure 5. Luciferase fluorescence signal detected by IVIS using NE-4-mLuc, NC-4-DX-mLuc, NC-4-PP, and NC-5-PP (prepared by microfluidic mixing) at different time points (6, 24, and 48 hours), after intramuscular administration

Abbreviations: DX: dextran sulfate. mLuc: mRNA encoding luciferase. NE: nanoemulsion. NC: nanocapsule. PEG-PGA or PP: PEG (5 kDa)-b-PGA (10) (Na). PR: protamine sulphate EP.

6. ACKNOWLEDGMENTS

This work was supported by the Preclinical development of innovative mRNA/MVA vaccines against SARS-CoV-2, COVARNA Consortium, Instituto de Salud Carlos III, and Generalitat de Catalunya. Mireya L. Borrajo acknowledges the financial support by Instituto de Salud Carlos III, through the "Contratos i-PFIS: Doctorados ISS-empresa en Ciencias y Tecnologías de la Salud" grant.

In vitro cytotoxicity and transfection efficacy studies were performed in collaboration with David Moreira Ph.D. and Prof. Mabel Loza from CiMUS (Spain). *In vitro* cytotoxicity and transfection efficacy studies in hDCs were performed in collaboration with the laboratory of Montserrat Plana, Ph.D., in the IDIBAPS (Spain). *In vivo* studies with mLuc were performed in collaboration with the laboratory of Prof. Andreas Meyerhans, from University of Pompeu Fabra (Spain); and the laboratory of Prof. Kris Thielemans, from Vrije University Brussels (Belgium). *In vivo* studies with different SARS-CoV-2 derived mRNAs were performed in collaboration with the laboratory of Prof. Andreas Meyerhans, from University of Pompeu Fabra (Spain); and the laboratory of Prof. Mariano Esteban, from CNB-CSIC (Spain).

7. REFERENCES

[1] D. Cucinotta, M. Vanelli, WHO declares COVID-19 a pandemic, Acta Biomed. 91 (2020) 157–160. https://doi.org/10.23750/abm.v91i1.9397.

[2] B. Hu, H. Guo, P. Zhou, Z.L. Shi, Characteristics of SARS-CoV-2 and COVID-19, Nat. Rev. Microbiol. 19 (2021) 141–154. https://doi.org/10.1038/s41579-020-00459-7.

[3] Y. Liu, J. Liu, K.S. Plante, J.A. Plante, X. Xie, X. Zhang, Z. Ku, Z. An, D. Scharton, C. Schindewolf, S.G. Widen, V.D. Menachery, P.Y. Shi, S.C. Weaver, The N501Y spike substitution enhances SARS-CoV-2 infection and transmission, Nature. 602 (2022) 294–299. https://doi.org/10.1038/s41586-021-04245-0.

[4] World Health Organization, WHO Coronavirus (COVID-19) Dashboard, (2023). https://covid19.who.int/ (accessed May 29, 2023).

[5] K.S. Corbett, D.K. Edwards, S.R. Leist, O.M. Abiona, S. Boyoglu-Barnum, R.A. Gillespie, S. Himansu, A. Schäfer, C.T. Ziwawo, A.T. DiPiazza, K.H. Dinnon, S.M. Elbashir, C.A. Shaw, A. Woods, E.J. Fritch, D.R. Martinez, K.W. Bock, M. Minai, B.M. Nagata, G.B. Hutchinson, K. Wu, C. Henry, K. Bahl, D. Garcia-Dominguez, L.Z. Ma, I. Renzi, W.P. Kong, S.D. Schmidt, L. Wang, Y. Zhang, E. Phung, L.A. Chang, R.J. Loomis, N.E. Altaras, E. Narayanan, M. Metkar, V. Presnyak, C. Liu, M.K. Louder, W. Shi, K. Leung, E.S. Yang, A. West, K.L. Gully, L.J. Stevens, N. Wang, D. Wrapp, N.A. Doria-Rose, G. Stewart-Jones, H. Bennett, G.S. Alvarado, M.C. Nason, T.J. Ruckwardt, J.S. McLellan, M.R. Denison, J.D. Chappell, I.N. Moore, K.M. Morabito, J.R. Mascola, R.S. Baric, A. Carfi, B.S. Graham, SARS-CoV-2 mRNA vaccine design enabled by prototype pathogen preparedness, Nature. 586 (2020) 567–571. https://doi.org/10.1038/s41586-020-2622-0.

[6] F.P. Polack, S.J. Thomas, N. Kitchin, J. Absalon, A. Gurtman, S. Lockhart, J.L. Perez, G. Pérez Marc, E.D. Moreira, C. Zerbini, R. Bailey, K.A. Swanson, S. Roychoudhury, K. Koury, P. Li, W. V. Kalina, D. Cooper, R.W. Frenck, L.L. Hammitt, Ö. Türeci, H. Nell, A. Schaefer, S. Ünal, D.B. Tresnan, S. Mather, P.R. Dormitzer, U. Şahin, K.U. Jansen, W.C. Gruber, Safety and Efficacy of the BNT162b2 mRNA Covid-19 Vaccine, N. Engl. J. Med. 383 (2020) 2603–2615. https://doi.org/10.1056/nejmoa2034577.

[7] L.R. Baden, H.M. El Sahly, B. Essink, K. Kotloff, S. Frey, R. Novak, D. Diemert, S.A. Spector, N. Rouphael, C.B. Creech, J. McGettigan, S. Khetan, N. Segall, J. Solis, A. Brosz, C. Fierro, H. Schwartz, K. Neuzil, L. Corey, P. Gilbert, H. Janes, D. Follmann, M. Marovich, J. Mascola, L. Polakowski, J. Ledgerwood, B.S. Graham, H. Bennett, R. Pajon, C. Knightly, B. Leav, W. Deng, H. Zhou, S. Han, M. Ivarsson, J. Miller, T. Zaks, Efficacy and Safety of the mRNA-1273 SARS-

CoV-2 Vaccine, N. Engl. J. Med. 384 (2021) 403–416. https://doi.org/10.1056/nejmoa2035389.

[8] G.T. Szabó, A.J. Mahiny, I. Vlatkovic, COVID-19 mRNA vaccines: Platforms and current developments, Mol. Ther. 30 (2022) 1850–1868. https://doi.org/10.1016/j.ymthe.2022.02.016.

[9] N. Pardi, M.J. Hogan, D. Weissman, Recent advances in mRNA vaccine technology, Curr. Opin. Immunol. 65 (2020) 14–20. https://doi.org/10.1016/j.coi.2020.01.008.

[10] M. Alameh, D. Weissman, N. Pardi, Messenger RNA-Based Vaccines Against Infectious Diseases, Curr. Top. Microbiol. Immunol. 440 (2020). https://doi.org/10.1007/82_2020_202.

[11] Y. Wang, Z. Zhang, J. Luo, X. Han, Y. Wei, X. Wei, mRNA vaccine: a potential therapeutic strategy, Mol. Cancer. 20 (2021) 1–23. https://doi.org/10.1186/s12943-021-01311-z.

[12] M. Hoffmann, H. Kleine-Weber, S. Schroeder, N. Krüger, T. Herrler, S. Erichsen, T.S. Schiergens, G. Herrler, N.H. Wu, A. Nitsche, M.A. Müller, C. Drosten, S. Pöhlmann, SARS-CoV-2 Cell Entry Depends on ACE2 and TMPRSS2 and Is Blocked by a Clinically Proven Protease Inhibitor, Cell. 181 (2020) 271-280.e8. https://doi.org/10.1016/j.cell.2020.02.052.

[13] N. Csaba, A. Sánchez, M.J. Alonso, PLGA: Poloxamer and PLGA: Poloxamine blend nanostructures as carriers for nasal gene delivery, J. Control. Release. 113 (2006) 164–172. https://doi.org/10.1016/j.jconrel.2006.03.017.

[14] N. Csaba, M. Köping-Höggård, M.J. Alonso, Ionically crosslinked chitosan/tripolyphosphate nanoparticles for oligonucleotide and plasmid DNA delivery, Int. J. Pharm. 382 (2009) 205–214. https://doi.org/10.1016/j.ijpharm.2009.07.028.

[15] M. De La Fuente, M. Raviña, A. Sousa-Herves, J. Correa, R. Riguera, E. Fernandez-Megia, A. Sánchez, M.J. Alonso, Exploring the efficiency of gallic acid-based dendrimers and their block copolymers with PEG as gene carriers, Nanomedicine. 7 (2012) 1667–1681. https://doi.org/10.2217/nnm.12.51.

[16] S. Vicente, M. Peleteiro, B. Díaz-Freitas, A. Sanchez, Á. González-Fernández, M.J. Alonso, Co-delivery of viral proteins and a TLR7 agonist from polysaccharide nanocapsules: A needle-free vaccination strategy, J. Control. Release. 172 (2013) 773–781. https://doi.org/10.1016/j.jconrel.2013.09.012.

[17] J. Crecente-Campo, S. Lorenzo-Abalde, A. Mora, J. Marzoa, N. Csaba, J. Blanco, Á. González-Fernández, M.J. Alonso, Bilayer polymeric nanocapsules: A formulation approach for a thermostable and adjuvanted E. coli antigen vaccine, J. Control. Release. 286 (2018) 20–32. https://doi.org/10.1016/j.jconrel.2018.07.018.

[18] T.G. Dacoba, R.W. Omange, H. Li, J. Crecente-Campo, M. Luo, M.J. Alonso, Polysaccharide Nanoparticles Can Efficiently Modulate the Immune Response against an HIV Peptide Antigen, ACS Nano. 13 (2019) 4947–4959. https://doi.org/10.1021/acsnano.8b07662.

[19] A.M. Ledo, M.S. Sasso, V. Bronte, I. Marigo, B.J. Boyd, M. Garcia-Fuentes, M.J. Alonso, Co-delivery of RNAi and chemokine by polyarginine nanocapsules enables the modulation of myeloid-derived suppressor cells, J. Control. Release. 295 (2019) 60–73. https://doi.org/10.1016/j.jconrel.2018.12.041.

[20] A.S. Cordeiro, J. Crecente-Campo, B.L. Bouzo, S.F. González, M. de la Fuente, M.J. Alonso, Engineering polymeric nanocapsules for an efficient drainage and biodistribution in the

lymphatic system, J. Drug Target. 27 (2019) 646–658. https://doi.org/10.1080/1061186X.2018.1561886.

[21] E. Samaridou, H. Walgrave, E. Salta, D.M. Álvarez, V. Castro-López, M. Loza, M.J. Alonso, Nose-to-brain delivery of enveloped RNA - cell permeating peptide nanocomplexes for the treatment of neurodegenerative diseases, Biomaterials. 230 (2020) 119657. https://doi.org/10.1016/j.biomaterials.2019.119657.

[22] P. Calvo, C. Remuñán-López, J.L. Vila-Jato, M.J. Alonso, Development of positively charged colloidal drug carriers: Chitosan-coated polyester nanocapsules and submicron-emulsions, Colloid Polym. Sci. 275 (1997) 46–53. https://doi.org/10.1007/s003960050050.

[23] D.P. Ivanov, A.M. Grabowska, M.C. Garnett, High-throughput spheroid screens using volume, resazurin reduction, and acid phosphatase activity, Methods Mol. Biol. 1601 (2017) 43–59. https://doi.org/10.1007/978-1-4939-6960-9_4.

[24] C.E. Gómez, B. Perdiguero, L. Usero, L. Marcos-Villar, L. Miralles, L. Leal, C.Ó.S. Sorzano, C. Sánchez-Corzo, M. Plana, F. García, M. Esteban, Enhancement of the HIV-1-Specific Immune Response Induced by an mRNA Vaccine through Boosting with a Poxvirus MVA Vector Expressing the Same Antigen, Vaccines. 9 (2021) 1–17. https://doi.org/10.3390/vaccines9090959.

[25] S. Sharma, T.K. Mukkur, H.A. Benson, Y. Chen, Enhanced immune response against pertussis toxoid by IgA-loaded chitosan-dextran sulfate nanoparticles, J. Pharm. Sci. 101 (2012) 233–244. https://doi.org/10.1002/jps.22763.

[26] S. Sharma, H.A.E. Benson, T.K.S. Mukkur, P. Rigby, Y. Chen, Preliminary studies on the development of IgA-loaded chitosan-dextran sulphate nanoparticles as a potential nasal delivery system for protein antigens, J. Microencapsul. 30 (2013) 283–294. https://doi.org/10.3109/02652048.2012.726279.

[27] J.V. González-Aramundiz, M. Peleteiro Olmedo, Á. González-Fernández, M.J. Alonso Fernández, N.S. Csaba, Protamine-based nanoparticles as new antigen delivery systems, Eur. J. Pharm. Biopharm. 97 (2015) 51–59. https://doi.org/10.1016/j.ejpb.2015.09.019.

[28] I. Ruseska, K. Fresacher, C. Petschacher, A. Zimmer, Use of protamine in nanopharmaceuticals—a review, Nanomaterials. 11 (2021). https://doi.org/10.3390/nano11061508.

[29] Y. Lin, B. Sun, Z. Jin, K. Zhao, Enhanced Immune Responses to Mucosa by Functionalized Chitosan-Based Composite Nanoparticles as a Vaccine Adjuvant for Intranasal Delivery, ACS Appl. Mater. Interfaces. 14 (2022) 52691–52701. https://doi.org/10.1021/acsami.2c17627.

[30] N.N. Zhang, X.F. Li, Y.Q. Deng, H. Zhao, Y.J. Huang, G. Yang, W.J. Huang, P. Gao, C. Zhou, R.R. Zhang, Y. Guo, S.H. Sun, H. Fan, S.L. Zu, Q. Chen, Q. He, T.S. Cao, X.Y. Huang, H.Y. Qiu, J.H. Nie, Y. Jiang, H.Y. Yan, Q. Ye, X. Zhong, X.L. Xue, Z.Y. Zha, D. Zhou, X. Yang, Y.C. Wang, B. Ying, C.F. Qin, A Thermostable mRNA Vaccine against COVID-19, Cell. 182 (2020) 1271-1283.e16. https://doi.org/10.1016/j.cell.2020.07.024.

[31] B. Bogaert, F. Sauvage, R. Guagliardo, C. Muntean, V.P. Nguyen, E. Pottie, M. Wels, A.K. Minnaert, R. De Rycke, Q. Yang, D. Peer, N. Sanders, K. Remaut, Y.M. Paulus, C. Stove, S.C. De Smedt, K. Raemdonck, A lipid nanoparticle platform for mRNA delivery through repurposing of cationic amphiphilic drugs, J. Control. Release. 350 (2022) 256–270.

https://doi.org/10.1016/j.jconrel.2022.08.009.

[32] J. You, M. Kamihira, S. Iijima, Surfactant-mediated gene transfer for animal cells, Cytotechnology. 25 (1997) 45–52. https://doi.org/10.1023/A:1007955631313.

[33] K. Palucka, J. Banchereau, I. Mellman, Designing Vaccines Based on Biology of Human Dendritic Cell Subsets, Immunity. 33 (2010) 464–478. https://doi.org/10.1016/j.immuni.2010.10.007.

[34] R. Firdessa-Fite, R.J. Creusot, Nanoparticles versus Dendritic Cells as Vehicles to Deliver mRNA Encoding Multiple Epitopes for Immunotherapy, Mol. Ther. - Methods Clin. Dev. 16 (2020) 50–62. https://doi.org/10.1016/j.omtm.2019.10.015.

[35] Y. Zeng, O. Escalona-Rayo, R. Knol, A. Kros, B. Slütter, Lipid nanoparticle-based mRNA candidates elicit potent T cell responses, Biomater. Sci. 11 (2023) 964–974. https://doi.org/10.1039/D2BM01581A.

[36] D.C. Jürgens, L. Deßloch, D. Porras-Gonzalez, J. Winkeljann, S. Zielinski, M. Munschauer, A.L. Hörner, G. Burgstaller, B. Winkeljann, O.M. Merkel, Lab-scale siRNA and mRNA LNP manufacturing by various microfluidic mixing techniques – an evaluation of particle properties and efficiency, OpenNano. 12 (2023) 100161. https://doi.org/10.1016/j.onano.2023.100161.

[37] B. Garulli, M.G. Stillitano, V. Barnaba, M.R. Castrucci, Primary CD8+ T-cell response to soluble ovalbumin is improved by chloroquine treatment in vivo, Clin. Vaccine Immunol. 15 (2008) 1497–1504. https://doi.org/10.1128/CVI.00166-08.

[38] T.G. Dacoba, A. Olivera, D. Torres, J. Crecente-Campo, M.J. Alonso, Modulating the immune system through nanotechnology, Semin. Immunol. 34 (2017) 78–102. https://doi.org/10.1016/j.smim.2017.09.007.

[39] P. Moss, The T cell immune response against SARS-CoV-2, Nat. Immunol. 23 (2022) 186–193. https://doi.org/10.1038/s41590-021-01122-w.

[40] K. Schroder, P.J. Hertzog, T. Ravasi, D.A. Hume, Interferon-γ: an overview of signals, mechanisms and functions, J. Leukoc. Biol. 75 (2004) 163–189. https://doi.org/10.1189/jlb.0603252.

[41] Y. Shi, J. Huang, Y. Liu, J. Liu, X. Guo, J. Li, L. Gong, X. Zhou, G. Cheng, Y. Qiu, J. You, Y. Lou, Structural and biochemical characteristics of mRNA nanoparticles determine anti–SARS-CoV-2 humoral and cellular immune responses, Sci. Adv. 8 (2022) 1–14. https://doi.org/10.1126/sciadv.abo1827.

[42] Y. Liu, L. Huang, Designer lipids advance systemic siRNA delivery, Mol. Ther. 18 (2010) 669–670. https://doi.org/10.1038/mt.2010.39.

[43] K.A. Whitehead, J.R. Dorkin, A.J. Vegas, P.H. Chang, O. Veiseh, J. Matthews, O.S. Fenton, Y. Zhang, K.T. Olejnik, V. Yesilyurt, D. Chen, S. Barros, B. Klebanov, T. Novobrantseva, R. Langer, D.G. Anderson, Degradable lipid nanoparticles with predictable in vivo siRNA delivery activity, Nat. Commun. 5 (2014). https://doi.org/10.1038/ncomms5277.

[44] K.J. Kauffman, J.R. Dorkin, J.H. Yang, M.W. Heartlein, F. Derosa, F.F. Mir, O.S. Fenton, D.G. Anderson, Optimization of Lipid Nanoparticle Formulations for mRNA Delivery in Vivo with Fractional Factorial and Definitive Screening Designs, Nano Lett. 15 (2015) 7300–7306.

https://doi.org/10.1021/acs.nanolett.5b02497.

[45] R.A. Seder, R. Ahmed, Similarities and differences in CD4+ and CD8+ effector and memory T cell generation, Nat. Immunol. 4 (2003) 835–842. https://doi.org/10.1038/ni969.

[46] G. Alter, J.M. Malenfant, M. Altfeld, CD107a as a functional marker for the identification of natural killer cell activity, J. Immunol. Methods. 294 (2004) 15–22. https://doi.org/10.1016/j.jim.2004.08.008.

OVERALL DISCUSSION

1. OVERALL DISCUSSION

Gene therapies are emerging and groundbreaking solutions for a wide range of medical challenges, owing to their ability to influence, inhibit, or modify the expression of specific crucial genes involved in the progression and development of certain diseases [1,2]. Over the past few decades, numerous chemical modifications have been used to optimize oligonucleotides, aiming to improve their efficacy, protection, or delivery capabilities [3,4]. Despite these advancements, delivery systems remain pivotal components of the genetic therapy strategies, aiming to reach diverse tissues and enhance the stability and protection of oligonucleotides [5,6]. For instance, lipid nanoparticles (LNPs) are the most well-known nanocarriers for ribonucleic acid (RNA) delivery [7,8]. However, LNPs are mainly delivered to the liver, limiting their use in other tissues or diseases. Consequently, alternative nanocarriers or delivery strategies are being explored to improve the delivery and applications of genetic therapeutics [5,9].

Within the framework of this work, we have developed various nanoemulsions (NE) and nanocapsules (NCs) as carriers for different genetic cargos, including small interfering RNA (siRNA), microRNA-mimics (miRNA) and messenger RNA (mRNA), intended for delivery into the central nervous system (CNS) or deployment as vaccines. Our group was among the first to develop polymer-based nanocarriers for polynucleotide delivery. Some of these nanocarriers were intended to deliver plasmid deoxyribonucleic acid (pDNA) across ocular and respiratory mucosa [10–12]. More recently, we developed encapsulated polymeric nanocomplexes for the nose-to-brain (N-to-B) delivery of miRNA. These nanocarriers were found to have access to distinct brain regions and modulate the targeted mRNA levels [13]. In the area of cancer, we have also designed nanocapsules loaded with miRNA, with the capacity to modulate the tumor microenvironment [14]. Finally, we have explored the functionalization of LNPs for the targeted delivery of siRNA in a lung tumor animal model. The results showed an increased tumor accumulation and a significant reduction of tumor growth as compared to the untargeted nanocarriers [15].

Moreover, our laboratory has decades of experience in the field of vaccinology. Initially, efforts were made to design poly(lactic acid) microparticles and different derivatives for the development of a single-dose vaccine against tetanus toxoid [16,17]. Building upon this foundation, we have developed various polymeric NPs and NCs aimed at modulating the immune response against multiple pathogens, including tetanus toxoid, hepatitis B, and uropathogenic *E. coli*, following either parenteral or nasal administration [18–27]. More recently, we have designed a human immunodeficiency virus (HIV) vaccine, comprising a polysaccharide NP for peptide antigen delivery, yielding promising immune responses and protection against viral infection in macaques following nasal administration [28].

Considering this background, this PhD thesis is organized into three different chapters, each addressing the following topics:

1. The design of ionizable NEs for facilitating the diffusion of diverse oligonucleotides within the brain.
2. The development of NEs and polymeric NCs for the N-to-B and intracerebroventricular (ICV) delivery of siRNA.

3. The potential of NEs and polymeric NCs as a vaccine against the severe acute respiratory syndrome coronavirus 2 (SARS-CoV-2).

1.1. IONIZABLE NANOEMULSIONS FOR RNA DELIVERY IN THE BRAIN

Among the numerous challenges associated with the delivery of genetic material to the CNS, a major hurdle that remains unaddressed is the limited diffusivity of nanoparticles. For example, the current gold standard for RNA delivery, LNPs, can only diffuse approximately 1-1.5 mm from the site of injection in the brain [29,30]. This restricted mobility can be attributed to the dense inner core of the LNPs, which confers relatively high rigidity to these nanocarriers [31].

Given this context, our hypothesis is founded on the combination of the potency of the LNPs, with more fluid and deformable cores, similar to those present in NEs, to engineer the next generation of ionizable NEs (iNEs) (Figure 1). The designed iNE consisted of a classical LNP containing C12-200 as an ionizable lipid, known for enhancing the endosomal scape [32]. The substitution of cholesterol with an oil (Vitamin E) was intended to enhance the core flexibility.

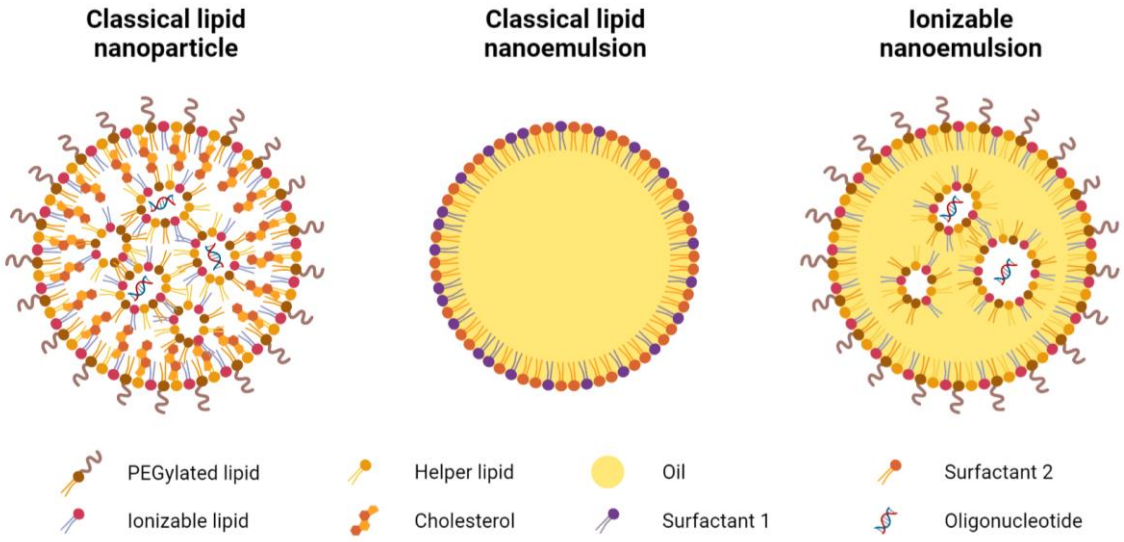

Figure 1. Hypothetical schematic representation of LNPs (left), NEs (middle), and iNE (right)

Abbreviations: iNE: ionizable nanoemulsion. NE: nanoemulsion. LNP: lipid nanoparticle. Created with https://biorender.com.

To prove the versatility of the developed iNE, various types of oligonucleotides were used to formulate the nanocarrier (Table 1). Notably, no significant differences in physicochemical properties were found across all formulations, with consistent sizes around 70 nm and neutral surface charges. Moreover, regardless of oligonucleotide type, over 80% of the RNA was fully encapsulated within the iNE. Importantly, these properties remained unchanged after subjecting the iNE to a more than 9-fold concentration process. This highlights the multifunctionality of the iNE, capable of entrapping various types of nucleic acids without altering their physicochemical characteristics.

Table 1. Physicochemical properties of iNE developed, in combination with siGFP, mGFP, and miR-132

Type of RNA	Size (nm)	PDI	ζ-Potential (mV)	Encapsulation efficiency (%)
siGFP	64 ± 7	0.23 ± 0.03	-2 ± 1	80-90
miR-132	60 ± 7	0.2 ± 0.05	-1 ± 1	80-90
mGFP	72 ± 9	0.17 ± 0.07	-4 ± 2	80-90

Encapsulation efficiency was measured by agarose gel, and values were corroborated by RiboGreen assay. **Abbreviations:** GFP: green fluorescence protein. mGFP: mRNA encoding GFP. miR-132: miRNA-132 mimic. PDI: polydispersity index. siGFP: siRNA anti-GFP. Values represent the mean ± standard deviation (n ≥ 3).

The diffusivity potential of the developed iNE was assessed in an Alzheimer's disease mouse model, using miRNA-132 mimic (miR-132) as the nucleic acid cargo (Figure 2). miR-132 is known to be downregulated in Alzheimer's disease progression, and restoring it in the hippocampus can restore neurogenesis and memory deficits in Alzheimer's disease animal models [33]. iNE-miR-132 was administered to the dentate gyrus (DG), a region severely affected by Alzheimer's disease, and miR-132 levels were determined in both the DG and the Cornu Ammonis (CA), a surrounding hippocampus region [34,35]. For comparison, the classical LNP used in Ompattro® was employed to encapsulate miR-132, given its established reputation as a nanocarrier for RNA interference (RNAi) delivery [36,37].

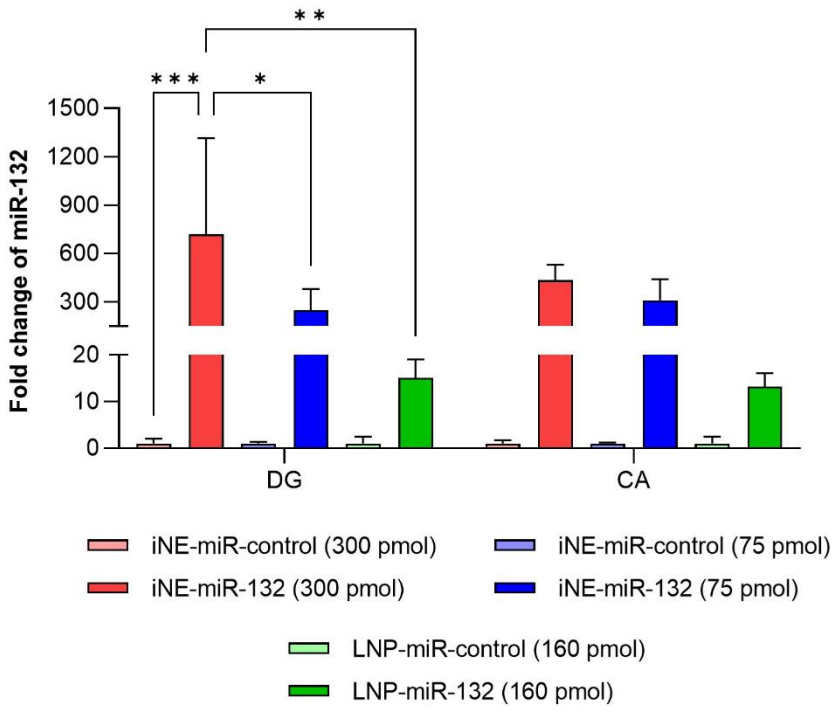

Figure 2. Semi-quantitative real-time PCR of miR-132 levels in the DG and surrounding CA regions, 48 hours post-injection of iNE (at a dose of 300 pmol in red, and 75 pmol in blue) and LNPs (green), loaded with miR-132 (bright color) or miR-control (pale color)

Abbreviations: iNE: ionizable nanoemulsions. LNP: lipid nanoparticle. miR-132: miRNA-132 mimic. A significant comparison was performed using two-way ANOVA followed by Turkey's multiple comparison tests between groups. *p*-values < 0.05 were considered statistically significant (*). Also, (**) if *p*-value < 0.01, (***) if *p*-value < 0.001. Values represent the mean ± standard deviation (n ≥ 3).

Various miR-132 concentrations were tested: 300 and 85 pmol for the iNE, and an intermediate concentration of 160 pmol for the LNP. In all cases, a miR-control was employed to discern if miR-132 levels were influenced by other regulatory pathways. iNE exhibited a significant accumulation in the DG, followed by diffusion to the CA in a dose-dependent manner, indicating specific modulation of miR-132 levels. At the highest concentration tested (300 pmol), iNE-miR-132 demonstrated a more than 600-fold increase in miR-132 levels in the DG, and over 400-fold increase in CA, highlighting the diffusion potential of the carrier. Even at the lowest concentration (75 pmol), iNE-miR-132 induced an approximately 300-fold increase in both the DG and the CA, surpassing the performance of LNP-miR-132, tested at a higher concentration (160 pmol). These results emphasize the diffusivity capacity of iNE, compared to classical LNPs, allowing them to efficiently reach different brain regions.

To further assess the diffusivity of iNEs, intra-parenchymal administration was performed with iNE-mRNA encoding green fluorescence protein (mGFP) (Figure 3). The results showed a substantial diffusion of the iNE from the administration site to various brain regions, along with a successful cellular transfection. Overall, these findings confirm the diffusion and transfection efficiency within the injected hemisphere reaffirming the potential of iNEs for RNA brain delivery.

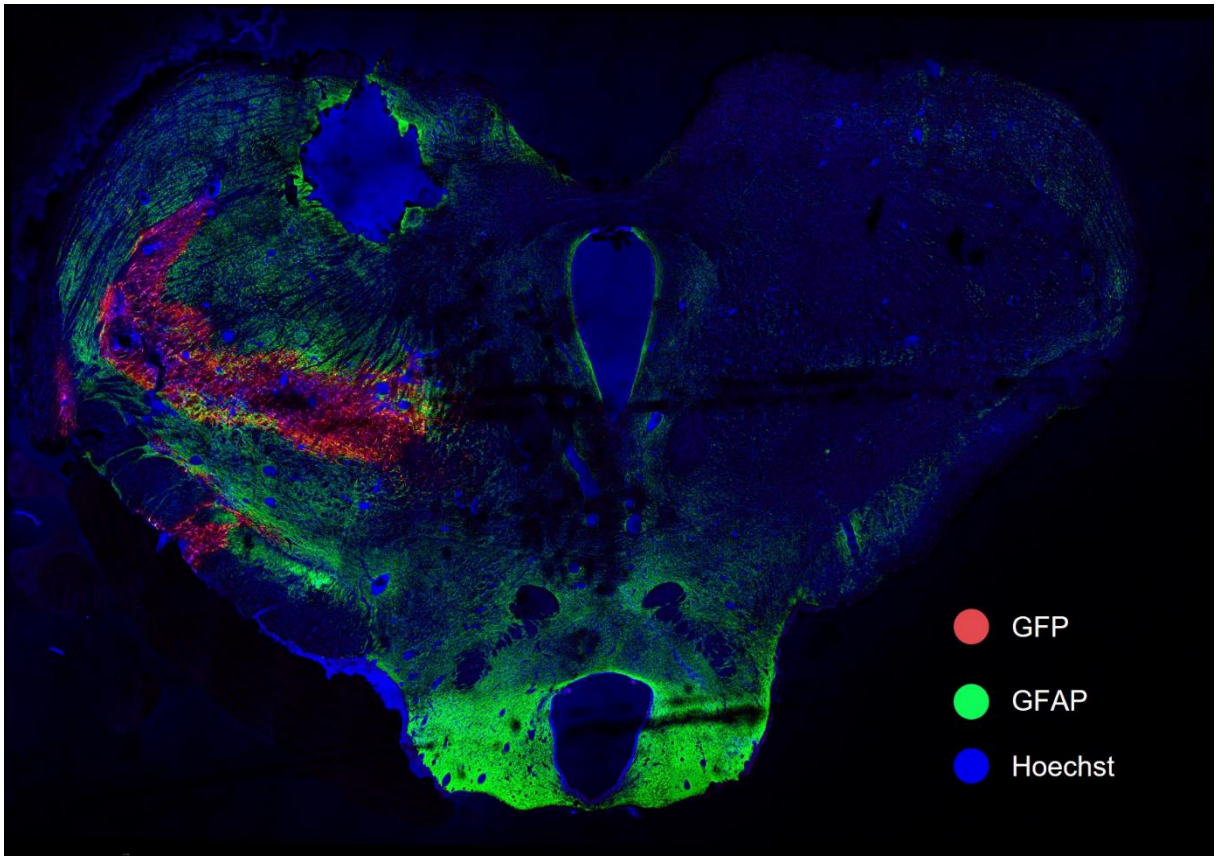

Figure 3. Double immunolabeling in the whole brain for GFP (red) and astrocytes (marked with GFAP, green), after intraparenchymal administration of iNE-mGFP. Hoechst was used as nuclei marker (blue)

Abbreviations: GFAP: glial fibrillary acidic protein. GFP: green fluorescence protein. iNE: ionizable nanoemulsion. mGFP: mRNA encoding GFP.

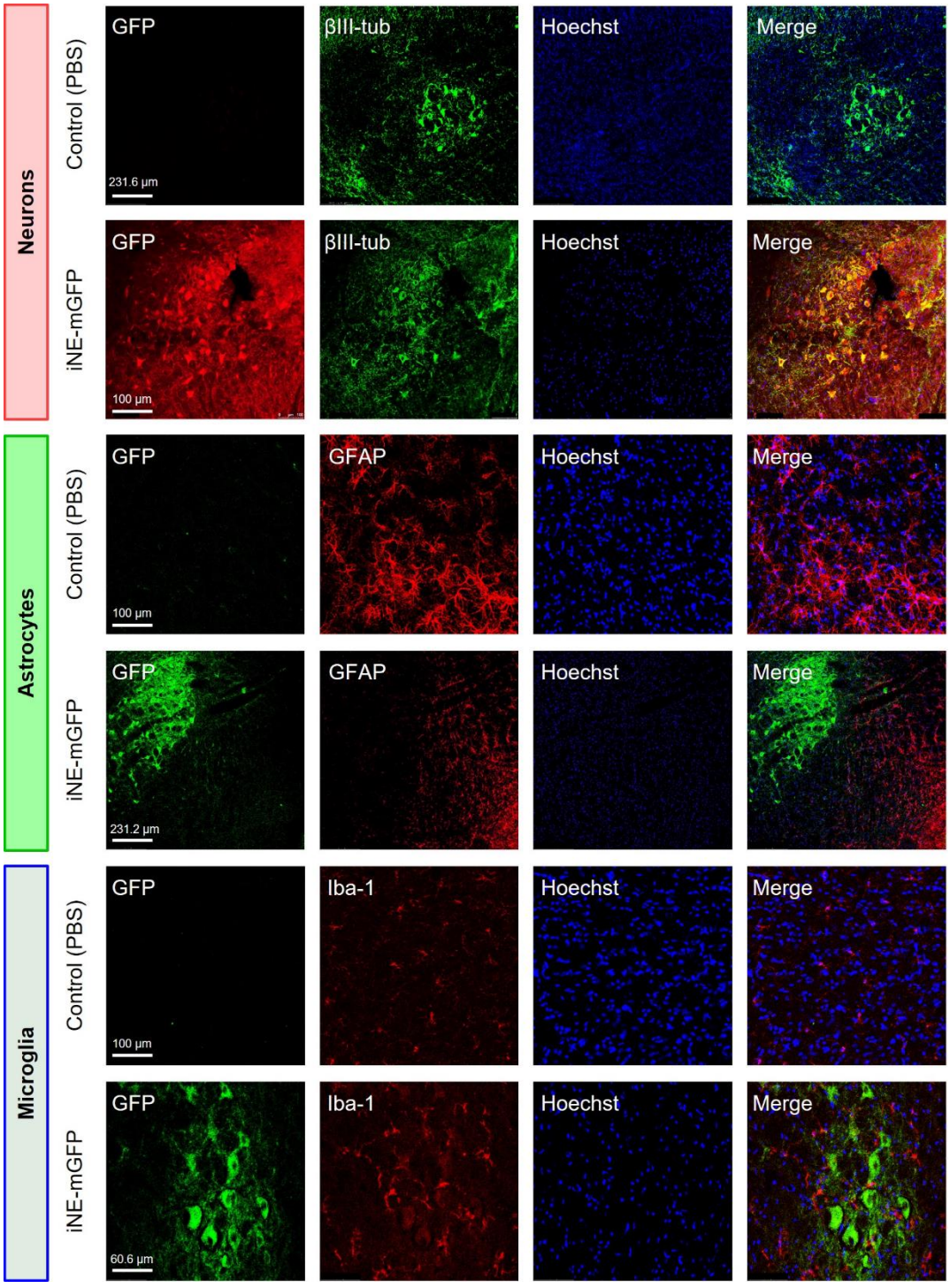

Figure 4. Immunolabelling for GFP in neurons (labeled with ßIII-tubulin), astrocytes (labeled with GFAP), and microglia (labeled with Iba-1) cells in rats after intraparenchymal administration of control or iNE-mGFP. Hoechst was used as nuclei marker

Abbreviations: ßIII-tubulin: class III ß-tubulin. GFAP: glial fibrillary acidic protein. GFP: green fluorescence protein. Iba-1: ionized calcium-binding adaptor molecule 1. iNE: ionizable nanoemulsion. mGFP: mRNA encoding GFP.

Finally, the images in Figure 4 show the GFP signal in neurons and microglia, thus indicating the uptake of the iNE-mGFP by these cell types and subsequent translation of the reporter fluorescence protein. This behavior was less prominent in astrocytes, suggesting the specificity of iNE uptake by neurons and microglia. These findings hold promise for treating neuron-specific conditions, like amyotrophic lateral sclerosis (ALS), or diseases related to microglia malfunction, such as Alzheimer's disease or Parkinson's disease [38,39]. However, the explanation for this preferred uptake by neurons and microglia remains unclear at this point.

In brief, this part of the thesis outlines the development of an iNE as a novel highly diffusive nanocarrier for RNA delivery to the brain. Nevertheless, further studies are required to validate this potential for treating CNS diseases, such as Alzheimer's or Parkinson's diseases. Additionally, the exploration of less invasive administration routes that do not imply direct brain injection, such as N-to-B, could be a promising avenue for further research.

1.2. NANOEMULSIONS AND POLYMERIC NANOCAPSULES FOR NOSE-TO-BRAIN AND INTRACEREBROVENTRICULAR DELIVERY OF SIRNA

Access to the CNS is primarily impeded by the presence of the blood-brain barrier (BBB), which plays a fundamental role in maintaining CNS homeostasis. However, this defense mechanism presents a significant challenge for delivering therapeutics into the brain [40–43]. Overcoming the BBB is a major challenge in CNS disease therapy, and researchers have explored various technological approaches to facilitate transport into the brain [44,45]. Among these approaches, the use of alternative delivery routes in combination with delivery systems has the potential to revolutionize CNS disease treatment. These methods aim to facilitate the delivery of biological cargo, including RNA therapeutics, using less invasive delivery routes and improving their ability to diffuse within different regions of the brain.

To achieve a successful siRNA delivery into the CNS, we have developed a library of NEs and polymeric NCs capable of encapsulating, protecting, and delivering siRNA to the CNS. These nanocarriers can be administered through promising alternative routes, including N-to-B and ICV administrations. Initially, we conducted a screening to select adequate oils and surfactants, aiming to generate a collection of nanocarriers with specific characteristics: a particle size below or around 100 nm, reproducible and scalable production, various surface charges (including positive, negative, and neutral), a final siRNA concentration of at least 0.25 mg/mL, and stability of at least one-month at 4 °C. Five different NEs met these requirements in terms of particle size (bellow 100 nm) and surface charge (positively charged), with an overall encapsulation efficiency close to 100% (Table 2). Among these NEs, NE-2 was successfully functionalized with the rabies virus glycoprotein (RVG), which facilitates cellular entry and virus fusion and has the capacity to bind to the nicotinic acetylcholine receptor, present in the CNS [46].

Due to their small particle size, NE-2 and NE-3 were selected for further coating with a polymeric shell, resulting in the formation of siRNA-loaded NCs (Table 3). Various polymers were employed to formulate these NCs, including polyethylene glycol-polyglutamic acid (PEG-PGA), hyaluronic acid (HA), polysialic acid (PSA), and chitosan (CS). The resulting nanocarriers exhibited a range of particle sizes and surface charges, spanning from highly negative (as in the case of NC-3, with a surface charge of -48 mV, attributed to the external HA coating), to highly positive (as seen in MNC-1, consisting of a double polymeric layer of HA

and CS, resulting in a surface charge of +49 mV). Additionally, neutral nanocarriers like NC-1 were obtained, due to the PEG-PGA shell.

Given the potential of these developed nanocarriers, specific candidates were chosen based on their physicochemical properties for testing in animal models. This involved exploring alternative administration routes, such as N-to-B and ICV routes.

Table 2. Physicochemical properties of siRNA-loaded NE-1, NE-2, NE-3, NE-4 and NE-5

	NE-1	NE-2	NE-2-RVG	NE-3	NE-4	NE-5
Composition	DOTAP: Vit E: K-HS15®	DOTAP: Vit E: Tween 80	DOTAP: Vit E: Tween 80 + RVG	DOTAP: Lab™: Tween 80	DOTAP: Vit E: Labrasol®	DOTAP: Vit E: Inulin
Molar ratio (mol%)	16.9:65.8: 17.3	19.4:75.4: 5.2	19.4:75.4: 5.1:0.1	25:56.5: 18.5	19.4:75.4: 5.2	19.4:75.4: 5.2
Particle diameter (nm)	90 ± 16	73 ± 10	84 ± 37	86 ± 10	100 ± 8	68 ± 5
PDI	0.20 ± 0.04	0.20 ± 0.04	0.25 ± 0.01	0.24 ± 0.03	0.18 ± 0.01	0.26 ± 0.03
ζ-Potential (mV)	+51 ± 3	+47 ± 4	+57 ± 6	+38 ± 6	+50 ± 3	+48 ± 2
Encapsulation efficiency (%)	100	100	100	100	100	100

Encapsulation efficiency was measured by agarose gel, and values were corroborated by RiboGreen assay and/or UPLC analysis. **Abbreviations:** DOTAP: 1,2-dioleoyl-3-trimethylammonium-propane chloride. K-HS15®: Kolliphor® HS15. Lab™: Labrafac™ Lipophile, WL 1349. NE: nanoemulsion. PDI: polydispersity index. RVG: rabies virus glyocoprotein. Vit E: D, L-α-tocopherol. Values represent the mean ± standard deviation (n ≥ 3).

Table 3. Physicochemical properties of siRNA-loaded NC-1, NC-2, NC-3, NC-4, NC-5 and MNC-1

	NC-1	NC-2	NC-3	NC-4	NC-5	MNC-1
Base nanosystem	NE-2	NE-2	NE-2	NE-3	NE-3	NC-2
Base composition	DOTAP: Vit E: T80	DOTAP: Vit E: T80	DOTAP: Vit E: T80	DOTAP: Lab™: T80	DOTAP: Lab™: T80	DOTAP: Vit E: T80 + HA
Polymer coating	PEG-PGA	HA	PSA	HA	PSA	CS
siRNA: polymer ratio (mol/mol)	1:2	1:4	-	1:4	-	-
siRNA: polymer ratio (w/w)	-	-	1:2	-	1:4	1:3.8
Particle diameter (nm)	73 ± 5	87 ± 6	116 ± 3	70 ± 8	79 ± 11	100 ± 16
PDI	0.15 ± 0.03	0.15 ± 0.02	0.13 ± 0.03	0.24 ± 0.03	0.23 ± 0.02	0.18 ± 0.02
ζ-Potential (mV)	-1 ± 6	-28 ± 2	-48 ± 1	-23 ± 5	-44 ± 8	+49 ± 4
Encapsulation efficiency (%)	100	100	100	100	100	100

Encapsulation efficiency was measured by agarose gel, and values were corroborated by RiboGreen assay and/or UPLC analysis. **Abbreviations:** CS: chitosan. DOTAP: 1,2-dioleoyl-3-trimethylammonium-propane chloride. HA: hyaluronic acid (40 kDa). Lab™: Labrafac™ Lipophile, WL 1349. MNC: multi-layer nanocapsule. mol/mol: mol to mol ratio. NC: nanocapsule. NE: nanoemulsion. PEG-PGA: PEG (5 kDa)-b-PGA (10) (Na). PDI: polydispersity index. PSA: polysialic acid (30 kDa). T80: Tween 80. Vit E: D, L-α-tocopherol. w/w: weight-to-weight ratio. Values represent the mean ± standard deviation (n ≥ 3).

N-to-B administration of NE-2, NE-2-RVG and NC-5, all containing siRNA-1, resulted in a noticeable accumulation in the nasal epithelium of all candidates, surpassing the accumulation observed with the positive control (LY-06D), as depicted in Figure 5 (top left). This increased retention could potentially facilitate access to the olfactory and trigeminal nerves [47,48]. Notably, only NE-2-RVG and NC-5 demonstrated increased accumulation in the olfactory bulb, indicating access via the olfactory nerves (Figure 5, top right). These results suggest that positively charged NPs (NE-2) may become entrapped within the nasal cavity, while negatively charged or those functionalized with targeting ligands (NC-5 and NE-2-RVG, respectively) might exhibit an enhanced diffusion into the olfactory bulb. Conversely, minor accumulation was observed in the trigeminal nerve and frontal cortex (Figure 5, bottom). However, these results must be interpreted with caution due to the high experimental variability observed.

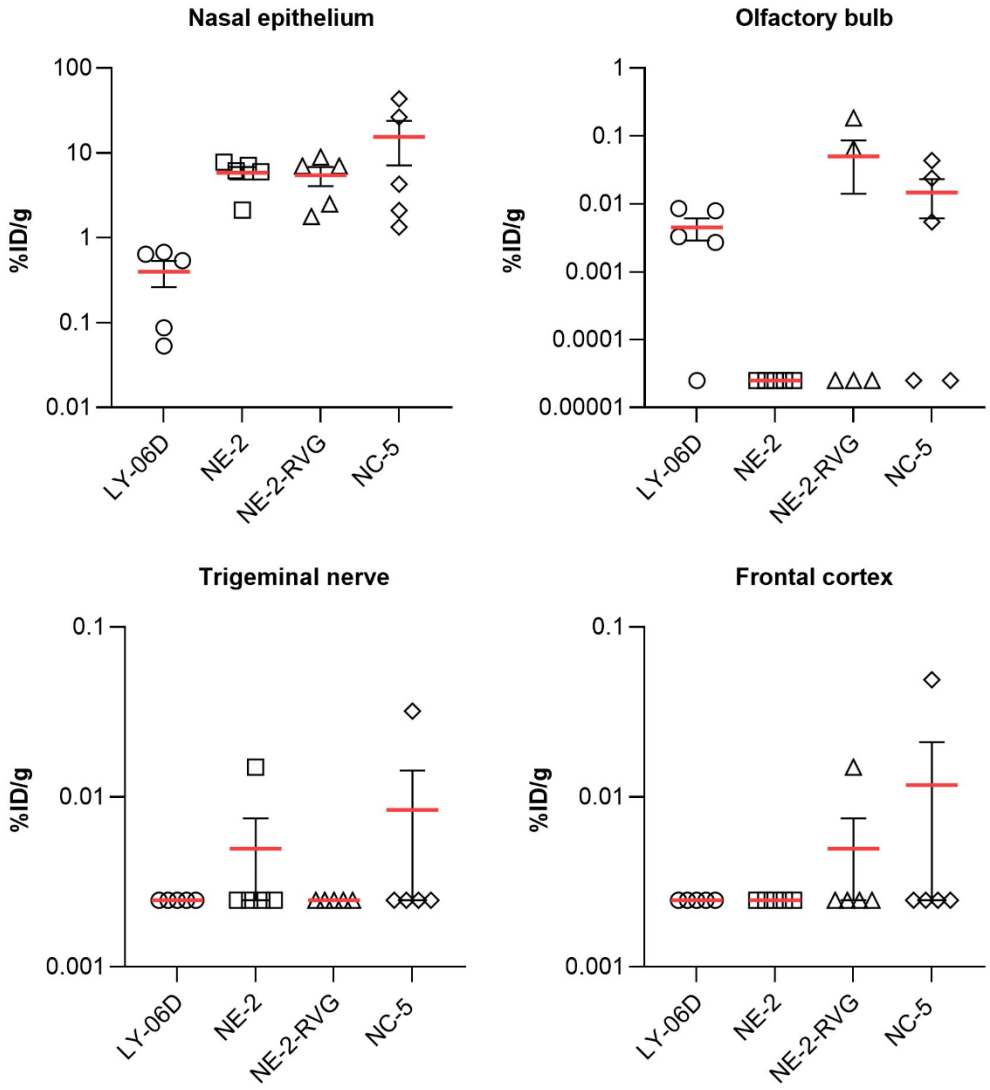

Figure 5. Mean percentage injected dose of siRNA-1 per gram (%ID/g) in different nasal and brain regions, including nasal epithelium (top, left), olfactory bulb (top, right), trigeminal nerve (bottom, left), and frontal cortex (bottom, right)

Abbreviations: LY-06D: internal positive control. NC: nanocapsule. NE: nanoemulsion. RVG: rabies virus glycoprotein. Values represent the mean ± standard deviation (n ≥ 3).

Lastly, the formulation named NC-1 was chosen for the evaluation of its diffusion and transfection performance upon ICV administration, using siRNA-2 as genetic cargo (Figure 6). This selection was based on its favorable physicochemical properties (73 nm and neutral surface charge), and the promising results obtained by our group using neutral, PEGylated nanocarriers for RNA brain delivery [49]. NC-1 resulted in a reduction of the targeted mRNA levels of over 50% in all the brain areas analyzed. These results hold particular significance when compared to previous literature on LNPs, which have shown lower reduction of the targeted mRNA levels with the same administration modality [29]. To the best of our knowledge, this marks the first time extensive silencing effects have been reported across the entire brain, demonstrating not only the diffusivity potential of NC-1, but also its capacity for gene silencing.

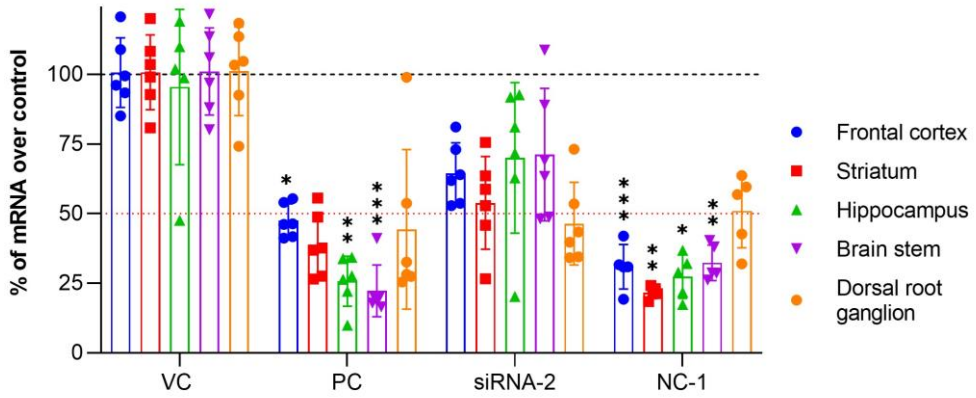

Figure 6. Quantitative qPCR of levels of targeted mRNA upon ICV administration of NC-1 encapsulating siRNA-2, in different brain areas, including the frontal cortex, striatum, hippocampus, brain stem, and dorsal root ganglion. Results were normalized using a housekeeping gene

Abbreviations: DRG: dorsal root ganglion. NC: nanocapsule. PC: internal positive control. VC: vehicle control (PBS). A significant comparison was performed using an ordinary one-way ANOVA followed by Tukey's multiple comparison tests of PC and NC-1 *vs*. siRNA-2. *p*-values < 0.05 were considered statistically significant (*). Also, (**) if *p*-value < 0.01, (***) if *p*-value < 0.001. Values represent the mean ± standard deviation (n ≥ 3).

Further observation of siRNA-2 confirmed the diffusion and distribution profile across the brain (Figure 7). Interestingly, the diffusion observed surpasses that of the current gold standard for RNA delivery, LNPs, which have been reported to only diffuse up to 4 mm from the administration site upon ICV injection [50]. Enhanced diffusion was observed in the areas proximate to the administration site, such as the striatum and frontal cortex, aligning nicely with the results obtained by PCR analysis (Figure 6).

To sum up, we have developed a library of multiple NEs and NCs for siRNA delivery to the brain. Among these candidates, NC-1 resulted in a highly promising nanocarrier for efficient siRNA diffusion and transfection within the brain. Given the preliminary evidence of delivery to the olfactory bulb following N-to-B administration, the potential applications of the diffusion and knockdown effects of NC-1 could benefit from less invasive routes, holding even greater promise for therapeutic use. Altogether, these results hold significant potential for the treatment of CNS conditions.

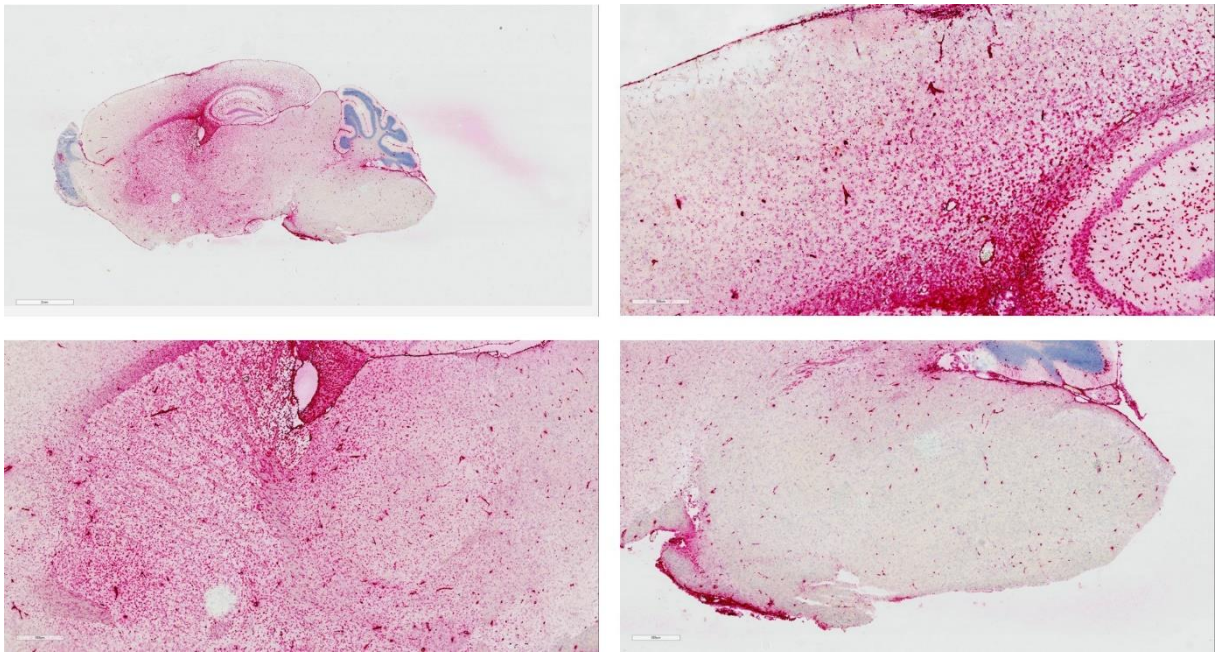

Figure 7. Detection of siRNA-2 in the brain after ICV administration of NC-1. Images were obtained for the complete brain (top, left), and close-up of the frontal cortex (top, right), the hippocampus (bottom, left), and the brain stem (bottom, right)

1.3. NANOEMULSIONS AND POLYMERIC NANOCAPSULES AS SARS-COV-2 VACCINES

On March 11, 2020, coronavirus disease 2019 (COVID-19) attained the status of global pandemic [51]. Researchers from around the world collaborated to develop vaccines against SARS-CoV-2, the virus responsible for the disease, which had resulted in over 760 million cases and 8 million deaths worldwide [52–54]. This collective effort led to the approval of two messenger RNA (mRNA) vaccines, Comirnaty® and Spikevax®, from BioNTech/Pfizer and Moderna, respectively. Both vaccines demonstrated over 90% protective efficacy against symptomatic SARS-CoV-2 infection and tolerable safety profiles in phase III clinical trials [55,56].

In April 2020, our laboratory joined the COVARNA consortium intending to develop an mRNA vaccine against SARS-CoV-2. Various mRNA constructs were developed to elicit the highest possible immune response against the receptor binding domain (RBD) of the spike protein on the surface of SARS-CoV-2, which is crucial for the virus' entry into the host cell. Four distinct mRNA immunogens were developed as part of this project: mRNA designed to stimulate T cell responses (SARS-CoV-2-T cells mRNA or mT), mRNA intended to elicit a B cell response (SARS-CoV-2-B cells mRNA or mB), mRNA encoding the RBD domain of the virus (SARS-CoV-2-RBD mRNA or mRBD) and mRNA encoding a highly immunogenic motif from the RBD domain (SARS-CoV-2-RBD_{epi} mRNA or $mRBD_{epi}$).

As a part of the consortium, we developed approximately 100 different prototypes of NEs and NCs for the entrapment and delivery of mRNA constructs. Among these prototypes, 15 were selected based on their ability to meet the target product profile criteria, including a particle size of less than or approximately 200 nm, excellent particle monodispersity, high

mRNA association efficiency, stability or potential for lyophilization, and compliance with the regulatory agency requirements (Table 4).

Table 4. Summary of the lipid compositions and molar ratios between the different components of the NEs (top) and NCs (bottom) investigated that successfully fulfill the target product profile

Nanosystem	Lipid composition	Molar composition (%)
NE-1	DOTAP: DOPE: Vit E	16.8: 15.7: 67.5
NE-2	DOTAP: DOPE: Vit E	40.7: 11.2: 48.1
NE-3	DOTAP: DOPE: Vit E: Tween 80	38.1: 10.5: 45.1: 6.4
NE-4	DOTAP: DOPE: Vit E: Tween 80	17.3: 8.1: 69.7: 4.9
NE-5	DOTAP: DOPE: Vit E: T80	46.2: 9: 35.6: 9.3

Nanosystem	Initial NE composition	Molar composition (%)	Polymer coating	w/w ratio
NC-1-PR	DOTAP: DOPE: Vit E	16.8: 15.7: 67.5	Protamine	1: 1
NC-3-PR	DOTAP: DOPE: Vit E: Tween 80	38.1: 10.5: 45.1: 6.4	Protamine	1: 1
NC-4-PR	DOTAP: DOPE: Vit E: Tween 80	17.3: 8.1: 69.7: 4.9	Protamine	1: 1
NC-3-DX	DOTAP: DOPE: Vit E: Tween 80	38.1: 10.5: 45.1: 6.4	Dextran Sulfate	1: 1
NC-4-DX	DOTAP: DOPE: Vit E: Tween 80	17.3: 8.1: 69.7: 4.9	Dextran Sulfate	1: 1 or 2: 1
NC-5-DX	DOTAP: DOPE: Vit E: Tween 80	46.2: 9: 35.6: 9.3	Dextran Sulfate	2: 1
NC-3-CS	DOTAP: DOPE: Vit E: Tween 80	38.1: 10.5: 45.1: 6.4	Chitosan	1: 1
NC-4-CS	DOTAP: DOPE: Vit E: Tween 80	17.3: 8.1: 69.7: 4.9	Chitosan	1: 1
NC-4-PP	DOTAP: DOPE: Vit E: Tween 80	17.3: 8.1: 69.7: 4.9	PEG-PGA	12: 1
NC-5-PP	DOTAP: DOPE: Vit E: Tween 80	46.2: 9: 35.6: 9.3	PEG-PGA	12: 1

Abbreviations: CS: chitosan. DOPE: 1,2-dioleoyl-3-trimethylammonium-propane chloride. DOTAP: 1,2-dioleoyl-3-trimethylammonium-propane chloride. DX: dextran sulfate. NE: nanoemulsion. NC: nanocapsule. PEG-PGA or PP: PEG (5 kDa)-b-PGA (10) (Na). PRT: protamine sulphate EP. Vit E: D, L-α-tocopherol. w/w ratio: weight-to-weight ratio between polymer and mRNA content.

These nanocarriers underwent several evaluations, including *in vitro* assessments using multiple cell lines (such as HeLa cells and human dendritic cells, using mGFP) and *in vivo* intramuscular administration of model mRNAs (mRNA encoding for luciferase). Overall, NC-4-DX, which consists of a NE containing DOTAP, DOPE, and Tween 80 (referred to as NE-4) and is coated with a dextran sulfate (DX) shell, exhibited superior performance compared to the others. These findings prompted the optimization of the N/P ratios used to prepare NE-4, and the w/w ratios for the DX shell (Figure 8, left and right, respectively).

Concerning the N/P ratio used, the transition from negatively charged surface to positively charged occurred at ratios greater than 1:1, as also demonstrated by the agarose gel results. A decision was made to employ a N/P ratio of 2:1, aiming for complete RNA complexation while avoiding potential toxicity effects associated with high N/P ratios [57]. Subsequently, NE-4 was employed to explore various weight-to-weight (w/w) ratios between the polymer and the RNA content. The objective was to reverse the highly positive charge of NE-4 while maintaining appropriate physicochemical properties. DX has previously been used as an adjuvant and antigen delivery system, capable of eliciting different T and B cellular responses [58,59]. Interestingly, no significant changes in particle size were found upon the incorporation of DX onto the nanocarrier, however, an increment on the negative charge was observed.

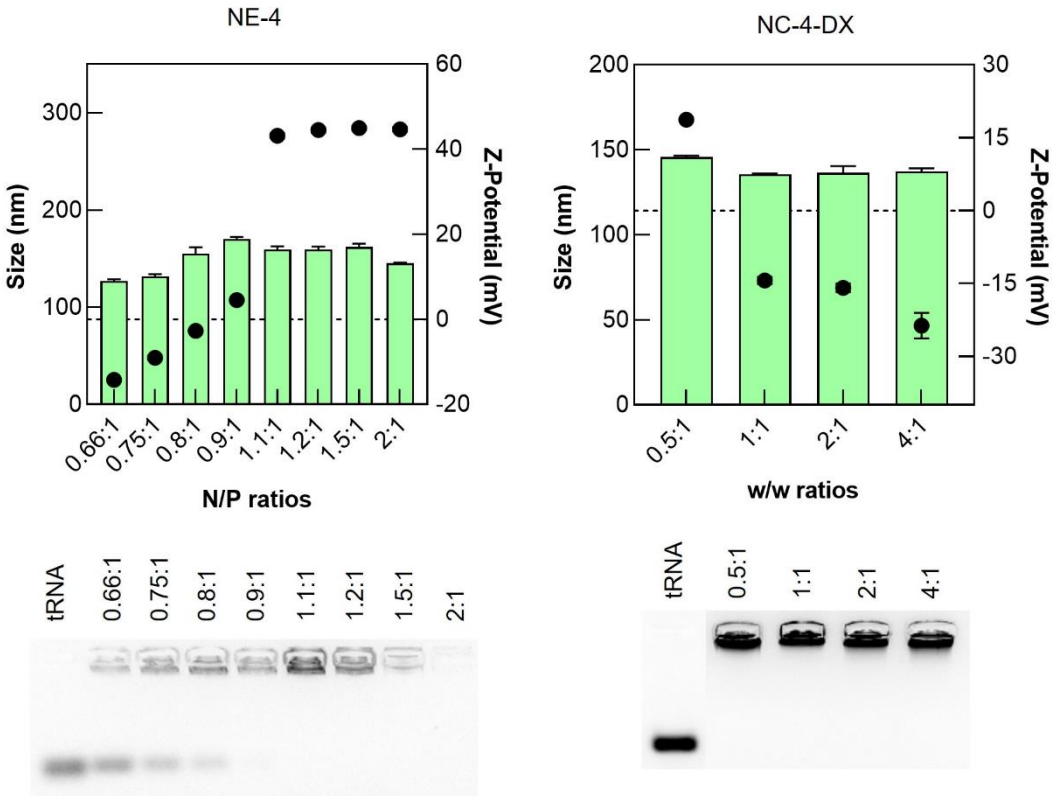

Figure 8. Physicochemical properties (top) and encapsulation efficiency (bottom) of NE-4-tRNA at different N/P ratios, and NC-4-DX-tRNA at different w/w ratios (left and right, respectively). Particle size corresponds with the left axis (bars), while surface charge corresponds with the right axis (dots)

Abbreviations: DX: dextran sulfate. NE: nanoemulsion. NC: nanocapsule. N/P ratio: nitrogen to phosphate ratio. tRNA: transfer RNA. w/w ratio: weight-to-weight ratio between the polymer and tRNA content.

Since NC-4-DX was our primary candidate, entrapment of different mRNAs was performed to assess its versatility. As indicated in Table 5, the particle size of NC-4-DX ranged from 105 to 130 nm, depending on the type of mRNA used, with consistently low polydispersity indices. Furthermore, the surface charge consistently remained negative, ranging from -13 to -20 mV. In all cases, the encapsulation efficiency exceeded 90%. These findings emphasize the potential of NC-4-DX as a delivery system for an mRNA vaccine candidate. This is particularly relevant in the case of SARS-CoV-2, as multiple mutations of the virus have required adjustments of the mRNA cargo, to maintain sufficient protective efficacy [60].

Table 5. Physicochemical properties of NC-4-DX with different types of mRNAs against SARS-CoV-2

Nanosystem	mRNA	w/w ratio	Particle diameter (nm)	PDI	ζ-Potential (mV)	EE (%)
NC-4-DX	mOVA	2: 1	132 ± 3	0.07 ± 0.03	-16 ± 2	100
NC-4-DX	mT	2: 1	111 ± 6	0.09 ± 0.02	-15 ± 5	100
NC-4-DX	mB	2: 1	114 ± 5	0.1 ± 0.02	-13 ± 5	100
NC-4-DX	mRBD	2: 1	109 ± 6	0.11 ± 0.01	-18 ± 2	90
NC-4-DX	$mRBD_{epi}$	2: 1	113 ± 6	0.09 ± 0.01	-19 ± 3	90
NC-4-DX	mT + mB	2: 1	113 ± 3	0.10 ± 0.02	-13 ± 4	100
NC-4-DX (n = 2)	mT + mRBD	2: 1	105 ± 1	0.09 ± 0.01	-19 ± 4	90
NC-4-DX (n = 2)	mT + $mRBD_{epi}$	2: 1	106 ± 1	0.10 ± 0.01	-17 ± 4	90

Abbreviations: DX: dextran sulfate. EE: encapsulation efficiency. mB: SARS-CoV-2-B cells mRNA. mRBD: SARS-CoV-2-RBD mRNA. $mRBD_{epi}$: SARS-CoV-2-RBD_{epi}. mT: SARS-CoV-2-T cells mRNA. NC: nanocapsule. PDI: polydispersity index. w/w ratio: weight-to-weight ratio between polymer and mRNA content. Values represent the mean ± standard deviation (n ≥ 3, unless indicated otherwise).

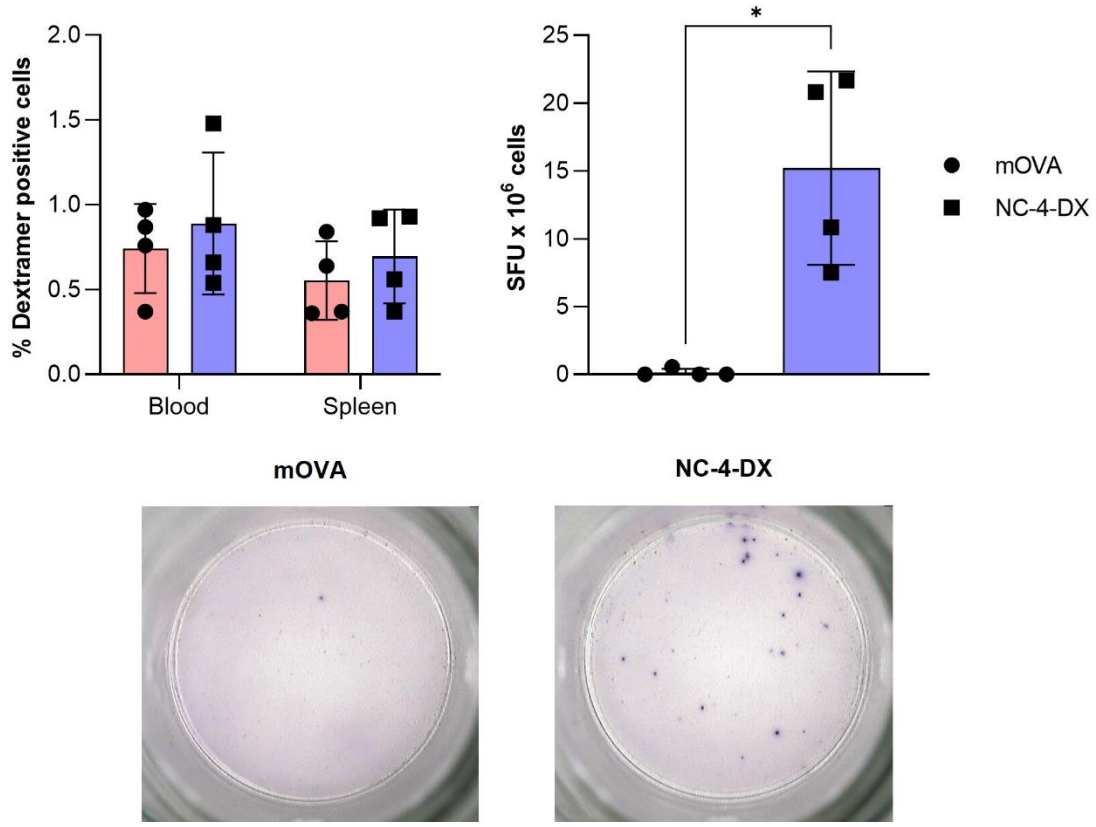

Figure 9. Percentage of dextramer-positive cells, obtained by flow cytometer, in the blood (collected on day 7 post-administration) and the spleen (collected on day 10 post-administration) (top, left), and IFN-γ-producing spot-forming units (SFU) from splenocytes, by ELISpot assay (collected in day 10-post administration) (top, right). Images of the INFγ-producing SFU of mOVA (bottom, left) and NC-4-DX (bottom, right)

Abbreviations: DX: dextran sulfate. IFN-γ: interferon gamma. mOVA: mRNA encoding ovalbumin protein. NC: nanocapsule. SFU: spot-forming units. A significant comparison was performed using multiple unpaired t-tests followed by a Welch correction. *p*-values < 0.05 were considered statistically significant (*). (n ≥ 3).

The first *in vivo* assessment of NC-4-DX as mRNA vaccine candidate involved the use of mRNA encoding the model immunology protein ovalbumin (OVA), known to induce $CD8^+$ T cell responses [61]. NC-4-DX was administered on days 0 and 7, with blood samples collected on day 7, and spleen samples on day 10. NC-4-DX-mOVA was found to elicit higher levels of dextramer-positive $CD8^+$ T cells than the free mOVA control, both in blood and spleen samples (Figure 9, top left). These activated $CD8^+$ T cells secreted interferon-gamma (IFN-γ), a cytokine involved in the immune response process [62]. Quantification of the IFN-γ responses concluded that NC-4-DX-mOVA induced higher levels of the cytokine compared to the free mOVA control (Figure 9, top right and bottom). These findings emphasize the significant role of the NC-4-DX in enhancing the immune responses triggered by the mRNA cargo, as both levels of $CD8^+$ T cells and IFN-γ induced by the nanoformulated mOVA surpassed those induced by the free mOVA control.

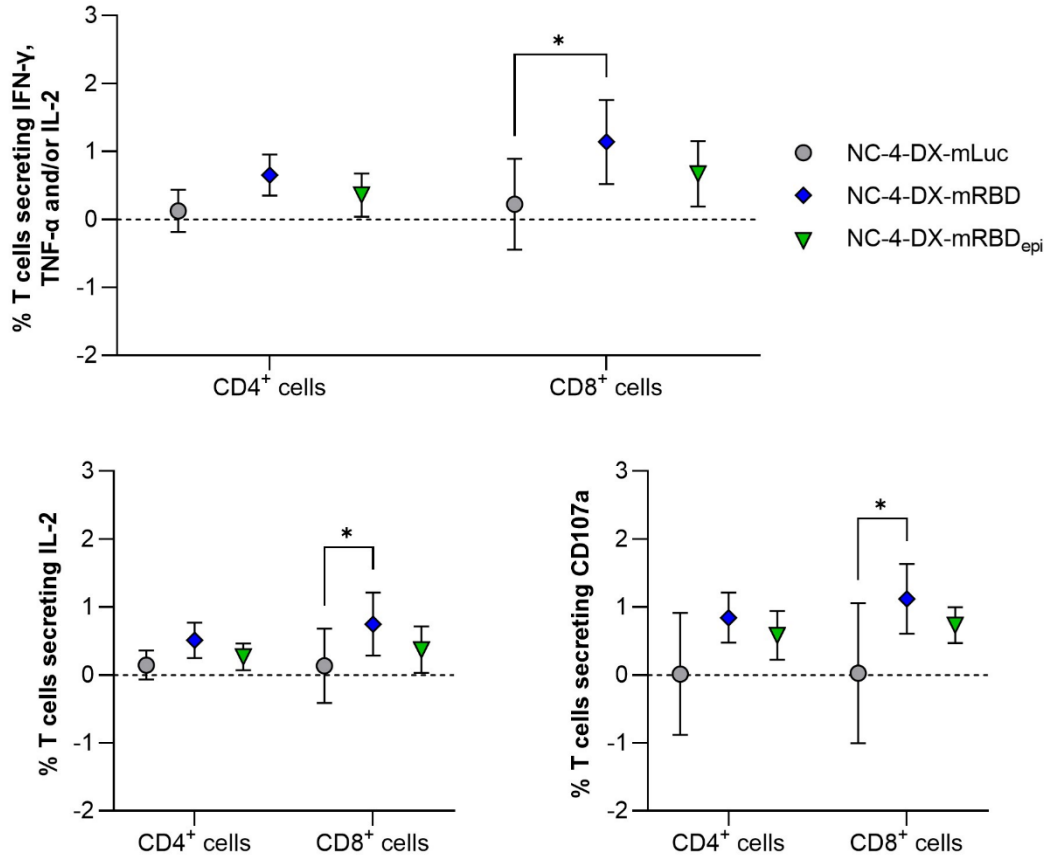

Figure 10. $CD4^+$ and $CD8^+$ T cell responses (top) considering IFN-γ, TNF-α, and IL-2 (bottom, left). C107a secretion from T cells was also determined (bottom, right)

Abbreviations: DX: dextran sulfate. IFN-γ: interferon gamma. IL-2: interleukin-2. mLuc: mRNA encoding luciferase. mRBD: SARS-CoV-2-RBD mRNA. $mRBD_{epi}$: SARS-CoV-2-RBD_{epi} mRNA. NC: nanocapsule. TNF-α: tumor necrosis factor-alpha. A significant comparison was performed using two-way ANOVA followed by Tukey's multiple comparison tests between groups. *p*-values < 0.05 were considered statistically significant (*). Values represent the mean ± standard deviation (n ≥ 3).

When used as a SARS-CoV-2 vaccine, NC-4-DX was evaluated in terms of the administration of a single mRNA (using the mRNAs developed for inducing B cell responses, namely mRBD and $mRBD_{epi}$, in Figure 10) or the combination of two mRNAs (one intended to induce T cell responses, mT, in combination mB, mRBD or $mRBD_{epi}$, in Figure 11). In all cases, animals received a prime administration at day 0 and a boost injection at day 21, and they were subsequently sacrificed and analyzed at day 36.

To distinguish the differences in the immunological responses between mRBD and $mRBD_{epi}$, both constructs were encapsulated onto NC-4-DX, and their $CD4^+$ and $CD8^+$ T cell responses were assessed (Figure 10, top). This evaluation revealed an overall stronger immune response when the construct mRBD was used. This was particularly evident in the case of $CD8^+$ T cell responses, where NC-4-DX-mRBD induced significantly higher responses in terms of $CD8^+$ T cells secreting IL-2 and CD107a, compared to the control group. These two cytokines play crucial roles in the immune responses mediated by T cells [63,64].

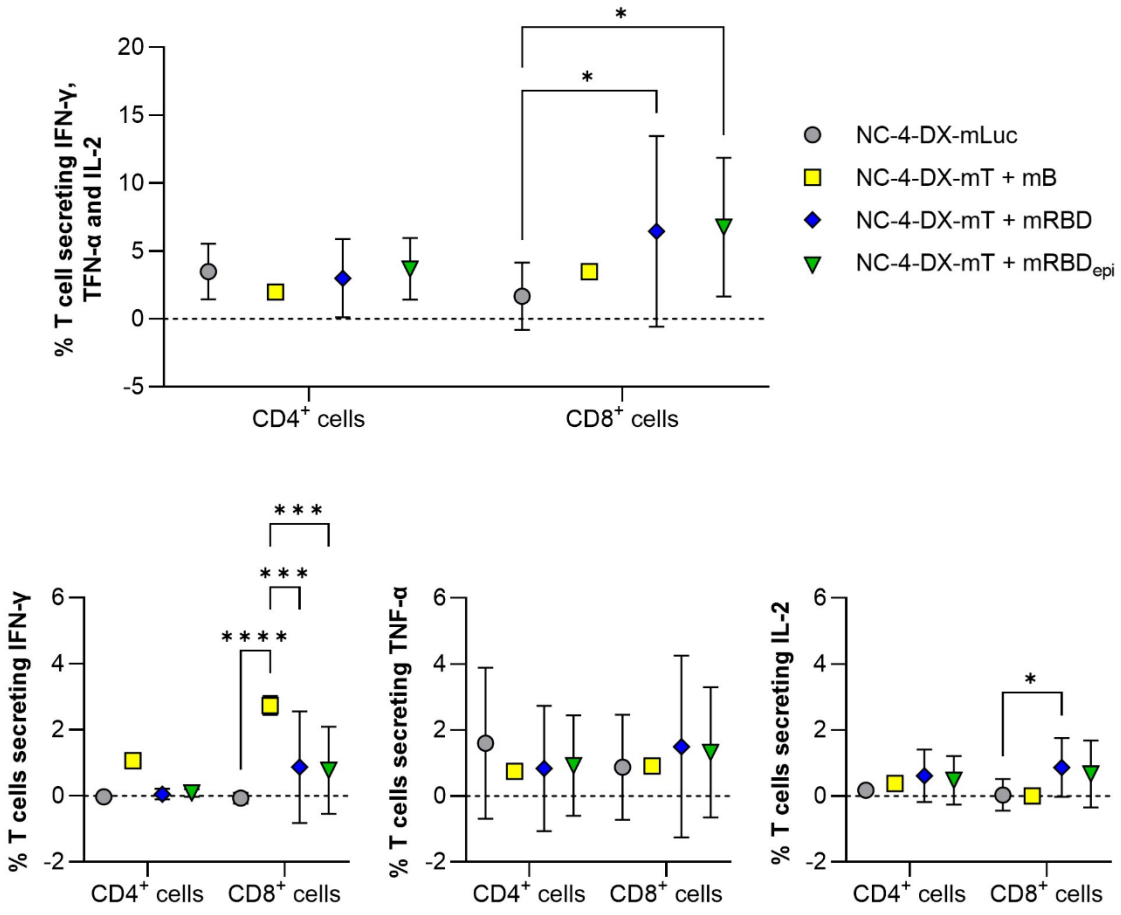

Figure 11. $CD4^+$ and $CD8^+$ T cell responses (top) considering IFN-γ, TNF-α, and IL-2 (bottom, left, center, and right, respectively)

Abbreviations: DX: dextran sulfate. IFN-γ: interferon gamma. IL-2: interleukin-2. mB: SARS-CoV-2-B cells mRNA. mLuc: mRNA encoding luciferase. mRBD: SARS-CoV-2-RBD mRNA. $mRBD_{epi}$: SARS-CoV-2-RBD_{epi} mRNA. mT: SARS-CoV-2-T cells mRNA. NC: nanocapsule. TNF-α: tumor necrosis factor-alpha. A significant comparison was performed using two-way ANOVA followed by Tukey's multiple comparison tests between groups. *p*-values < 0.05 were considered statistically significant (*). Values represent the mean ± standard deviation (n ≥ 3).

Finally, the combination of NC-4-DX-mT with different NC-4-DX-mRNA with the potential to depict B cell responses (-mB, -mRBD, and -RBD_{epi}) was evaluated (Figure 11). Significant differences were found in overall $CD8^+$ T cell responses when NC-4-DX-mT was combined with both NC-4-DX-mRBD and -RBDepi, compared with the control group (Figure 11, top). In terms of more specific response, the combination of mT and mB significantly increased the levels of secreted IFN-γ, compared to the other tested groups (Figure 11, bottom left). Additionally, the combination of mT and mRBD formulated onto NC-4-DX led to significantly higher levels of IL-2, compared to the control group (Figure 11, bottom right).

Overall, the results showed greater immune responses when combinations of mRNA were administered. However, it is worth noting that this effect may be partially attributed to the higher dose administered (10 µg of mRNA for single mRNA administration versus 20 µg of mRNA for the combinations of mRNA). Moreover, the predominant immune responses observed were $CD8^+$ cellular derived, and mRBD (either alone or in combination with mT) was found to induce the highest immune response among the explored SARS-CoV-2 derived mRNA.

In conclusion, this part of the thesis successfully designed and developed over 100 candidates for an mRNA vaccine and identified a potential candidate for a SARS-CoV-2 mRNA vaccine, namely NC-4-DX. This nanocarrier enhanced the levels of specific cellular immune responses following intramuscular administration of SARS-CoV-2-derived mRNAs. Further studies must be performed to optimize the potency of NC-4-DX or the mRNA sequences to elicit immune responses. To sum up, these results emphasize the potential of NEs and NCs as delivery carriers for mRNA vaccines.

2. REFERENCES

[1] T. Wirth, N. Parker, S. Ylä-Herttuala, History of gene therapy, Gene. 525 (2013) 162–169. https://doi.org/10.1016/j.gene.2013.03.137.

[2] V. Sudhakar, R.M. Richardson, Gene Therapy for Neurodegenerative Diseases, Neurotherapeutics. 16 (2019) 166–175. https://doi.org/10.1007/s13311-018-00694-0.

[3] A. Khvorova, J.K. Watts, The chemical evolution of oligonucleotide therapies of clinical utility, Nat. Biotechnol. 35 (2017) 238–248. https://doi.org/10.1038/nbt.3765.

[4] M. Egli, M. Manoharan, Chemistry, structure and function of approved oligonucleotide therapeutics, Nucleic Acids Res. 51 (2023) 2529–2573. https://doi.org/10.1093/nar/gkad067.

[5] Y. Yan, X.-Y. Liu, A. Lu, X.-Y. Wang, L.-X. Jiang, J.-C. Wang, Non-viral vectors for RNA delivery, J. Control. Release. 342 (2022) 241–279. https://doi.org/10.1016/j.jconrel.2022.01.008.

[6] A. Cox, S.A. Lim, E.J. Chung, Strategies to deliver RNA by nanoparticles for therapeutic potential, Mol. Aspects Med. 83 (2022) 100991. https://doi.org/10.1016/j.mam.2021.100991.

[7] X. Hou, T. Zaks, R. Langer, Y. Dong, Lipid nanoparticles for mRNA delivery, Nat. Rev. Mater. 6 (2021) 1078–1094. https://doi.org/10.1038/s41578-021-00358-0.

[8] C. Hald Albertsen, J.A. Kulkarni, D. Witzigmann, M. Lind, K. Petersson, J.B. Simonsen, The role of lipid components in lipid nanoparticles for vaccines and gene therapy, Adv. Drug Deliv. Rev. 188 (2022) 114416. https://doi.org/10.1016/j.addr.2022.114416.

[9] H. Xu, Z. Li, J. Si, Nanocarriers in gene therapy: A review, J. Biomed. Nanotechnol. 10 (2014) 3483–3507. https://doi.org/10.1166/jbn.2014.2044.

[10] M. de la Fuente, B. Seijo, M.J. Alonso, Novel Hyaluronic Acid-Chitosan Nanoparticles for Ocular Gene Therapy, Investig. Opthalmology Vis. Sci. 49 (2008) 2016. https://doi.org/10.1167/iovs.07-1077.

[11] M. de la Fuente, B. Seijo, M.J. Alonso, Bioadhesive hyaluronan–chitosan nanoparticles can transport genes across the ocular mucosa and transfect ocular tissue, Gene Ther. 15 (2008) 668–676. https://doi.org/10.1038/gt.2008.16.

[12] D. Teijeiro-Osorio, C. Remuñán-López, M.J. Alonso, Chitosan/cyclodextrin nanoparticles can efficiently transfect the airway epithelium in vitro, Eur. J. Pharm. Biopharm. 71 (2009) 257–263. https://doi.org/10.1016/j.ejpb.2008.09.020.

[13] E. Samaridou, H. Walgrave, E. Salta, D.M. Álvarez, V. Castro-López, M. Loza, M.J. Alonso, Nose-to-brain delivery of enveloped RNA - cell permeating peptide nanocomplexes for the treatment of neurodegenerative diseases, Biomaterials. 230 (2020) 119657. https://doi.org/10.1016/j.biomaterials.2019.119657.

[14] A.M. Ledo, M.S. Sasso, V. Bronte, I. Marigo, B.J. Boyd, M. Garcia-Fuentes, M.J. Alonso, Co-delivery of RNAi and chemokine by polyarginine nanocapsules enables the modulation of myeloid-derived suppressor cells, J. Control. Release. 295 (2019) 60–73. https://doi.org/10.1016/j.jconrel.2018.12.041.

[15] S. Anthiya, S.C. Öztürk, H. Yanik, E. Tavukcuoglu, A. Şahin, D. Datta, K. Charisse, D.M. Álvarez, M.I. Loza, A. Calvo, E. Sulheim, S. Loevenich, G. Klinkenberg, R. Schmid, M. Manoharan, G. Esendağlı, M.J. Alonso, Targeted siRNA lipid nanoparticles for the treatment of KRAS-mutant tumors, J. Control. Release. 357 (2023) 67–83. https://doi.org/10.1016/j.jconrel.2023.03.016.

[16] M. Tobío, R. Gref, A. Sánchez, R. Langer, M.J. Alonso, Stealth PLA-PEG nanoparticles as protein carriers for nasal administration, Pharm. Res. 15 (1998) 270–275. https://doi.org/10.1023/A:1011922819926.

[17] A. Vila, A. Sánchez, C. Évora, I. Soriano, J.L. Vila Jato, M.J. Alonso, PEG-PLA Nanoparticles as Carriers for Nasal Vaccine Delivery, J. Aerosol Med. 17 (2004) 174–185. https://doi.org/10.1089/0894268041457183.

[18] P. Calvo, C. Remuñán-López, J.L. Vila-Jato, M.J. Alonso, Novel Hydrophilic Chitosan – Polyethylene Oxide Nanoparticles as Protein Carriers, J. Appl. Polym. Sci. 63 (1997) 125–132. https://doi.org/10.1002/(SICI)1097-4628(19970103)63:1<125::AID-APP13>3.0.CO;2-4.

[19] C. Prego, P. Paolicelli, B. Díaz, S. Vicente, A. Sánchez, Á. González-Fernández, M.J. Alonso, Chitosan-based nanoparticles for improving immunization against hepatitis B infection, Vaccine. 28 (2010) 2607–2614. https://doi.org/10.1016/j.vaccine.2010.01.011.

[20] S. Vicente, M. Peleteiro, B. Díaz-Freitas, A. Sanchez, Á. González-Fernández, M.J. Alonso, Co-delivery of viral proteins and a TLR7 agonist from polysaccharide nanocapsules: A needle-free

vaccination strategy, J. Control. Release. 172 (2013) 773–781. https://doi.org/10.1016/j.jconrel.2013.09.012.

[21] J. Correia-Pinto, N. Csaba, J. Schiller, M. Alonso, Chitosan-Poly (I:C)-PADRE Based Nanoparticles as Delivery Vehicles for Synthetic Peptide Vaccines, Vaccines. 3 (2015) 730–750. https://doi.org/10.3390/vaccines3030730.

[22] J.V. González-Aramundiz, E. Presas, I. Dalmau-Mena, S. Martínez-Pulgarín, C. Alonso, J.M. Escribano, M.J. Alonso, N.S. Csaba, Rational design of protamine nanocapsules as antigen delivery carriers, J. Control. Release. 245 (2017) 62–69. https://doi.org/10.1016/j.jconrel.2016.11.012.

[23] M. Peleteiro, E. Presas, J.V. González-Aramundiz, B. Sánchez-Correa, R. Simón-Vázquez, N. Csaba, M.J. Alonso, Á. González-Fernández, Polymeric Nanocapsules for Vaccine Delivery: Influence of the Polymeric Shell on the Interaction With the Immune System, Front. Immunol. 9 (2018). https://doi.org/10.3389/fimmu.2018.00791.

[24] J. Crecente-Campo, S. Lorenzo-Abalde, A. Mora, J. Marzoa, N. Csaba, J. Blanco, Á. González-Fernández, M.J. Alonso, Bilayer polymeric nanocapsules: A formulation approach for a thermostable and adjuvanted E. coli antigen vaccine, J. Control. Release. 286 (2018) 20–32. https://doi.org/10.1016/j.jconrel.2018.07.018.

[25] A.S. Cordeiro, J. Crecente-Campo, B.L. Bouzo, S.F. González, M. de la Fuente, M.J. Alonso, Engineering polymeric nanocapsules for an efficient drainage and biodistribution in the lymphatic system, J. Drug Target. 27 (2019) 646–658. https://doi.org/10.1080/1061186X.2018.1561886.

[26] J. Crecente-Campo, J. Guerra-Varela, M. Peleteiro, C. Gutiérrez-Lovera, I. Fernández-Mariño, A. Diéguez-Docampo, Á. González-Fernández, L. Sánchez, M.J. Alonso, The size and composition of polymeric nanocapsules dictate their interaction with macrophages and biodistribution in zebrafish, J. Control. Release. 308 (2019) 98–108. https://doi.org/10.1016/j.jconrel.2019.07.011.

[27] J. Crecente-Campo, M.J. Alonso, Engineering, on-demand manufacturing, and scaling-up of polymeric nanocapsules, Bioeng. Transl. Med. 4 (2019) 38–50. https://doi.org/10.1002/btm2.10118.

[28] T.G. Dacoba, R.W. Omange, H. Li, J. Crecente-Campo, M. Luo, M.J. Alonso, Polysaccharide Nanoparticles Can Efficiently Modulate the Immune Response against an HIV Peptide Antigen, ACS Nano. 13 (2019) 4947–4959. https://doi.org/10.1021/acsnano.8b07662.

[29] R.L. Rungta, H.B. Choi, P.J. Lin, R.W. Ko, D. Ashby, J. Nair, M. Manoharan, P.R. Cullis, B.A. MacVicar, Lipid Nanoparticle Delivery of siRNA to Silence Neuronal Gene Expression in the Brain, Mol. Ther. Acids. 2 (2013) e136. https://doi.org/10.1038/mtna.2013.65.

[30] L.E. Waggoner, K.F. Miyasaki, E.J. Kwon, Analysis of PEG-lipid anchor length on lipid nanoparticle pharmacokinetics and activity in a mouse model of traumatic brain injury, Biomater. Sci. (2023) 4238–4253. https://doi.org/10.1039/d2bm01846b.

[31] Y. Eygeris, S. Patel, A. Jozic, G. Sahay, Deconvoluting Lipid Nanoparticle Structure for Messenger RNA Delivery, Nano Lett. 20 (2020) 4543–4549. https://doi.org/10.1021/acs.nanolett.0c01386.

[32] X. Han, H. Zhang, K. Butowska, K.L. Swingle, M.G. Alameh, D. Weissman, M.J. Mitchell, An ionizable lipid toolbox for RNA delivery, Nat. Commun. 12 (2021) 8–13. https://doi.org/10.1038/s41467-021-27493-0.

[33] H. Walgrave, S. Balusu, S. Snoeck, E. Vanden Eynden, K. Craessaerts, N. Thrupp, L. Wolfs, K. Horré, Y. Fourne, A. Ronisz, E. Silajdžić, A. Penning, G. Tosoni, Z. Callaerts-Vegh, R. D'Hooge, D.R. Thal, H. Zetterberg, S. Thuret, M. Fiers, C.S. Frigerio, B. De Strooper, E. Salta, Restoring miR-132 expression rescues adult hippocampal neurogenesis and memory deficits in Alzheimer's disease, Cell Stem Cell. 28 (2021) 1805-1821.e8. https://doi.org/10.1016/j.stem.2021.05.001.

[34] K. Richetin, P. Steullet, M. Pachoud, R. Perbet, E. Parietti, M. Maheswaran, S. Eddarkaoui, S. Bégard, C. Pythoud, M. Rey, R. Caillierez, K. Q Do, S. Halliez, P. Bezzi, L. Buée, G. Leuba, M. Colin, N. Toni, N. Déglon, Tau accumulation in astrocytes of the dentate gyrus induces neuronal dysfunction and memory deficits in Alzheimer's disease, Nat. Neurosci. 23 (2020) 1567–1579. https://doi.org/10.1038/s41593-020-00728-x.

[35] P. Chauhan, K. Jethwa, A. Rathawa, G. Chauhan, S. Mehra, The Anatomy of the Hippocampus, in: Cereb. Ischemia, Exon Publications, 2021: pp. 17–30. https://doi.org/10.36255/exonpublications.cerebralischemia.2021.hippocampus.

[36] D. Adams, A. Gonzalez-Duarte, W.D. O'Riordan, C.-C. Yang, M. Ueda, A. V. Kristen, I. Tournev, H.H. Schmidt, T. Coelho, J.L. Berk, K.-P. Lin, G. Vita, S. Attarian, V. Planté-Bordeneuve, M.M. Mezei, J.M. Campistol, J. Buades, T.H. Brannagan, B.J. Kim, J. Oh, Y. Parman, Y. Sekijima, P.N. Hawkins, S.D. Solomon, M. Polydefkis, P.J. Dyck, P.J. Gandhi, S. Goyal, J. Chen, A.L. Strahs, S. V. Nochur, M.T. Sweetser, P.P. Garg, A.K. Vaishnaw, J.A. Gollob, O.B. Suhr, Patisiran, an RNAi Therapeutic, for Hereditary Transthyretin Amyloidosis, N. Engl. J. Med. 379 (2018) 11–21. https://doi.org/10.1056/NEJMoa1716153.

[37] J.A. Kulkarni, D. Witzigmann, S. Chen, P.R. Cullis, R. van der Meel, Lipid Nanoparticle Technology for Clinical Translation of siRNA Therapeutics, Acc. Chem. Res. 52 (2019) 2435–2444. https://doi.org/10.1021/acs.accounts.9b00368.

[38] M. Miceli, C. Exertier, M. Cavaglià, E. Gugole, M. Boccardo, R.R. Casaluci, N. Ceccarelli, A. De Maio, B. Vallone, M.A. Deriu, ALS2-Related Motor Neuron Diseases: From Symptoms to Molecules, Biology (Basel). 11 (2022) 77. https://doi.org/10.3390/biology11010077.

[39] S. Bachiller, I. Jiménez-Ferrer, A. Paulus, Y. Yang, M. Swanberg, T. Deierborg, A. Boza-Serrano, Microglia in Neurological Diseases: A Road Map to Brain-Disease Dependent-Inflammatory Response, Front. Cell. Neurosci. 12 (2018). https://doi.org/10.3389/fncel.2018.00488.

[40] D.J. Begley, Delivery of therapeutic agents to the central nervous system: The problems and the possibilities, Pharmacol. Ther. 104 (2004) 29–45. https://doi.org/10.1016/j.pharmthera.2004.08.001.

[41] B. Obermeier, R. Daneman, R.M. Ransohoff, Development, maintenance and disruption of blood-brain barrier, Nat. Med. 19 (2013) 1584–1596. https://doi.org/10.1038/nm.3407.Development.

[42] B. Engelhardt, L. Sorokin, The blood-brain and the blood-cerebrospinal fluid barriers: function and dysfunction, Semin. Immunopathol. 31 (2009) 497–511. https://doi.org/10.1007/s00281-009-0177-0.

[43] J.J. Lochhead, R.G. Thorne, Intranasal delivery of biologics to the central nervous system, Adv. Drug Deliv. Rev. 64 (2012) 614–628. https://doi.org/10.1016/j.addr.2011.11.002.

[44] D.S. Hersh, A.S. Wadajkar, N. Roberts, J.G. Perez, N.P. Connolly, V. Frenkel, J.A. Winkles, G.F. Woodworth, A.J. Kim, Evolving Drug Delivery Strategies to Overcome the Blood Brain Barrier., Curr. Pharm. Des. 22 (2016) 1177–1193.

[45] D. Furtado, M. Björnmalm, S. Ayton, A.I. Bush, K. Kempe, F. Caruso, Overcoming the Blood–Brain Barrier: The Role of Nanomaterials in Treating Neurological Diseases, Adv. Mater. 30 (2018). https://doi.org/10.1002/adma.201801362.

[46] R. Hao, B. Sun, L. Yang, C. Ma, S. Li, RVG29-modified microRNA-loaded nanoparticles improve ischemic brain injury by nasal delivery, Drug Deliv. 27 (2020) 772–781. https://doi.org/10.1080/10717544.2020.1760960.

[47] H. Wu, K. Hu, X. Jiang, From nose to brain: understanding transport capacity and transport rate of drugs, Expert Opin. Drug Deliv. 5 (2008) 1159–1168. https://doi.org/10.1517/17425247.5.10.1159.

[48] P.G. Djupesland, J.C. Messina, R.A. Mahmoud, The nasal approach to delivering treatment for brain diseases: An anatomic, physiologic, and delivery technology overview, Ther. Deliv. 5 (2014) 709–733. https://doi.org/10.4155/tde.14.41.

[49] E. Samaridou, H. Walgrave, E. Salta, D.M. Álvarez, V. Castro-López, M. Loza, M.J. Alonso, Nose-to-brain delivery of enveloped RNA - cell permeating peptide nanocomplexes for the treatment of neurodegenerative diseases, Biomaterials. 230 (2020) 119657. https://doi.org/10.1016/j.biomaterials.2019.119657.

[50] R.L. Rungta, H.B. Choi, P.J.C. Lin, R.W.Y. Ko, D. Ashby, J. Nair, M. Manoharan, P.R. Cullis, B.A. MacVicar, Lipid nanoparticle delivery of sirna to silence neuronal gene expression in the brain, Mol. Ther. - Nucleic Acids. 2 (2013) 1–12. https://doi.org/10.1038/mtna.2013.65.

[51] D. Cucinotta, M. Vanelli, WHO declares COVID-19 a pandemic, Acta Biomed. 91 (2020) 157–160. https://doi.org/10.23750/abm.v91i1.9397.

[52] B. Hu, H. Guo, P. Zhou, Z.L. Shi, Characteristics of SARS-CoV-2 and COVID-19, Nat. Rev. Microbiol. 19 (2021) 141–154. https://doi.org/10.1038/s41579-020-00459-7.

[53] Y. Liu, J. Liu, K.S. Plante, J.A. Plante, X. Xie, X. Zhang, Z. Ku, Z. An, D. Scharton, C. Schindewolf, S.G. Widen, V.D. Menachery, P.Y. Shi, S.C. Weaver, The N501Y spike substitution enhances SARS-CoV-2 infection and transmission, Nature. 602 (2022) 294–299. https://doi.org/10.1038/s41586-021-04245-0.

[54] World Health Organization, WHO Coronavirus (COVID-19) Dashboard, (2023). https://covid19.who.int/ (accessed May 29, 2023).

[55] F.P. Polack, S.J. Thomas, N. Kitchin, J. Absalon, A. Gurtman, S. Lockhart, J.L. Perez, G. Pérez Marc, E.D. Moreira, C. Zerbini, R. Bailey, K.A. Swanson, S. Roychoudhury, K. Koury, P. Li, W. V. Kalina, D. Cooper, R.W. Frenck, L.L. Hammitt, Ö. Türeci, H. Nell, A. Schaefer, S. Ünal, D.B. Tresnan, S. Mather, P.R. Dormitzer, U. Şahin, K.U. Jansen, W.C. Gruber, Safety and Efficacy of the BNT162b2 mRNA Covid-19 Vaccine, N. Engl. J. Med. 383 (2020) 2603–2615. https://doi.org/10.1056/nejmoa2034577.

[56] L.R. Baden, H.M. El Sahly, B. Essink, K. Kotloff, S. Frey, R. Novak, D. Diemert, S.A. Spector, N. Rouphael, C.B. Creech, J. McGettigan, S. Khetan, N. Segall, J. Solis, A. Brosz, C. Fierro, H. Schwartz, K. Neuzil, L. Corey, P. Gilbert, H. Janes, D. Follmann, M. Marovich, J. Mascola, L. Polakowski, J. Ledgerwood, B.S. Graham, H. Bennett, R. Pajon, C. Knightly, B. Leav, W. Deng, H. Zhou, S. Han, M. Ivarsson, J. Miller, T. Zaks, Efficacy and Safety of the mRNA-1273 SARS-CoV-2 Vaccine, N. Engl. J. Med. 384 (2021) 403–416. https://doi.org/10.1056/nejmoa2035389.

[57] Z. Liu, S. Wang, C. Tapeinos, G. Torrieri, V. Känkänen, N. El-Sayed, A. Python, J.T. Hirvonen, H.A. Santos, Non-viral nanoparticles for RNA interference: Principles of design and practical guidelines, Adv. Drug Deliv. Rev. 174 (2021) 576–612. https://doi.org/10.1016/j.addr.2021.05.018.

[58] S. Sharma, T.K. Mukkur, H.A. Benson, Y. Chen, Enhanced immune response against pertussis toxoid by IgA-loaded chitosan-dextran sulfate nanoparticles, J. Pharm. Sci. 101 (2012) 233–244. https://doi.org/10.1002/jps.22763.

[59] S. Sharma, H.A.E. Benson, T.K.S. Mukkur, P. Rigby, Y. Chen, Preliminary studies on the development of IgA-loaded chitosan-dextran sulphate nanoparticles as a potential nasal delivery system for protein antigens, J. Microencapsul. 30 (2013) 283–294. https://doi.org/10.3109/02652048.2012.726279.

[60] A.M. Carabelli, T.P. Peacock, L.G. Thorne, W.T. Harvey, J. Hughes, T.I. de Silva, S.J. Peacock, W.S. Barclay, T.I. de Silva, G.J. Towers, D.L. Robertson, SARS-CoV-2 variant biology: immune escape, transmission and fitness, Nat. Rev. Microbiol. (2023). https://doi.org/10.1038/s41579-022-00841-7.

[61] B. Garulli, M.G. Stillitano, V. Barnaba, M.R. Castrucci, Primary CD8+ T-cell response to soluble ovalbumin is improved by chloroquine treatment in vivo, Clin. Vaccine Immunol. 15 (2008) 1497–1504. https://doi.org/10.1128/CVI.00166-08.

[62] K. Schroder, P.J. Hertzog, T. Ravasi, D.A. Hume, Interferon-γ: an overview of signals, mechanisms and functions, J. Leukoc. Biol. 75 (2004) 163–189. https://doi.org/10.1189/jlb.0603252.

[63] R.A. Seder, R. Ahmed, Similarities and differences in CD4+ and CD8+ effector and memory T cell generation, Nat. Immunol. 4 (2003) 835–842. https://doi.org/10.1038/ni969.

[64] G. Alter, J.M. Malenfant, M. Altfeld, CD107a as a functional marker for the identification of natural killer cell activity, J. Immunol. Methods. 294 (2004) 15–22. https://doi.org/10.1016/j.jim.2004.08.008.

CONCLUSIONS

The conclusions of the work performed in this thesis have been formulated taking into account the three primary experimental objectives:

1. With regard to the ionizable NEs for RNA delivery and diffusion in the CNS:

   RNA-loaded NEs containing ionizable lipids exhibited a significant diffusion within the brain, surpassing the diffusion capabilities of LNPs. Furthermore, transfection was achieved in distant brain areas from the injection site, specifically targeting neurons and microglia.

2. With regard to the NEs and polymeric NCs loaded with siRNA and the exploration of alternative routes to access the brain:

   NEs and polymer NCs are promising nanosystems for diffusion and transfection in the brain. Specifically, our selected candidate NC-1 was found to show exceptional diffusivity upon ICV administration and decreased the mRNA-targeted levels below 50% in the frontal cortex, striatum, hippocampus, brain stem, and DRG.

3. With regard to the NEs and polymeric NCs as mRNA vaccine candidates against SARS-CoV-2:

   Among the 100 prototypes developed, a formulation named NC-4-DX was identified as a promising delivery vehicle for mRNA vaccines against SARS-CoV-2. Enhanced levels of specific cellular immune responses following intramuscular administration of NC-4-DX loaded with mRNA derived from SARS-CoV-2 were found.

Overall, this thesis highlights the considerable potential of NEs and polymeric NCs for efficient RNA delivery to the brain. It emphasizes the role of nanocarrier composition in the enhanced diffusion within the CNS and in the modulation of targeted mRNA levels. Additionally, this thesis contributes to the progress achieved in the development of mRNA vaccine formulations and underlines the opportunities that exist for the optimization of mRNA vaccines through the adequate design of RNA nanocarriers.

LIST OF ABBREVIATIONS

%0123

β III-tubulin: Class III β-tubulin
ζpot: ζ-potential

A

A: Adenine
A/P: Anterior-posterior
AAV: Adeno-associated virus
Ab: Antibody
AD: Alzheimer's disease
AL: Alabama
AMA1: Apical membrane antigen 1
AMD: Age-related macular degeneration
APP: β-amyloid precursor protein
ASCVD: Clinical atherosclerotic cardiovascular disease
ASGPR-CRD: Asialoglycoprotein receptor carbohydrate recognition domine
ASL: Amyotrophic lateral sclerosis
ASO: Antisense oligonucleotide
AUC: Areas under the curve

B

BACE-1: β-secretase 1
BBB: Blood-brain barrier
BMDC: Bone-marrow-derived dendritic cell
bp: Base pair
BSA: Bovine serum albumin
BZT: Benzethonium

C

C: Cytosine
C12-200: 1,1′-((2-(4-(2-((2-(bis(2-hydroxydodecyl)amino)ethyl)(2-hydroxydodecyl)amino)ethyl)piperazin-1-yl)ethyl)azanediyl)bis(dodecan-2-ol)
C-PEG3-RVG: C-PEG3-rabies virus glycoprotein derived peptide
CA: Cornu ammonius
Cas9: CRISPR-associated protein 9
CB: Citrate buffer
CD: Cyclodextrin
$CD4^+$: Cluster of differentiation 4
$CD8^+$: Cluster of differentiation 8
CD107a or LMAP-1: Lysosomal-associated membrane protein-1

CMV: Cytomegalovirus
CNS: Central nervous system
CO: Colorado
COVID-19: Coronavirus disease 2019
CPT: Camptothecin
CRISPR: Cluster regularly interspaced short palindromic repeats
CS: Chitosan
CSF: Cerebrospinal fluid
CTL: Cytotoxic T cell

D

D/V: Dorsal-ventral
DCR: Derived count rate
DEAE-DX or DEAE-dextran: Diethylaminoethyl-dextran
DG: Dentate gyrus
DLin-MC3-DMA: (6Z,9Z,28Z,31Z)-heptatriacont-6,9,28,31-tetraene-19-yl 4(dimethylamino) butanoate
DLS: Dynamic light scattering
DMD: Duchenne muscular atrophy
DMG-PEG_{2000}: (*R*)-methoxy-polyethyleneglycol-2000-carbamoyl-di-O-myristyl-sn-glyceride
DNA: Deoxyribonucleic acid
DODAP: 1,2-dioleoyl-3-dimethylammonium propane
DOPE: 1,2-dioleoyl-sn-glycero-3-phosphoethanolamine
DOTAP: 1,2-dioleoyl-3-trimethylammonium propane
DOX: Doxorubicin
DRG: Dorsal root ganglion
DSPC: 1,2-distearoyl-sn-glycero-3-phosphocholine
DSPE-PEG_{2000}-maleimide: 1,2-distearoyl-sn-glycero-3-phosphoethanolamine-N-[maleimide(polyethylene glycol)-2000]
dsRNA: Double-stranded ribonucleic acid
DTX: Docetaxel
DX: Dextran sufate

E

EBOV: Ebola virus
EDTA: Ethylenediaminetetraacetic acid
EE%: Encapsulation efficiency
EGFR: Epidermal growth factor receptor
EMA: European Medicines Agency

F

F: Fusion glycoprotein
FAM: Fluorescein amidite

FBS: Fetal bovine serum
FCS: Familial chylomicronemia syndrome
FDA: Food and Drug Administration

G

G: Guanine
gag: group-specific antigen
Gal-1: Galectin-1
GalNAc: N-acetylgalactosamine
gB: Enveloped glycoprotein B
Ge: Gefitinib
GFAP: Glial fibrillary acidic protein
GFP: Green fluorescence protein
Glut1: Glucose transporter 1
GOLPH3: Golgi phosphoprotein 3
gp120: enveloped glycoprotein 120
gp140: enveloped glycoprotein 140
GRA6: Dense granule protein 6
GRIN1: Glutamate *N*-mehtyl-D-aspartic acid receptor subunit zeta-1
Gu: Guanidinium

H

H_{II}: Inverted hexagonal
HA: Hyaluronic acid
HAp: Hemagglutinin protein
hATTR: Hereditary transthyretin amyloidosis
hCMV: Human cytomegalovirus
hDC: Human dendritic cell
HeFH: Heterozygous familial hypercholesterolemia
hELISA: Hybridization enzyme-linked immunosorbent assay
HEPES: 4-(2-hydroxyethyl)-1-piperazineethanesulfonic acid
HIV-1: Human immunodeficiency virus
hMDDC: Human monocyte-derived dendritic cell
HoFD: Homozygous familial hypercholesterolemia
HPLC: High performance liquid chromatography
HSV: Herpes simplex virus

I

Iba-1: Ionized calcium-binding adaptor molecule 1
ICV: Intracerebroventircular
IFN-γ: Interferon γ
IgG: Immunoglobulin G
Il-1β: Interleukin-1β

Il-6: Interleukin-6
IM: Intramuscular
IN: Intranasal
iNE: Ionizable nanoemulsion
Inulin: Inutec® SL1
IT: Intrathecal
IV: Intravenous
IVIS: *In vivo* imaging system
IVT: Intravitreal

K

kbp: kilobase pair
K-HS15®: Kolliphor® HS15

L

Lab™ or Labrafac™: Labrafac™ Lipophile, WL 1349, medium chain triglycerides of caprylic and capric acids
Labrasol®: PEG-8 (MW 400) mono- and diesters of caprylic and capric acids
LAE: Ethyl lauroyl arginate
LDH: Lactate dehydrogenase
LNA: Locked nucleic acid
LNP: Lipid nanoparticle
LP: Lipofectamine
LRP1: Low-density lipoprotein receptor-related protein-1
LSINCT5: Long stress-induced non-coding transcript 5

M

M/L: Medial-Lateral
MA: Massachusetts
Mal: Maleimide
mB or SARS-CoV-2-B cells mRNA: Messenger ribonucleic acid intended to trigger a B cell response
MEM: Minimum essential medium
MFI: Mean fluorescence intensity
mGFP: Messenger ribonucleic acid encoding for green fluorescence protein
MHC-I: Major histocompatibility complex I
mLuc: Messenger ribonucleic acid encoding for luciferase
mOVA: Messenger ribonucleic acid encoding for ovalbumin protein
mRBD or SARS-CoV-2-RBD mRNA: Messenger ribonucleic acid encoding for RBD domain of SARS-CoV-2
$mRBD_{epi}$ or SARS-CoV-2-RBD_{epi} mRNA: Messenger ribonucleic acid encoding for a highly immunogenic motif from the RBD domain of SARS-CoV-2
mRNA: Messenger ribonucleic acid

miR: Micro ribonucleic acid
miR-132: Micro ribonucleic acid 132 mimic
miR-control: Scrambled micro ribonucleic acid
miRNA: Micro ribonucleic acid
MNC: Multi-layer nanocapsule
MO: Missouri
mT or SARS-CoV-2-T cells mRNA: Messenger ribonucleic acid intended to trigger a T cell response
MTT: 3-(4,5-dimethylthiazol-2-yl)-2,5-diphenyltetrazolium bromide
MW: Molecular weight

N

N-to-B: Nose-to-brain
N/P: nitrogen/phosphate
NC: Nanocapsule
NCX: Nanocomplex
NE: Nanoemulsion
NK: Natural killer
NMR: Nuclear magnetic resonance
NP: Nanoparticle
ns: Not significative
NY: New York

O

ORF: Open reading frame
OVA: Ovalbumin

P

PA: Pennsylvania
PArg: Poly-L-arginine
PBS: Phosphate-buffered saline
PC: Positive control
PCL: Poly(ε-caprolactone)
PCR: Polymerase chain reaction
PD: Parkinson's disease
PD-1: Programmed cell death protein 1
PDI: Polydispersity index
PEG: Polyethylene glycol
PEI: Poly(ethylenimine)
PGA: Polyglutamic acid
PGA-PEG or PP: Polyethylene glycol (5 kDa)-block-poly(α-glumatic acid) (10u)
PGS: Polyglucan-spermidine
PH1: Primary hyperoxaluria type 1

PLA: Poly(D,L-lactic acid)
PLGA: Poly(lactic-co-glycolic acid)
PLK1: Polo-like kinase 1
PLL: Poly-L-lysine
PMAM: Poly(amido amine)
PMO: Phosphorodiamidate morpholino
pp65-IE1: Phosphoprotein 65-immediate early protein 1
PRT or PR: Protamine Sulphate EP
PSA: Polysialic acid
PTEN: Phosphatase and tensin homolog 1

Q

qPCR: Quantitative real-time polymerase chain reaction

R

r^2: Lineal coefficient of determination
r8-C12: Octaarginine-lauric acid
Raf-1: Serine-threonine kinase 1
RBD: Receptor binding domain
RISC: Ribonucleic acid-induced silencing complex
RNA: Ribonucleic acid
RNAi: Ribonucleic acid interference
RNase: Ribonuclease
ROP2A: Rhoptry protein 2A
ROP18: Rhoptry protein 18
RSV: Respiratory syncytial virus
RT: Reverse transcription
RVG: Rabies virus glycoprotein

S

S1: Subunit 1 SARS-CoV-2 spike protein
S2: Subunit 2 SARS-CoV-2 spike protein
SA: Stearic acid
SAG1: Surface antigen 1
SAG2A: Surface antigen 2A
SAM: Self-amplifying messenger ribonucleic acid
SARS-CoV-2: Severe acute respiratory syndrome coronavirus 2
SC: Subcutaneous
SCA3: Spinocerebellar ataxia 3
SG: Sodium glycocholate
siGFP: Small interfering ribonucleic acid against green fluorescence protein
siRNA: Small interfering ribonucleic acid
SMA: Spinal muscular dystrophy

SPAN 80: Span 80-LQ-(MV)
SPM: Spermine

T

T. gondii: *Toxoplasma gondii*
T80: Tween 80
Tat: Trans-activator of transcription protein
TE: Tris-ethylenediaminetetraacetic acid
TEA: Triethylamine
TEER: Transepithelial electrical resistance
TFR: Total flow rate
TLR: Toll-like receptor
tLyP-1: Truncated form of LyP-1 (sequence: CGNKRTR)
TNF-α: Tumor necrosis factor-α
TPP: Target product profile
tRNA: Transfer ribonucleic acid

U

U: Uracil
UPLC: Ultra-performance liquid chromatography
USA: United States of America
UT: Untreated
UTR: Untranslated region
UV: Ultraviolet

V

VC: Vehicle control
VEGF: Vascular endothelial growth factor
VEGFR2: Vascular endothelial growth factor receptor 2
Vit E or Vitamin E: D, L-α-tocopherol
vs.: *versus*
VT: Vermont
v/v: volume/volume

W

WGA: Wheat germ agglutinin
w/v: weight/volume
w/w: weight/weight

ETHICAL CONSIDERATIONS

The studies in mice described in Chapter 1 were done at KU-Leuven (Leuven, Belgium), and approved by the ethical committee under approval number LA1210596, following European regulations (Directive 2010/63/EU, on the protection of animals used for scientific purposes).

The studies performed in rats described in Chapter 1 were done at University of Santiago de Compostela (Santiago de Compostela, Spain), and approved by the ethical committee under approval number 15005/15/002 and 15012/2021/012, following European (Directive 2010/63/EU, on the protection of animal used for scientific purposes), and National (RD 53/2013) regulations.

The studies performed in mice described in Chapter 2 were done at Charles Rivers Laboratories Research Models (CRDL) (Cambridge, USA), approved by the ethical committee under approval number DS16-00496 (A3863-01), following regulations from the National Institute of Health Office for Laboratory Animal Welfare (NIH OLAW) and the Assurance of Compliance with Public Health Services (PHS) Policy on Humane Care and Use of Laboratory Animals.

The studies performed with human dendritic cells, obtained from human donors, in Chapter 3 were done at Institute for Research in Biomedicine (Barcelona, Spain), and the Hospital Clinic of Barcelona (Barcelona, Spain), and approved by the ethical committee under approval number HCB/2020/0387, following National regulations (RD 14/2007).

The studies performed in mice using mLuc in Chapter 3 were done at University Pompeu Fabra (Barcelona, Spain), and approved by the ethical committee under approval number FUE-2020-01825389, following European (Directive 2010/63/EU, on the protection of animals used for scientific purposes), and National (RD 53/2013) regulations. These studies were also performed at Vrije University Brussel (Brussel, Belgium), and approved by the ethical committee under approval number 17-214-7, following European regulations (Directive 2010/63/EU, on the protection of animals used for scientific purposes).

The studies performed using mOVA using mLuc in Chapter 3 were done at Vrije University Brussel (Brussel, Belgium), and approved by the ethical committee under approval number 17-214-7, following European regulations (Directive 2010/63/EU, on the protection of animals used for scientific purposes).

The studies performed using SARS-CoV-2 derived mRNAs in Chapter 3 were done at University Pompeu Fabra (Barcelona, Spain), and approved by the ethical committee under approval number FUE-2020-01825389, following European (Directive 2010/63/EU, on the protection of animal used for scientific purposes), and National (RD 53/2013) regulations. These studies were also performed at the National Center of Biotechnology, Spanish National Research Council (CNB-CSIC) (Madrid, Spain), and approved by the ethical committee under approval number ES200790000182, following European (Directive 2010/63/EU, on the protection of animal used for scientific purposes), and National (RD 53/2013) regulations.

De ondertekende formulieren sturen naar:
Erna Dewil, Proefdierencentrum, Herestraat 49 bus 501, 3000 Leuven.

KATHOLIEKE UNIVERSITEIT LEUVEN

Aanvraag tot aanpassing aan een proefdierexperiment – *application for a modification to an animal experiment*

Laboratorium (*laboratory*): Laboratory for the Research of Neurodegenerative Diseases

Erkenningsnr laboratorium (*license number*): LA1210596

Laboratoriumdirecteur (*laboratory director*): Bart De Strooper

Projectnummer (*project number*)**:** 286/2014

Titel van het onderzoeksproject (*title of the research project*)**:**

miR-132 role in mammalian neurogenesis

Gelieve aan te geven om welke aanpassing het gaat (*please indicate what the modification is about*)

☐ **Verlenging van het project (maximum 1 jaar, voor verlenging van meer dan 1 jaar dient een volledig dossier te worden ingevuld)** (*change in duration of the project, max 1 year allowed*) Begindatum/*starting date*: 1 Einddatum/*end date*:

☐ **Wijziging in techniek/manipulatie**/*change in technique or manipulation*

☒ **Wijziging in proefdieren – extra dieren nodig – inschatting pijn, lijden en letsel**/ *change in animals – need for extra animals - estimate of pain, suffering and lasting harm*

Aantal *number*	Diersoort *species and strain*	Gemiddelde duur van de proef (dagen, weken, maanden) *Mean duration of the experiment (days, weeks, months)*	Gemiddelde duur van pijn, lijden en letsel (dagen, weken, maanden) *Mean duration of pain, suffering and lasting harm (days, weeks, months)*	Graad van pijn, lijden en letsel (geen, gering, matig, ernstig, ondefinieerbaar) *Estimate of pain, suffering and lasting harm (none, low, moderate, severe, undefinable)*
301	APPswe/PS1L166P	30 days	30 days	Severe*
301	C57BL/6	30 days	30 days	Severe*
301	APP-NLGF	30 days	30 days	Severe*

**The additional possible burden due to behavioral testing was encountered*

Motivatie voor de gevraagde aanpassing en van het aantal benodigde dieren of **motivatie voor en beschrijving van de aangepaste technieken**/ *justification for the modification and the number of animals and justification for the modified techniques*

Motivation

microRNAs have indispensable roles in the development and functioning of the nervous system. microRNA-132 (miR-132) has been shown to be a crucial regulator of neuronal plasticity and its deficiency is observed in several neurodegenerative disorders including Alzheimer's and Huntington's disease. We recently reported a novel role for miR-132 in the cell fate specification of radial glial progenitors in embryonic zebrafish spinal cord (Salta et al, 2014, DevCell). We have followed up on these observations to further study the regulatory function of miR-132 in mammalian neurogenesis.

To achieve this, we have performed initial experiments making use of an adult neurogenesis mouse paradigm which is based on the inductive effect of physical exercise (housing with a running wheel) on adult neurogenesis in the subgranular zone of dentate gyrus. This currently constitutes the most well accepted system to study adult neurogenesis and it cannot be replaced by any *in vitro* model. Subsequently, we manipulated the levels of miR-132 by intracerebroventricular (ICV) injections (miR-132 mimics/antagomiRs) and assessed the effect of miR-132 gain- and loss-of-function on the glial progenitor proliferation and neuronal differentiation in the adult mammalian brain. Possible alterations were assessed biochemically and histologically.

These initial experiments (which were primarily used to help establish the most appropriate experimental conditions) provided preliminary evidence that A. miR-132 responds to the induction of adult hippocampal neurogenesis by becoming upregulated, B. is required for adult neurogenesis to occur (miR-132 knockdown in C57/Bl6 mice inhibits neural stem cell proliferation) and C. is sufficient for the induction of adult neurogenesis (miR-132 overexpression in APPPS1 mice restores levels of neural stem cell proliferation in the dentate gyrus).

We now aim at: A. confirming these findings by increasing the number of animals for each experiment (APPPS1 and C57/Bl6) to be able to perform accurate statistical analysis, B. validating these initial data in a non overexpressing (knock-in) and therefore more physiologically relevant AD mouse model, namely the APP-NLGF mice, C. assessing the effect of these manipulations on memory and cognition, and D. testing an alternative non invasive delivery route of miR-132 into the brain (intranasal instillation) and its effect on memory and cognition to assess the possible therapeutic potential of miR-132 targeting in AD.

This project represents a thorough study of the role of miR-132 in radial glial stem cells of the adult brain both in health and

disease and explores the therapeutic potential of miR-132 replacement therapy in AD.

Statistics

For sample size estimation, the following online algorithm combined with our lab's previous experience on the expected within-group variability in the described experimental set-ups was used:

www.stat.ubc.ca/~rollin/stats/ssize/n2.html

Mean and standard deviation values were derived from the already performed pilot experiments. Since for each experimental set-up a series of analyses will be performed, the read-out exhibiting the highest standard deviation was considered for power analysis (see below for specifications). On certain occasions the results will be further controlled for multiple testing by applying the Benjamini-Hochberg correction to minimize the false discovery rate (FDR) [e.g. in real-time PCR for multiple microRNAs (to assess off-target effects) or for *in situ* quantification of multiple cell populations].

**In order to minimize the total number of animals used, biochemical (protein and RNA analysis) and histological analysis (immunofluorescence and ISH) will be performed in the same samples (2 hemispheres are differentially processed), which will be obtained following the voluntary running period or the behavioral testing.*

>> Running+Biochemistry+Histology OR Behavioral testing+Biochemistry+Histology

** The same experimental approach and therefore statistical analysis are used for all three strains*

** One additional animal per experiment per genotype was eventually calculated in case of experimental drop-out (please see Summary Table)*

ICV injections – running (48 animals/genotype):

Basis for sample size calculation: % of BrdU-positive cells co-staining for neuronal or glial markers

Statistical analyses to be applied: 2-way Anova (with Tukey's multiple comparison post hoc test)

Statistical significance: 0.05

Power: 0.90

Mean of population 1: 10

Mean of population 2: 21.5

Common standard variation: 8.5

Sample size: n=12/group

-48 animals per injection experiment are needed:

	With running (n=)	Without running (n=)
Control injection	12	12
miRNA manipulation	12	12
Grant total / genotype	48	

The miRNA manipulation will entail a miR-132 antisense (AS) treatment for C57BL/6 mice and miR-132 overexpression for APPPS1 and APP-NLGF mice.

ICV injections – behavioral testing: 2 behavioral testing rounds with 2 distinct animal cohorts/genotype have to be carried out, due to the fact that miR-132 expression change upon ICV injection persists only for 2 wk (mice have to be re-injected bi-weekly for 1 month prior to behavioral testing). This means that if all the behavioral tests were to be combined in one cohort of mice (i.e. open fiel + T-maze + contextual fear conditioning + Morris water maze -> 3 wk testing), mice would have to be re-injected in the middle of the the testing period. Since this would interfere with the subsequent behavioral testing (due to unwanted side effects possibly because of oligonucleotide differential dosing), we will assign 2 different groups to the different behavioral tests, trying to combine as many compatible tests as possible: 1 cohort will be tested in open field + T-maze + contextual fear conditioning, while the other cohort will be tested in Morris water maze. The three genotypes will be tested independently in distinct testing rounds.

A. 1st testing round – Open field/T-maze/Contextual fear conditioning (44 animals/genotype):

Basis for sample size calculation: % freezing values in contextual fear conditioning testing

Statistical analyses to be applied: Student's t-test

Statistical significance: 0.05

Power: 0.90

Mean of population 1: 40

De ondertekende formulieren sturen naar:
Erna Dewil, Proefdierencentrum, Herestraat 49 bus 501, 3000 Leuven.

Aanvraag tot aanpassing aan een proefdierexperiment – *application for a modification to an animal experiment*

KATHOLIEKE UNIVERSITEIT LEUVEN

Mean of population 2: 50
Common standard variation: 10
Sample size: n=22/group OK

-44 animals per genotype will be used:
22x control injections
22x miR-132 or miR-132 AS injections

B. 2nd testing round –Morris water maze (50 animals/genotype):
Basis for sample size calculation: % of time in TQ
Statistical analyses to be applied: Student's t-test
Statistical significance: 0.05
Power: 0.90
Mean of population 1: 42
Mean of population 2: 29 OK
Common standard variation: 14
Sample size: n=25/group

-50 animals per genotype will be used:
25x control injections
25x miR-132 or miR-132 AS injections

Intranasal instillation – technical optimization (60 animals/genotype):

Initially we have to troubleshoot/optimize the intranasal delivery method, since this is a newly-implemented technique in our lab. In this case, miR-132 will be overexpressed (and not down regulated) in WT mice to assess the baseline beneficial effects of miR-132 on memory. The optimization of the administration scheme has to be conducted independently for the 3 genotypes as the olfactory mucosa (and thus the uptake of the miR-132 oligonucleotide by the olfactory nerve terminals) might be differentially affected in each of them.

The following conditions will be tested:

-5 timepoints post intranasal instillation

-6 treatments (control & miR-132 using 3 different carriers)

-2 mice/treatment/timepoint

>> 2 mice * 5 timepoints * 6 treatments = 60 mice for protocol optimization/genotype.

Intranasal instillation – behavioral testing

-2 behavioral testing rounds with 2 distinct animal cohorts have to be carried out, for similar reasons to the ones discussed earlier.

A. 1st testing round – Open field/T-maze/Contextual fear conditioning (44 animals/genotype):
Basis for sample size calculation: % freezing values in contextual fear conditioning testing
Statistical analyses to be applied: Student's t-test
Statistical significance: 0.05
Power: 0.90
Mean of population 1: 40
Mean of population 2: 50
Common standard variation: 10

Sample size: n=22/group

-44 animals per genotype will be used:
22x control injections
22x miR-132 or miR-132 AS injections

B. 2nd testing round –Morris water maze (50 animals/genotype):
Basis for sample size calculation: % of time in TQ
Statistical analyses to be applied: Student's t-test
Statistical significance: 0.05
Power: 0.90
Mean of population 1: 42
Mean of population 2: 29
Common standard variation: 14
Sample size: n=25/group

-50 animals per genotype will be used:
25x control injections
25x miR-132 or miR-132 AS injections

Summary Table

Genotype	Experiment	Nr of animals	Total/genotype
APPswe/PS1L166P	ICV injections/running	48	
	ICV Behavioral testing-1st round	44	
	ICV Behavioral testing-2nd round	50	
	Intranasal instillation (I.N.)setup	60	
	I.N. Behavioral testing-1st round	44	
	I.N. Behavioral testing-2nd round	50	
	Additional mice to replace experimental drop-outs	5	
			301
APP-NLGF	ICV injections/running	48	
	ICV Behavioral testing-1st round	44	
	ICV Behavioral testing-2nd round	50	
	Intranasal instillation (I.N.)setup	60	
	I.N. Behavioral testing-1st round	44	
	I.N. Behavioral testing-2nd round	50	
	Additional mice to replace experimental drop-outs	5	
			301
C57BL/6	ICV injections/running	48	
	ICV Behavioral testing-1st round	44	
	ICV Behavioral testing-2nd round	50	
	Intranasal instillation (I.N.)setup	60	
	I.N. Behavioral testing-1st round	44	
	I.N. Behavioral testing-2nd round	50	
	Additional mice to replace experimental drop-outs	5	
			301

Protocols

De ondertekende formulieren sturen naar:
Erna Dewil, Proefdierencentrum, Herestraat 49 bus 501, 3000 Leuven.

KATHOLIEKE UNIVERSITEIT LEUVEN

Aanvraag tot aanpassing aan een proefdierexperiment – *application for a modification to an animal experiment*

ICV injections (take place on a heating mat) [8-9 month old mice]

1. Administration of isoflurane (5% induction, 2-2.5% maintenance) and 0.25% Marcaine (3ul/gram) s.c. under scalp
2. Incision of the skin under aseptic conditions
3. Drilling of the skull to insert a guide cannula
4. Stereotactic implantation of the guide cannula based on Bregma coordinates
5. Intracerebroventricular injection (2ul) via an injection cannula
6. Saline injection ip (900 ul/mouse)
7. Recovery from anesthesia and transfer to home cage (heated by a lamp)
8. Monitoring for signs of discomfort / infection (this over the defined period prior the subsequent analysis / in case of disconfort/ infection (the experiment will be stopped and animals will be euthanised).
9. Following a period defined by the subsequent analysis [biochemistry (RNA and protein extraction), histology (cryopreservation of tissue blocks), behavioral testing] the animals will be euthanized by cervical dislocation and tissue samples will be collected (Note: all tissue collection procedures will be performed after euthanasia).

Intranasal instillation (takes place in induction box under constant heating by a heating lamp) [8-9 month old mice]

1. Put mouse in induction box and open isoflurane at 5%
2. Reduce isoflurane (2.5 – 2.0 %), make sure mouse breaths normally
3. Instillation:
   - 3µl in right nostril
   - Wait 2 min
   - 3µl in left nostril
   - Wait 2 min
   - Repeat 4 times: final volume = 24µl
4. Following a period defined by the subsequent analysis [biochemistry (RNA and protein extraction), histology (cryopreservation of tissue blocks), behavioral testing], the animals will be euthanized by cervical dislocation and tissue samples will be collected (Note: all tissue collection procedures will be performed after euthanasia).

Datum/*date*: 30/09/2016

Handtekening van de laboratoriumdirecteur/*signature of the laboratory director*:

Advies (voorbehouden aan de Ethische Commissie) (*for the Ethical Committee*):

☑ gunstig/*favorable* ☐ gunstig mits aanpassingen/*provided favorable adjustment* ☐ ongunstig/*rejected*

Inschatting van pijn, lijden of letsel door de Ethische Commissie/*estimate bij the Ethical Comittee*

☐ geen/*none* ☐ gering/*minor* ☐ matig/*moderate* ☑ ernstig/*severe* ☐ ondefinieerbaar/*undefinable* Datum/*date*: 11.10.2016

Commentaar en opmerkingen/*comments and remarks*

10.

De Voorzitter/ *the Chairman*

XUNTA DE GALICIA
DELEGACIÓN TERRITORIAL
DA CORUÑA
Xefatura Territorial da Consellería do Medio Rural e do Mar

Edificio Administrativo Monelos
Vicente Ferrer, 2
15071 A Coruña

galicia

REXISTRO XERAL DA XUNTA DE GALICIA
REXISTRO DO EDIFICIO ADMINISTRATIVO DA CORUÑA
A CORUÑA
SAÍDA 108582 / RX 1039888
Data 01/09/2015 09:09:34

José Manuel Cifuentes
Departamento de Anatomía
Facultade de Veterinaria
Campus Universitario
27002 Lugo

NOTIFICACIÓN DE RESOLUCIÓN DE AUTORIZACIÓN DE PROXECTOS DE EXPERIMENTACIÓN ANIMAL

Expediente núm.: 15005/15/002
Interesado: José Luis Labandeira García
Procedemento: resolución de autorización
Data de inicio: 21.7.2015
Forma de inicio: solicitude do interesado

Notifícolle que con data 29 de xullo de 2015, o xefe territorial da Consellería do Medio Rural e do Mar emitiu unha resolución de autorización do proxecto de experimentación animal, cuxo texto íntegro é o seguinte:

ANTECEDENTES

A interesada, como representante do centro da Facultade de Medicina (Universidade de Santiago de Compostela), presentou con data 3.7.2015 e rexistro de entrada 79260 RX 1272914, unha solicitude para a realización do proxecto de experimentación animal, cuxos datos se detallan a continuación:

Denominación do proxecto: Estudio de novas terapias en modelos de Párkinson e outras enfermidades neurodexenerativas
Nome do centro usuario: Facultade de Medicina (USC)
Persoa responsable do proxecto: José Luis Labandeira García
Establecemento onde se realizarán os procedementos do proxecto (ou lugar xeográfico no caso de traballos de campo): Laboratorio de Neuroloxía Experimental e Neuroanatomía da Facultade de Medicina
Clasificación do proxecto : Tipo I ☐ Tipo II ☒ Tipo III ☐

CONSIDERACIÓNS LEGAIS E TÉCNICAS

1. O Real decreto 53/2013, de 1 de febreiro (BOE núm. 34, do 8 de febreiro), polo que se establecen as normas básicas aplicables para a protección dos animais utilizados en experimentación e outros fins científicos, incluíndo a docencia, establece no seu artigo 33 as condicións de autorizacións dos proxectos con animais de experimentación.
2. O artigo 89 da Lei 30/1992, de 26 de novembro, do réxime xurídico das administracións públicas e do procedemento administrativo común (BOE núm. 285, 27 de novembro de 1992), modificada pola Lei 4/1999, de 14 de xaneiro, establece que a resolución que poña fin o procedemento decidirá todas as cuestións expostas polos interesados e aquelas outras derivadas deste.

XUNTA DE GALICIA
DELEGACIÓN TERRITORIAL DA CORUÑA
Xefatura Territorial da Consellería do Medio Rural e do Mar

Edificio Administrativo Monelos
Vicente Ferrer, 2
15071 A Coruña

galicia

3. O Servizo de Gandaría da Coruña revisou a documentación achegada na solicitude e o resultado favorable da avaliación do proxecto, realizada polo órgano habilitado Sección de Experimentación animal do Comité de Bioética da Universidade de Santiago de Compostela.

Esta xefatura territorial é competente para ditar unha resolución, de conformidade co artigo 11 do Decreto 245/2009 de 3 de abril, polo que se regulan as delegacións territoriais da Xunta de Galicia e o Decreto 46/2012, de 19 de xaneiro, polo que establece a estrutura orgánica da Consellería do Medio Rural e do Mar e do Fondo Galego de Garantía Agraria.

De acordo con todo o indicado, RESOLVO:

1. Autorizar o proxecto solicitado.
2. Notificarlle esta resolución ao interesado.

O mencionado proxecto non deberá someterse a unha avaliación retrospectiva.

A autorización deste proxecto terá unha duración de 5 anos, transcorridos os cales, deberá ser renovada esta autorización.

A citada autorización é unicamente válida nas condicións que figuran no expediente. Ante calquera cambio significativo no proxecto que poida ter efectos negativos sobre o benestar dos animais, deberá solicitar a confirmación da autorización ao Servizo Provincial de Gandaría.

Esta autorización poderá ser suspendida, no caso de que o proxecto non se leve a cabo de acordo coas condicións de autorización e retirala, previo expediente tramitado ao que se lle dará audiencia.

Contra a presente resolución, que non pon fin á vía administrativa, poderá interpor recurso de alzada ante a conselleira de Medio Rural e do Mar da Xunta de Galicia no prazo dun mes contado a partir da recepción da notificación da presente resolución, conforme coa Lei 30/1992, do 26 de novembro, (BOE núm.: 285, 27 de novembro de 1992), de réxime xurídico das administracións públicas e do procedemento administrativo común na súa redacción dada pola Lei 4/1999, do 13 de xaneiro.

A Coruña, 31 de xullo de 2015
O xefe do Servizo de Gandaría

Eugenio Romero Senande

DE ASIS A COMPOSTELA
800 aniversario
1214 2014

XUNTA DE GALICIA
CONSELLERÍA DO MEDIO RURAL

Xefatura Territorial
Sº de Gandaría
Edificio administrativo Monelos, 4º andar
Rúa Vicente Ferrer, Nº 2
15008 A Coruña
Tfno.: 981 184 565
Correo electrónico: servizo.gandaria.a.coruna@xunta.gal

galicia

RESOLUCIÓN DE AUTORIZACIÓN DE PROXECTO DE EXPERIMENTACIÓN ANIMAL

Expediente núm.: 15012/2021/012
Persoa solicitante: Anxo Vidal Figueroa
Forma de inicio: solicitude da persoa interesada

Data de inicio do expediente: 16.4.2021
Procedemento: resolución de autorización

ANTECEDENTES

A persoa solicitante presentou con data 16.4.2021 unha solicitude para a realización do proxecto de experimentación animal (entrada no Rexistro electrónico da Xunta de Galicia 2021/880369), cuxos datos se detallan a continuación:

Denominación do proxecto: Estudos de novas terapias en modelos de enfermidade de Parkinson e outras enfermidades neurodexenerativas

Nome do centro usuario: Centro de Biomedicina Experimental (CEBEGA) da Universidade de Santiago de Compostela
Persoa responsable do proxecto: José Luis Labandeira García

Establecemento onde se realizarán os procedementos do proxecto (ou lugar xeográfico no caso de traballos de campo): Centro de Biomedicina Experimental (CEBEGA)

Clasificación do proxecto : Tipo I ☐ Tipo II [X] Tipo III ☐

CONSIDERACIÓNS LEGAIS E TÉCNICAS

1 O Real decreto 53/2013, de 1 de febreiro (BOE 34, do 8 de febreiro), polo que se establecen as normas básicas aplicables para a protección dos animais utilizados en experimentación e outros fins científicos, incluíndo a docencia, establece no seu artigo 33 as condicións de autorizacións dos proxectos con animais de experimentación.

2 O artigo 88 da Lei 39/2015, de 1 de outubro, do procedemento administrativo común das administracións públicas (BOE 236, do 2 de outubro de 2015) establece que a resolución que poña fin o procedemento decidirá todas as cuestións expostas polos interesados e aquelas outras derivadas deste.

Xacobeo 21·22

XUNTA DE GALICIA
CONSELLERÍA DO MEDIO RURAL

Xefatura Territorial
Sº de Gandaría
Edificio administrativo Monelos, 4º andar
Rúa Vicente Ferrer, Nº 2
15008 A Coruña
Tfno.: 981 184 565
Correo electrónico: servizo.gandaria.a.coruna@xunta.gal

galicia

3 O Servizo de Gandaría da Coruña revisou a documentación achegada na solicitude e o resultado favorable da avaliación do proxecto realizada polo órgano habilitado, a Sección de Experimentación Animal do Comité de Bioética da Universidade de Santiago de Compostela.

Esta xefatura territorial é competente para ditar unha resolución, de conformidade co Decreto 149/2018, do 5 de decembro, polo que se establece a estrutura orgánica da Consellería do Medio Rural e se modifica parcialmente o Decreto 177/2016, do 15 de decembro, polo que se fixa a estrutura orgánica da Vicepresidencia e das consellerías da Xunta de Galicia (DOG 235, do 11 de novembro).

De acordo con todo o indicado, RESOLVO:

1 Autorizar o proxecto solicitado.

2 O proxecto non precisa someterse a unha avaliación retrospectiva.

3 A autorización deste proxecto terá unha duración de cinco anos e unha vez transcorrido este tempo, deberá ser renovada.

A citada autorización é unicamente válida nas condicións que figuran no expediente. Ante calquera cambio significativo no proxecto que poida ter efectos negativos sobre o benestar dos animais, deberá solicitar a confirmación da autorización ao Servizo Provincial de Gandaría.

Esta autorización poderá ser suspendida no caso de que o proxecto non se leve a cabo de acordo coas condicións de autorización e retirala, previo expediente tramitado ao que se lle dará audiencia.

Contra a presente resolución, que non pon fin á vía administrativa, poderá interpoñer un recurso de alzada ante o conselleiro de Medio Rural. O prazo comezará a contar dende o día seguinte ao da recepción desta resolución. Todo isto, segundo o disposto nos artigos 121 e 122 da citada Lei 39/2015.

Mediante este escrito notifícaselle a Anxo Vidal Figueroa esta resolución segundo o esixido no artigo 40.1 da antedita Lei 39/2015.

Xacobeo 21·22

cradl charles river accelerator & development lab

Institutional Animal Care and Use Committee
Charles River Accelerator & Development lab (CRADL)
Charles River Laboratories

September 27th, 2023

Eli Lilly

To Whom it May Concern:

This letter is to inform you that the study protocols to support the animal use activities conducted by Eli Lilly at the Charles River 100 Binney site were reviewed and approved by the CRADL IACUC as outlined below:

Protocol	Description	Approval Date
2021-1433	**Platform screening of LNPs/PNPs for Extra-Hepatic Targets**	**11/22/2021**
2021-1452	**Local Delivery of Nucleic Acids to CNS**	**07/18/2022**
2022-1512	**Screening of nanomedicine delivery approaches for central and peripheral nervous system deilvery**	**02/25/2022**

All active protocols are reviewed annually, with a *de novo* submission required every 3 years for ongoing activities.

The CRADL site is included in the Charles River Laboratories Research Models registration with the National Institutes of Health Office for Laboratory Animal Welfare (NIH OLAW) and the Assurance of Compliance with Public Health Service (PHS) Policy on Humane Care and Use of Laboratory Animals statement number is D16-00496 (A3863-01) with the current effective term of 27July2022 through 31July2026. Should you have any questions regarding this matter, please contact me.

Sincerely,

DocuSigned by:
Michael Tetreault
4F55B2A4CE4F4A4...

Michael Tetreault, BS RLATg
CRADL IACUC Chairperson
Operations Manager Insourcing Solutions | Charles River
225 Gateway Suite 100.
South San Francisco, CA 94080
michael.tetreault@crl.com ; 508-245-0401

CLÍNIC BARCELONA
Hospital Universitari

DICTAMEN DEL COMITÉ ÉTICO DE INVESTIGACIÓN CLÍNICA

ANA LUCIA ARELLANO ANDRINO, Secretario del **Comité Ético de Investigación Clínica del Hospital Clínic de Barcelona.**

Certifica:
Que este Comité ha evaluado la propuesta del promotor, para que se realice:

Enmienda al protocolo y a la HIP/CI

Protocolo v2_18/02/2021. HIP/CI v2_18/02/2021

del estudio:

CÓDIGO: **COVARNA** NÚMERO EUDRACT:

CIF – G-08431173

TÍTULO: Preclinical development of innovative mRNA/MVA vaccines against SARS-CoV2

y emite

DICTAMEN FAVORABLE

Y hace constar que:

1º En la reunión celebrada el día 25/02/2021, acta 4/2021 se decidió emitir el informe correspondiente a la enmienda de referencia.

2º El CEIC del Hospital Clínic de Barcelona, tanto en su composición como en sus PNTs, cumple con las normas de EMA/CHMP/ICH/135/1995.

3º Listado de miembros:

Presidente:

- JOAQUIM FORÉS I VIÑETA (Médico Traumatólogo, HCB)

Vicepresidente:

- JOSEP MARÍA MIRÓ MEDA (Médico Enfermedades Infecciosas, HCB)

Reg.HCB/2020/0387

HOSPITAL CLÍNIC DE BARCELONA
Villarroel, 170 - 08036 Barcelona (España)
Tel. 93 227 54 00 Fax 93 227 54 54
www.clinicbarcelona.org

CLÍNIC BARCELONA Hospital Universitari

Secretario:

- ANA LUCIA ARELLANO ANDRINO (Médico Farmacólogo Clínico, HCB)

Vocales:

- MONTSERRAT GONZALEZ CREUS (Trabajadora Social, Servicio de Atención al Usuario, HCB)
- JOSE RIOS GUILLERMO (Estadístico. Plataforma de Estadística Médica. IDIBAPS)
- OCTAVI SANCHEZ LOPEZ (Representante de los pacientes)
- MARIA JESÚS BERTRAN LUENGO (Médico Epidemiólogo, HCB)
- JOAQUÍN SÁEZ PEÑATARO (Médico Farmacólogo Clínico, HCB)
- SERGI AMARO DELGADO (Médico Neurólogo, HCB)
- EDUARD GUASCH CASANY (Médico Cardiólogo, HCB)
- VIRGINIA HERNANDEZ GEA (Médico Hepatólogo, HCB)
- MARINA ROVIRA ILLAMOLA (Farmacéutico Atención Primaria, CAP Eixample)
- PAU ALCUBILLA PRATS (Médico Farmacólogo Clínico, HCB)
- JOSE TOMAS ORTIZ PEREZ (Médico Cardiólogo, HCB)
- ELENA CALVO CIDONCHA (Farmacéutica Hospitalaria, HCB)
- CECILIA CUZCO CABELLOS (Enfermera, HCB)
- PAULA MARTÍN FARGAS (Abogada, HCB)
- SALVATORE BRUGALETTA (Médico Cardiólogo, HCB. Miembro del CEA, HCB)
- XAVIER CANALS-RIERA (Ingeniero Telecomunicaciones)
- FRANCESC XAVIER CORBELLE (Informático, HCB)
- JOSEP DÍAZ CORT (Licenciado en Ciencias Físicas. Catedrático en Informática)
- GASPAR MESTRES ALOMAR (Médico, Angiología, Cirugía Vascular, HCB)
- FRANCESC TORRALBA ROSELLÓ (Doctor en Filosofía)

HOSPITAL CLÍNIC DE BARCELONA
Villarroel, 170 - 08036 Barcelona (España)
Tel. 93 227 54 00 Fax 93 227 54 54
www.clinicbarcelona.org

CLÍNIC BARCELONA Hospital Universitari

- MARTA FRANCH SAGUER (Abogada)
- PATRICIA AMOROS REBOREDO (Farmacéutica Hospitalaria, HCB)

Que en el caso de que se evalúe algún proyecto del que un miembro sea investigador/colaborador, éste se ausentará de la reunión durante la discusión del proyecto.

ANA LUCIA ARELLANO ANDRINO - DNI 43590424L

Firmado digitalmente por ANA LUCIA ARELLANO ANDRINO - DNI 43590424L
Fecha: 2021.03.04 14:50:13 +01'00'

Barcelona, a 03 de marzo de 2021

CIF – G-08431173

HOSPITAL CLÍNIC DE BARCELONA
Villarroel, 170 - 08036 Barcelona (España)
Tel. 93 227 54 00 Fax 93 227 54 54
www.clinicbarcelona.org

Generalitat de Catalunya Departament de Salut

UNIVERSITAT DE BARCELONA

USC UNIVERSIDADE DE SANTIAGO DE COMPOSTELA

Generalitat de Catalunya
Departament de Territori i Sostenibilitat
Direcció General de Polítiques Ambientals
i Medi Natural
Comissió d'Experimentació Animal
Òrgan Habilitat

Ref. núm. informe: CEA-OH/11282/1

INFORME D'AVALUACIÓ D'UN PROJECTE PER LA COMISSIÓ D'EXPERIMENTACIÓ ANIMAL COM A ÒRGAN HABILITAT PER LA GENERALITAT DE CATALUNYA (Reial Decret 53/2013, d'1 de febrer)
Ref. núm. de projecte: 11282
Títol del projecte: **Desenvolupament d'una vacuna contra SARS-COV-2 empleant el ratolí**
Projecte tipus: ☐ I ☒ II ☐ III
Persona responsable del projecte: Marta Sisteré Oró
Data d'admissió de la documentació: 15.12.2020
Data d'avaluació per la CEA com a OH: 20.01.2021

Revisada la documentació presentada, s'informen, d'acord amb la normativa vigent*, els punts següents:

1. Avaluada la informació relativa a la procedència dels animals (art.19 del RD 53/2013 d'1 de febrer i només per a les espècies* incloses a l'annex I del RD 53/2013 d'1 de febrer o a l'annex de la Llei 5/1995, de 21 de juny), s'informa,
(*) la utilització de gossos i gats rodamóns, i els provinents de centres de recollida d'animals abandonats està prohibida a Catalunya (art. 4.1.a de la Llei 5/1995)
☐ No procedeix, atès que l'espècie animal no està inclosa a l'annex I del RD 53/2013, d'1 de febrer.
☒ Favorablement
☐ Desfavorablement, atès que
Observacions/Justificació:

2. Avaluada la informació presentada relativa a la utilització de primats no humans en el projecte, d'acord amb l'art. 21 del RD 53/2013 d'1 de febrer, s'informa,
☒ No procedeix, atès que no s'utilitzen primats no humans.
☐ Favorablement.
☐ Desfavorablement, atès que
Observacions/Justificació:

3. Avaluada la informació relativa a l'ús d'anestèsia durant el projecte (art. 26 del RD 53/2013 d'1 de febrer), s'informa,
☐ No procedeix, atès que el projecte no ho requereix.
☒ Favorablement el protocol d'anestèsia a aplicar.
☐ Favorablement la justificació presentada pel responsable del projecte en relació amb la no utilització de l'anestèsia per ser incompatible amb el projecte o per estar contraindicada.
☐ Desfavorablement, atès que
Observacions/Justificació:

1

Provença, 204-208
08036 Barcelona
Telèfon: 93 495 80 00
http://territori.gencat.cat

Generalitat de Catalunya
Departament de Territori i Sostenibilitat
Direcció General de Polítiques Ambientals
i Medi Natural
Comissió d'Experimentació Animal
Òrgan Habilitat

Ref. núm. informe: CEA-OH/11282/1

4. Avaluada la informació relativa a l'ús d'analgèsia o altres mètodes destinats a eliminar al màxim el dolor, el sofriment durant el projecte (art. 26 del RD 53/2013 d'1 de febrer), s'informa,
☐ No procedeix, atès que el projecte no ho requereix.
☒ Favorablement el protocol d'analgèsia o altres mètodes a aplicar destinats a eliminar al màxim el dolor.
☐ Favorablement la justificació presentada pel responsable del projecte en relació amb la no utilització de l'analgèsia per ser incompatible amb el projecte o per estar contraindicada.
☐ Desfavorablement, atès que
Observacions/Justificació:

5. Avaluada la informació relativa a les condicions d'allotjament, zootècniques i de cura dels animals en el projecte (art. 6 del RD53/2013 d'1 de febrer), s'informa,
☐ No procedeix, atès que el projecte no ho requereix.
☒ Favorablement.
☐ Desfavorablement, atès que
Observacions/Justificació:

6. Mètode d'eutanàsia:
6.1. Avaluada la informació relativa al mètode d'eutanàsia (art. 7 i annex III del RD 53/2013 d'1 de febrer) en finalitzar el projecte, s'informa,
☐ No procedeix, atès que els animals no són eutanasiats
☒ Favorablement
☐ Desfavorablement, atès que
Observacions/Justificació:

6.2. I en relació amb el mètode d'eutanàsia en aplicació a criteris de punt final, s'informa,
☐ No procedeix, atès que el projecte no ho requereix.
☒ Favorablement.
☐ Desfavorablement, atès que
Observacions/Justificació:

7. Avaluades les condicions generals previstes en l'execució del projecte (art. 25.3 del RD 53/2013 d'1 de febrer) s'informa,
☒ Favorablement, atès que el projecte es realitzaria tenint en compte evitar als animals qualsevol dolor, sofriment, angoixa o dany durador innecessari.
☐ Desfavorablement, atès que
Observacions/Justificació:

8. Avaluada la informació presentada en relació amb l'acreditació/capacitació del personal que participa en el projecte (art. 25.5 del RD 53/2013 d'1 de febrer), s'informa,
☒ Favorablement.
☐ Desfavorablement, atès que
Observacions/Justificació:

2

Provença, 204-208
08036 Barcelona
Telèfon: 93 495 80 00
http://territori.gencat.cat

Generalitat de Catalunya
Departament de Territori i Sostenibilitat
Direcció General de Polítiques Ambientals
i Medi Natural
Comissió d'Experimentació Animal
Òrgan Habilitat

Ref. núm. informe: CEA-OH/11282/1

9. Avaluada la informació relacionada amb el transport dels animals (art. 9.1 del RD 53/2013 d'1 de febrer), s'informa,
☐ No procedeix, atès que els animals no són transportats durant el projecte.
☒ Favorablement.
☐ Desfavorablement, atès que
Observacions/Justificació:

10. Avaluada la informació relativa a la utilització d'animals d'espècies amenaçades (art. 20 del RD 53/2013 d'1 de febrer), s'informa,
☒ No procedeix
☐ Favorablement.
☐ Desfavorablement, atès que
Observacions/Justificació:

11. Avaluada la informació relativa a la utilització d'animals capturats en la natura (art. 22 del RD 53/2013 d'1 de febrer), s'informa,
☒ No procedeix.
☐ Favorablement.
☐ Desfavorablement, atès que
Observacions/Justificació:

12. Avaluada la informació relativa a la reutilització d'animals (utilització d'animals que han esta sotmesos prèviament a un altre projecte) (art. 29 del RD 53/2013 d'1 de febrer), s'informa,
☒ No procedeix.
☐ Favorablement.
☐ Desfavorablement, atès que
Observacions/Justificació:

13. Avaluada la finalitat, els beneficis científics i, si s'escau, el valor docent del projecte (art. 34.2a del RD 53/2013 d'1 de febrer) s'informa,
☒ Favorablement.
☐ Desfavorablement, atès que
Observacions/Justificació:

14. Avaluada la conformitat amb les 3Rs (art.34.2b del RD 53/2013 d'1 de febrer), s'informa,
☒ Favorablement.
☐ Desfavorablement.
Observacions/Justificació:

3

Provença, 204-208
08036 Barcelona
Telèfon: 93 495 80 00
http://territori.gencat.cat

Generalitat de Catalunya
Departament de Territori i Sostenibilitat
Direcció General de Polítiques Ambientals
i Medi Natural
Comissió d'Experimentació Animal
Òrgan Habilitat

Ref. núm. informe: CEA-OH/11282/1

15. Avaluat el grau de severitat indicat a la memòria del projecte (art.34.2c del RD 53/2013 d'1 de febrer) s'informa,
☒ Favorablement.
☐ Desfavorablement, atès
Observacions/Justificació:

Amb la classificació de:
☐ Sense recuperació ☐ Lleu ☒ Moderat ☐ Sever

16. Balanç ètic: analitzats els danys i beneficis del projecte (art.34.2d del RD 53/2013 d'1 de febrer), s'informa,
☒ Favorablement.
☐ Desfavorablement.
Observacions/Justificació:

17. El projecte requereix un resum no tècnic (art. 33.1 del RD 53/2013 d'1 de febrer).
☒ Sí
☐ No
Atès que és de Tipus II

18. Avaluació retrospectiva del projecte (art. 35.1 del RD 53/2013 d'1 de febrer).
Atès que el projecte,
☐ Utilitza primats.
☐ S'utilitzen primats per a finalitats diferents a les previstes a l'art. 21.2.a del RD 53/2013 d'1 de febrer.
☐ Ha estat classificat com a sever.
☐ El projecte implica un dolor greu i perllongat que no pot ser alleujat.
☐ Altres: Article 33.6 f) del RD 53/2013
Justificació:

S'informa que el projecte,
☒ No requereix avaluació retrospectiva.
☐ Sí requereix avaluació retrospectiva, la qual s'ha de realitzar

19. Altres comentaris:

4

Provença, 204-208
08036 Barcelona
Telèfon: 93 495 80 00
http://territori.gencat.cat

Generalitat de Catalunya
Departament de Territori i Sostenibilitat
Direcció General de Polítiques Ambientals
i Medi Natural
Comissió d'Experimentació Animal
Òrgan Habilitat

Ref. núm. informe: CEA-OH/11282/1

RESULTAT FINAL DE L'INFORME.

Per tant, tenint en compte l'informe de cadascun dels punts anteriors,

☒ S'informa FAVORABLEMENT

☐ S'informa DESFAVORABLEMENT
Justificació:

Sílvia Lleonart Roura
La secretària de la Comissió d'Experimentació Animal

Signat electrònicament

5

Provença, 204-208
08036 Barcelona
Telèfon: 93 495 80 00
http://territori.gencat.cat

Generalitat de Catalunya
Departament de Territori i Sostenibilitat
Direcció General de Polítiques Ambientals i Medi Natural

RESOLUCIÓ

Assumpte: autorització de projecte d'experimentació núm. 11282

Identificació de l'expedient

Expedient núm. FUE-2020-01825389 i ID Q35FKW3B7 relatiu a la sol·licitud d'autorització d'un projecte d'experimentació amb animals.

Antecedents

1. El centre usuari Parc de Recerca Biomèdica de Barcelona va presentar sol·licitud d'autorització per a l'execució del projecte d'experimentació:
    a. Títol: Desenvolupament d'una vacuna contra SARS-COV-2 empleant el ratolí
    b. Responsable del projecte: Marta Sisteré Oró
2. La Comissió d'Experimentació Animal, com a òrgan habilitat, en data 20.01.2021 va avaluar el projecte d'acord amb l'article 34 del Reial Decret 53/2013, d'1 de febrer, amb un informe Favorable.

Fonaments de dret

1. Llei 5/1995, de 21 de juny, de protecció dels animals utilitzats per a experimentació i per a altres finalitats científiques.
2. El Decret 214/1997, de 30 de juliol, pel qual es regula la utilització d'animals per a experimentació i per altres finalitats científiques.
3. Directiva 2010/63/UE del Parlament Europeu i del Consell de 22 de setembre de 2010 relativa a la protecció dels animals utilitzats per a finalitats científiques.
4. Reial Decret 53/2013, d'1 de febrer, pel qual s'estableixen les normes bàsiques aplicables per a la protecció dels animals utilitzats en experimentació i altres fins científics, incloent-hi la docència.
5. Llei 6/2013, d'11 de juny, de modificació de la Llei 32/2007, de 7 de novembre, per a la cura dels animals, en la seva explotació, transport, experimentació i sacrifici.
6. Reial decret 1386/2018, de 19 de novembre, pel qual es modifica el Reial decret 53/2013, d'1 de febrer, pel qual s'estableixen les normes bàsiques aplicables per a la protecció dels animals utilitzats en experimentació i altres finalitats científiques, incloent la docència.

Provença, 204-208
08036 Barcelona
Tel. 93 495 80 00
http://territori.gencat.cat

Generalitat de Catalunya
www.gencat.cat

GENERALITAT DE CATALUNYA

Resolució

Per tant, resolc:

1. Informar Favorablement la sol·licitud d'autorització del projecte d'experimentació que es relaciona a continuació:

   Títol: Desenvolupament d'una vacuna contra SARS-COV-2 empleant el ratolí

   Responsable del projecte: Marta Sisteré Oró

   Usuari: Parc de Recerca Biomèdica de Barcelona

   Instal·lació on es realitzarà el projecte: Estabulari del Parc de Recerca Biomèdica de Barcelona

2. Assignar al projecte el núm. d'ordre: 11282

3. Autoritzar la realització d'aquest projecte d'experimentació durant cinc anys a partir de la data de signatura d'aquesta resolució. En el moment que es disposi d'un mètode validat alternatiu a l'ús d'animals per a qualsevol dels procediments que integren el projecte, aquesta autorització quedarà suspesa i sense efecte.

Aquesta autorització no eximeix del compliment i disposició d'altres autoritzacions, d'acord amb la normativa sectorial vigent.

Contra aquesta resolució que no exhaureix la via administrativa, es pot interposar recurs d'alçada davant la secretària de Medi Ambient i Sostenibilitat en el termini d'un mes, a comptar de l'endemà de la notificació d'aquesta resolució, segons el que estableix l'article 112, 121 i 122 de la Llei 39/2015, d'1 d'octubre, del procediment administratiu comú de les administracions públiques.

Ferran Miralles i Sabadell
El director general de Polítiques Ambientals i Medi Natural

Signat electrònicament

Doc.original signat per:
Ferran Miralles Sabadell
14/02/2021

Document electrònic garantit amb signatura electrònica. Podeu verificar la integritat d'aquest document a l'adreça web csv.gencat.cat

Original electrònic / Còpia electrònica autèntica

CODI SEGUR DE VERIFICACIÓ

0AMY3PSM5CI0VZNLG7I9HVVSLSHZQRSX

Data creació còpia:
15/02/2021 15:41:29

Data caducitat còpia:
15/02/2026 00:00:00

Pàgina 2 de 2

VRIJE UNIVERSITEIT BRUSSEL

Ethische Commissie Dierproeven
Ethical Committee for Animal Experiments

VERGUNNING - *LICENCE*

De Ethische Commissie Dierproeven geeft een gunstig advies voor onderstaand project en verleent hierbij de vergunning om het project te starten met inachtneming van onderstaande voorwaarden.

Based on a positive evaluation, the Ethical Committee for Animal Experiments hereby grants permission for this project to start, under the following conditions.

Deze vergunning wordt toegekend naar aanleiding van een aanpassing van het project.
This license is issued after approval of an adaptation:
R6

PROJECTNUMMER / *PROJECT NUMBER*: 17-214-7

TITEL PROJECT / *TITLE*: Anti-neoantigen respons: vergelijking van peptide en RNA immunizatie en optimalizatie van mRNA productie systemen

DUUR / DURATION

Oorspronkelijke startdatum / *Initial start date:*	Oorspronkelijke einddatum / *Initial end date*:	Nieuwe einddatum / *New end date*:
15/06/2017	01/05/2021	01:11/2021

GEBRUIKERS / *USERS*

Verantwoordelijke laboratoriumdirecteur / *Responsible laboratory director*:	Kris Thielemans
Proefleider / *Experiment manager*:	Wout de Mey
Overige uitvoerende personen / *Other researcher(s):*	Jan Spitaels Marian Crabbé Lukasz Bialkowski Sanne Bevers Nikolai Hendriks Sofie Seghers Elien van De Velde Patrick Tjok Sarah Maenhout
Verantwoordelijke van het laboratorium waar het project (deels) plaatsvindt, indien verschillend van hierboven / *Responsible of the laboratory where the experiments are (partially) conducted:*	

AANTAL DIEREN / NUMBER OF ANIMALS: 1521

INSCHATTING VAN ERNSTKLASSE DOOR DE COMMISSIE /
ASSESSMENT OF PAIN AND SUFFERING BY THE COMMITTEE

☐ Licht / *Mild*
☒ Matig / *Moderate*
☐ Ernstig / *Severe*: (duur/duration: dagen/days)

RETROSPECTIEVE ANALYSE / *RETROSPECTIVE ANALYSIS*
Gelieve binnen de 2 maanden na het beëindigen van het project de retrospectieve analyse en aangepaste NTS op te sturen naar ecd-secretariaat@minf.be.
A retrospective analysis with an adjusted NTS should be submitted within 2 months after conclusion of the project. Please send it to ecd-secretariaat@minf.be.

DE VOORZITTER / THE *CHAIR*:
Prof. dr. Eline Menu

DATUM / *DATE*:
14/04/2021

1/1

Ref: 10/296822.9/20

Comunidad de Madrid

Dirección General de Agricultura,
Ganadería y Alimentación
CONSEJERÍA DE MEDIO AMBIENTE, ORDENACIÓN
DEL TERRITORIO Y SOSTENIBILIDAD

Vista la solicitud presentada por MARIANO ESTEBAN RODRÍGUEZ, para la autorización del proyecto de memoria técnica titulada "ANÁLISIS DE LA RESPUESTA INMUNE DE VACUNAS FRENTE A SARS-COV-2/COVID-19" a desarrollar en el centro usuario CN BIOTECNOLOGÍA-CSIC con código de registro ES200790000182 y siendo el responsable del proyecto JUAN FRANCISCO GARCÍA ARRIAZA.

Visto el informe del Área de Protección Animal de la Subdirección General de Producción Agroalimentaria

Considerando que el citado proyecto se ajusta a lo establecido en el Real Decreto 53/2013 de 1 de febrero por el que se establecen las normas básicas aplicables para la protección de los animales utilizados en experimentación y otros fines científicos, incluyendo la docencia.

Esta Dirección General ha resuelto: autorizar la realización del proyecto referenciado siempre que se mantengan las condiciones que dieron lugar a la autorización y que el personal que intervenga tenga la preparación y formación adecuada que se especifica en el citado Real Decreto.

Tal y como se establece en el informe de evaluación aportado, este proyecto no deberá ser sometido a la realización de una evaluación retrospectiva.

Contra esta Resolución, que no agota la vía administrativa, cabe interponer recurso de alzada en el plazo de un mes, contado desde el día siguiente a la recepción de esta notificación, ante el Viceconsejero de Medio Ambiente, Ordenación del Territorio y Sostenibilidad, conforme a lo establecido en el artículo 121 y siguientes de la Ley 39/2015, de 1 de octubre, del Procedimiento Administrativo Común de las Administraciones Públicas.

Madrid, a fecha de la firma
EL DIRECTOR GENERAL DE AGRICULTURA, GANADERIA Y ALIMENTACION
(P.D.F. Resolución de 16 de julio de 2020)
EL COMISIONADO DEL GOBIERNO DE BIENESTAR ANIMAL
(documento firmado en el lateral)

Ref PROEX 169.4/20

Firmado digitalmente por: ALTOZANO SOLER PABLO
Fecha: 2020.07.28 17:10

La autenticidad de este documento se puede comprobar en www.madrid.org/cove mediante el siguiente código seguro de verificación: 0962993789213468799271

PUBLICATIONS DERIVED FROM THIS THESIS

Publications derived from this thesis

Title: Using nanotechnology to deliver biomolecules from nose to brain – peptides, proteins, monoclonal antibodies and RNA.

Authors: L. Borrajo, M. & Alonso, M. J.

Drug Delivery and Translational Research. 12, 862-880. (2022).

DOI: https://doi.org/10.1007/s13346-021-01086-2

ISSN: 21903948, 2190393X

Specific contribution to the publication

Literature review. Structuring of information. Manuscript and figure preparation.

Quality indexes

Journal Impact factor: 5.4 (2023 Journal Citation Reports). Journal CiteScore: 9.8 (calculated by Scopus on the 4th of Oct of 2023). Quartiles: quartile 1 (Q1) in Pharmaceutical Science (SJR 2022 0.81) calculated by Scimago (https://www.scimagojr.com/journalsearch.php?q=19700182043&tip=sid)

Journal authorization

Genetic therapies show great potential for treating various diseases through modulation of the expression of specific genes. Their effective delivery is crucial, particularly for challenging conditions like CNS diseases and SARS-CoV-2 vaccines. Here, we used nanotechnology as a fundamental tool for RNA delivery. First, we engineered an ionizable nanoemulsion designed for brain diffusion and delivery of RNA. Second, we explored nanocarriers loaded with siRNA for brain delivery, exploring their performance following alternative administration routes. Finally, we encapsulated mRNAs derived from SARS-CoV-2 within nanoemulsions and polymeric nanocapsules, achieving significant cellular immune responses.